University College London

# Pharmacokinetic and Pharmacodynamic Challenges of Antibody-Directed Enzyme Prodrug Therapy (ADEPT)

A thesis submitted to the University College London (UCL) for the degree of Doctor of Philosophy in the faculty of Biomedical Sciences, Department of Oncology, UCL Cancer Institute, UCL

**Carima Andrady**

2014

# Declaration of Originality

'I Carima Andrady confirm that the work presented in this thesis is my own. Where information has been derived from other sources; I confirm that this has been indicated in the thesis.'

# Abstract

Antibody-Directed Enzyme Prodrug Therapy (ADEPT) is an experimental cancer treatment. First, an antibody-enzyme is targeted to the tumour. After clearance from healthy tissue, a prodrug is administered and activated by the enzyme. MFE-CP, an anti-carcinoembryonic antibody fragment fused to the enzyme carboxypeptidase G2, has been used for ADEPT in combination with a nitrogen mustard prodrug. Clinical trials are encouraging but highlight major challenges of sub-optimal MFE-CP pharmacokinetics and drug resistance. This thesis explores means to address these challenges.

MFE-CP, manufactured in *P. pastoris*, clears rapidly from the circulation due to yeast mannosylation. This leads to excellent tumour:blood ratios but decreased opportunity for tumour uptake. MFE-CP was therefore mutated in an attempt to reduce glycosylation. Initially, N-linked glycosylated asparagine residues were mutated to glutamine. The enzyme remained active but cleared rapidly *in vivo*. O-linked residue mutations were then explored. Changes that would least impede enzyme function were predicted using bioinformatics and a series of mutated constructs generated. The T55V mutation generated a functional enzyme that also cleared rapidly *in vivo*.

The DNA damage response was investigated as a mechanism of drug resistance. Using the comet assay, DNA interstrand cross-links were shown to form rapidly in carcinoma cells and xenografts in response to ADEPT, but these were unhooked over 48 hours. The $\gamma$-H2AX and RAD51 response indicated unhooking was due to DNA damage repair. Cell cycle studies showed that ADEPT treatment also led to G2/M arrest. G2/M arrest allowed DNA repair to occur and it was hypothesised that ADEPT could be made more effective by blocking arrest and driving entry into mitosis. To test this hypothesis, Chk1 inhibitors, UCN-01 and PF-477736, were investigated. Results demonstrated an enhanced anticancer effect with the ADEPT and PF-477736 combination, whereby increased cell death was observed at 48 hours post treatment. The approach has potential for clinical translation.

# Contents

# List of Figures

# List of Tables

# List of Abbreviations

| | |
|---|---|
| γ-H2AX | gamma (phosphorylated) H2AX |
| μg | micro gram |
| μM | micro molar |
| A375M | human melanoma cell line |
| ADC | antibody-drug conjugate |
| ADEPT | Antibody Directed Enzyme Prodrug Therapy |
| BER | base excision repair |
| bp | base pairs |
| BSA | bovine serum albumin |
| cDNA | complementary DNA |
| CEA | Carcinoembryonic antigen |
| Con A | Concanavalin A |
| CPG2 | Carboxypeptidase G2 |
| Ct | cycling threshold |
| dH20 | distilled water |
| DMSO | dimethyl sulphoxide |
| DNA | Deoxyribonucleic acid |
| DSB | double strand break |
| *E. coli* | *Escherichia coli* |
| Fab | fragment released from papain digestion of an IgG |
| FACS | fluorescence-activated cell sorting |
| Fc | antibody constant region |
| FcRn | neonatal Fc receptor |
| FDA | Food and Drug Administration (USA) |
| FPLC | Fast protein liquid chromatography |
| Fv | variable region fragment |
| g | gram |
| *x*g | gravity |
| $GI_{50}$ | growth inhibition by 50% |
| GlcNAc | N-acetylglucosamine |
| Gy | gray |

| | |
|---|---|
| HPLC | High performance liquid chromatography |
| HR | homologous recombination |
| HRP | horseradish peroxidase |
| ICL | DNA interstrand crosslink |
| Ig | immunoglobulin |
| IMAC | immobilised metal affinity chromatography |
| kDa | kilo Dalton |
| kV | kilo Volt |
| L | litre |
| M | molar |
| mAbs | monoclonal antibodies |
| mCPG2 | codon-optimised CPG2 sequence generated by Mologic Ltd |
| mg | milligram |
| ml | millilitre |
| MS | mass spectrometry |
| mV | milli Volts |
| MW | molecular weight |
| nM | nanomolar |
| nm | nanometer |
| OD | optical density |
| PAGE | polyacrylamide gel electreophoresis |
| PBLs | peripheral blood lymphocytes |
| PI | propidium iodide |
| *P. pastoris* | *Pichia pastoris* |
| PBS | phosphate buffered saline |
| PCR | polymerase chain reaction |
| RES | reticulo-endothelial system |
| RNA | Ribonucleic acid |
| rpm | revolutions per minute |
| RT-PCR | reverse transcriptase PCR |
| scFv | single chain variable fragment |
| SDS | sodium dodecyl sulphate |
| SRB | sulphorhodamine B |
| SW1222 | human colorectal carcinoma cell line |

| | |
|---|---|
| TBS/T | Tris buffered saline/0.1% Tween-20 |
| Tm | tail moment |
| U | (enzyme) unit |
| $V_H$ | variable heavy chain antibody fragment |
| $V_L$ | variable light chain antibody fragment |

# Acknowledgements

I would like to gratefully acknowledge my supervisor Prof Kerry Chester for her constant support, guidance and enthusiasm. I would also like to thank Dr Surinder Sharma for her unfailing support, and the Clement Wheeler-Bennett Trust for the financial support of my studentship and for allowing me to have the opportunity to be a part of and contribute to an exceptional research team. I would like to especially acknowledge the postdoctoral researchers – Dr Berend Tolner, Dr Enrique Miranda Rota, Dr Jenny Yeung and Dr Hassan Shahbakhti - who have helped me tremendously by providing guidance, technical knowledge and encouragement throughout my PhD. To the other members and fellow students in my group who I want to thank for their technical assistance and emotional support: Gaurav Bhavsar, Maria Livanos, Maha Abdollah, Elizabeth Hull, Fatemeh Vahid Dastjerdi, Alex Kinna and Tom Oxenham.

I would like to acknowledge Prof Barbara Pedley and her group for their supervision and expert advice regarding xenograft tissue storage, sectioning and microscopic analysis. I am grateful to Prof John Hartley of the Cancer Research UK Drug-DNA Interactions Research Group for his guidance and allowing me to work in his lab; and staff members - Dr Victoria Spanswick and Dr John Bingham - for their unfailing support and guidance. I would also like to acknowledge the following external collaborators: Dr Paul Gane from Medicinal Chemistry (UCL) who helped me with the enzyme molecular modelling; Daniel Spencer from Ludger Institute (Oxford) who carried out the mass spectrometry analyses; and Mologic Ltd who provided the codon-optimised CPG2 sequence.

Finally, I would like to acknowledge my family, in particular, Vincent Fernandez-Sanchez, for their continual encouragement throughout my PhD.

University College London

# CHAPTER 1

Pharmacokinetic and Pharmacodynamic Challenges of Antibody-Directed Enzyme Prodrug Therapy (ADEPT)

Carima Andrady

# 1 Introduction

## 1.1 Cancer

Cancer is a malignant disease characterised by the growth of tumours with a series of defined hallmarks (1) (2): uncontrolled cell growth, self-sufficiency in growth factors, insensitivity to anti-growth factors, evasion of apoptosis, limitless replicative potential, sustained angiogenesis, invasion and metastasis (spread to other organs), genome instability, chronic inflammation, evasion of immune destruction and reprogramming of energy metabolism. Cancer arises from the accumulation of genetic and epigenetic alterations within proto-oncogenes and tumour suppressor genes, which can lead to the disruption of various signalling pathways (3). De-regulation of a single pathway can provoke unscheduled proliferation leading to genomic and chromosomal instability – all of which contribute to the development of the primary tumour (4) (5).

As the leading cause of mortality world-wide, cancer accounted for 13% of all deaths in 2008 (6). One in four of all deaths in UK are caused by cancer; in particular, cancer of the lung, bowel, breast and prostate (7). The latter being solid tumour carcinomas, highlights a great need for treatments in these areas.

Traditional cancer treatments include surgery, radiotherapy, chemotherapy, or a combination of these for aggressive tumours. Chemotherapeutic agents tend to act systemically and exert their effects on proliferating cells, including healthy cells - hair follicles, blood cells and cells of the intestinal tract. This causes unwanted toxicity to healthy tissue. Targeted therapy aims to overcome these limitations by destroying the tumour while sparing healthy tissue. Monoclonal antibodies and small molecule drugs, developed for targeted therapy, have both demonstrated anti-tumour efficacy. Although antibodies dominate the sales market there is still a need for more effective targeted therapies, given the multiple types of cancer (8).

## 1.2 Antibodies for cancer therapy

In the early twentieth century, Paul Ehrlich envisioned treating cancer with a "magic bullet" that would specifically target a therapeutic agent to cancer cells, whilst leaving healthy cells unharmed (9). Antibodies form an integral part of the immune defence system, in which they are designed to specifically bind to foreign proteins (or antigens). This specificity and exquisite selectivity means antibodies can be harnessed for therapeutic uses in the rationally targeted approach proposed by Ehrlich.

Behring and Kitasoto were first to suggest that antibodies could be used for therapy using horse antisera. Initial attempts to treat cancer was with polyclonal antisera, that is, antibodies of differing specificity raised in animals against fragments of the patient's own tumours (10) (11). Despite their potential efficacy, the use of polyclonal antibodies for cancer therapy was (and is) limited by safety concerns and short supply of antisera from immunized animals. The use of antibodies for targeting cancer was limited, until 1975, when the development of hybridoma technology enabled the production of mouse monoclonal antibodies (12) (13). These monoclonal antibodies (mAbs) could be generated in large quantities from the fusion of antigen-specific antibody-producing B cell clones isolated from spleens of immunised mice with immortalised myeloma cells. This revolutionary work paved the way for the generation of highly specific therapeutic antibodies. Antibodies derived from hybridoma technology that are currently used in the clinic for cancer therapy are listed in Table 1.1.

### 1.2.1 Antibody structure

Antibodies, also known as immunoglobulins (Ig), are a group of glycoproteins. They are produced by B-lymphocytes and act as soluble surface receptors for antigen recognition. Antibodies were first identified in 1939 by Kabat and Tiselius (14) and their structure was later elucidated by Porter (15) and Edelman (16) (17). Antibodies are bi-functional molecules composed of a highly specific antigen-binding half and an immunological effector half. In vertebrates, 5 classes of

antibodies exist based on the sequence of their heavy chain constant regions (IgG, IgM, IgA, IgE and IgD). IgG is the most frequently used for cancer therapy and its structure, as reviewed by Padlan (18), is shown in Figure 1.1. A full-size IgG antibody is a Y-shaped complex molecule composed of two identical light chains, each with a variable and constant domain; and two heavy chains, each with one variable and three constant domains. Each heavy chain is attached to a light chain by disulphide bonds, and the $C_{H1}$ and $C_{H2}$ heavy domains are also linked together by disulphide bonds. The antibody is subdivided into two distinct functional moieties: the antigen-binding region F(ab')$_2$ and the constant region (Fc). The Fab or F(ab')$_2$ region contains the variable fragments (Fv), $V_L$ and $V_H$, each of which consists of three hypervariable complementarity-determining regions (CDRs) (19). These constitute the highly specific antigen binding site of the antibody (20). The IgG molecule has an exposed hinge region; a flexible proline-rich region between the $C_{H1}$ and $C_{H2}$ domains that is susceptible to proteases (Figure 1.1). Pepsin cleaves the Fc and releases the large F(ab')$_2$ moiety, which retains the bivalent antigen-binding properties of the parent IgG but without the effector capacity (Figure 1.2B). Alternatively, papain digestion releases the two identical Fab fragments containing the $V_H$-$C_{H1}$ and $V_L$-$C_L$ segments linked together by disulphide bonds - each with monovalent antigen binding capacity, and the Fc region that has no antigen binding ability (21).

The Fc portion of an antibody mediates both the biological half-life of the IgG and its ability to direct immunological effector functions for targeted cell-killing, including antibody-dependent cellular cytotoxicity (ADCC), complement-dependent cytotoxicity (CDC) and immune complex clearance (22). IgG isotypes (e.g. IgG1, IgG2, IgG3 and IgG4) are defined by structural differences associated with the Fc region and these isotypes differ in their ability to elicit immune effector functions (23) (24)). The IgG serum half-life of antibodies is regulated by neonatal Fc receptors (FcRns) on various immune cells and is described in more detail in Section 1.7.
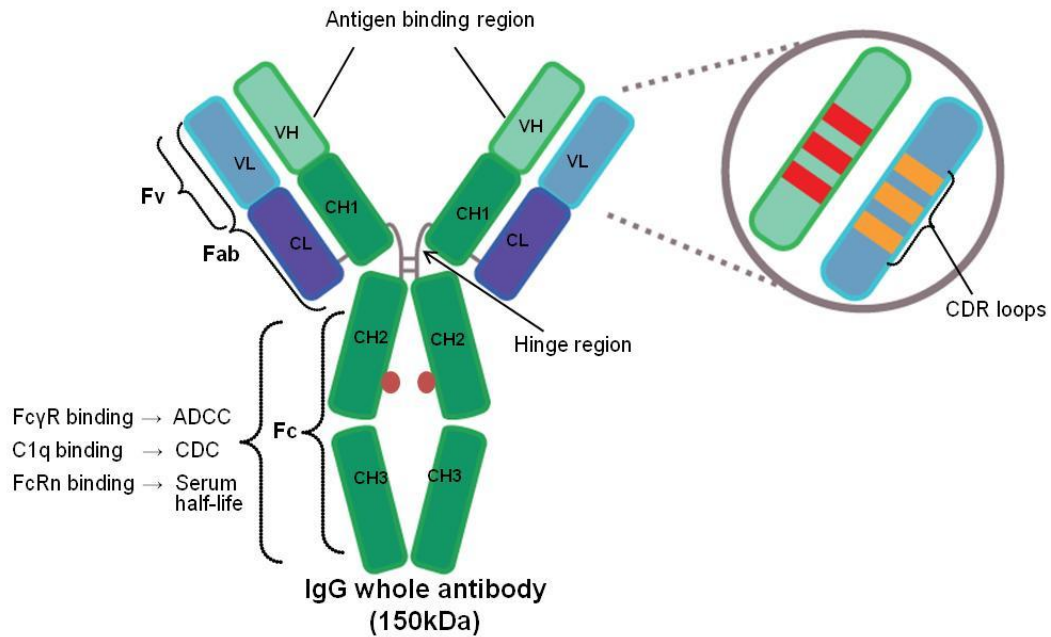
**Figure 1.1 IgG antibody framework**

The antibody can be divided into fragment regions, which are each composed of variable and constant polypeptide chain domains, as described in the text. A flexible proline-rich hinge region separates the CH1 and CH2 domains of the heavy chain. The heavy and light chains are linked together through a disulphide bridge. Red spheres indicate glycosylation on the CH2 domain. Binding of the Fc region to various Fc receptors leads to the initiation of immune effector functions including, antibody-dependent cellular cytotoxicity (ADCC) and complement-dependent cytotoxicity (CDC); or influences antibody retention. CDR, complementarity determining regions; $C_H$, constant heavy; $C_L$, constant light; Fc, constant fragment; Fab, variable fragment antigen binding region; Fv, variable fragment; $V_H$, variable heavy; $V_L$, variable light.

## 1.2.2 Engineering antibodies for therapy

During their initial use in the 1980s, clinical therapeutic success with murine monoclonal antibodies was limited by a number of factors, principally, their ability to invoke immune reactions in humans resulting in human anti-mouse antibodies (HAMA) after repeated treatments (25) (26) (27), and their poor ability to induce immune effector responses (23). This prompted the development of alternative strategies to improve the tumour targeting potential of antibodies.

Approaches to overcome the immunogenicity presented by murine antibodies have involved incorporating the murine antigen-binding regions into the human

IgG framework. This has allowed the generation of chimeric and humanised antibodies, as illustrated in Figure 1.2A. A chimeric antibody consists of linking the variable domains of a murine antibody with the human constant regions (28) (29) (30). The first chimeric antibody to be approved by the US Food and Drugs Administration (FDA) was rituximab in 1997 for the treatment of B-cell non-Hodgkin's lymphoma (see Table 1.1).

A humanised antibody contains only the murine CDRs grafted into the human IgG framework at the gene level (31) (32) (33). Multiple strategies have been developed to humanise antibodies as a result of intellectual property rights. However, they are all based on the CDR-grafting approach originally described by Winter and colleagues (33). The humanised antibodies clinically approved for the treatment of cancer are listed in Table 1.1.
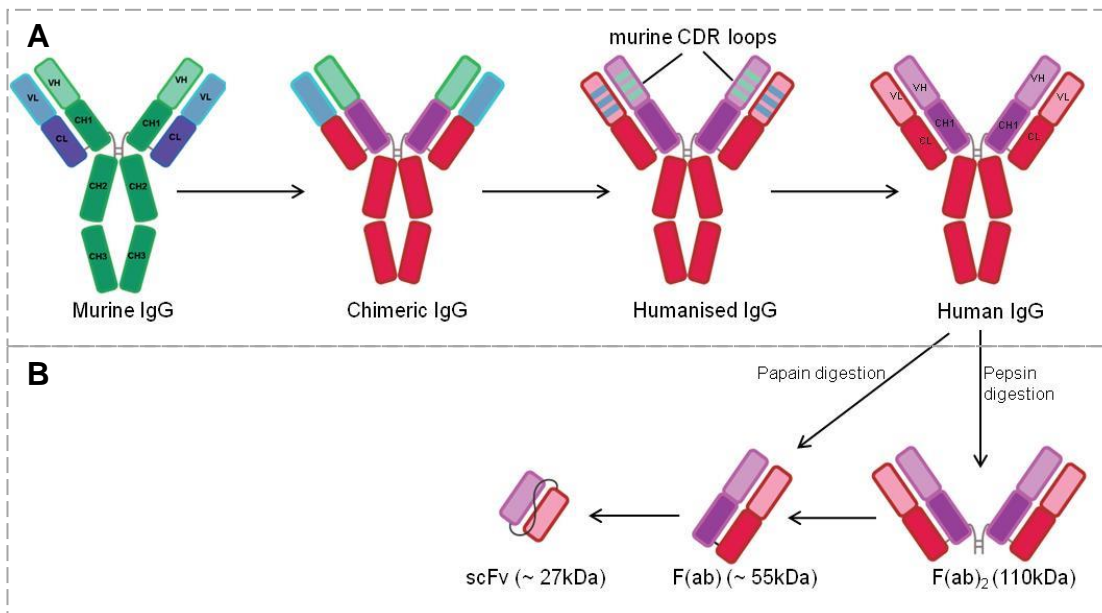
**Figure 1.2 Schematic diagram illustrating monoclonal antibody development**

A) murine IgG (green/blue shading) to humanised IgG (purple/pink shading); B) antibody fragments derived from an IgG antibody. Fabs and F(ab)$_2$ can be derived directly from proteolytic digestion, and scFvs are engineered from the Fv fragment. Murine, chimeric and humanised can also be engineered into antibody fragments (see Figure

**Figure 1.3**). (scFv, single chain variable fragment).

**Table 1.1 US Food and Drugs Administration (FDA)-approved anticancer monoclonal antibodies (mAb)**

ADCC: antibody-dependent cell-mediated cytotoxicity, ALCL: systemic anaplastic large cell lymphoma, BLyS: B-lymphocyte stimulator, CDC: complement-dependent cytotoxicity, CLL: chronic lymphoid leukaemia, CTLA-4: cytotoxic T-lymphocyte-associated antigen 4, EGFR: epidermal growth factor receptor, EpCAM: epithelial cell adhesion molecule NHL: non-Hodgkin's lymphoma, NSCLC: non-small-cell lung cancer, RANKL: receptor activator of nuclear factor kappa-B ligand (belongs to the tumour necrosis family), VEGF: vascular endothelial growth factor. *Not approved in the European Union; **Approved in the European Union only.

| Drug name | Antibody | Antigen | Type of mAb | Indication | Mechanism of action | Year of approval |
|---|---|---|---|---|---|---|
| *Naked antibodies* | | | | | | |
| Rituxan | Rituximab | CD20 | Chimeric | NHL | ADCC, CDC | 1997 |
| Herceptin | Trastuzumab | HER2 | Humanised | HER2$^+$ breast cancer | ADCC, receptor blockade | 1998 |
| Campath | Alemtuzumab | CD52 | Humanised | B cell CLL | ADCC, CDC | 2001 |
| Avastin | Bevacizumab | VEGF | Humanised | Metastatic cancer of colon, breast; NSCLC | Ligand blockade | 2004 |
| Erbitux | Cetuximab | EGFR | Chimeric | Metastatic cancer of colon and head and neck | Receptor blockade | 2004 |
| Vectibix | Panitumumab | EGFR | Human | Metastatic colon cancer | Receptor blockade | 2006 |
| Arzerrza | Ofatumumab | CD20 | Human | CLL | ADCC, CDC | 2009 |
| ** Removab | Catumaxomab | EpCAM and CD3 | Chimeric | Malignant ascites | Bispecific, tri-functional | 2009 |
| Xgeva | Denosumab | RANKL | Human | Bone metastases from solid tumours | Ligand blockade | 2010 |
| Yervoy | Ipilimumab | CTLA-4 | Human | Unresectable or metastatic melanoma | Receptor blockade | 2011 |
| Perjeta | Pertuzumab | HER2 | Humanised | Late-stage breast cancer | Receptor blockade | 2012 |
| Gazyva | Obinutuzumab | CD20 | Humanised | CLL | ADCC | 2013 |

| Drug name | Antibody | Antigen | Type of mAb | Indication | Mechanism of action | Year of approval |
|---|---|---|---|---|---|---|
| *Immunoconjugates* | | | | | | |
| Zevalin | $^{90}$Y-Ibritumomab | CD20 | Murine | Relapsed/refractory NHL | Radiation (β-emission) | 2002 |
| Bexxar | $^{131}$I-Tositumomab | CD20 | Murine | Relapsed/refractory NHL | Radiation (β- and γ-emissions) | 2003 |
| *Adcetris | Brentuximab vedotin | CD30 | Chimeric | Hodgkin's lymphoma and ALCL | Toxin blocks polymerisation of tubulin | 2011 |
| Kadcyla | Ado-trastuzumab emtansine | HER2 | Humanised | Late-stage breast cancer | Toxin binds to tubulin | 2013 |

Antibody therapy has had a profound impact on revolutionising cancer treatments, but its effectiveness has been limited due to poor tumour penetration because of the large IgG size (34), long *in vivo* half-life leading to increased toxicity, immunogenicity, and ability to initiate effector functions is often too toxic for repeat administrations (35). Other factors include mechanism-dependent toxicity, for example, in the binding of rituximab to normal B cells expressing CD20 antigen (36), and cardiotoxicity induced by trastuzumab binding to receptors in the heart tissue (37) (38). The limiting factors are currently being addressed through advances in recombinant antibody engineering (39).

## 1.3   Recombinant antibodies

### 1.3.1   Recombinant technology

Shortly after the introduction of antibody humanisation, technological advances facilitated the isolation of antibodies derived directly from human germ-line sequences and with enhanced features for tumour targeting, such as, defined affinity, avidity, specificity, and reduced immunogenicity. These technologies can be broadly classified into two distinct approaches: *in vitro* assembly of recombinant human antibody (fragment) libraries for use in phage display (40) (41) (42); and *in vivo* generation of human antibodies using transgenic mice engineered to encode human IgG heavy and light chains (43) (44) (45). At least 66 different therapeutic drugs, derived from either phage display or transgenic mouse platforms, have entered human clinical trials (45).

#### 1.3.1.1   *Phage display*

*In vitro* selection of antibodies was made possible by the introduction of phage display in the 1980s (46) (47) (20). Phage display involves the presentation of a library of antibody fragments on the surface of filamentous phage, by fusing the antibody fragment genes to the phage genome. For example, phage carrying

variable antibody fragment genes, express the antibody $V_H$ and $V_L$ domains on the surface of the phage as a single chain variable fragment (scFv) (see Section 1.3.2.1). Affinity selection of antibody-phage by binding to an antigen (panning) (48) is followed by elution of bound antibody-phage, which can be used to infect *E. coli*, and generate a large amount of specific antibodies after several rounds of selections and re-amplification of the selected antibody-phage (49). In 2002, adalimumab became the first FDA-approved fully human antibody created by phage display technology (50) (51). Adalimumab is a monoclonal antibody for the treatment of rheumatoid arthritis, but has also been approved for other inflammatory diseases.

Compared to hybridoma technology, antibodies selected from a phage display library are generally more stable, give high yields (> $10^{10}$ compared $10^2$ to $10^3$ clones) and easier to genetically engineer to create higher affinity binding molecules (52). The antibody phage libraries are classified as naive (from non-immunised donors) (40) (53) or immune (from immunised donors, but with biased antibody specificity) (54). The complexity of combinatorial libraries has been increased by creating semi-synthetic or synthetic libraries. For example, the fully synthetic Human Combinatorial Antibody Libraries (HuCAL) have been created to mimic the variable domains of antibodies seen in immune responses (55) (56). Other molecular selection strategies employed for engineering human antibodies include ribosome and mRNA display (57), yeast cell display (58) (59) (60), and lymphocyte display (61). The latter is a novel antibody selection platform based on T-cell activation.

### 1.3.1.2 *Transgenic mice*

Creating human antibodies from transgenic mice provides diverse, high affinity and high specificity monoclonal antibodies that aim to eliminate the production of HAMA reactions. Fully human monoclonal antibodies can be produced using this method which eliminates the need to "humanise" identified antibodies using earlier technologies. For example, the anti-EGFR monoclonal antibody, Panitunumab, was developed in this way (62) (63) (Table 1.1). In patients, the

antibody revealed decreased immunogenicity compared to an earlier chimeric antibody (cetuximab) for the same cancer (64) (65).

## 1.3.2 Recombinant antibody fragments

Intact IgGs are bivalent, that is, they have the ability to bind two antigens which greatly increases their functional affinity and avidity (retention). However, their large size means that they diffuse less efficiently through solid tumour mass (66) and are retained in the circulation for longer, which can lead to off-target toxic effects caused by Fc-mediated effector reactions. The advent of phage library technology has made it easier to generate a large variety of smaller, recombinant antibody fragments from the intact IgG with different binding kinetics, affinities and biophysical properties.

The IgG molecule (150 kDa) can be dissected into smaller antigen-binding fragments by proteolytic digestion, as shown in Figure 1.2B. These include, $F(ab')_2$ (~100 kDa), (2x) Fabs (~ 55 kDa each), and the Fv (fragment variable), which is composed of the $V_L$ and $V_H$ regions only (67). These $V_L$ and $V_H$ domains can be expressed in recombinant form as a single polypeptide chain by joining the two regions using a flexible, neutral linker. The fragment is termed single chain variable fragment, scFv (~ 27 kDa) (68) (69), as shown in Figure 1.2B. The impact of molecular size on tumour penetration was revealed in early studies comparing the *in vitro* binding of IgG antibody fragments [scFv, Fab, $F(ab)_2$] with the intact IgG, such that tumour penetration is inversely proportional to the size of the antibody molecules (70).

### *1.3.2.1 ScFv*

ScFvs represent the smallest IgG fragment carrying the whole antigenic binding site and are sufficiently stable (35). Their small size means scFvs are an ideal platform for targeted-therapies because of their ease of use in display technologies and high production yields in non-mammalian expression systems for clinical use (71). In 2009, it was reported that scFvs accounted for 53% of recombinant

fragments in clinical development, although none of the FDA-approved fragments were anti-neoplastic antibodies (72).

A scFv can have two possible orientations, $V_H$-$V_L$ or $V_L$-$V_H$, which can affect the expression efficiency, stability and affinity of the resulting antibody. The most commonly used linker, $(Gly_4Ser)_3$, provides flexibility, hydrophilicity and resistance to proteases (68) (69). The small size of antibody fragments means they are capable of penetrating and distributing homogenously in tumours more efficiently which is advantageous in imaging and therapeutic applications (73) (74) (75). Antibodies < 50-65 kDa undergo rapid, first-pass renal clearance (76), and the monomeric nature of scFvs means these antibodies show fast dissociation rates and modest retention times on the antigen (35) (77). Although this can be advantageous for avoiding toxicity, it is a drawback for clinical therapy because of the low absolute concentrations of antibody in the tumour.

One of the ways to improve retention of scFvs (and Fabs) is by increasing their valency, that is, the number of binding sites. ScFvs can be forced to form multivalent multimers by shortening the peptide linker (< 12 residues long), which encourages spontaneous multimerisation (78) (see Figure 1.3). Bivalent antibodies can be chemically or genetically engineered (79). Diabodies are scFv dimers (60 kDa) consisting of two non-covalently associated scFvs, in which the variable domains of one scFv pair with complementary domains of another scFv (80). These bivalent diabodies can be further stabilised by a disulphide linkage (81) (82) (83). Bispecific diabodies are two scFvs of different antigen specificities linked together (~55-60 kDa). When the peptide linker is < 3 residues long, scFvs can be forced to associate into multimers of 3 or 4 scFvs together - known as triabodies (90 kDa) or tetrabodies (120 kDa), respectively. Larger fragments such as minibodies (~75 kDa) comprise of two scFv-hinge-$CH_3$ chains covalently linked by disulfide bonds (81). ScFvs fused to intact Fc domains (scF-Fc; ~ 110 kDa) have similar pharmacokinetic profiles as intact IgGs (84) because of the presence of the entire Fc region, including the FcRn binding site. However, it has been shown that inducing mutations in the FcRn binding site of the Fc region can alter the pharmacokinetic profile of these antibodies (85) (86).

Other strategies to address the poor retention times and rapid clearance of scFvs include: chemical coupling with polyethylene glycol (87) (88) (89); engineering fusions with albumin (90) (91); affinity maturation (92); and modification of size through conjugation/genetic fusions with radioisotopes, toxins, enzymes or drugs (93) (94) (95) (96) (Figure 1.3). In the latter strategy, antibodies are used to deliver a toxic payload to tumours, which greatly increases the efficacy of antibody-targeted anti-cancer therapy. This is discussed in more detail in Section 1.4.
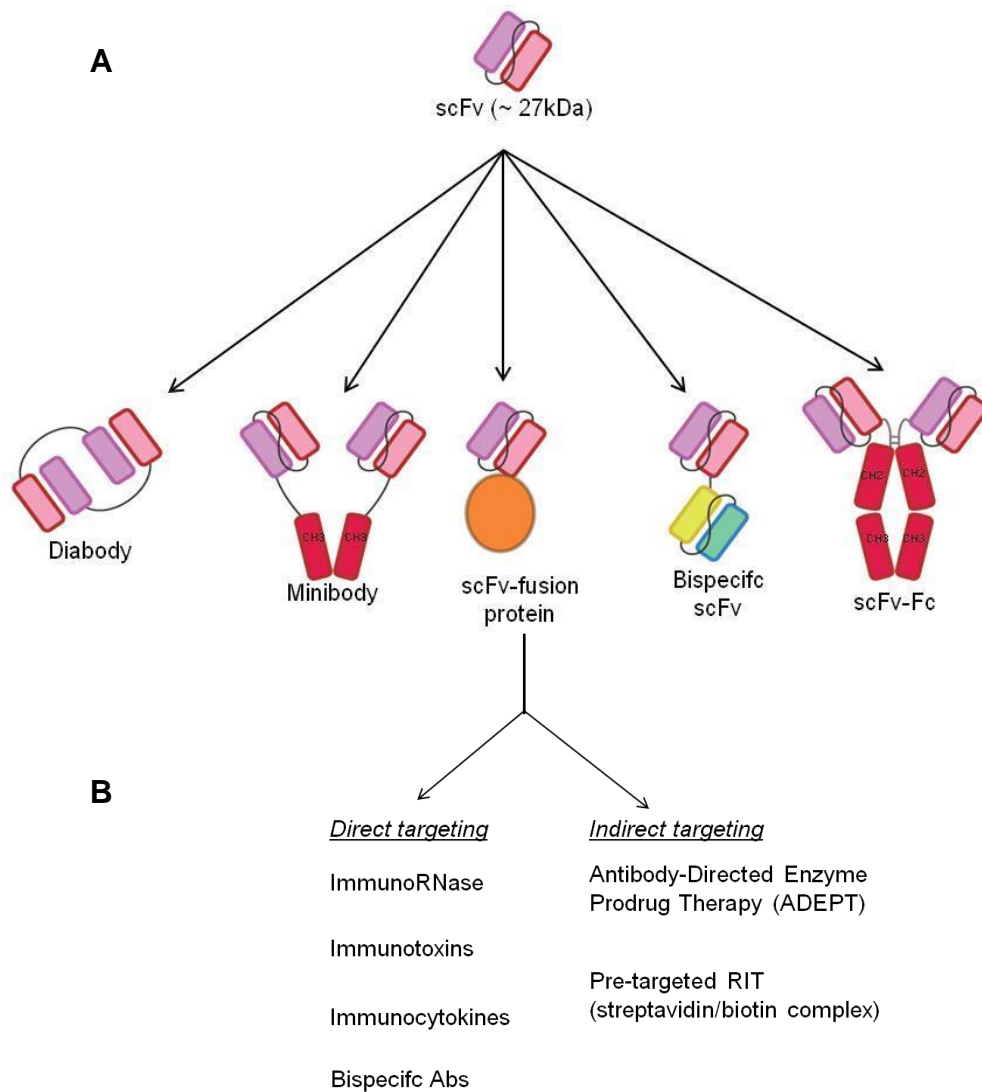


**Figure 1.3 Recombinant antibody fragments**

A) The single chain variable fragment (scFv) can be manipulated to create different antibody formats of different size and avidity. B) The scFv-fusion protein can be created with various effector proteins. Some of these are explained in more detail in Section 1.4. (RIT, radioimmunotherapy).

## 1.4 Modified antibodies for targeted therapy

As single agents, monoclonal antibodies cause tumour cell-killing by altering the progression of signal transduction pathways (receptor blockade, agonist activity, induction of apoptosis); or by immune-mediated mechanisms (including CDC, ADCC and regulation of T-cell function). To increase the potency of tumour cell-killing, whole antibodies and recombinant antibody fragments are being increasingly exploited as vehicles to deliver a toxic payload, such as radionuclides, toxins, drugs or enzymes (Figure 1.3).

### 1.4.1 Radioimmunotherapy (RIT)

Radio-labelled antibodies act by delivering lethal doses of radiation to disseminated tumour cells, primarily resulting in DNA damage, but do not always deliver enough radiation to completely eradicate solid tumours (97) (98). There are currently two approved therapeutic radio-immunoconjugates in the clinic (see Table 1.1). Pre-targeted RIT is a way of indirectly targeting radionuclides to the tumour using antibodies. A specific antibody localises to the tumour and is allowed to progress independently of the radiation-delivery phase. Once the target cell has achieved maximum antibody uptake, radioactivity can be delivered via a small ligand (e.g. biotin-labelled radionuclide) possessing high affinity for the pre-targeted antibody (e.g. fused with streptavidin) (99). The separation between the two phases of antibody distribution and radionuclide delivery results in more favourable tumour-to-normal tissue ratios compared to conventional RIT.

### 1.4.2 Immunotoxins

Immunotoxins are antibodies conjugated or fused to bacterial- or plant-derived toxins. These conjugate/fusion proteins are very potent and generally well-tolerated by haematological cancers because the patients are immunosuppressed from their disease and previous drug treatment. However, these agents are immunogenic and cause toxicity in patients, such as vascular leak syndrome (94).

Antibodies conjugated or fused to ribonucleases (immunoRNases) offer the potential of a less immunogenic cancer therapeutic with similar potency to immunotoxins (100) (101) (102). A review of antibody-enzyme fusion proteins for cancer therapy can be found by Andrady *et al*., 2011 (96).

### 1.4.3   Antibody-drug conjugates

The first antibody-drug conjugate (ADC) to gain FDA approval for the treatment of cancer was gemtuzumab-ozogamicin (Mylotarg) (103) – a humanised anti-CD33 IgG4 antibody conjugated to a DNA-binding cytotoxic antibiotic. Unfortunately, the drug was recently withdrawn from FDA-approval because it failed to show any clinical benefit compared to standard chemotherapy in a post-approval study (104). In spite of this, antibody-drug conjugates are gaining renewed interest in the last couple of years as anticancer therapeutics. There are currently more than 20 ADCs in early phase cancer clinical trials (105) compared to 6 that entered the clinic between the years 2000-2005 (106). The FDA recently approved the ado-trastuzumab emtansine (T-DM1) antibody-drug conjugate for patients with HER2-positive, late-stage (metastatic) breast cancer (see Table 1.1). It comprises an anti-HER2 antibody conjugated to a microtubule-depolymerizing agent through a non-reducible thioether linkage that is cleaved upon internalisation into cancer cells (107) (108). The clinical efficacy of T-DM1 was evaluated in a recent clinical study of 991 patients randomly assigned to receive T-DM1 or HER2-specific tyrosine kinase inhibitor plus chemotherapy (109). Results showed that patients treated with T-DM1 had a median progression-free survival of 9.6 months compared to 6.4 months in patients treated with the alternative drug combination. One of the pitfalls of ADCs is combining highly potent drugs with safe, stable linkers.

### 1.4.4   Antibody-directed enzyme prodrug therapy

Another form of targeted therapy, involves pre-targeting of an antibody-enzyme followed by administration of an inactive prodrug that is converted by the targeted enzyme to an active drug. The targeting approach is known as antibody-directed enzyme prodrug therapy (ADEPT). ADEPT has a number of potential advantages

over standard chemotherapy and single antibody agents, by intending to eliminate the weaknesses of each individual approach. As opposed to ADCs, a high concentration of cytotoxic drug can be generated at the tumour site quickly and safely, all the while overcoming the non-specificity posed by chemotherapeutic compounds alone. ADEPT is the principal topic under investigation in this thesis and is discussed further in Section 1.5.

## 1.5   ADEPT

Chemotherapy kills cancer cells but also damages healthy cells, meaning less than optimal drug doses can be administered. If cytotoxic agents could be generated *in vivo* and restricted to cancer sites this would have the potential to deliver more drug to the tumours and avoid normal tissue toxicity. This is the principal concept behind antibody-directed enzyme prodrug therapy (ADEPT), which was first described in the late 1980s (110) (111) (112).

ADEPT is a staged therapy (as shown in Figure 1.4), whereby an antibody-enzyme is delivered systemically and allowed to localize to the target tumour antigen *in vivo*. After clearance of the antibody-enzyme from normal tissues, a low-toxicity prodrug is administered and activated by the enzyme to the toxic drug at the tumour site. The active drug can diffuse to nearby cells, creating a local bystander effect where antigen negative cells and tumour supportive stromal elements are destroyed.
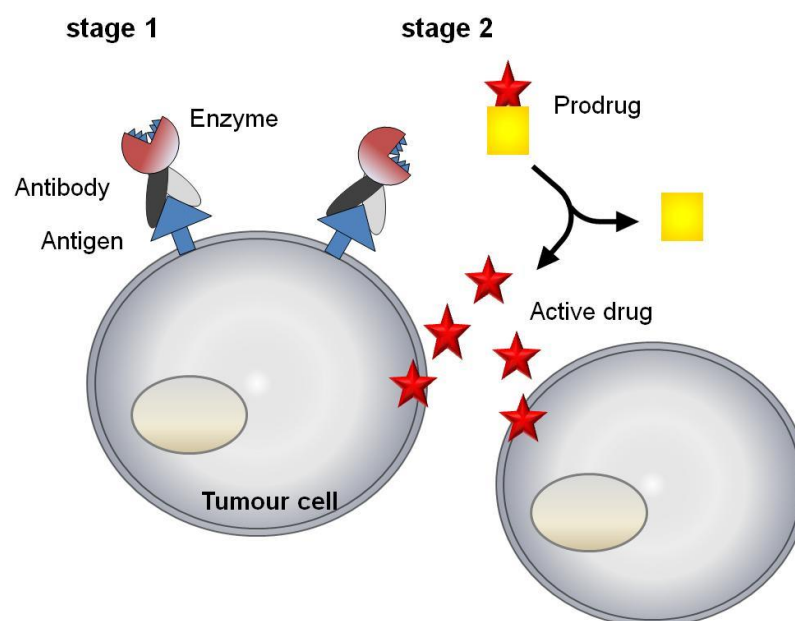
**Figure 1.4 Antibody-directed enzyme prodrug therapy (ADEPT)**

A staged system of cancer therapy. **Stage 1:** The antibody-enzyme fusion protein is allowed to localise in tumour tissue and is cleared or deactivated in healthy tissue. **Stage 2:** After administration, a non-toxic prodrug is converted by the targeted enzyme to the active drug. The active drug causes localised cytotoxicity to tumour cells bearing the antigen and mediates bystander effects to neighbouring tumour cells. (Adapted from Andrady *et al.*, 2011 (96))

ADEPT allows the selective and specific generation of highly toxic chemotherapeutic drugs, which has many advantages over standard chemotherapy. By giving a relatively non-toxic prodrug, larger doses can be prescribed and result in less or ultimately no systemic side effects, thus toxicity is restricted to the tumour site. Furthermore, the efficacy of ADEPT is boosted by the fact that many prodrug molecules can be converted by one enzyme, so the tumour essentially becomes a factory for its own destruction.

Most prodrugs for ADEPT are designed around the use of cytotoxic drugs currently licensed for chemotherapy (as noted in Table 1.2). This may be due to the fact that using a known drug for the therapy would reduce the clinical trial arms by one parameter. Since ADEPT provides the possibility of on-site generation of active drug, it is theoretically possible to use new and more potent drugs that would be too toxic to administer as standard chemotherapeutics. Whilst being a crucial part of ADEPT development, the field of prodrug/drug design is

beyond the scope of this Chapter. The reader is referred to further publications in this area (113) (114) (115). An ideal prodrug for ADEPT is one with a large differential in cytotoxicity between drug and prodrug, and is also a good substrate for the enzyme under physiologic conditions.

A wide range of enzymes (human and non-human) have undergone pre-clinical investigation for ADEPT (see Table 1.2). The majority are of bacterial origin and do not have a human equivalent. Non-human enzymes are often highly immunogenic and ADEPT therapy can only be administered prior to the patient eliciting an immune response. The ideal enzyme would be human but inevitably these are not suitable for ADEPT systems as they would cause endogenous conversion of prodrugs at sites other than the tumour, leading to off-target toxicity. Human enzymes can, however, be mutated so that they no longer recognise their native substrates, and would therefore be useful in an ADEPT setting (116) (117). Carboxypeptidase G2 (CPG2) is the only enzyme to have been clinically investigated, and forms the basis of this PhD thesis.

**Table 1.2 Summary of ADEPT systems – chemical conjugates and fusion proteins**

CEA, carcinoembryonic antigen; EpCAM, epithelial cell adhesion molecule; dsFv, disulfide-linked variable fragment; EDB, extra domain-B; TAG-72, tumour-associated glycoprotein-72; TfR, transferrin receptor. (Taken and adapted from Helen *et al.*, 2009 (118)).

| Enzyme | Antibody | Format | Active Drug | References |
|---|---|---|---|---|
| Alkaline Phosphatase | IgG2a antibody to carbohydrate antigen on carcinomas | Chemical Conjugate | Etoposide, Mitomycin C, Doxorubicin, Phenol mustard | (112) (119) (120) (121) |
| Carboxypeptidase A | Monoclonal antibody to human lung adenocarcinoma | Chemical Conjugate | Methotrexate | (122) (123) |
| | Monoclonal antibody to glycosylated surface protein on human ovarian teratocarcinoma | | | (124) |
| | Monoclonal antibody to Ep-CAM | | | (125) |
| Carboxypeptidase A1 Mutant (Human) | Monoclonal antibody to EpCAM | | | (126) |
| | scFv to seminoprotein | Fusion Protein | | (127) |
| Carboxypeptidase G2 | hCG antibody | Chemical Conjugate | Nitrogen mustard | (111) (128) (129) |
| | CEA F(Ab')2 | | | (130) (131) (132) (133) (134) (135) |
| | CEA scFv | Fusion Protein | | (136) (137) (138) (139) |

| Enzyme | Antibody/Target | Type | Drug | References |
|---|---|---|---|---|
| Cytosine Deaminase | IgG2a to carcinoma | Chemical Conjugate | 5-Fluorouracil | (140) (141) (142) (143) |
| | scFv to gpA33 antigen in colon cancers | Fusion Protein | | (144) (145) |
| | L19 scFv to extradomain B of fibronectin expressed in ovaries, uterus and during wound healing | | | (146) |
| β-Galactosidase | Monoclonal anti-CEA antibody | Chemical Conjugate | | (147) |
| | Humanised anti-TAG-72 (C$_{H2}$ knocked-out) | | Geldanamycin | (148) (149) |
| β-Glucuronidase | Monoclonal Antibody to carcinomas | | Daunorubicin and Doxorubicin | (150) (151) (152) |
| | IgG2a antibody expressed on AS-30D cell line | | Phenol mustard | (153) |
| β-Glucuronidase (Human) | CEA | Fusion Protein | Doxorubicin | (154) (155) |
| | scFv to EpCAM | | | (156) |
| | F(Ab')2 to a tumour necrosis antigen | | | (157) |
| | humanised scFV to TAG-72 | | p-Hydroxyaniline mustard glucuronide | (158) |
| β-Lactamase | IgG2a F(Ab')2 to carbohydrate antigen on carcinomas | Chemical Conjugate | Nitrogen mustard | (159) (160) |
| | dsFv to p185$^{HER2}$ | Fusion Protein | Doxorubicin | (161) |
| | scFv to melanotransferrin p97 | | Nitrogen mustard | (162) (163) |
| | scFv to melanoma | | Paclitaxel | (164) |
| | scFv to TAG72 carbohydrate epitope | | Melphalan | (165) |
| | Nanobody to CEA | | Nitrogen mustard | (166) |

| Penicillin-G-Amidase | IgG2a Monoclonal antibody to carcinoma cells | Chemical Conjugate | N-(4-hydroxyphenylacetyl) palytoxin, Doxorubicin, Melphalan | (167) (160) |
|---|---|---|---|---|
| Penicillin V Amidase | IgG2a antibody to carbohydrate antigen on carcinomas | | Doxorubicin and melphalan | (168) |
| Prolyl Endopeptidase (Human) | Monoclonal antibody to EDB domain of fibronectin | | Methotrexate, Cephalosporin analogues and Melphalan | (169) |
| Purine Nucleoside Phosphorylase (Mutant, Human) | Anti-HER-/neu peptide mimetic (AHNP) (breast cancer) | Fusion Protein | 2-Fluoroadenine | (170) |

## 1.5.1 Carboxypeptidase G2 ADEPT system

Carboxypeptidase G2 (CPG2) (also known as glucarpidase), originally identified from *Pseudomonas sp*. (strain RS-16) (171), is a bacterial, zinc-dependent exopepetidase with a molecular weight of 41.8 kDa (per monomer). It forms a natural homodimer, comprised of two subunits, each of which contains two zinc ions necessary for catalysis (172). CPG2 has a natural affinity for mediating the hydrolysis of folates, which has made it ideal for controlling the side-effects of high-dose chemotherapy with methotrexate (173) (174). In ADEPT, nitrogen mustard L-glutamate prodrugs have been specifically designed for cleavage by CPG2 (175) (176).

### 1.5.1.1 Chemical conjugate

The first reported *in vivo* studies utilised CPG2 conjugated to anti-human chorionic gonadotrophin (hCG) murine monoclonal F(ab')$_2$ antibody (111). The antibody-enzyme conjugate was used to target choriocarcinoma xenografts in nude mice, which were previously resistant to conventional chemotherapy. Due to the large concentration of hCG antigens in the blood, antibody-CPG2 bound to hCG to form immuno-complexes which accelerated clearance of the conjugate from the blood. This immune-complex formation had been demonstrated earlier by Begent *et al*. (177). The dichlorobenzoic acid mustard prodrug could then be safely administered between 56 and 72 hr after the conjugate. The ADEPT system proved to be successful, resulting in complete tumour growth regression of 9 out of 12 xenograft tumours (129).

Following on from this initial success, a F(ab')$_2$ fragment derived from a murine monoclonal antibody was chemically conjugated to CPG2 to target carcinoembryonic antigen (CEA) (178). CEA (CEACAM5) is a tumour-associated glycoprotein that is highly expressed on epithelial cells of various adenocarcinomas, in particular colorectal carcinoma (179). CEA is an oncofoetal antigen. It is also present on normal adult colon tissue, but restricted to the luminal surface of the gut where it is virtually inaccessible by intravenously administered antibodies. CEA was the target of choice for the CPG2-ADEPT system, as there was a clinical need at the time.

The anti-CEA antibody-enzyme conjugate was tested for efficacy in mice bearing LS174T human colorectal carcinoma xenografts (180). However, clearance of the conjugate from the plasma was slow possibly due to low circulating levels of CEA (181). This meant that it was necessary to delay prodrug administration for several days to avoid toxicity (182). As a result, no tumour response was observed.

To increase the speed of conjugate clearance from the blood and healthy tissue, a hybridoma-derived anti-CPG2 (SB43) monoclonal antibody was generated to inactivate circulating antibody-enzyme conjugates (183). The enzyme-inactivating antibody was galactosylated (SB43gal) in order to accelerate the clearance of conjugate from the blood via carbohydrate-specific receptors in the liver (184) and without affecting enzyme levels in the tumour. It was found that the prodrug, 4-[2-chloroethyl-(2-mesyloxyethyl) amino]benzoyl-L-glutamic acid (CMDA), (128) could be given within 24 hr after the conjugate without toxicity and this resulted in significant tumour growth delays of the human colon and ovarian carcinoma xenografts (180) (185) (186). Incorporating a glycosylated anti-enzyme antibody into the ADEPT system increased tumour-to-plasma ratios and meant that the prodrug could be administered safely. A pilot clinical trial of this ADEPT system was initiated following its *in vivo* success (130) (131).

### 1.5.1.2   *Chemical conjugate clinical trials*

The first ADEPT clinical trial used the system consisting of 3 components administered in the following order: 1) anti-CEA-CPG2 conjugate; 2) SB43gal and 3) CMDA prodrug (130) (131) (187). The trial demonstrated that this ADEPT system could achieve high tumour levels of conjugate whilst levels remained low in healthy tissues and blood of patients with advanced metastatic colorectal cancer. Eight (out of 17) patients who received the highest prodrug doses showed a good response to therapy, 4 patients had partial responses and one had a mixed response (131) (187) (188). Moreover, seven of the eight patients with a life expectancy of less than eight weeks, survived more than six months including three who survived 18, 25 and 36 months (188). Most patients suffered myelosuppression and it was alleged that the active drug had leaked into the plasma from the tumour.

The same (3-phase) system was subsequently used in a smaller clinical trial (10 patients) to investigate a lower dose of antibody-enzyme conjugate (134). One patient achieved a partial response and most of the other patients had stable disease for several months. The tumour-to-blood ratios of enzyme were in excess of 10,000:1 and the myelosuppression seen in the patients was believed to result from the leak-back of active drug from the tumours and not from prodrug conversion in the blood. It was, therefore, confirmed that the active drug as originally suggested (110) should have a very short half-life to avoid toxicity due to the leak-back effect. The active drug of CMDA has a half-life of approximately 20-30 minutes in humans (133). All patients developed anti-CPG2 antibodies and anti-mouse antibodies (HAMAs) which limited repeat therapy treatments.

A new nitrogen mustard prodrug (ZD2767P) was synthesised to address this potential toxicity (176) (176) (189). ZD2767P had a shorter half-life than the CMDA drug and the active drug was found to be 300 times more potent than the prodrug (133). Together with the antibody-enzyme conjugate, the new prodrug generated impressive cell kill results *in vivo* (133). However, in a trial designed to simplify the 3-phase system, the use of the clearing antibody was omitted and there was no evidence of therapeutic efficacy (135). Without a clearing antibody the conjugate took too long to be eliminated from the blood and eventually insufficient conjugate remained in the tumour at the time of prodrug administration (135).

### 1.5.1.3   *Recombinant fusion protein*

Building on the early work with antibody-CPG2 chemical conjugates, CPG2 was tested for use as a fusion protein with an anti-CEA scFv antibody, MFE-23. MFE-23 is a phage-derived, murine scFv (190). MFE-23 is specific for the N and A1 domains of CEA (191) (192) with an affinity of 2.4 nM (193). MFE-23 has been effective in radio-immunodetection (73), radio-immunoguided surgery (RIGS) (194) and as a fusion protein in ADEPT. It has been fully humanised with 29 mutations, affinity matured with 2 mutations and stabilised with 4 mutations. This new humanised MFE-23 was named SM3E (92).

The first antibody-enzyme fusion protein construct, MFE23-CPG2 (abbreviated to MFECP), was expressed in *E.coli* as a stable homodimer that exhibited high tumour specificity and functional affinity *in vitro* and *in vivo* (195). MFECP proved to effectively target LS174T CEA$^+$ colon carcinoma xenografts in nude mice (136). However, the tumour-to-normal tissue ratios for MFECP were found to be considerably higher than the tumour-to-plasma ratios. Whilst the tumour-to-liver ratio was 371:1, tumour-to-lung 450:1, tumour-to-kidney 521:1 and tumour-to-colon 1477:1, the tumour-to-plasma ratio was only 19:1 – it's maximum within 48 hr (136). Thus, the study highlighted the need for greater tumour-to-plasma ratios to be established. Furthermore, antibody-enzyme production in *E. coli* was insufficient for clinical studies, at 0.7-1.4 mg/L (195).

More favourable tumour-to-plasma ratios were subsequently obtained using the yeast (*P. pastoris*) expression system to generate glycosylated MFECP, that is, with the post-translational N-linked (Asn) addition of branched mannose (137). (Further explanation of glycosylation of proteins in *P. pastoris* can be found in Section 1.7). The rationale was to clear unbound MFECP from the circulation via mannose receptors in the liver, thus mediating rapid clearance and resulting in higher tumour-to-normal tissue ratios. *P. pastoris*-expressed MFECP was tested in nude mice and shown to clear rapidly from the blood to less than 1/1000 of its original plasma value by 6 hr after administration (137) (138) and via the mannose receptors (196). Despite the rapid clearance, *P. pastoris*-expressed MFECP was able to penetrate xenograft tumours and co-localize with its cognate antigen (CEA) on the tumour cell surface leading to excellent tumour-to-normal tissue ratios within 6 hr after injection. Tumour-to-plasma ratios of 1400:1 in the LS174T colon carcinoma xenograft model and 339:1 in the SW1222 colon carcinoma xenograft model were obtained (138). A single therapy dose of MFECP followed by the bis-iodo-phenol mustard prodrug, given to mice with LS174T or SW1222 tumour xenografts, led to significant tumour regression; and repeat cycles of therapy led to sustained tumour regressions (138).

### 1.5.1.4   *Fusion protein clinical trial*

*P. pastoris*-expressed MFECP was manufactured to clinical grade and named MFECP1 - the first ADEPT antibody-enzyme fusion protein to enter clinical trials

(197) (198) (71). In its final genetic construct, a sequence encoding a hexa-histidine (His) tag was added to the C-terminal end of the CPG2 gene for column purification by Immobilized Metal Affinity Chromatography (IMAC) (197). MFECP1 was tested in a dose escalating Phase I/II clinical trial to test the safety and pharmacokinetics in patients with advanced metastatic colon cancer (139). Eleven out of 28 patients had disease stabilization and one patient had a 10% reduction in the tumour diameter (139). DNA interstrand cross-links were detected in the tumour, implying that prodrug activation had occurred and the active alkylating drug had been effective at the tumour site. However, after a single dose of MFECP1, 36% (11 out of 30) patients elicited an immune response to the CPG2 (139).

More recently, a Phase I/II ADEPT study with the fusion protein and BIP prodrug was conducted to test the feasibility of repeat treatments in patients with colorectal adenocarcinoma (199). A therapeutic response was observed in only one of three patients treated successfully with 2 ADEPT cycles. Myelosuppression was the principal toxicity and repeat treatments significantly increased the incidence of anti-CPG2 antibodies.

### 1.5.2   Current challenges of ADEPT

ADEPT has the potential to be a very potent anti-cancer therapy that combines the specificity and selectivity of drug delivery to tumour cells, but there are still major challenges to be addressed (200). ADEPT requires a balance of individual components (antibody, enzyme, antibody-enzyme, prodrug), each of which present their own challenges. Clinical trials with the CPG2 ADEPT systems highlighted immunogenicity of the fusion protein (or conjugate) as a limitation. However, before this issue can be addressed, the more immediate challenge is to overcome repeat treatment cycles for ADEPT to be more effective. This involves exploring the following two areas of ADEPT:

1) ADEPT pharmacokinetics - the need to obtain high tumour-to-blood ratios prior to prodrug administration, whilst sustaining low or no circulating enzyme in the blood for reduced toxicity

2) ADEPT pharmacodynamics – the need to understand the DNA damage response after a single cycle of ADEPT, and be able to manipulate DNA damage repair to improve therapeutic efficacy.

The ways these challenges can be met are discussed further in Sections 1.7 and 1.6.

## 1.6   ADEPT Pharmacokinetics: Clearance mechanisms

Pharmacokinetics is the study of how the body processes the drug after administration. Pharmacokinetics can be divided into the study of the following areas: absorption, distribution, metabolism and excretion. Within these areas, circulatory half-life, volumes of distribution, clearance rates and total bioavailability are of particular significance for protein drugs.

Whole antibodies have their own built-in clearing/recycling system via the Fc region. IgGs are above the renal threshold and cleared through the cells of the reticulo-endothelial system (RES), which is regulated through the interaction with various Fc receptors. The neonatal Fc receptors (FcRns), expressed on phagocytic cells of the RES, protect IgGs from rapid clearance, and thus are critical regulators of the half-life of antibodies (201). Antibody fragments lack the Fc portion and therefore, depending on their size, are eliminated by renal filtration (<50kDa), proteolytic cleavage, hepatic uptake or immune complex formation (>50kDa). The same is true for most proteins. Antibody fragments lack the Fc domain and do not bind to FcRns, thus have substantially shorter half-lives (hrs) than the intact IgG (days). The Fc region can be manipulated to alter the clearance (and pharmacokinetic) profile of IgGs and antibody fragments for imaging or therapeutic applications. For example, it has been shown that introducing mutations into the Fc region at the FcRn binding site of anti-CEA scFv-Fc fragments results in variants exhibiting distinct clearance patterns in mice (85) (86). This demonstrated that serum half-life can be shortened by reducing the Fc-Rn interaction.

Cells of the RES also express various types of Fcγ receptors and interactions with these could potentially impact antibody clearance (202), such that polymorphism in the Fcγ receptors impacted the therapeutic response to rituximab (203) (204). In addition, the persistence of therapeutic antibodies in circulation depends, in part, on the structure and identity of N-linked oligosaccharides attached to Asn-297 within the Fc region. Human IgGs in serum consist of a number of glycoforms differing in number and heterogeneity of N-linked sugars on the Fc region. Glycosylation also plays a role in the plasma half-life of antibodies via binding to neonatal Fc gamma receptors (FcγRn) (205). Glycosylations can influence the half-life, clearance and effector function of antibodies, and can be manipulated to enhance efficacy and safety, as detailed in Section 1.6.2.

For effective therapy with ADEPT, it is necessary that there is adequate antibody-enzyme on the tumour and as little antibody-enzyme as possible in non-tumour tissue at the time of prodrug administration to minimise off-target toxicity. Without a clearing system, high concentrations of the antibody-enzyme can remain in the blood for extended periods of time (up to 72 hr (182) before the prodrug can be administered safely. This leads to low tumour-to-blood ratios. Strategies to increase the rate of clearance of the antibody-enzyme whilst attaining high tumour-to-blood ratios have been studied. Clearance strategies have included: the use of high-affinity complexing agents such as avidin/streptavidin (206) (207), EDTA (208), polyethylene glycol (PEG) (209) and sugars (210) (184); transfusion techniques such as plasmapheresis (211); and second antibody systems (212) (213). In the CPG2 ADEPT system, strategies to accelerate the clearance of the antibody-enzyme conjugate or fusion protein have included second antibody systems and/or glycosylation. The significance of these two systems is explained in the following sections.

## 1.6.1 Second antibody systems

As mentioned in Section 1.5.1, a galactosylated anti-enzyme antibody was employed to inactivate and clear the antibody-enzyme conjugate in the 3-phase CPG2 ADEPT system, which greatly reduced residual enzyme in the blood and normal tissues without affecting enzyme in the tumour. The use of a second antibody to improve

tumour-to-blood ratios and therapeutic efficacy of ADEPT has also been demonstrated with the β-glucuronidase (214) (152) and cytosine deaminase (141) (142) enzyme systems.

Initially, second antibody systems involved a liposome-entrapped antibody directed against anti-tumour antibodies (215). This was later followed by 'free' secondary antibodies (212), which have proven effective in radioimmunodetection studies (216) (217) (213) (218). The pioneering work with the anti-CPG2 enzyme inactivating antibody demonstrated effective clearance of the antibody-enzyme conjugate from blood, and addition of galactose sugars to the second antibody allowed rapid clearance of the conjugates via galactose receptors in the liver (183) (184) (186). Studies with the galactosylated anti-CPG2 antibody, SB43gal, showed a decrease in radiolabelled conjugate [percentage injected dose per gram (%ID/g)] in the blood, while %ID/g in the tumour remained unaltered (180). Rapid clearance of residual conjugates in the tumour improved tumour-to-blood ratios and minimised non-specific uptake by healthy tissues, which would otherwise lead to toxicity (183) (180) (184). The mechanism of SB43 inactivation is thought to involve its binding at or near the active site or at a distant site of the CPG2 enzyme causing a conformational change in the enzyme and loss of its biological activity. SB43gal was also shown to inactivate and clear PEG-conjugated antibody-enzyme conjugates in the blood without affecting the tumour levels (219).

In studies with the cytosine deaminase (CD) ADEPT system, a non-inactivating anti-enzyme antibody was incorporated to clear the antibody-CD conjugates from the circulation *in vivo* (141). The anti-CD antibody bound to both free and conjugated enzyme, with a minimum loss of enzyme activity. Tumour-to-blood ratios increased from 1 to > 38. However, a 50% reduction in conjugate level in the tumour was also observed. The same group also reported the use of an anti-idiotype antibody to accelerate the clearance of the same conjugate from blood which led to a 30-fold reduction in enzyme activity in blood but also a 30% reduction in the tumour (142). Other studies have shown anti-idiotype antibodies to accelerate clearance from tumour cells (220) (221).

Haisma and colleagues (214) developed an antibody against the enzyme β-glucuronidase. Antibody-enzyme conjugate levels were reduced in the blood of mice by 50% within 5 min after administration and it was believed that the antibody complexes formed were rapidly removed via the RES. No other pharmacokinetic data regarding the effect of the second antibody in other tissues was or has been reported. The same group also reported a 3-phase system to test a new glucuronide prodrug using the same anti-enzyme antibody (152). The *in vivo* studies revealed improved tumour growth inhibition by 3-fold compared to the prodrug alone; and tumour regression in 9 out of 11 compared to 0 out of 12 xenografts, respectively.

### 1.6.2 Glycosylation

Ong and colleagues (210) found that if antibodies were conjugated with galactose, their clearance could be modulated by the use of competitive inhibitors to galactose receptors in the liver. In this way, high concentrations of antibody can be maintained in the circulation for longer periods of time to obtain high tumour-to-blood ratios prior to rapid clearance. The group also mention the liver-receptor inhibition method to be advantageous over the second antibody method. For example, clearance of circulating antibody is more orderly involving the uptake and degradation at only one site, whereas the second antibody would form immune complexes in the circulation and interstitial fluid. Immune complexes in the interstitial fluid may persist in the tissues for longer and be degraded much less efficiently.

The initial understanding of the role of the *in vivo* circulatory behaviour of glycoproteins can be attributed in part to the discovery of the hepatic asialoglycoprotein receptor in the 1970s (222) (223). Galactose-terminating proteins are eliminated by specific endocytosis, which is mediated by these asialoglycoprotein receptors expressed by the hepatocytes. It is also known that glycoproteins with terminating mannose, N-acetylglucosamine (GlcNAc) or fucose residues can also be removed from the circulation via the liver by specific mammalian lectin-like receptors. For example, the uptake of mannosylated albumins by mannose receptors was shown in isolated perfused rat livers (224), hepatic sinusoidal cells (225) and *in vivo* in mice (226).

Glycosylation by attachment of galactose to the antibody-CPG2 conjugate was studied as another approach to accelerate clearance in ADEPT without the need for a secondary antibody (184). However, radiolabelled galactosylated conjugates cleared from the blood too rapidly and no localisation in the tumour occurred. Galactose receptors in the liver were blocked with various competitive protein binders, e.g. asialo-fetuin (AF) or asialo-bovine sub-maxillary gland mucin (a-BSM) (210), to inhibit rapid clearance. Studies in mice using the a-BSM receptor blocking protein prior to the administration of the radiolabelled galactosylated conjugate was shown to inhibit conjugate clearance for up to 10 hrs. As the inhibitor degraded, the conjugate was cleared rapidly from the blood and tissues except the tumour. This led to higher tumour-to-blood ratios of 45:1 at 24hrs increasing to 100:1 at 72 hr after injection (186). This allowed prodrug to be given 24 hr after conjugate injection without toxicity. The likelihood of this going to clinical trials was small because of the possible immunogenicity of a-BSM and its associated toxicity was unknown.

The development of the genetic fusion protein, MFECP, and its expression in yeast allowed for its self-clearance via mannose receptors in the liver (138), which created a 2-phase ADEPT system. However, the high tumour-to-blood ratios obtained with the secondary antibody system were never achieved with MFECP, because it cleared from the circulation too quickly as a result of the glycosylation. One of the objectives in this thesis is to remove these glycosylations and generate a non-glycosylated fusion protein. Glycosylation by yeast *P. pastoris* is explained in more detail below.

### 1.6.2.1   *Protein glycosylation by yeast P. pastoris*

Protein glycosylation is an essential post-translational modification in eukaryotic cells. Glycosylation can play an important role in determining the function, pharmacokinetics, pharmacodynamics, stability and immunogenicity of antibodies and protein drugs (205) (227) (228). Protein glycosylation can be manipulated to modify various properties of a protein including: physical properties (stability, increased solubility, resistance to proteolysis or denaturation); folding (prevents aggregation); activity (altered protein recognition, increased/decreased multimerisation); and targeting (intracellular/extracellular, altered clearance) (229).

In yeast, secretory proteins are commonly mannosylated by protein mannosyltransferases (pmts) in the endoplasmic reticulum (ER), and subsequently glycosylated by several glycosyltransferases in the Golgi apparatus to form glycoproteins with diverse N and O-glycan structures (230). The type of glycosylation (N- or O-linked), site occupancy, and the site of glycosylation can vary from glycoprotein to glycoprotein, in addition, the actual oligosaccharide structures (branching or linkages) can differ, even on the same site. The structural variation arises because glycosylation is a process that is not driven by a template, thus making full characterisation of protein glycosylations a challenge. The glycosylation pattern at a given site depends on many factors, including cell-specific and growth-dependent availability of glycosyltransferases and exo-glycosidases found in the Golgi bodies and ER. In yeast, the enzymatic N- and O-linked glycosylations are the two most studied glycosylations that affect the bioactivity of a protein.

1.6.2.1.1   N-linked glycosylation

The role of N-glycosylation is usually protein trafficking and secretion of the protein. N-glycosylation occurs via the amide nitrogen of asparagine residues in the consensus sequence Asn-Xaa-Ser/Thr (where X is any amino acid except proline) (231) (232) (233). N-glycans are categorised as high mannose, hybrid, or complex, depending on the extent of processing. High-mannose N-glycans contain two core GlcNAc residues and 5 to 9 mannose residues, and lack galactose or GlcNAc at the distal ends on the branched chains. Such chains are typically found in yeast-expressed proteins (232). N-glycosylation on MFECP was found to comprise 5 to 13 sugar units per site (196). In the yeast *Saccharomyces cerevisiae*, however, the Asn residues are hypermannosylated with 50-150 mannose residues making them very long chains. In hybrid mannose structures, both substituted GlcNAc residues and terminal mannose residues are present in the antennae, whereas complex mannose structures have both 1,6- and 1,3-mannose residues substituted with GlcNAc moieties.

1.6.2.1.2   O-linked glycosylation

The O-glycosylation pathway and glycan structures differ between species/host and the type of protein expressed. O-linked glycosylation occurs via the hydroxyl groups on serine or threonine residues (predominantly), but no consensus primary amino acid sequence exists for O-glycosylation (234) (235). Various types or structural motifs of O-glycosylation exist (236). Examples include: addition of N-acetylgalactosamine (GalNAc) to Ser/Thr of animal proteins especially mucins; addition of mannose to Ser/Thr residues of yeast proteins; addition of arabinose to hydroxyproline residues and galactose to Ser of plant proteins; addition of galactose to hydroxylysine residues of collagen and addition of N-acetylglucosamine (GlcNAc) to Ser/Thr residues of cytoplasmic and nuclear proteins. In *P. pastoris*, the most common O-mannosyl glycan structures are α1-2-mannose polymers of 2 or 3, or rarely, 4 mannose residues long and arranged in linear chains (237). A common feature of O-glycosylated proteins is that the side-chains are often clustered together in distinct Ser/Thr-rich regions (238). Such areas are thought to adopt rod-like structures important for protein function. In yeast, O-glycosylation is usually favoured by the presence of proline, one residue before or 3 residues after the glycosylation site and the absence of charged amino acids proximal to Ser/Thr (239). The sequence and isomeric linkage of monosaccharides in O-glycans show greater variety than in N-glycans. It has been suggested that O-mannosylation precedes and potentially controls N-glycosylation of glycoproteins (240).

## 1.7   ADEPT Pharmacodynamics: DNA damage response

Pharmacodynamics is the study of the biochemical and physiological effects of a drug on an organism; the mechanisms of drug action and the relationship between drug concentration and effect. Knowledge of the mechanisms of therapeutic response to ADEPT at the DNA level could help to improve the efficacy of treatment.

## 1.7.1   ADEPT-induced DNA damage

The prodrug used in the CPG2 ADEPT system, ZD2767P (chemically known as 4-[bis(2-iodoethyl)amino]phenoxycarbonyl-L-glutamic acid or bis-iodophenol-L-glutamate), is the inactive form of a toxic nitrogen mustard chemotherapeutic drug. The chemical structures of the two drug forms are illustrated in Figure 1.5.
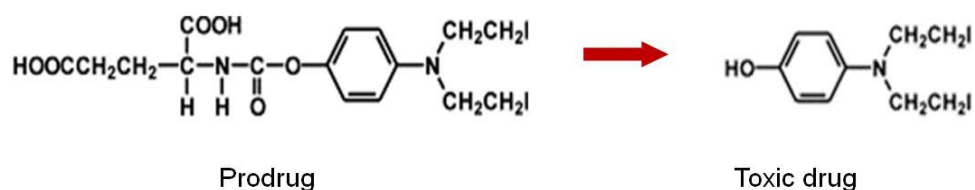


**Figure 1.5 Chemical structure of the ZD2767P prodrug and its conversion to the active drug, ZD2767D, in the presence of CPG2 enzyme**
(Taken with permission from a presentation by Prof. Kerry Chester).

The ZD2767D active drug is a bifunctional alkylating agent. Alkylating agents have the ability to bind covalently to electron-rich bases in DNA, especially the guanine-rich sequences (241). Nitrogen-7 of guanine is strongly nucleophilic, and is the main target for alkylating agents. Most chemotherapeutic agents have two alkylating groups, that is, they are bifunctional and capable of producing various DNA strand cross-links. These include cross-links formed within the same DNA strand (intrastrand), between the two complementary strands of DNA (interstrand) or with a reactive group on a protein (DNA-protein). DNA interstrand cross-links (ICLs) are generally considered to be cytotoxic lesions (242) and difficult to repair because they greatly distort the DNA structure, and thus inhibit DNA replication (243) and transcription (244). However, ICLs only constitute a small proportion (5-10% induced by alkylating agents) of the total adducts formed (245); the majority being monoadducts. ZD2767P/ZD2767D has previously been shown to induce DNA ICLs in tumour cells, xenograft tumour tissue and patient tumour biopsies upon treatment with ADEPT (242) (246) (139). The mechanism of repair of these ADEPT-induced ICLs has not been investigated in detail, but is thought to be similar to other classical nitrogen mustard drugs, such as melphalan and chorambucil (242) (247). The mechanisms determining the cellular pharmacology of these nitrogen mustards, such

as membrane transport, intracellular detoxification (both chemical and enzymatic) and DNA damage repair, (248) (249) may be equally the same for ZD2767D.

## 1.7.2    The DNA damage response (DDR)

The DNA damage response (DDR) constitutes a network of evolutionary conserved signalling cascades, which involves sensing DNA damage, followed by amplification and transmission of the damage signal to evoke a multitude of effector responses (250) (251). These effector responses either promote the survival or death of a cell, either by stalling the cell cycle to provide time for repair, or activating cell death pathways, respectively (252) (253) (254).

Cell cycle arrest is mediated by specific checkpoints in response to DNA damage. The main checkpoints include the G1/S checkpoint (preparation for DNA synthesis), intra-S or S checkpoint (DNA replication) and the G2/M checkpoint (preparation for cell division). These checkpoints are activated by the DDR transducers: ataxia telangiectasia mutated (ATM), which triggers the G1 checkpoint; and ataxia telangiectasia and Rad3-related protein (ATR), which triggers the S and G2/M checkpoints. ATM and ATR are both members of the phosphatidyl-inositol-3 (PI-3) kinase family and their association with checkpoint kinases, Chk1 and Chk2 (respectively), further amplifies the cell cycle signalling and arrest depending on the nature of the DNA damage (255). To some extent there is cross-talk between ATM/Chk2 and ATR/Chk1 pathways (256). Cyclins and cyclin-dependent kinases (CDKs) are also key regulatory molecules that determine a cell's progress through the cell cycle checkpoints (257).

DNA repair is arguably the most important component of the DDR. However, repair of DNA damage in cancer cells can reduce the highly potent activity of DNA damaging agents by removing lesions before they become toxic - a common mechanism for cancer-therapy resistance. Current research investigates and develops approaches to overcome therapy resistance, whilst limiting toxicity to healthy cells, by exploiting defective or lost signalling genes or controls, such as BRCA1/2 or p53 deficiency, in cancer cells (258) (259).

Repair of genetic lesions is mediated by different pathways and even a combination of pathways. These are summarized in Figure 1.6. The choice of repair mechanism is largely defined by the type of lesion, but other factors including p53 status and cell cycle phase also play a role. Detailed explanations of each of the different repair pathways are beyond the scope of this thesis, thus the reader is referred to the following reviews: (260) (261) (262) (258). The principal DNA damage repair pathways believed to be associated with the response to the CPG2 ADEPT system are explained in context in the following sections.
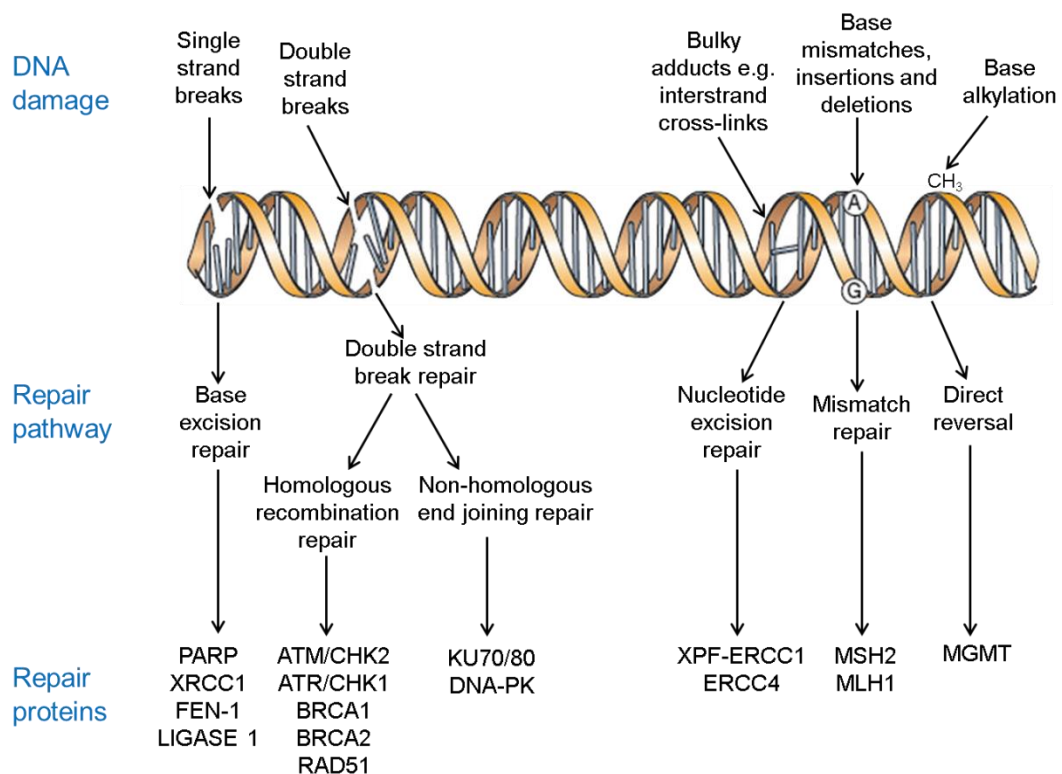
**Figure 1.6 The principal DNA repair pathways in mammalian cells**

Only key repair proteins are noted. Full term and genes expressing these proteins are listed in the Appendix. (Adapted from Lord and Ashworth (250)).

### 1.7.3   Repair of DNA ICLs

Drug resistance to nitrogen mustards has been associated with increased repair of DNA ICLs (263) (264). ICL repair is a well-established pathway in *E. coli* (265) and is thought to be different to that in yeast (266) (267), which is different to that in mammalian cells. ICL repair in mammalian cells is complex and is thought to require

the co-ordinated activities of different repair pathways, most notably nucleotide excision repair (NER), homologous recombination (HR) and translesion bypass synthesis (TLS) (268) (269) (270) (271) (272). Other repair pathways have also been reported to be involved in ICL repair, including base excision repair (BER) (273) and mismatch repair (274). A considerable amount of the knowledge of ICL repair mechanisms in mammalian cells has come from studies conducted in cells from patients with Fanconi anaemia (FA) - a human cancer-prone disorder that is particularly sensitive to ICL-inducing agents (275) (276) (277) (278) (279) (280).

It is believed that ICLs alone do not activate the G1 or G2 cell cycle checkpoint, but are tolerated by the cell until a DNA replication fork is encountered (281). ICLs cause the replication fork to stall during S phase of the cell cycle, thus allowing repair of the damage. However, if the checkpoint proteins for stabilising the fork are not activated in time, the replication fork will collapse because of the strong covalent bond linking the DNA strands together. If the ICL lesion is recognised as too cytotoxic and cannot be repaired, the cell will ultimately undergo apoptosis. The proposed model for ICL repair in mammalian cells is illustrated in Figure 1.7. The stalled replication fork is recognised and cleaved by a specific NER-related endonuclease in the leading-strand template, which makes an initial 3' incision. The incision is thought to be made by an enzyme called XPG, but there have also been reports that another enzyme, MUS81-EME1, may be responsible (282) (283) (284) (285). This event creates a one-sided double-strand break (DSB) (as shown in Figure 1.7). A second structure-specific heterodimeric NER-related endonuclease, XPF-ERCC1, creates a 5' incision on the other side of the ICL, thus releasing the covalent linkage between the DNA strands (286) (287). The importance of XPF-ERCC1 in mammalian cells was recognised when mutant cells deficient in this and other NER-related proteins were sensitive to nitrogen mustard (288) (289) (290). This initial ICL repair process is known as the "unhooking" step. The "unhooking" step creates a gap in the gene sequence which requires resection by proteins involved in HR repair (288) (269) and post-replication TLS (291) (292) (293). The classic model of DSB repair by HR (as shown in Figure 1.7) is based on experimental data from *Saccharomyces cerevisiae* (266) (294) and involves exchange of genetic information between the undamaged intact duplex and the break-containing duplex in order to

restart the replication fork (295). DSB repair in the context of ICL repair is described in more detail below.
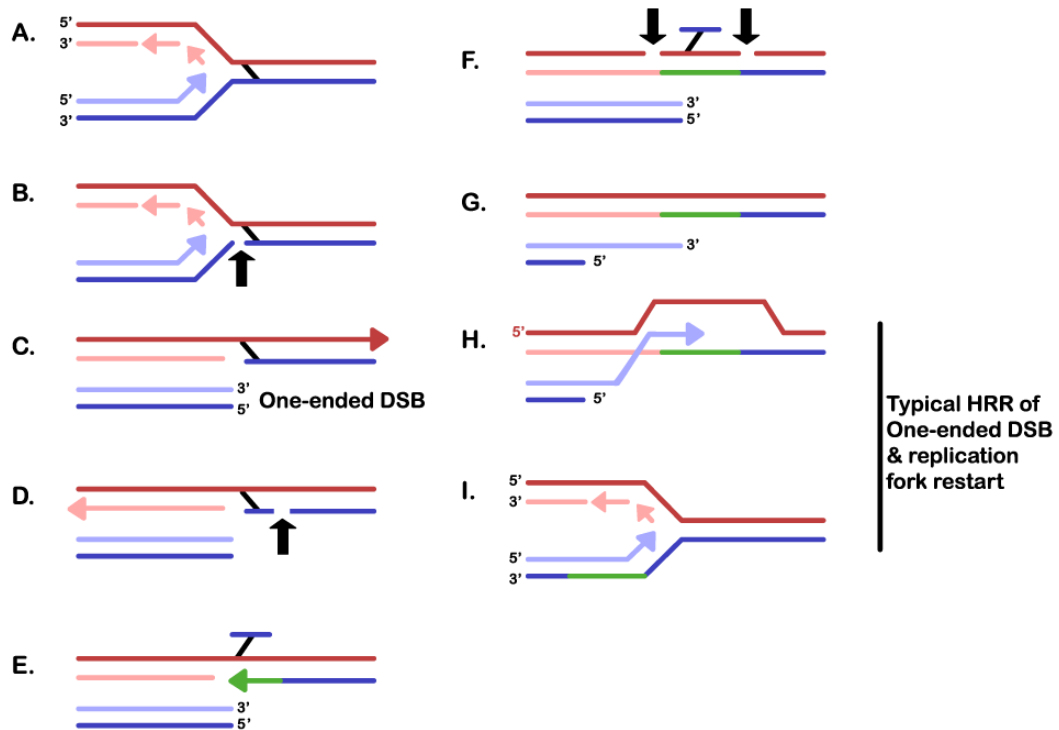


**Figure 1.7 Schematic of ICL repair during S phase in mammalian cells**

(**A**) When a replication fork approaches an ICL, the replication fork stalls. (**B**) An initial 3' incision is made in the leading-strand template adjacent to the lesion by a NER-related endonuclease (MUS81-EME1). This creates a one-sided double-strand break (DSB) (**C**). (**D**) A second incision is made by XPF-ERCC1 which unhooks the ICL. (**E**) Translesion synthesis (TLS) provides the missing sequence across from the unhooked ICL. (**F** and **G**) Removal of the unhooked cross-link and a second excision-resynthesis event occurs to fill in the single-strand gap. End resection of the DSB generates a 3'-OH-ending single-stranded tail. (**H**) This tail invades the template DNA to generate a D-loop. Homologous recombination takes place. (**I**) The replication fork is restored as the 3' end of the DSB is integrated into the homologous duplex. Taken and adapted from Hinz (296) and Niedernhofer *et al*., (284), (HRR: homologous recombination repair).

## 1.7.4 Repair of ICL-associated DSBs

DSBs are extremely cytotoxic lesions and difficult to repair (297) (298). If mis-repaired or left unrepaired, this can lead to translocations and other potentially carcinogenic abnormalities. DSBs are well-characterised lesions formed upon

exposure to ionising radiation, but they are less well-known as an intermediate lesion formed during ICL repair (as shown in Figure 1.7). The endogenous formation of DSBs is also not unusual. For example, DSBs may form during rearrangement of gene segments (VDJ recombination) in meiosis and antibody and T-cell receptor development (299); and they may also form as a result of normal metabolic processes which generate reactive oxygen species that attack DNA (300).

There are two pathways for DSB repair: the homology-driven HR pathway or the non-homology-driven non-homologous end joining (NHEJ) pathway. HR allows for replication-dependent error-free repair of ICL-associated DSBs during S or G2 phase of the cell cycle (301) (285). HR is not favoured during G0/G1 phase and ICL lesions may be by-passed altogether by TLS although this mechanism is less well-known and prone to errors (302) (303). In NHEJ the two ends of the DSB are directly joined together, requiring little or no sequence homology, and thus prone to error. DSB repair by NHEJ is particularly favoured in the G1 phase. NHEJ is thought to not be important for mediating ICL repair (304) (305), but recent evidence suggests that some proteins from the NHEJ pathway may be involved in repair of DSBs formed during ICL repair (306).

### *1.7.4.1   Gamma-H2AX*

In response to ionising radiation, DSBs have been shown to rapidly induce the phosphorylation of the histone variant, H2AX (on Ser139 in mammalian cells) (307) (308). H2AX is a member of the histone H2A family, which constitutes one of the 5 types of histones that package and organise eukaryotic DNA into chromatin. It has been reported that phosphorylated H2AX, $\gamma$-H2AX (309), accumulates at sites of DSBs to form discrete nuclear foci (310) (or ionising radiation induced foci (308)). These foci are thought to contain a collection of DNA damage signalling and repair proteins required for DSB repair (307) (311) (312) (313).

$\gamma$-H2AX is a key component of the DDR network and is widely used as a highly sensitive, prognostic marker of DNA damage, namely DSBs formed in response to ionising radiation (314) (315) (316) (317) (318). H2AX phosphorylation in response to ICL agents is considered to reflect the presence of ICL-associated DSBs.

However, it has been suggested that this may not be true for all ICL-inducing agents, as some γH2AX foci may form independently of readily detectable ICL-associated DSBs (319) (284) (320) (321). Nitrogen mustard has been shown to rapidly induce ICL-associated DNA DSBs in dividing human and Chinese hamster ovary (CHO) cells, but the same was not true after treatment with cisplatin (288) (322) (320) (323). Thus, suggesting that γH2AX may represent a DNA damage response to ICL-inducing agents rather than a prognostic biomarker.

### 1.7.4.2 RAD51

One the repair proteins recruited by γ-H2AX is RAD51. RAD51 is a key protein involved in HR-mediated repair of DSBs. DSBs are first processed by exonucleases to generate protruding ssDNA tails in a process called resection (324). A single-stranded DNA-binding heterotrimeric complex, known as replication protein A (RPA), then binds to the exposed ssDNA. The bound RPA serves to protect the DNA from degradation by nucleases and formation of secondary structures. RPA is then removed from DNA to allow binding of RAD51, forming a helical nucleoprotein filament (325) (326). The RAD51 filament carries out the search for homologous dsDNA in a process known as strand invasion and this promotes the exchange of genetic information (327) - the fundamental step of HR. Following strand invasion by RAD51, DSBs may be resolved via a number of HR sub-pathways, including break-induced repair, double Holliday Junction, synthesis-dependent strand annealing. These models of HR repair are beyond the scope of this Chapter and are described in detail in the following reviews by Li *et al.* (302) and Hinz *et al.* (296).

The presence of RAD51 in S-phase has been linked to repair of stalled or arrested replication forks (328). Indeed, the role of RAD51 has previously been observed in experiments investigating ICL repair in cross-linked plasmids (329) (330). Single-stranded DNA bound by RPA at stalled replication forks recruits ATR and other ATR signalling components to the sites of replication stress (331). Other factors recruited that are critical for RAD51 activity and DSB repair include BRCA1 and BRCA2 (307) (332). This accumulation of factors centred on RAD51 forms discrete nuclear foci (333) (334) and this formation is thought to be controlled by cyclin-

dependent kinases and checkpoint kinases (335) (332). RAD51 foci formation has been used as a functional assay to indicate HR repair or even it's deficiency (336) (337) (338).

## 1.8 Thesis Aims

The aim of this thesis was to explore a means to address the sub-optimal pharmacokinetics and pharmacodynamics of ADEPT.

For pharmacokinetics, it was hypothesised that mutation of *P pastoris*-produced MFECP could lead to non-mannosylated protein with potential for longer circulatory times. The aim was to test this hypothesis by systematic informatics-based mutation of potential glycosylation sites and testing of the newly generated MFECP variants *in vitro* and *in vivo*.

For pharmacodynamics, it was hypothesised that interfering with the DNA damage response would lead to impairment of drug resistance. The aim was to discover potential targets for intervention by study of the DNA repair response to ADEPT.

University College London

# CHAPTER 2

Pharmacokinetic and Pharmacodynamic Challenges of Antibody-Directed
Enzyme Prodrug Therapy (ADEPT)

Carima Andrady

# 2 Materials and Methods

## 2.1 Materials

All chemicals were purchased from Sigma (Poole, UK) unless otherwise stated.

### 2.1.1 Molecular Biology Reagents

#### 2.1.1.1 Primers and enzymes

Rationally designed oligonucleotide primers were ordered from Integrated DNA Technologies (Glasgow, Scotland). Each vial was reconstituted to a working dilution of 100 μM in double distilled water. The restriction enzymes, *EcoR*I, *Not*I, *Pme*I, *Pst*I, *Xba*I and *Xho*I were obtained from New England Biolabs (Hitchin, Hertfordshire, UK) with their respective buffers for optimal use (see Table 2.4). T4 DNA Ligase was also purchased from New England Biolabs (Hitchin, Hertfordshire, UK).

**Table 2.1 Primers**

| Primer | Sequence |
|---|---|
| AOX1 5' | 5' GACTGGTTCCAATTGACAAGC 3' |
| AOX1 3' | 5' GCAAATGGCATTCTGACATCC 3' |
| Rev_MFE_NOT | 5' AATATTTATAGCGGCCGCTTTCAGCTCCAGCTTGGTGC 3' |
| MFE_FW_seq1 | 5' GTACTACTTTGACTACTGG 3' |
| MFE_FW_seq2 | 5' GAATGGAGGCTGAAGATGCTGC 3' |
| MFE_FW_seq3 | 5' TCGCGGTCACGCGAAGCAAG 3' |
| CP_Rev_seq1 | 5' GTGTCCATGTGCGACATCAGC 3' |
| CPMOL_Rev1 | 5' TAATTATCTAGATTATTAGTGGTGGTGATGATGGTGCTTACCAGC 3' |
| CPMOL_FW1 | 5' ATTAATCTCGAGAAAAGAATGGCGGCCGCTGACAACGTTTTGTTCCAGGCTGC 3' |
| GAPDH 5' | 5' ACCACAGTCCATGCCATCAC 3' |
| GAPDH 3' | 5' TCCACCCTGTTGCTGTA 3' |

## *2.1.1.2   Plasmids*

All CPG2 and MFECP constructs generated in this thesis were cloned into the yeast expression vector, pPICZαB (Invitrogen, Paisley, UK) unless otherwise stated. Mutated CPG2 constructs were based on the CPG2-3Q or mCPG2_3Q sequences, as described in Table 2.2 CPG2 template sequencesThe *P. pastoris* CPG2_3Q sequence is shown in Figure 2.1. Bacterial CPG2, kindly provided by Mologic Ltd (Bedford, UK), was used as a non-glycosylated comparison for the mutated CPG2 constructs.

**Table 2.2 CPG2 template sequences**

| Construct name | Mutations in the CPG2 gene sequence | Cloning |
|---|---|---|
| CPG2_3Q | 3x Asn mutated to Gln | 3_Q mutations were previously constructed by site-directed mutagenesis by Dr Berend Tolner |
| mCPG2_3Q | 3x Asn mutated to Gln | codon-optimised CPG2 sequence ordered from GenScript with permission from Mologic Ltd |

```
                                                     ATGagattt......

                                                     M   R   F......

         .........agagaggctgaagctgccgctcagaagcgcgacaacgtgctgttccag
           .........R   E   A   E   A   A   A   Q   K   R   D   N   V   L   F   Q
         gcagctaccgacgagcagccggccgtgatcaagacggtggagaagctggtcaacatcgag
           A   A   T   D   E   Q   P   A   V   I   K   T   L   E   K   L   V   N   I   E
         accggcaccggtgacgccgagggcatcgccgctgcgggcaacttcctcgaggccgagctc
           T   G   T   G   D   A   E   G   I   A   A   A   G   N   F   L   E   A   E   L
         aagaacctcggcttcacggtcacgcgaagcaagtcggccggcctggtggtgggcgacaac
           K   N   L   G   F   T   V   T   R   S   K   S   A   G   L   V   V   G   D   N
         atcgtgggcaagatcaagggccgcggcggcaagaacctgctgctgatgtcgcacatggac
           I   V   G   K   I   K   G   R   G   G   K   N   L   L   L   M   S   H   M   D
         accgtctacctcaagggcattctcgcgaaggccccgttccgcgtcgaaggcgacaaggcc
           T   V   Y   L   K   G   I   L   A   K   A   P   F   R   V   E   G   D   K   A
         tacggcccgggcatcgccgacgacaagggcggcaacgcggtcatcctgcacacgctcaag
           Y   G   P   G   I   A   D   D   K   G   G   N   A   V   I   L   H   T   L   K
         ctgctgaaggaatacggcgtgcgcgactacggcaccatcaccgtgctgttcaacaccgac
           L   L   K   E   Y   G   V   R   D   Y   G   T   I   T   V   L   F   N   T   D
         gaggaaaagggttccttcggctcgcgcgacctgatccaggaagaagccaagctggccgac
           E   E   K   G   S   F   G   S   R   D   L   I   Q   E   E   A   K   L   A   D
         tacgtgctctccttcgagcccaccagcgcaggcgacgaaaaactctcgctgggcacctcg
           Y   V   L   S   F   E   P   T   S   A   G   D   E   K   L   S   L   G   T   S
         ggcatcgcctacgtgcaggtccaaatcaccggcaaggcctcgcatgccggcgccgcgccc
           G   I   A   Y   V   Q   V   Q   I   T   G   K   A   S   H   A   G   A   A   P
         gagctgggcgtgaacgcgctggtcgaggcttccgacctcgtgctgcgcacgatgaacatc
           E   L   G   V   N   A   L   V   E   A   S   D   L   V   L   R   T   M   N   I
         gacgacaaggcgaagaacctgcgcttccaatggaccatcgccaaggccggccaagtctcc
           D   D   K   A   K   N   L   R   F   Q   W   T   I   A   K   A   G   Q   V   S
         aacatcatccccgccagcgccacgctgaacgccgacgtgcgctacgcgcgcaacgaggac
           N   I   I   P   A   S   A   T   L   N   A   D   V   R   Y   A   R   N   E   D
         ttcgacgccgccatgaagacgctggaagagcgcgcgcagcagaagaagctgcccgaggcc
           F   D   A   A   M   K   T   L   E   E   R   A   Q   Q   K   K   L   P   E   A
         gacgtgaaggtgatcgtcacgcgcggtcgcccggccttcaatgccggcgaaggcggcaag
           D   V   K   V   I   V   T   R   G   R   P   A   F   N   A   G   E   G   G   K
         aagctggtcgacaaggcggtggcctactacaaggaagccggcggcacgctgggcgtggaa
           K   L   V   D   K   A   V   A   Y   Y   K   E   A   G   G   T   L   G   V   E
         gagcgcaccggcggcggcaccgacgcggcctacgccgcgctctcaggcaagccagtgatc
           E   R   T   G   G   G   T   D   A   A   Y   A   A   L   S   G   K   P   V   I
         gagagcctgggcctgccgggcttcggctaccacagcgacaaggccgagtacgtggacatc
           E   S   L   G   L   P   G   F   G   Y   H   S   D   K   A   E   Y   V   D   I
         agcgcgattccgcgccgcctgtacatggctgcgcgcctgatcatggatctgggcgccggc
           S   A   I   P   R   R   L   Y   M   A   A   R   L   I   M   D   L   G   A   G
         aagcatcaccatcatcaccattaataa
           K   H   H   H   H   H   H   -   -
                     His tag
```

**Figure 2.1 CPG2_3Q DNA and protein sequence**

The pPICzαB plasmid α-factor signal sequence is shown in part in bold, and is 225bp long. The mature CPG2 protein is represented after the dashed vertical line. The black arrow represents the Kex2 signal cleavage site; the blue arrows represent the Ste 13 signal cleavage sites. The internal Kex2 cleavage site is highlighted in green. Asn-to-Gln (x3) mutations are highlighted in blue. (The sequence originates from the CPG2 wild-type Genbank entry: AAA62842.1 - bacterial CPG2 *Variovorax paradoxus*).

Commercial kits were used to clean-up and purify genomic DNA. These are stated in Table 2.3.

**Table 2.3 Commercial kits for purifying genomic DNA**

| Name of Kit | Company |
|---|---|
| Wizard® Minipreps DNA purification system | Promega, Madison, WI, USA |
| Plasmid Midi Kit | Qiagen, Crawley, UK |
| Wizard® SV Gel and PCR Clean-Up system | Promega, Madison, WI, USA |

### 2.1.1.3 *Electrophoresis consumables*

For agarose gel electrophoresis, DNA Molecular Weight Markers II (*Hind* III-digested λ DNA) and IX (*Hae* III-digested φx174 DNA) were obtained from Roche Diagnostics Ltd (Burgess Hill, East Sussex, UK). A 1 kbp DNA from Promega (Madison, WI, USA) was also used in this thesis. The sizes of the standards for each ladder are shown in Figure 2.2.
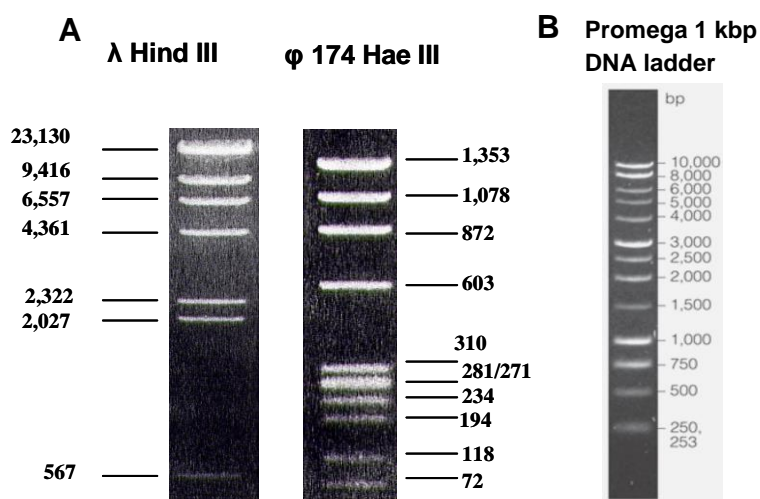


**Figure 2.2 DNA ladders used in agarose gel electrophoresis**

The separation and sizes of the DNA standards for *Hind* III and *Hae* III are shown on a 1% agarose gel (A); and the Promega ladder is shown on a 0.7 % gel (B). (Images take from catalogues Roche Diagnostics and Promega, respectively).

Pre-cast Tris-Glycine SDS-PAGE gels (10 or 17 well, 4-20% polyacrylamide, 1 mm thick) and protein molecular weight marker (See Blue Plus2) were obtained from Invitrogen Ltd (Paisley, UK). The Pro™Sieve™ QuadColor™ protein molecular weight marker from Lonza (Basel, Switzerland) is also mentioned in this thesis. Figure 2.3 shows the molecular weight markers. Polyvinylidene difluoride (PVDF) membrane and chromatography Whatman filter paper was purchased from BioRad (Herts., UK).
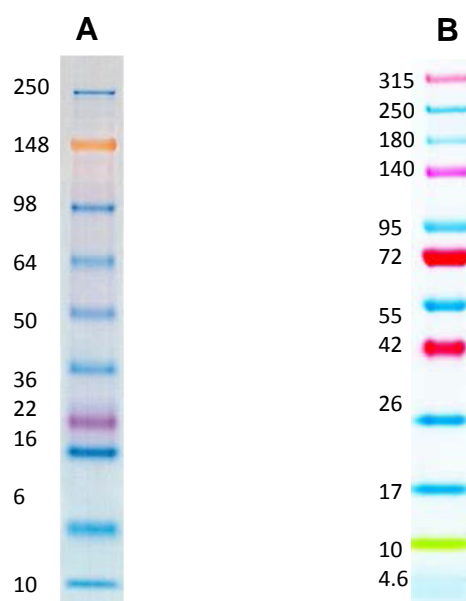


**Figure 2.3 Pre-stained protein molecular weight markers used with precast Tris-Gly gels for SDS-PAGE**

(A) SeeBlue Plus2 and (B) Pro™Sieve™ QuadColor™. (Taken from the Invitrogen and Lonza catalogues, respectively).

For determining the molecular weights of proteins run on the FPLC, molecular weight markers were run routinely on the Superdex 75 and 200 columns using the Gel Filtration Standard kit (Bio-Rad, UK). Figure 2.4 shows the molecular weight markers run on both columns.
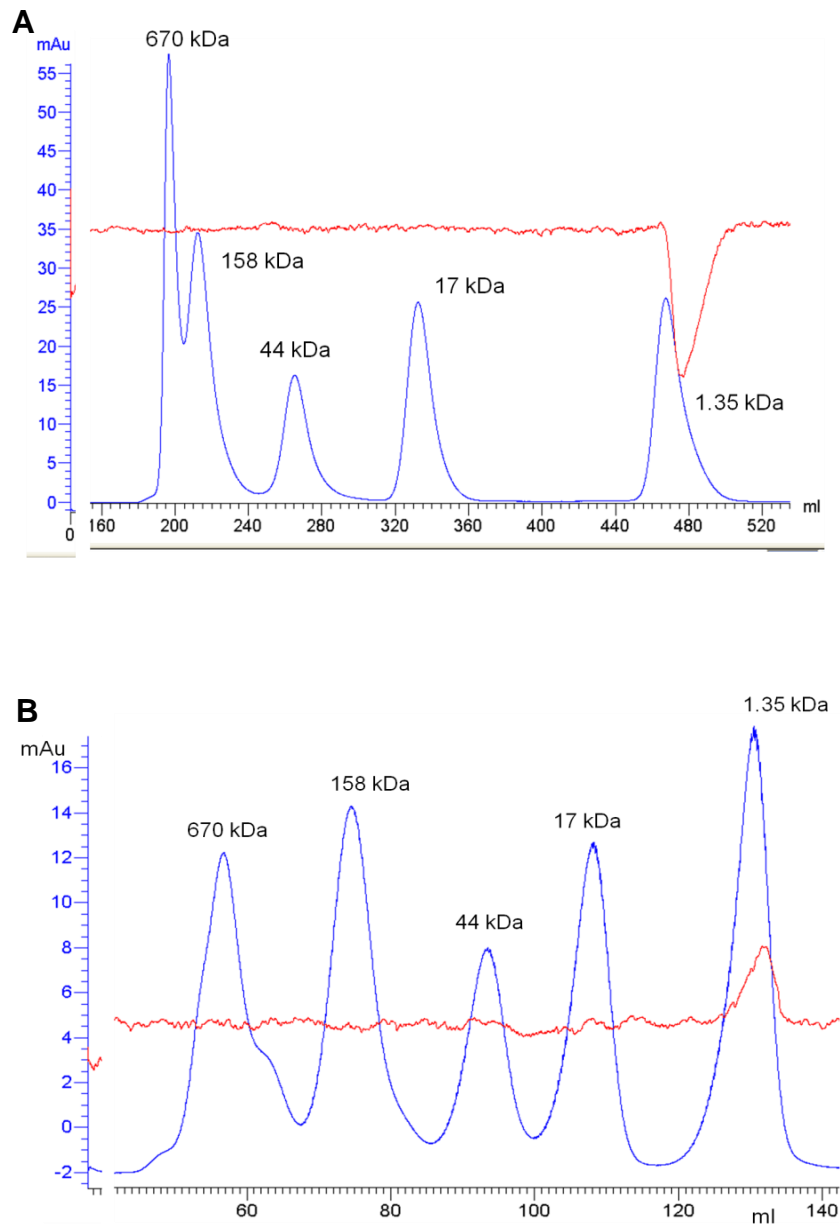
**Figure 2.4 Gel filtration molecular weight markers**

A) Superdex 75, 500 ml column. Flow rate 4 ml/min. B) Superdex 200, 125 ml column. Flow rate 1.5 ml/min.

**Table 2.4 Buffers for DNA manipulation**

| Buffer | Formula |
|---|---|
| Tris-borate (TBE) buffer stock (10X) | 100mM Tris, 10mM Boric acid, 1.25mM EDTA |
| Tris-acetate (TAE) buffer stock (50X) | 40mM Tris, 1mM EDTA, 20mM glacial acetic acid, pH 8.0 |
| Loading Dye blue/orange 6x (Promega, Madison, WI, USA) | 0.03% Bromophenol Blue, 0.03% Xylene Cyanol FF, 0.4% orange G, 15% Ficoll® 400, 10mM Tris-HCl (pH 7.5), 50mM EDTA (pH 8.00) |
| PCR 'master' mix (GeneAmp® PCR reagent kit, Applied Biosystems) | 1000µl 10 x PCR buffer, 250µl each 2.5mM dATP, dCTP, dGTP, dTTP, 6.5ml sterile $dH_2O$ |
| 1 x NEBuffer 1 (NEBiolabs Ltd, UK) | 10mM Bis Tris Propane-HCl, 10mM $MgCl_2$, 1mM dithiothreitol (pH 7.0 @ 25ºC) |
| 1 x NEBuffer 2(NEBiolabs Ltd, UK) | 10mM Tris-HCl, 10mM $MgCl_2$, 50mM NaCl, 1mM dithiothreitol (pH 7.9 @ 25ºC) |
| 1 x NEBuffer 3 (NEBiolabs Ltd, UK) | 50mM Tris-HCl, 10mM $MgCl_2$, 100mM NaCl, 1mM dithiothreitol (pH 7.9 @ 25ºC) |
| 1 x NEBuffer 4 (NEBiolabs Ltd, UK) | 20mM Tris-acetate, 10mM magnesium acetate, 50mM potassium acetate, 1mM dithiothreitol (pH 7.9 @ 25ºC) |
| 1 x T4 DNA Ligase buffer (NEBiolabs Ltd, UK) | 50mM Tris-HCl (pH 7.5), 10mM $MgCl_2$, 10mM dithiothreitol, 1mM ATP |

**Table 2.5 Buffers for protein manipulation**

| Buffer | Formula |
|---|---|
| 2 x Reducing SDS-PAGE loading buffer | 4% SDS, 10% β-mercaptoethanol, 20% glycerol, 0.02% bromophenol blue, 100mM Tris |
| 1 x SDS-PAGE running buffer | 25mM Tris base; 192mM glycine; 0.1%( w/v) SDS |
| 1 x Transfer buffer | 25mM Tris base; 192mM glycine; 20% (v/v) methanol |
| Coomassie gel stain | 0.1% (w/v) Coomassie Blue R-250; 45% (v/v) methanol; 10% (v/v) glacial acetic acid |
| Coomassie gel destain | 30% (v/v) methanol; 10% (v/v) glacial acetic acid |

## *2.1.1.4  Microbial strains*

Bacterial (*E.coli*) TOP10 and the wild-type yeast (*P. pastoris*) X-33 cells were obtained from Invitrogen (Paisley, UK). Genotypes are given in Table 2.6.

**Table 2.6 Microbial genotypes**

| Strain | Genotype | Transformation vector and use |
|---|---|---|
| TOP10F' | F' {*pro*AB, *lac*I$^q$, *lac*Z$\Delta$M15, Tn*10*, (Tet$^R$)} *mcr*A, $\Delta$(*mrr-hsd*RMS-*mcr*BC), $\Phi$80*lac*Z$\Delta$M15, $\Delta$*lac*X74, *deo*R, *rec*A1, $\lambda^-$ *ara*D139, $\Delta$(*ara-leu*)7697, *gal*U, *gal*K, *rps*L(Str$^R$), *end*A1, *nup*G | pPICZαB-based vectors used for DNA propagation |
| X-33 | Wild-type Mut$^+$ (phenotype) | pPICZαB-based vectors used for protein expression in *Pichia pastoris* |

**Table 2.7 Culture media for bacterial expression**

| Media | Formula |
|---|---|
| 2TY broth | 16g tryptone, 10g yeast extract, 5g NaCl. Complete to 1L with dH$_2$0. Autoclave. For 2 X TY Agar, add 15g/L agar prior to autoclaving. |
| Luria Bertani Broth (LB ) | 10g tryptone, 5g yeast extract, 10g NaCl. Complete to 1L with dH$_2$0. Autoclave. For LB Agar, add 15g/L agar prior to autoclaving. |
| Low salt LB | 10g tryptone, 5g yeast extract, 5g NaCl. Complete to 1L with dH$_2$0. Autoclave. For Low salt LB Agar, add 15g/L agar prior to autoclaving. |

**Table 2.8 Culture media and solutions for yeast expression**

| Media | Formula |
|---|---|
| Yeast Extract Peptone Dextrose Medium (YPD) (2% peptone; 1% yeast extract; 2% dextrose) | Dissolve 10g yeast extract and 20g peptone in 900ml $dH_2O$. Autoclave. When cool add 100ml 20% glucose solution. Store at 4°C. For YPD agar add 20g/L agar prior to autoclaving. |
| YPD with sorbitol (YPDS) (2 % peptone; 1% yeast extract; 2% dextrose; 1M sorbitol) | Dissolve 10g yeast extract, 20g peptone and 182.2g sorbitol in 900ml $dH_2O$. Autoclave. When cool add 100ml 20% glucose solution. Store at 4°C. For YPDS agar add 20g/L agar prior to autoclaving. |
| Buffered Glycerol-complex Medium (BMGY) (1% yeast extract; 2% peptone; 100mM potassium phosphate pH 6.0; 1.34% YNB; 4 x $10^{-5}$% biotin; 2% caseamino acids; 1% glycerol) | Dissolve 10g yeast extract and 20g peptone in 600ml $dH_2O$. Autoclave. When cool add 100ml 1M potassium phosphate buffer, pH 6.0, 100ml 13.4% YNB, 600µl 0.02% biotin, 100ml 20% caseamino acids, 100ml 10% glycerol. Store at 4°C. |
| Buffered Methanol-complex Medium (BMMY) (1% yeast extract; 2% peptone; 100mM potassium phosphate, pH 6.0; 1.34% YNB; 4 x $10^{-5}$% biotin; 2% caseamino acids;  0.5% methanol) | Dissolve 10g yeast extract and 20g peptone in 600ml $dH_2O$. Autoclave. When cool add 100ml 1M potassium phosphate buffer, pH 6.0, 100ml 13.4% YNB, 600µl 0.02% biotin, 100ml 20% caseamino acids, 100ml 5% methanol. Store at 4°C. |

Colonies containing gene of interest were selected against ampicillin (Roche Diagnostics, Burgess Hill, UK) or Zeocin™, both of which were purchased from Invitrogen (Paisley, UK).

### 2.1.1.5  RT-PCR

The following kits were employed for determining gene expression levels by RT-PCR using the $RT^2$ Profiler™ PCR array system (SABiosciences, West Sussex, UK), Table 2.9. The DNA Damage Signalling Pathway PCR array plate was also purchased from SABiosciences (PAHS-029A, human-specific). The 96-well plate contained primers for 84 pre-selected DNA damage signalling genes and the remainder were for regulatory control genes. A list of the genes can be found in the Appendix 1.

**Table 2.9 Commercial kits used for RT-PCR prep**

| Name of Kit | Use |
|---|---|
| RNeasy mini kit (Qiagen, Crawley, UK) | Purification of total RNA from mammalian cells |
| First strand cDNA synthesis kit (SABiosciences, West Sussex, UK) | Synthesis of cDNA using reverse transcriptase |
| RT$^2$ qPCR master mix (SABiosciences, West Sussex, UK) | Initiating PCR reaction |

## 2.1.2   Detection of proteins

The following details a list of antibodies and various buffers for detecting proteins using various methods.

### *2.1.2.1   Antibodies*

Antibodies used for Western blotting and immunofluorescence, are provided in Table 2.10.

**Table 2.10  Antibodies for protein detection**

(HRP, Hydrogen peroxidase)

| Antibody | Manufacturer | Clone | Working dilution |
|---|---|---|---|
| Mouse anti-tetra His | Qiagen, Crawley, UK | Monoclonal | 1:1000 |
| Rabbit anti-MFE-23 (serum) | In-house | Polyclonal | 1:1000 |
| Rabbit anti-CPG2 (serum) | In-house (183) | SB43gal, monoclonal | 1:1000 |
| Mouse anti-CPG2 (serum) | Mologic Ltd, Bedfordshire, UK | Polyclonal | 1:1000 |
| Biotinylated mouse anti-γ-H2AX (Ser 139) | Millipore, Watford, UK | JBW301, Monoclonal | 1:1000 |
| Mouse anti-γ-H2AX (Ser 139) | Millipore, Watford, UK | JBW301, Monoclonal | 1:1000 |
| Rabbit anti-RAD51 | Santa Cruz Biotech, Texas, USA | H-92, Polyclonal | 1:100 |
| Mouse anti-PCNA | Dako, Glostrup, Denmark | PC10, Monoclonal | 1:1500 |
| Mouse anti-NBS1 | BD, NJ, USA | 34/NBS1, Monoclonal | 1:1000 |
| Rabbit anti-phospho-CHK1 (Ser296) | Cell Signalling Tech, Danvers, MA, USA | Polyclonal | 1:1000 |
| Rabbit anti-phospho-CHK2 (Thr68) | Cell Signalling Tech, Danvers, MA, USA | Polyclonal | 1:1000 |
| Mouse anti-α-tubulin | Sigma | Monoclonal | 1:5000 |
| Goat anti-actin | Santa Cruz Biotech, Texas, USA | I-19, Polyclonal | 1:1000 |
| Sheep anti-mouse-HRP | GE Healthcare, Buckinghamshire, UK | | 1:1000 |
| Goat anti-rabbit-Alexa Fluor® 488 | Invitrogen, Paisley, UK | | 1:1000 |
| Rabbit anti-goat-HRP | Sigma | | 1:6000 |
| Goat anti-mouse- Alexa Fluor® 488 | Invitrogen, Paisley, UK | | 1:2000 |
| Goat anti-rabbit-HRP | Sigma | | 1:3000 |

Non-antibody detecting agents included: biotinylated Con A (1mg/ml), streptavidin-HRP (Invitrogen) (1/1000 dilution) and streptavidin-Alexa Fluor® 488 (Invitrogen) (1 in 1000 dilution).

## *2.1.2.2 Buffers*

Table 2.11 details a list of the buffers used with antibodies for protein detection.

**Table 2.11 Buffers for protein detection using antibodies**

(Marvel skimmed milk powder; 10x TBS: 0.15 M Tris-HCl, 1.37 M NaCl, pH 7.6).

| Buffer | Formula |
|---|---|
| **Western blot** | |
| Wash | PBS |
| Blocking | 5% Marvel/PBS |
| **Western blot, detection of phosphorylated proteins** | |
| Wash | 1x TBS/0.1% Tween-20 (TBST) |
| Blocking | 5% BSA/TBST |
| **Immunofluorescence** | |
| Permeabilisation | 0.5% Triton-X-100/PBS |
| Blocking | 0.2% Marvel/0.1% Triton-X-100/PBS |
| Wash buffer | 0.1% Triton-X-100/PBS |

For reblotting PVDF membranes, primary and secondary antibodies were removed using a stripping buffer containing the following: 10% SDS, 0.5M Tris HCl pH 6.8 and 0.8% β-mercaptoethanol.

## 2.1.3   Protein deglycosylation

## *2.1.3.1 Deglycosylating enzymes*

The enzymes used for removing the N-glycosylations on proteins included: endoglycosidase Hf (EndoH, EC 3.2.1.96) (100 U/ml or $1 \times 10^6$ NEB U/ml) or peptide-N-glycosidase F (PNGase F, EC 3.5.1.52) (7.7 U/ml or $5 \times 10^5$ NEB U/ml). Enzymes purchased from New England Biolabs Ltd (Hitchin, Hertfordshire, UK) were each stored in enzyme buffer (20 mM Tris/HCl, 50 mM NaCl, 5 mM EDTA, pH 7.5).

## 2.1.3.2 *Chromatography buffers*

The glycosylation status of proteins were analysed by affinity chromatography using the HiTrap Con A 4B 1 ml column (GE Healthcare, Amersham, UK) and the buffers were made up accordingly, as listed in Table 2.12.

**Table 2.12 HiTrap Con A 4B column buffers**

| Buffer | Formula |
|---|---|
| Binding Buffer | 20mM Tris-HCl, 0.5M NaCl, 1mM MnCl$_2$, 1mM CaCl$_2$, pH7.4 |
| Elution Buffer | 0.25M methyl-α-D-mannopyranoside, 20mM Tris-HCl, 0.5M NaCl, pH7.4 |
| Equilibration Buffer | 20mM Tris-HCl, 0.5M NaCl, pH 8.5 |

## 2.1.4 **Modified single-cell gel electrophoresis (comet) assay**

The comet assay buffers are listed in Table 2.13. All buffers were kept at 4ºC prior to usage.

**Table 2.13 Comet assay buffers**

| Buffer | Formula |
|---|---|
| Lysis buffer | 100mM disodium EDTA , 2.5M NaCl, 10mM, Tris-HCl, 1% Triton-X-100, pH 10.5 |
| Alkali buffer | 50mM NaOH, 1mM Disodium EDTA, pH 12.5 |
| Neutralisation buffer | 0.5M Tris-HCl, pH 7.5 |

## 2.1.5 **Cell culture**

The human colorectal carcinoma SW1222 CEA$^{+ve}$ cell line was obtained from within the Department and A375M CEA$^{-ve}$ amelanotic human melanoma cell line was obtained from ATCC. Both cell types are adherent. Cell lines were passaged under sterile conditions in microbiological Class II safety cabinets and cultured into vented flasks in medium containing the necessary nutrients for optimal growth (see Table

2.14). Cells were incubated at 37ºC humidified with 5% $CO_2$. Cells were grown in the exponential phase prior to conducting *in vitro* assays. All cells were tested for mycoplasma on a regular basis. For long term storage, aliquots of cells (1 x$10^6$cells/ml) were stored in freezing medium (see Table 2.14) in liquid nitrogen.

**Table 2.14  Tissue culture and freezing media**

Cell culture media was purchased from PAA (PAA, Pasching, Austria), unless otherwise stated.

| Media | Formula |
|---|---|
| Dulbecco'S Modified Eagle Medium (DMEM) culture medium for SW1222 and A375M cell lines | DMEM containing  10% foetal calf serum (Bio Sera Ltd, East Sussex, UK), 2mM L-glutamine, 1% Non-essential amino acids, 100U/ml penicillin and 100µg/ml streptomycin |
| Freezing medium | 90% foetal calf serum, 10% dimethyl sulphoxide (DMSO) |

### 2.1.5.1  ADEPT reagents

MFECP was supplied as a clinical grade sample (MFECP1, Batch B0131, 0.63 mg/ml in PBS, 78.1 U/ml) previously produced and purified for the Phase I clinical trial (139) (198) (197). This particular batch was used consistently for all *in vitro* and *in vivo* experiments, unless otherwise stated.

The bis-iodophenol prodrug (ZD27267P) was generously supplied by AstraZeneca (UK), supplied as a salt to be dissolved in DMSO. Stock concentration was 100 mM. A detailed account of its synthesis was published by Springer *et al.* (176).

### 2.1.5.2  Cell cycle inhibitors

Checkpoint kinase 1 (Chk1) inhibitors were purchased from Sigma: UCN-01 (2 mM stock) and PF477736 (2.38 mM stock) were stored as aliquots at -80°C.

### 2.1.6  *In vivo* studies

Therapy studies were conducted in nude mice bearing SW1222 human colorectal carcinoma xenografts. SW1222 cells were cultured *in vitro* and implanted (5 x10$^6$ cells per 100 µl serum-free media) subcutaneously into the flanks of 2-3 month old female nude mice, each weighing 20-25 g. Treatment occurred when the tumours had grown to ~ 2.5-3.5 mm in diameter. Clearance studies were conducted in 2-3 month old female, balb/c hairy mice, each weighing 20-25 g.

All animal handling was undertaken by Mr Matthew Robson (Dept. of Oncology, UCL Cancer Institute, London) under the project licence held by Professor Barbara Pedley (Dept. of Oncology, UCL Cancer Institute, London). All animal experiments complied with the UK Coordinating Committee on Cancer Research Guidelines for the Welfare of Animals in Experimental Neoplasia, UK Home Office and UCL regulations.

## 2.2  Methods

### 2.2.1  Cloning and propagation of DNA

#### 2.2.1.1  *Plasmids*

The DNA sequences for the CPG2 mutated constructs, CPG2_3Q_12A (1236bp) and mCPG2_3Q (1224bp), were ordered from GenScript Corporation (New Jersey, USA) in a bacterial pUC57 plasmid. These sequences were modelled on the CPG2_3Q sequence previously mutated within the Department. The CPG2_3Q_12A sequence was flanked by the restriction enzyme sites EcoRI and Xba I for genetic manipulation into the yeast pPICzαB plasmid (Invitrogen, Paisley, UK). The mCPG2-3Q sequence was flanked by XhoI and XbaI for cloning and genetic insertion into pPICzαB. Oligonucleotides (145bp each) for cloning into mCPG2_3Q were also ordered from GenScript Corporation cloned into a pUC57 plasmid, and each gene sequence was flanked by restriction sites XhoI and PstI.

Bacterial puc57 plasmid DNA was propagated into bacterial TOP10 cells (see Sections 2.2.1.4-2.2.1.6 for more details) prior to being cloned into the pPICZαB vector for further genetic manipulation and protein expression.

## 2.2.1.2  Plasmid digestion

Vector (pPICZαB) and inserts were cut with respective restriction enzymes (as mentioned above) using the correct buffers specific for the enzymes for 2hrs at 37°C followed by heat inactivation at 65ºC for 10 minutes. Restriction digest mix included approximately (vector:insert) 10:5 μg, 5 μl each of restriction enzymes (New England Biolabs), 10 μl 10X NEBuffer (New England Biolabs), 10 μl BSA (10X BSA; final concentration 100 μg/ml), and made up to a final volume of 100 μl with sterile $dH_2O$.

To check the vectors and inserts were cut and digested and to the correct size, the samples were run on an agarose gel. 2% (inserts) and 0.8-1% (vectors) agarose gels containing 5 μl (10 mg/ml) ethidium bromide were made in TBE buffer and run in a Hi-Set mini horizontal electrophoresis unit (Anachem, UK) at 50-60V for 30 minutes. Samples were mixed with 20% loading dye and molecular weight markers (Figure 2.2) were used to determine size. Gels were visualised using a G:BOX Gel Doc transilluminator (Syngene, Cambridge, UK). A sample of the uncut vector or insert was run alongside the cut samples to distinguish differences in size, confirming that the restriction enzymes had cut.

Provided the digested DNA was the correct size, the bands were cut from the gel under UV light and put into an Eppendorf tube. The isolated fragments of DNA were cleaned using the Wizard® Gel and PCR Clean-Up System (Promega, Madison, WI, USA) kit according to manufacturer's instructions. DNA fragments were purified to a final volume of 50 μl in nuclease-free $dH_2O$. DNA was measured in ng/μl at 260nm on the Nanodrop® ND-1000 UV-VIS spectrophotometer.

## 2.2.1.3   Ligation and clean-up

Ligation reactions were carried out using different molar ratios of vector: insert (1:1, 3:1 or 1:3). Reactions were carried out at 16ºC overnight using 2 µl T4 DNA Ligase (NEBiolabs), 5 µl T4 Ligase buffer (NEBiolabs) and proportionally enough vector and insert. A reaction without the insert was also prepared as a control. Distilled water was added to give a final volume of 50 µl.

Ligated DNA was extracted from the mix using phenol/chloroform extraction and the DNA precipitated. Samples were made up to 100 µl with $dH_2O$ and an equal amount of phenol was added, samples shaken vigorously and centrifuged for 10 min (14, 000 x g) at room temperature. The aqueous phase was then carefully transferred to a clean tube and an equal volume of phenol:chloroform:isoamyl alcohol (25:24:1 v/v/v) (saturated with 10 mM Tris, pH 8.0, 1mM EDTA) was added, shaken vigorously and centrifuged for 10 min (14, 000 x g) at room temperature. The aqueous phase was then carefully transferred to a clean tube and to this 1/10 volume of 3 M sodium acetate (pH 6.0), 2.5x volumes of 100% ethanol and 1 µl glycogen were added. The reaction mixture was incubated at -80°C for 1hr or -20°C overnight. Precipitated DNA was recovered by centrifugation (14, 000 x g) for 10 min at room temperature. The pellet was then washed with 70% (v/v) ethanol by centrifugation (14, 000 x g) for 10 min and resuspended in 10 µl of dH20.

## 2.2.1.4   Transformation into competent bacterial cells

Electro-competent TOP10 *E.coli* cells were thawed on ice. To a 50 µl aliquot of cells, 2 µl of the pPICZαB ligation or puc57 plasmid was added and mixed by gentle pipetting. (Control samples included vector DNA/cells mixture and cells only). The mixture of cells and DNA was transferred to an ice-cold, sterile 0.2 cm disposable cuvette (BioRad Laboratories, Hertfordshire, UK) and pulsed once for 4-5 ms in the electroporator (BioRad MicroPulser™, Bio-Rad Laboratories Ltd., Hemel Hampstead, U.K.). The apparatus was set to 2.5kV, 25µFD, and 200Ω (Ec2 programme). One millilitre of LB (puc57) or low salt LB (pPICZαB) (see Table 2.7) was immediately added to the pulsed cells and the culture was incubated for 1hr at 37°C. 50, 100 and 200 µl of culture was spread onto LB agar plates containing 100

µg/ml ampicillin or low-salt LB agar plates containing 100 µg/ml Zeocin™ and incubated at 37°C overnight.

### 2.2.1.5  *Checking for positive clones*

The polymerase chain reaction (PCR) was performed to determine whether the correct size insert was expressed in bacterial cells. Single colonies were picked with an inoculating loop and mixed into 20 µl sterile $H_2O$ and labelled for reference. All reagents were mixed on ice in the following PCR reaction mixture: 104 µl PCR 'mix' (Applied Biosystems, Life technologies, UK), 16 µl forward primer (AOX1 5' for pPICZαB) and 16 µl reverse primer (AOX1 3' for pPICZαB), 3.2µl Taq polymerase (Applied Biosystems, Life technologies, UK) and 12.8 µl d$H_2O$. 20 µl aliquots were added to 0.5 ml Eppendorf tubes and 1 µl of single colonies from the reference tubes were mixed well to each of the tubes. PCR was carried out using a Biometra Personal Cycler programmed as follows (1 kb per 90 sec): one cycle of 95°C for 3 min to detach the DNA from the template; 30 cycles of 95ºC for 60 sec, 60ºC for 60 sec (annealing), 72ºC for 90 sec (elongation); one cycle of 72ºC for 600 sec and cooled at 4ºC until the samples were required. PCR products were run on agarose gel electrophoresis, as described above.

### 2.2.1.6  *Isolation of plasmid DNA*

Plasmids were isolated using two systems depending on the amount of DNA required. For small-scale DNA purification (10-20 µg) the Wizard Plus SV DNA Miniprep Kit (Promega, Southampton, UK) was used, and for larger-scale purification the Qiagen Midi Kit (up to 100 µg) was used. For mini-prep cultures, a single bacterial colony transformed with plasmid DNA (plate or reference tubes, as described above) was used to inoculate 5 ml of the appropriate medium (LB with 100 µg/ml ampicillin for bacterial vectors, low salt LB with 25 µg/ml Zeocin™ for yeast vectors) in a sterile, 20 ml polypropylene tube. The culture was grown overnight at 37°C in an orbital shaker (Innova 4000 incubator shaker, New Brunswick Scientific) at 250 rpm. For midi-prep cultures, 25 ml of fresh medium plus antibiotic was inoculated in a sterile, 250 ml conical flask and grown overnight shaking at 37°C.

100 ng/µl of purified plasmid was sent for sequencing (UCL Cancer Institute Support Services, London, UK) together with 2-5 pmoles/µl of suitable primers, listed in Table 2.1.

### 2.2.2    Expression and purification of proteins from *P. pastoris*

#### 2.2.2.1    *Linearisation of plasmid DNA*

pPICZαB plasmids containing DNA insert were linearised for transformation into the X-33 yeast genome. 10 µg of plasmid DNA was digested with 2.5 µl Pme I (New England Biolabs) for 2 hr at 37°C in the presence of 5 µl 10X NEB buffer 4 (New England Biolabs), 5 µl BSA (10X BSA; final concentration 100 µg/ml), and made up to 50 µl with sterile $dH_2O$. Reactions were stopped by heat inactivation at 65°C for 20 min. Digested DNA was purified by phenol:chloroform extraction and precipitated, as described in Section 2.2.1.3.

#### 2.2.2.2    *Preparation of electro-competent X-33 cells*

Yeast wild-type X-33 cells were prepared for electroporation following protocols by Invitrogen. Five millilitres of YPD media (see Table 2.8) was inoculated with X-33 cells. The inoculated culture was grown overnight at 30°C, 250 rpm in an orbital shaker. The next day, 500 ml YPD media was inoculated with 0.5 ml of the overnight culture and grown at 30°C, 250 rpm until an OD600 of 1.3 was reached.

Cultures were centrifuged at 1,500 x g for 5 min at 4°C and pellets resuspended in 500 ml ice cold sterile $dH_2O$. Cells were centrifuged as before, and pellets resuspended in 250 ml ice cold sterile $dH_2O$. Cells were again centrifuged and the pellet resuspended in 20 ml ice cold sterile 1 M sorbitol. The process was repeated once more and the cells were resuspended in 1 ml ice cold sterile 1 M sorbitol. Cell were stored on ice and used the same day.

### *2.2.2.3   Electroporation of electro-competent yeast cells*

80µl of freshly prepared X33 electro-competent cells were added to 10 µl of linearised plasmid DNA and incubated on ice for 1 min. Cells were transferred to a pre-chilled 0.2 µm cuvette (Biorad) and pulsed once using a BioRad MicroPulser™ set at 2.0kV, 5ms (Pic programme). One millilitre of ice-cold, sterile 1 M sorbitol was added to the cuvette immediately after pulsing and cells were incubated at 30°C for 2 hr with no shaking. 10, 50, 100 and 200 µl of transformed cells were spread onto YPDS/Zeocin™ (100 µg/ml) plates and incubated at 30°C for 3-5 days until colonies formed.

### *2.2.2.4   Protein expression in yeast*

With an inoculating loop, individual colonies (4 colonies per construct) were picked and dabbed on to separate YPDS plates for glycerol stocks and the same loop was used to inoculate 5 ml BMGY medium (containing 100 µg/ml Zeocin™) (see Table 2.8) and grown (overnight) at 30°C, 250 rpm until an OD600 of 2-5 was reached. Cultures were centrifuged at 3,000 x g for 5 min and pellets were resuspended in 50 ml BMMY (containing 100 µg/ml Zeocin™) (see Table 2.8) to a final OD600 = 1. The cultures were transferred to sterile 250 ml conical flasks and protein of interest was expressed at 30°C, 250 rpm with the addition of 100% methanol for a final concentration of 0.5% (v/v) every 24 hr for 72 hrs. Supernatant was extracted every 24 hr and visualised by Western blot. At the final time point cultures were centrifuged for 30 min at 3,000 x g and supernatants were filtered through 0.2 um Nalgene filters and stored at 4°C for enzyme activity testing and at -80°C for long-term storage.

### *2.2.2.5   Preparation of glycerol stocks*

Seed lots of the clones that expressed protein were prepared and taken forward for scaled-up fermentation and purification. Preparations took place in a sterile microbiological Class II safety cabinets with UV lamp turned on. Using a sterile inoculating loop, a single yeast colony was transferred into 50ml YPD (containing 100 µg/ml Zeocin™) in a 250 ml conical flask and grown overnight at 30ºC, 250 rpm

until an OD600nm of 15-20 was reached (doubling time ~ 2-3 hr). Cultures were transferred to 50 ml falcon tube and centrifuged at 3000 rpm for 5 min, 4ºC. Supernatant was discarded and pellet resuspended in YPD and 15% (final concentration) glycerol. For example, if OD600nm is 15, then 10 ml YPD was added with 5 ml 60% glycerol. 1 ml aliquots were dispensed into cryovials (Nunc International, Hereford, UK) and stored at -80°C.

### 2.2.2.6   Fermentation and purification of proteins

Large-scale protein production was carried out in a 10 litre Bioflo 3000 Batch/Continuous Bioreactor (New Brunswick Scientific, Edison, NJ, USA) by Dr Berend Tolner and Mr Gaurav Bhavsar, according to Good Manufacturing Practice (GMP) guidelines (198) (197). The protein was purified by radial bed IMAC and concentrated on a lab-scale Tangential Flow Filtration (TFF) system (Millipore, UK). Final purification was performed by gel filtration chromatography using an ÄKTA *FPLC*™ system (GE Healthcare, Little Chalfont, UK). A HiLoad™ Superdex 200 column (16/60, 150 ml or 200 ml; GE Healthcare, UK) was used to separate proteins larger than 100 kDa and a HiLoad™ Superdex 75 column (16/60, 120 ml or 200 ml; GE Healthcare, UK) was used for proteins less than 75 kDa. Proteins were filter sterilised (0.2 μm; Acrodisc, UK) and injected onto the column at a constant flow rate of 1.5 ml/min PBS. Fractions (1.5 ml) were collected immediately after the void volume (40 ml for S200 and 34 ml for S75 column) for a total of 120 ml. Peak fractions were pooled and stored at -80°C.

### 2.2.2.7   Determination of protein concentration

Protein samples were measured at 280nm using a spectrophotometer (Cecil, CE2041, Cecil Instruments Ltd, Cambridge, UK). The protein concentration was determined using the Beer-Lambert's law:

$$OD_{280} = \varepsilon 280 \times c \times l$$

$OD_{280}$ is the absorbance of the protein sample at 280 nm, $\varepsilon 280$ is the extinction coefficient of the protein at 280nm (0.1%, 280 nm, 1 cm path length) (mg/ml$^{-1}$ cm$^{-1}$), $c$ is the concentration of protein (mg/ml), $l$ is the path length of the cuvette (cm).

ε280 was calculated from the primary amino acid sequence of each protein using the EXPASY Protparam web tool (http://www.expasy.ch/tools/protparam.html).

For protein from cell lysates, protein concentration was determined using the Bradford Assay (Bio-Rad Protein Assay kit, California, USA).

### 2.2.3 Characterisation of proteins

#### 2.2.3.1 *Sodium Dodecyl Sulphate Polyacrylamide Gel Electrophoresis (SDS-PAGE)*

Proteins were characterised by SDS-PAGE and Coomassie staining. The samples were diluted in 2x reducing buffer loading and boiled for 5 minutes prior to loading on a pre-cast 4-20% Tris-glycine gel (Novex, San Diego, CA). A protein ladder of known molecular weights was also loaded in order to determine size and presence of the protein of interest (Figure 2.3). Proteins were subject to electrophoresis at 125V 35mA for 90 min. Once the gel had run it was removed from its casing and incubated overnight in Coomassie dye. Destaining eliminated the dye from the gel leaving only the protein bands stained. This is carried out with several washes of destain buffer over a period of 3-4 hours. The gel was dried using the DryEase kit (Invitrogen, Paisley, UK).

#### 2.2.3.2 *Western Blotting*

Western blotting was performed following SDS-PAGE to determine the true presence of a protein of interest. After electrophoresis the gel was removed from the casing and proteins transferred onto polyvinyl difluoride (PVDF) membrane (BioRad) by electro-blotting at 25V 125mA for 90 mins. The membrane was then blocked with 5% Marvel/PBS overnight to remove any non-specific binding. The membrane was then washed three times with PBS and the primary antibody (diluted in 1% blocking buffer) was added for 1 hr with gentle agitation. The membrane was washed five times with PBS. The secondary antibody conjugated to horse radish peroxidase (HRP) (diluted in 1% blocking buffer) was added for 1 hr and then washed as before. The antibodies were stained using 10 mg 3,3'-diamino-benzidine

(DAB) in 40 ml water in the presence of 20 µl hydrogen peroxide. The reaction was stopped with tap water and the membrane was left to air dry. The Amersham ECL™ Western Blotting System (GE Healthcare, Buckinghamshire, UK) was also used in some cases for a more sensitive mode of detection. The chemiluminescent signal was captured on photographic film.

### 2.2.3.3 Glycosylation analysis of proteins

Proteins were checked for glycosylation by affinity chromatography using the HiTrap™ Con A 4B 1 ml column (GE Healthcare, Amersham, UK). The column is pre-packed with concanavalin A Sepharose™, a medium used for the separation and purification of glycoproteins, polysaccharides and glycolipids. Con A is a tetrameric metalloprotein (lectin) that binds molecules containing α-mannopyranosyl, α-D-glucopyranosyl and sterically related residues (339).

The protocol provided by GE Healthcare was followed using a peristaltic pump (Pharmacia LKB-Pump P-1) or the chromatographic ÄKTA *FPLC*™ system. The column was primed with 10 ml of Con A binding buffer (Table 2.12 HiTrap Con A 4B column buffers). Up to 500 µg protein was diluted in binding buffer and applied to the column. The column was washed with binding buffer and unbound material (flow through) fractions were collected in 500 µl aliquots. Bound protein was recovered with 5 ml of Con A elution buffer (Table 2.12 HiTrap Con A 4B column buffers). Fractions were analysed by SDS-PAGE and Western blotting.

Protein samples were also sent to Dr. Daniel Spencer (Ludger, Oxford) for expert analysis of the glycosylation patterns by mass spectrometry.

### 2.2.3.4 Enzymatic deglycosylation

MFECP was incubated with deglycosylating enzymes, EndoHf or PNGaseF, for 24 hr at 37°C under non-denaturing conditions. Deglycosylation was assessed by Con A column chromatography, followed by SDS-PAGE and Western blotting.

## 2.2.3.5 *Enzyme kinetics*

The enzyme activity (U/ml) of MFECP and CPG2 protein variants was measured using a dual beam spectrophotometer fitted with a cell temperature controller (U-2001, Hitachi Instruments Inc., Japan). As described previously (137), protein was diluted 100x and added to 1 ml assay buffer (5x PBS tablets and 0.2 mM $ZnCl_2$) containing methotrexate (MTX) (60 mM) at 37°C and the rate of change of absorbance at 320nm was measured. Activity was calculated from standard regression analysis using the UV solutions software, version 1.2 (where 1 U/ml of enzyme activity is defined as the amount of enzyme catalysing the hydrolysis of 1 µM of MTX per min per ml at 37°C).

## 2.2.4 *In vitro* assays

### 2.2.4.1 *Drug treatment*

Cells were incubated with 0.1 U/ml MFECP for 1 hr at 37°C and this was followed by incubation with the 0.25 µM or 50 nM prodrug (unless stated otherwise) for 1 hr. For tumour response measured over time, cells were incubated in drug-free medium before harvesting at different time points. For Chk1 inhibitor combination experiments, cells were exposed to 25 nM UCN-01 or 0.1 µM PF-477736 during and after ADEPT treatment.

### 2.2.4.2 *Growth inhibition assay*

Sulphorhodamine B (SRB) assay was used to determine the cellular growth inhibition of ADEPT-treated cells, which was conducted in accordance with the first published protocol (340). Preliminary experiments using different cell-seeding densities (non-drug-treated) were conducted in order to determine the optimal cell seeding densities per well for each cell line.

Cells were seeded in a 96-well plate and left to adhere overnight prior to drug exposure. SW1222 cells were seeded at a density of 5 $\times 10^4$ cells/well and A375M cells were seeded at 2.5 $\times 10^4$ cells/well. Cells were treated with ADEPT (as

described in Section 2.2.4.1) using various concentrations of prodrug. Alternatively, cells were treated with the fusion protein and washed with PBS prior to addition of the prodrug; or treated with the fusion protein or prodrug, alone. Supernatant was aspirated, cells washed with PBS and drug-free medium replaced. Cells were incubated at 37°C for 96 hr or 120 hr for SW1222 cells or A375M cells, respectively.

Cells were fixed with 100 μl 10% trichloroacetic acid (TCA) for 20 min at 4°C. Wells were washed four times with water and tapped on paper towels to remove excess water. 100 μl of 0.4% SRB (in 1% acetic acid) was next added to stain the cells for 20 min at room temperature. Wells were washed with 1% acetic acid and tapped to remove excess. The SRB-stained cells were left to air-dry overnight before solubilising in 100 μl of 10 mM Tris base. OD540nm was measured using the plate reader (Varioskan Flash Multimode Reader, Thermoscientific, Philadelphia, US).

### 2.2.4.3 *Modified single-cell gel electrophoresis (comet) assay*

For drug treatment, 10 x$10^4$ cells/well SW1222 cells were seeded in a 6-well plate and allowed to adhere overnight. Next day, cells were treated with ADEPT, as described in Section 2.2.4.1 - using various concentrations of prodrug for determining ICL damage, and 0.25 μM prodrug for ICL repair. Drug-containing medium was then removed and cells incubated at 37°C in drug-free medium for up to 48 hr. Control experiments included cells incubated with fusion protein only, prodrug only, and no treatment.

Following drug-treatment, media was aspirated and the cells were washed with PBS followed by Trypsin/EDTA 1x (PAA, Pasching, Austria) to detach the cells. The trypsin was neutralised with fresh medium and the suspension of cells were centrifuged at 1200 rpm for 4 min. The cell pellet resuspended in freezing mix (Table 2.14) and stored in cryovials at -80°C until required for the comet assay.

All procedures were carried out on ice and in subdued lighting. Cells were thawed and diluted to give a final concentration of 2.5 x$10^4$ cells/ml and irradiated with 17.5 Gy in a X-ray irradiator to deliver a fixed number of random DNA strand breaks. After embedding cells in 1% low gelling temperature agarose on pre-coated

microscope slides, the cells were lysed in lysis buffer (Table 2.13) for 1 hr, and then washed every 15 min with distilled water for 1 hr. Slides were then incubated in alkali buffer (Table 2.13) for 45 min followed by electrophoresis in the same buffer for 25 min at 18 V (0.6 V/cm), 250 mA. The slides were finally rinsed in neutralising buffer (Table 2.13) followed by PBS.

After drying, the slides were stained with propidium iodide (2.5 µg/ml) for 20 min and then rinsed in distilled water for 30 min. Comet images were visualised using an inverted fluorescent microscope (Nikon, UK) with a high-pressure mercury lamp (Nikon, UK) at 20x magnification. Images were captured using a digital camera and analysed using the Komet Analysis software Version 6 (Andor Technology, Kinetic Imaging, UK) (Figure 2.5). For each duplicate slide, 25 cells were analysed. The tail moment (Tm) was calculated as the product of the percentage DNA in the comet tail and the distance between the means of the head and tail distributions, based on the definition by Olive *et al.* (341). DNA interstrand cross-linking was expressed as the percentage decrease in tail moment compared to the irradiated non-treated samples, as calculated in Equation 2.1. Percentage repair was calculated at 48 hr following the peak of DNA interstrand cross-linking.

$$\% \text{ decrease in tail moment} = \left[1 - \left(\frac{(TMdi - TMcu)}{(TMci - TMcu)}\right)\right] x100$$

**Equation 2.1: Calculation for calculating the % decrease in tail moment in *in vitro* assays.**

TMdi = tail moment of drug-treated, irradiated sample

TMci = tail moment of irradiated non-treated sample

TMcu = tail moment of unirradiated non-treated sample
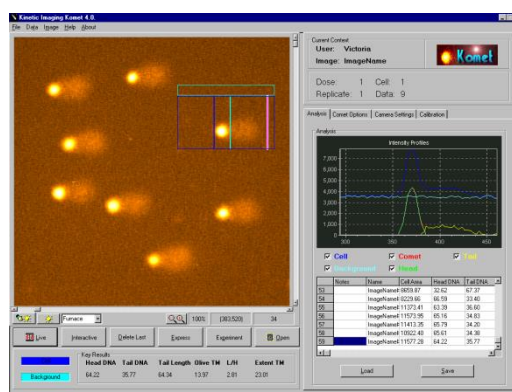
**Figure 2.5 Screen-shot of the Komet Analysis software used to calculate the tail moment of the captured comet images**

### 2.2.4.4  *Measurement of γ-H2AX and RAD51 foci by immunofluorescence*

SW1222 cells were seeded in 6-well plates and treated with ADEPT, as described in Section 2.2.4.1, using 50 nM prodrug and cells were then incubated in drug-free medium. At different time points cells were trypsinised, centrifuged, resuspended in freezing mix and stored in cryovials at -80°C, as previously described.

Frozen vials of cells were defrosted on ice, centrifuged at 430 x g for 5 min and re-suspended in 1 ml PBS. 16% paraformaldehyde (Alfa Aesar, MA, USA) was added to give a final concentration of 2% and cells were incubated for 20 min. Cells were washed with PBS, centrifuged again at the same speed, pellet resuspended in 1 ml 70% ice-cold ethanol and incubated for 10 min on ice. The cells were centrifuged and resuspended in 200 μl ice-cold 70% ethanol. The final cell resuspension was applied to a Shandon EZ single cytofunnel (Thermofisher Scientific, Loughborough, UK) and spun at 650 rpm for 5 min at room temperature onto Superfrost® Plus slides (25 x 75 x 0.1 mm, VWR International, Leicestershire, UK).

Fixed cells were permeabilised with 0.5 % Triton-X-100/PBS for 5min at room temperature. Cells were placed in a humidified chamber and blocked overnight at 4°C in blocking buffer (Table 2.11). Blocked cells were washed three times with cold PBS and then  incubated overnight at 4°C with either anti-γ-H2AX (Millipore, UK) at a 1:1000 dilution in blocking buffer or anti-RAD51 (Santa Cruz Biotech) at a 1:100 dilution in blocking buffer. After washing three times with cold wash buffer (Table 2.11), cells were then incubated for 4 hr at 4°C in the dark with either Alex Fluor® 488 goat anti-mouse secondary antibody (Invitrogen, Paisley, UK) at a dilution of 1:2000 in blocking buffer or Alex Fluor® 488 goat anti-rabbit secondary antibody (Invitrogen, Paisley, UK) at a dilution of 1:2000 in blocking buffer. Cells were then washed three times in cold wash buffer. Slides were mounted with Pro-Long® gold anti-fade reagent with DAPI (Invitrogen, Paisley, UK), a coverslip applied (24 x 50 mm thickness, VWR International VWR International, Leicestershire, UK) and the edges sealed with clear nail polish. Images were

visualised with a Perkin Elmer Ultraview Spinning Disk Confocal, driven by Volocity Acquisition (63x oil immersion objective) equipped with a cooled ECCD camera and laser lines at 405nm, 440nm, 488nm, 514nm, 568nm and 614nm wavelengths. Foci were counted in 100 cells per dose or time point and results expressed as average number of foci per cell (mean ±standard error).

### *2.2.4.5   Cell cycle analysis*

SW1222 cells were seeded at a density of 1 x$10^6$ cells in 6-well plates and left to adhere overnight at 37°C. The next day, cells were treated with ADEPT using 0.25 μM prodrug (as described in Section 2.2.4.1), and cells were incubated in drug-free media and harvested at different time points. Supernatant containing detached cells was removed and centrifuged at 1200 rpm for 4 min. Adherent cells were trypsinised and also centrifuged. Cell pellets from both supernatant and trypsinised mix (as per time point) were pooled together and fixed in 1 ml ice-cold 70% ethanol – drop-wise while vortexing before storing at 4°C, until required.

In preparation for cell cycle analysis, cells were centrifuged at high-speed > 3000 rpm for 6 min. The pellet was washed with PBS and centrifuged again at high speed. This process was repeated. The cell pellet was treated with 50 μl of 50 μg/ml Ribonuclease A (Invitrogen) to remove RNA and this was followed by the addition of 500 μl of 0.1 mg/ml propidium iodide (PI) per million cells and mixed well. The PI/RNase cell suspension was then incubated for 10 min at room temperature or overnight at 4 ºC. Samples were passed through a 40 μm cell strainer (BD, JY, USA) to remove cell clumps prior to analysis by flow cytometry using the CyAn ADP High-Performance Flow Cytometer and Summit analysis software (Dako, Cambridge, UK). A blue 488 nm laser line was employed for propidium excitation and red fluorescence was measured using 670 LP filter. Samples were analysed at a low flow rate, that is, fewer than 800 events/second. Ten thousand events were collected per sample. PI fluorescence data was collected in a linear scale and a dot plot (PI area versus pulse width) was used to gate out cell doublets and higher aggregates.

### 2.2.4.6 Real-time PCR array

Exponentially growing cells seeded at a density of 3 x10$^6$ cells per T25 flask (Corning® Tewksbury, MA, USA) were treated with ADEPT, as described in Section 2.2.4.1, and replaced with drug-free medium following prodrug incubation. Cells were harvested at 1, 3 and 24 hrs-post-ADEPT and total RNA was extracted from adherent cells using the RNeasy Mini kit (Qiagen) according to the manufacturer's instructions. (The on-column DNase treatment step was performed for each sample). Concentration (ng/μl) of RNA was measured at 260nm on the Nanodrop® ND-1000 UV-VIS spectrophotometer. RNA purity and integrity was verified on the Agilent 2100 Bioanalyser and associated RNA 6000 Nano LabChip kit (25-500 ng/μl) (Agilent Technologies UK, Cheshire), and using the Eukaryote Total RNA assay. RNA samples were stored at -80°C until required.

Template cDNA was generated from 1 μg of RNA using the RT$^2$ First Strand (SABiosciences). cDNA was checked with PCR (as described in Section 2.2.1.5) using GAPDH forward and reverse primers and the PCR reaction per sample was run on a 1.5% agarose gel. The cDNA template was then amplified in 24 μl volumes using the DNA Damage Signalling Pathway PCR array plate and RT$^2$ qPCR Mastermix (SABiosciences) which contained Hot-Start Taq DNA polymerase, dNTPs, SYBR green and ROX. Amplification was carried out in an Applied Biosystems ABI7500 RT-PCR machine. The cycling conditions were as follows: 1 cycle of 95ºC for 10 min followed by 45 cycles of 95ºC for 15 sec and 60ºC for 60 sec. Cycle Threshold (CT) values were automatically calculated using the Applied Biosystems SDS software version 1.3.1 and changes in gene expression were analysed using the online RT$^2$ Profiler™ PCR array data analysis application at http://www.sabiosciences.com/pcrarraydataanalysis.php.

### 2.2.4.7 Detection of intracellular proteins by Western blotting

Equal numbers of cells were seeded in a 25 cm$^2$ tissue culture flask (1 x10$^6$ cells/25 cm$^2$) and allowed to adhere overnight. The next day cells were treated with ADEPT, as described in Section 2.2.4.1, and replaced with drug-free medium following prodrug incubation. Cells were harvested at 1, 3 and 24 hrs-post-ADEPT. Cells were

lysed in lysis buffer [150 mM sodium chloride, 1 % Triton-X-100, 1 % sodium deoxycholate, 0.1 % SDS, 50 mM Tris, pH 7.2 and 1x protease inhibitor cocktail (Roche Diagnostics Ltd, West Sussex)] on ice (1 ml per $10^7$ cells per 150 $cm^2$ flask). A cell scraper was used to lift the cells and then left on ice for 30 min. Insoluble debris was pelleted (12, 000 rpm, 10 min, 4 °C) and the protein concentration of the resulting supernatant was determined using the Bio-Rad DC Protein Assay kit (California, USA), according to the manufacturer's protocol. Total cell lysates (15-20 μg of protein) were mixed with loading buffer (Table 2.5) and boiled for 5 min before loading onto a 4-20% pre-cast SDS-gradient gel (Novex, San Diego, CA). SDS-PAGE and protein transfer onto PVDF membrane was carried out as previously described in Sections 2.2.3.1 and 2.2.3.2

Membranes were blocked overnight in blocking buffer: 5% Marvel/PBS or 5% BSA/TBST (for phoshorylated proteins). The membrane was then washed briefly with PBS or TBST and the primary antibody (diluted in 1% blocking buffer) was applied and incubated overnight at 4°C with gentle agitation. The membrane was then washed in PBS or TBST 3x 10 min. The secondary antibody conjugated to horseradish peroxidase (HRP) (diluted in 1% blocking buffer) was added and incubated with the membrane for 1 hr at room temperature, followed by washing 3x 10 min. Bands were visualised using Amersham ECL™ Western Blotting System (GE Healthcare, Buckinghamshire, UK) or the Luminata™ Classico ECL reagent and autoradiographic film. For re-blotting: membranes were stripped by incubating in stripping buffer (Section 2.1.2.1) at 50°C for 30 min, washed with distilled water for 1-2 hs with a final 5 min extensive wash with TBST, and then blocked with 5% BSA/TBST.

Specific bands were quantified by densiometry using Image J software (v.1.44, National Institutes of Health, USA). The relative density value of protein in the ADEPT-treated samples was calculated against non-treated samples, and these values were normalised against the relative densities of the loading control protein.

### 2.2.5   *In vivo* studies

### *2.2.5.1 Clearance study*

Balb/c hairy mice were injected with 1000 U/kg (i.v.) bacterial or yeast CPG2 and blood was taken at 1, 3 and 5 hrs. The blood was diluted 10x in PBS and the amount of enzyme present in the blood was measured by determining the enzyme activity using the UV-spectrophotometer (as described in Section 2.2.3.5) or high performance liquid chromatography (HPLC). HPLC analysis was performed according to the protocol described by Bhatia *et al.* (136) with the help of Dr. Surinder Sharma (Dept. of Oncology, UCL Cancer Institute, London).

### *2.2.5.2 Analysis of therapeutic response*

The therapeutic response to ADEPT was conducted in nude mice bearing SW1222 human colorectal carcinoma xenografts. ADEPT-treated mice were injected with 1000 U/kg (i.v.) of MFECP fusion protein followed by 70 mg/kg (i.p.) of ZD2767P prodrug (x3) at 6, 7 and 8 hr later. Tumours were excised at 1, 3 and 24 hr after the last prodrug dose. Each tumour tissue was cut into 3 equal pieces and processed accordingly: snap-frozen, snap-frozen in iso-pentane and fresh tissue. Fresh tumour tissue was cut into tiny fragments with a sterile scalpel to create a single-cell suspension and stored in freezing medium at -80°C until required for analysis. Blood, also withdrawn at these time points, were collected into 4 ml EDTA Vacutainer® tubes (Becton Dickinson, Oxford, UK) and processed into a single-cell suspension of peripheral blood lymphocytes. To do this, blood was gently added to 2 ml Ficoll-Paque™ PLUS (GE Healthcare) and centrifuged at 450xg for 20 min at room temperature with slow deceleration. PBLs were obtained by removing the fluffy white mononuclear layer at the interface of the two layers with a pipette and transferring to 15 ml Falcon tube (VWR International Limited, Leicestershire, UK). Cells were washed with PBS, centrifuged at 450xg for 5 min and resuspended in freezing medium for -80°C storage until required for analysis.

Analysis using the comet assay was carried out in the same way as described in Section 2.2.4.3. The percentage decrease in tail moment was calculated using Equation 2.2 which takes into consideration the unirradiated drug-treated tail

moment and is used to compensate for additional single strand breaks that may have been induced by drug treatment.

$$\% \text{ decrease in tail moment} = \left[1 - \left(\frac{(TMdi - TMcu)}{(TMci - TMcu) + (TMdu - TMcu)}\right)\right] x100$$

**Equation 2.2: Calculation for calculating the % decrease in tail moment in *in vivo* assays.**

TMdi = tail moment of drug-treated, irradiated sample

TMci = tail moment of irradiated non-treated sample

TMcu = tail moment of unirradiated non-treated sample

TMdu = tail moment of the drug-treated, unirradiated sample

## 2.2.6 Statistical analysis

Statistical analysis was performed using Prism 6 (GraphPad Software Inc.). For ADEPT experiments conducted *in vivo* all post-treatment samples were compared with pre-treatment samples by using ordinary one-way ANOVA analysis. For cell cycle analyses, the two-way ANOVA (repeated-measures) was used with the Bonferroni post-test for determining the p value. The significance level was expressed as ns = non-significant, * $p < 0.05$, ** $p < 0.005$, *** $p < 0.001$ and **** $p < 0.0001$.

University College London

# CHAPTER 3

Pharmacokinetic and Pharmacodynamic Challenges of Antibody-Directed
Enzyme Prodrug Therapy (ADEPT)

Carima Andrady

# 3  Modifying Antibody-Enzyme Pharmacokinetics

## 3.1  Introduction

Early ADEPT clinical trials with the antibody-enzyme conjugate incorporated an additional component, that is, a glycosylated anti-enzyme antibody to inactivate and clear circulating antibody-enzyme conjugates (183) (184). The system increased tumour-to-blood ratios in excess of 10, 000:1 (134), the highest recorded with CPG2. The 2-phase ADEPT system, which incorporates the glycosylation on the antibody-enzyme fusion protein, showed promise in Phase I/II clinical trials (139), but its efficacy was limited by rapid clearance and myelosuppression caused by activated drug in the bone marrow (199).

Obtaining maximal antibody-enzyme in the tumour, whilst maintaining low enzyme activity in the blood is crucial to the efficacy of ADEPT. Using a bacterially-generated non-glycosylated form of MFECP (137) allows the antibody-enzyme to remain in circulation longer than the *P. pastoris*-generated glycosylated form (139); with consequent improvement in tumour loading. Theoretically, non-glycosylated MFECP could be followed by a CPG2-inactivating/clearance step prior to the administration of the prodrug: mimicking the early clinical trials (135). This would create a 3-phase ADEPT, as outlined diagrammatically in Figure 3.1. Unfortunately, it has proved to be too difficult to generate sufficient quantities of MFECP in bacteria, although *P. pastoris* manufacture was readily achievable to clinical grade (140). It was therefore hypothesised that *P. pastoris*-generated MFECP could be modified to remove glycosylations in order to prolong its circulation time and maximise tumour loading.
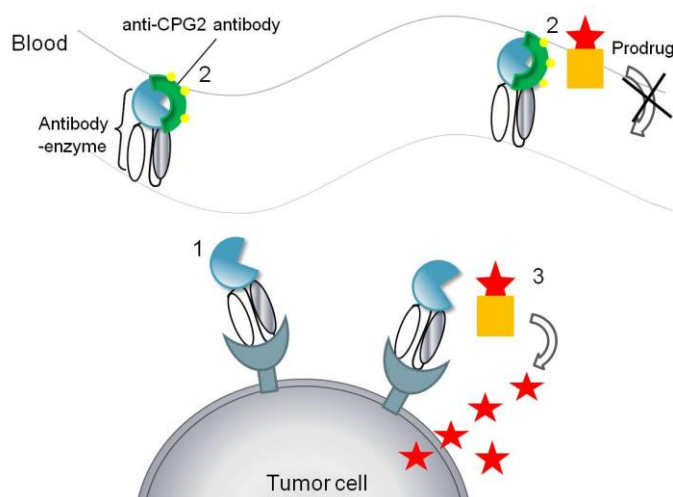
**Figure 3.1 Proposed 3-Phase ADEPT**
1. An antibody-enzyme localises *in vivo* to the target tumour antigen
2. An enzyme-inactivating antibody/agent binds to non-bound fusion protein
3. After circulatory clearance, an un-harmful prodrug is administered. The prodrug is converted to a potent DNA-damaging toxic drug by the pre-targeted enzyme in the tumour.

### 3.1.1 Aims and Objectives

The aim: to remove glycosylations from MFECP in order to prolong its circulation time in blood prior to addition of a clearing agent. The objectives:

1. To remove N-linked glycosylations.

2. To determine the presence and sites of O-linked glycosylations.

3. To remove O-linked glycosylations.

## 3.2 Results

### 3.2.1 MFECP stability

Several batches of clinical grade MFECP were checked for degradation, purity and activity by SDS-PAGE and size-exclusion chromatography (Figure 3.2A and B). 2 ml of a 1 in 10 dilution of each batch of MFECP was run (separately) onto a Superdex 200 column and the FPLC profile of each batch is shown in Figure 3.2B. The proteins each produced a single peak, all eluting at approximately 78 ml. Coomassie staining (Figure 3.2A) revealed several bands: one at ~ 72 kDa, which represents MFECP; and two thinner bands close together at ~ 45 kDa, which

represents the CPG2 moiety of MFECP. This was an indication that the protein had degraded over time during storage at -80ºC, and/or the expressed protein was susceptible to protease cleavage. The smear of Coomassie stain above the MFECP band indicated the presence of glycosylation. MFECP, batch B0131, was chosen for use throughout this thesis. Functional activity of MFECP was also checked by measuring the absorbance of enzyme-catalysed reduction of methotrexate in the dual beam spectrophotometer (as described in Section 2.2.3.5) and found to be 120 U/mg (where 1 U is the amount of enzyme required to hydrolyse 1 mmol of methotrexate per min at 37ºC). The fusion protein was checked for thermo-stability by incubating at 37ºC over several hours and then loading the protein onto a 12% Tris-Gly gel, as shown in Figure 3.3. The Western blot showed no change in the protein between 6 and 96 hr at 37ºC.
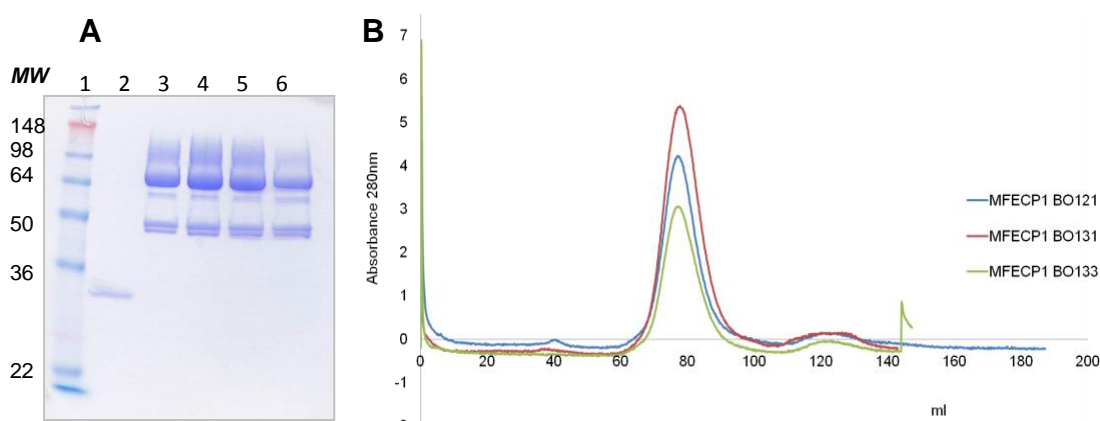


**Figure 3.2 MFECP clinical batches**

A) Coomassie gel of different MFECP1 clinical batches. Lane 1: marker, lane 2: positive control, lane 3: B0120 (0.5 mg/ml), lane 4: B0121 (0.71 mg/ml), lane 5: B0131 (0.63 mg/ml), B0133 (0.4mg/ml). B) FPLC profile of the MFECP batches B0121, B0131 and B0133. Superdex 200 separation column was used. (MW markers in kDa).
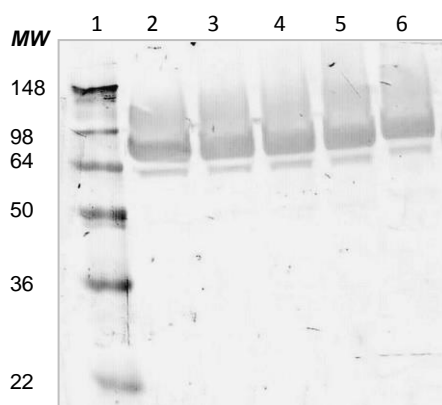
**Figure 3.3 Western Blot of MFECP (0.63 mg/ml) after incubation at 37ºC over several hours**
Lane 1: marker, lane 2: MFECP pre-incubation, and in subsequent lanes 3, 4, 5 and 6: MFECP incubated for 6, 24, 72 and 96 hr. Protein was detected with anti-MFE antibody/goat anti-rabbit-HRP. (MW markers in kDa).

## 3.2.2    Removal of N-linked glycosylation from MFECP or CPG2

### 3.2.2.1    Using enzymes

In the first instance, MFECP was deglycosylated with enzymes specific for N-linked glycans on MFECP using peptide-N-glyco-hydrolase F (PNGase F) and endo-β-N-acetylglucosaminidase (EndoH). PNGase F is not specific for the conserved N-glycan core structure and catalyses the hydrolysis of the GlcNAc$\beta$-Asn linkage. EndoHf catalyses the hydrolysis of the glycosidic bond between two N-acetylglucosamine residues (GlcNAc$\beta$-1,4GlcNAc) in the conserved N-glycan core structure resulting in the release of the GlcNAc residues. The effect of incubating MFECP with PNGase F at 37ºC was demonstrated, as shown in Figure 3.4. MFECP was identified without the smear above the protein band when treated with PNGase F (Figure 3.4A, lane 2), compared to non-treated MFECP (lane 1). The bands were detected with the mannose-binding lectin concanavalin A (Con A), which implied that the N-linked glycosylations had been cleaved. However, the smear above the PNGase-treated MFECP band (lane 2) remained in those blots detected with anti-His and anti-CPG2 antibody, suggesting that glycosylations other than N-glycosylation were present on the enzyme molecule (Figure 3.4 B and C). PNGase-treated MFECP

was detected with anti-His and anti-CPG2 antibodies also showed that the enzyme had no affect on the overall protein structure of MFECP.
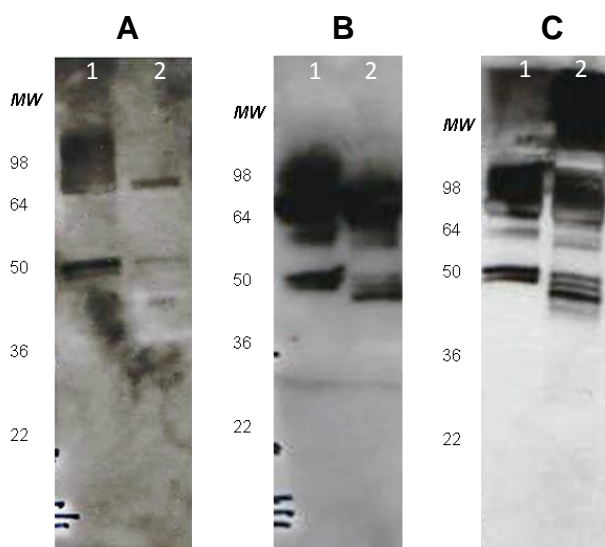


**Figure 3.4 X-ray film of MFECP digested with PNGase F and detected with biotinylated Con A (A), anti-His antibody (B) and anti-CPG2 antibody (C)**
Lane 1: 0.126 mg/ml MFECP, lane 2: MFECP (6 μg) treated with PNGase F. Enzymatic reaction was left for 24 hr at 37°C. Con A detects N-glycosylation which is absent in (A), whilst (B) and (C) suggest the presence of other glycosylations. Protein was detected with anti-mouse-HRP, anti-rabbit-HRP or streptavidin-HRP and the Amersham ECL™ Western Blotting System used.

Upon treatment of MFECP with EndoHf, the incubation mixture was loaded onto a Con A HiTrap affinity chromatography column to separate glycosylated proteins from non-glycosylated proteins. The purified fractions were run on a Tris-Gly gel, and Western blots of the column fractions of PNGase F- and EndoHf-treated MFECP are shown in Figure 3.5A and B (respectively). Both reactions revealed the presence of MFECP in the flow-through (binding buffer) as shown in lane 7. This revealed that sugars, notably the N-linked mannose sugars, had been removed from the fusion protein by the enzyme. MFECP, in the absence of deglycosylating enzymes, was also run through the Con A column for comparison and the fractions were analysed by Western blotting (Figure 3.6). Fractions that contained protein in the elution buffer confirmed N-glycosylation on MFECP.
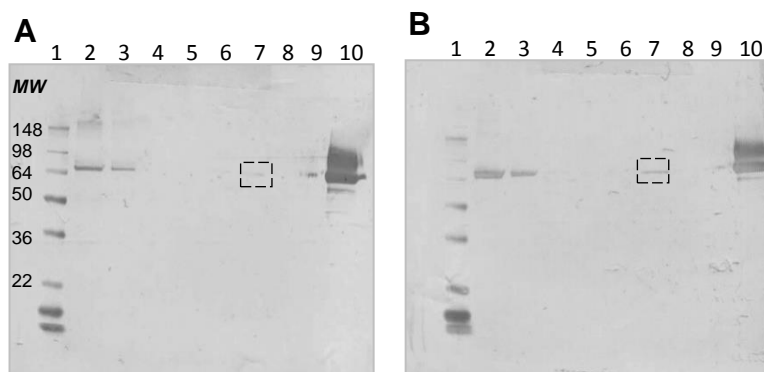
**Figure 3.5 Con A column fractions of MFECP digested with PNGase F (A) and EndoHf (B)**

Lane 1: marker, lane 2: MFECP (0.144 mg) treated with PNGase F (A) or EndoHf (B) after 24 hr incubation, lane 3: MFECP (35 µg) and enzymes – column load, lane 4-9: binding buffer fractions, lane 10: MFECP (0.63 mg/ml). The boxes mark the presence of MFECP band. Protein was detected with anti-MFE/goat anti-rabbit-HRP. (MW markers in kDa).
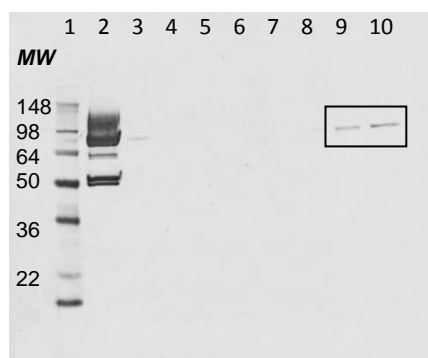


**Figure 3.6 Con A column fractions of MFECP only**

Lane 1: marker, lane 2: MFECP (0.315 mg/ml) column load, lanes 3-6: binding buffer fractions 1-4, lanes 7-10: elution buffer fractions 1-4. MFECP is present in lanes 9 and 10. Protein was detected with anti-CPG2/goat anti-rabbit-HRP. (MW markers in kDa).

### *3.2.2.2 Genetic manipulation of CPG2*

From previous studies, we know that there are 3 potential N-glycosylated asparagine (Asn) residues of CPG2 when it is expressed in yeast (137) and in mammalian cells (342). In addition, the CPG2 moiety of MFECP is most vulnerable since its structure dictates the enzyme's activity, affinity and specificity for its substrate - the prodrug. Thus, in order to properly address the issue of deglycosylation, it was decided to focus on CPG2. A mutated CPG2 variant was previously generated by mutating the 3

N-glycosylated Asn residues (Asn-222, Asn-272, Asn-264) to glutamine (Gln) and was found to be functionally active when expressed in mammalian cells (342). A similar CPG2 variant was also generated within the Department using site-directed mutagenesis and expressed in yeast when genetically fused to an antibody. For this work, the non-N-linked glycosylated CPG2, CPG2_3Q, was cloned into pPICzαB vector plasmid via NotI and XbaI restriction sites and the ligated plasmid sequence was transformed into X33 cells. Protein expressed in yeast *P. pastoris* supernatant at 48 and 72 hr after methanol induction in shake-flask cultures, as shown in Figure 3.7. Protein production from one of the yeast clones was scaled-up to 10 L batch fermentation. The protein was harvested after 72 hrs and purified. Twenty-five millilitre pooled fractions of purified protein was loaded and run through a 120 ml Superdex 75 size-exclusion column. The FPLC profile of the purified protein is shown in Figure 3.8A. The Gaussian shape of peak appears to be skewed, probably an indication of partial dimerisation of the enzyme. 0.4 ml fractions were collected and run on SDS-PAGE and from the Coomassie stain (Figure 3.8B) fractions 12 to 21 were pooled. Final protein concentration was 2.8 mg/ml and total protein yield was 20 mg. Enzyme activity of the purified protein was measured by methotrexate reduction on the UV-spectrophotometer and found to be 202 U/ml (specific activity 72 U/mg).
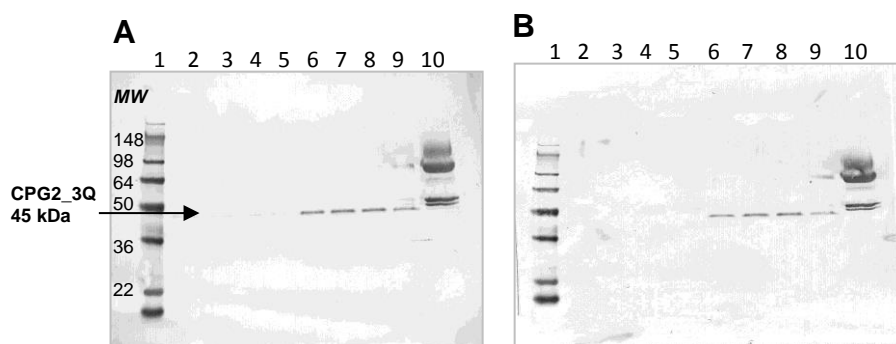


**Figure 3.7 Protein expression of CPG2_3Q at 48 hrs (A) and 72 hrs (B) from shake flask cultures**

A) Lane 1: marker, lane 2-5: expression of CPG2_3Q from 4 yeast cell clones at 24 hrs post-methanol induction; lane 6-9: expression of CPG2_3Q from the same yeast cell clones at 48 hrs post-methanol induction; lane 10: positive control. B) Lane 1: marker, lane 2-5: blank; lane 6-10: expression of CPG2_3Q from the same yeast cell clones at 72 hr post-methanol induction; lane 10: positive control. Protein was detected with anti-His/anti-mouse-HRP. (MW markers in kDa).
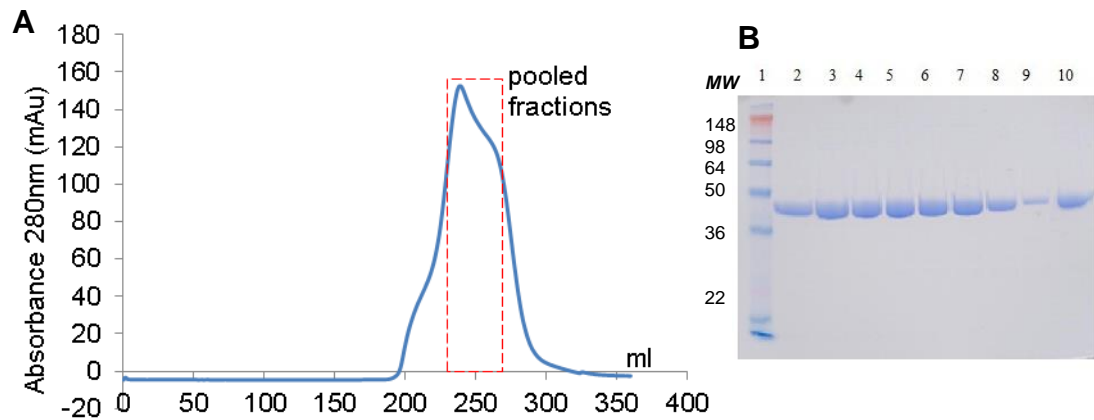
**Figure 3.8 Purified CPG2_3Q**

**A)** Size exclusion chromatography. 25 ml of purified protein from the fermentor was applied to a Superdex 75 column. 0.4 ml fractions were collected at a flow rate of 0.5 ml/min. **B)** SDS-PAGE/Coomassie stain of the collected fractions. Lane 1: MW marker, Lane 2-10: FPLC fractions 11, 13, 15, 19, 21, 23, 25, 27.

A codon-optimised sequence of CPG2 obtained with permission from Mologic Ltd (Bedford, UK) [used in later cloning experiments (Section 3.2.3.2)], was also cloned into pPICzαB with the N-linked glycosylations knocked-out (mCPG2_3Q), as before. The CPG2 DNA sequence is very GC-rich, and codon-optimisation reduces the GC content without affecting the overall protein structure and enzyme activity to facilitate genetic manipulation. In the fermentor, this protein was produced at a final concentration of 2.5 mg/ml (total protein yield 38 mg) and enzyme activity was found to be 578 U/ml (specific activity 231 U/mg). FPLC of the purified mCPG2_3Q protein is shown in Figure 3.9 and the pooled fractions indicated. The peak, also skewed here by the protein shoulder (200-220 mls), may indicate partial dimerization.
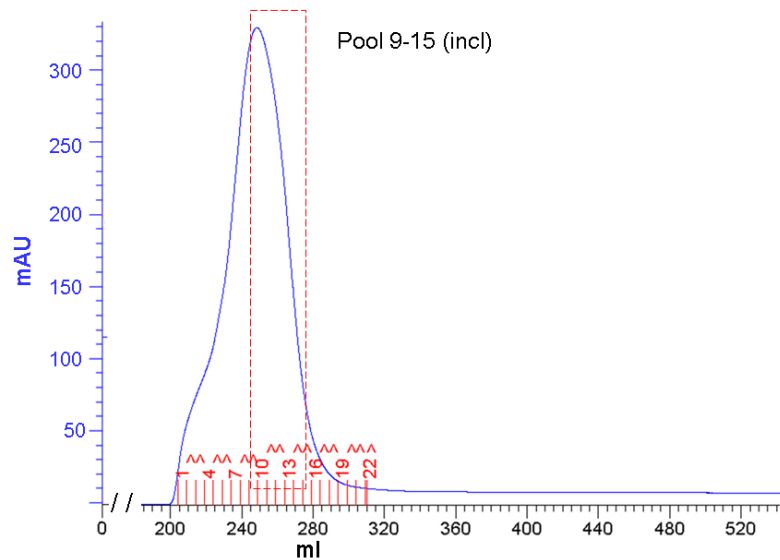
**Figure 3.9 FPLC profile of purified mCPG2_3Q (Mologic Ltd)**

25 ml of purified protein from the fermentor was applied to a Superdex 75 column. 0.4 ml fractions were collected at a flow rate of 0.5 ml/min.

### 3.2.2.2.1   Verifying glycosylation status of CPG2_3Q

Glycosylation status of the purified CPG2_3Q protein was checked using Con A affinity chromatography. Protein was diluted in Con A column binding buffer (see Section 2.1) and applied to a 1 ml Con A HiTrap affinity column. Fractions (0.5 ml) were collected in the binding and elution phases at a flow rate of 1 ml/min (Figure 3.10 A and B). An early peak in the binding phase indicated the presence of protein and protein was not detected in the elution buffer. There was, however, a very large peak upon exchange of buffers, as shown in Figure 3.10 A. This was the result of the methyl-$\alpha$-D-glucopyranoside in the elution buffer which caused a change in the absorbance (and conductivity). Fractions were analysed for the presence and activity of CPG2_3Q, as presented in Figure 3.11 and Table 3.1, (respectively). The Western blot in Figure 3.11 verified the presence of CPG2_3Q in the binding phase, indicating that it hadn't bound to the Con A lectin in the column and was, therefore, not glycosylated. The findings demonstrated an *in vitro* method of detection for the glycosylation status of CPG2_3Q, and subsequent testing *in vivo* would clarify the results.
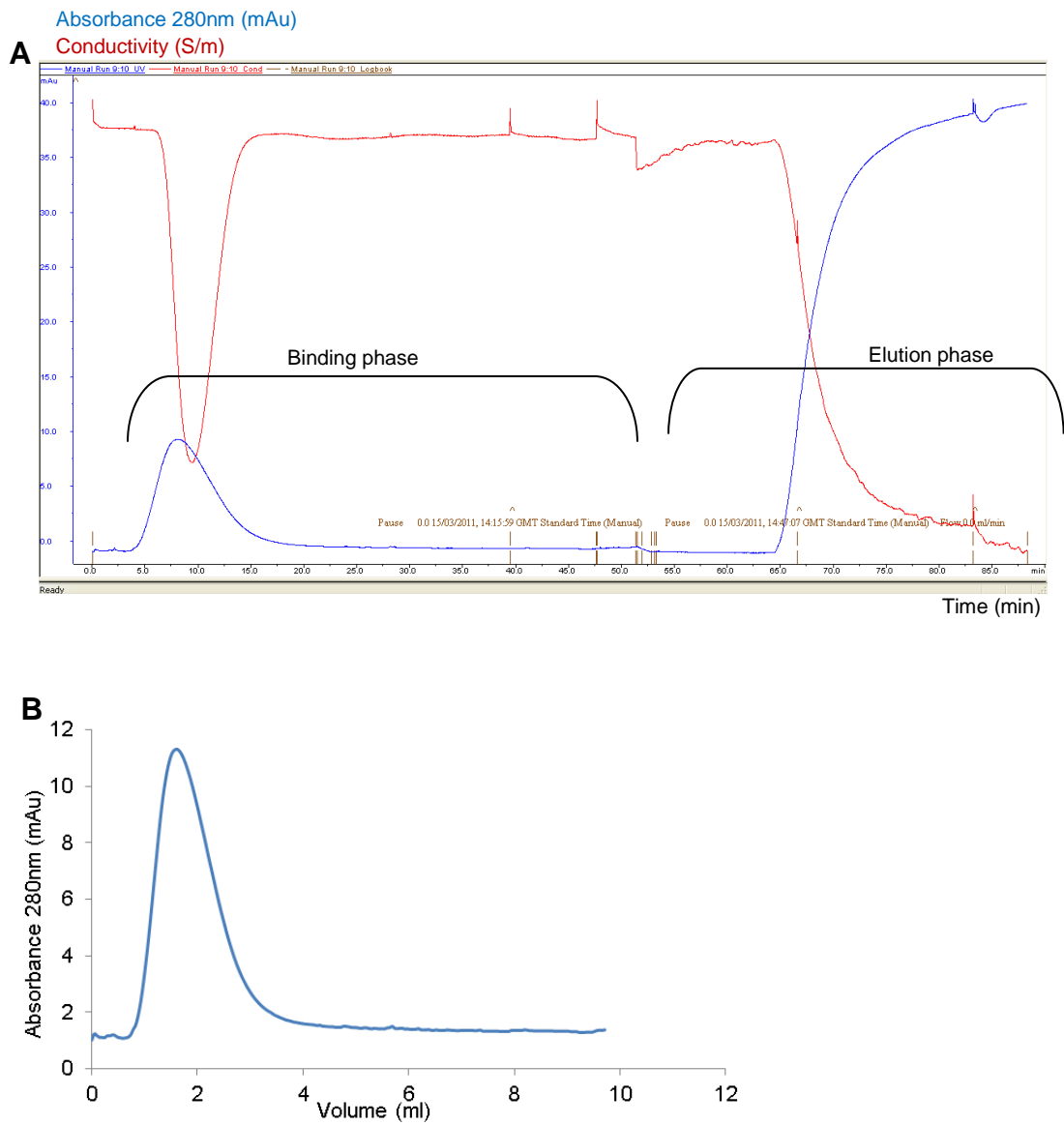
**Figure 3.10 Con A column FPLC elution profile of purified CPG2_3Q**

A) 0.56 mg of CPG2_3Q protein was loaded to a 1 ml Con A HiTrap affinity column and 0.5 ml fractions collected in the binding buffer and elution phases. The blue profile is the change in absorbance over time and the red profile is the change in conductivity over time. The small peak at 7-10 min is the column purified CPG2_3Q, also shown in B) in absorbance vs volume. The large peak at 65 min coincides with the absorbance detection of methyl-α-D-glucopyranoside in the elution phase.

**Figure 3.11 Western blot of the CPG2_3Q Con A column fractions**

Lane 1: marker, lane 2: CPG2_3Q (0.56 mg) column load, lane 3-9: column flow-through fractions 1-7, lane 10: MFECP (0.63 mg/ml; positive control). Protein was detected with antibodies anti-CPG2/anti-rabbit-HRP. (MW markers in kDa).

**Table 3.1 Enzyme activity of the Con A column flow-through fractions of CPG2_3Q**

Enzyme activity was determined by measuring the absorbance of enzyme-catalysed reduction of methotrexate, as described in Section 2.2.3.5. Each measurement is a mean of triplicate readings.

| Flow-through fractions (500 µl) | Activity U/ml |
|---|---|
| 1 | 0 |
| 2 | 0 |
| 3 | 5.61 |
| 4 | 8.50 |
| 5 | 8.41 |
| 6 | 5.78 |
| 7 | 3.21 |
| 8 | 1.17 |

A small clearance study was undertaken in hairy balb/c mice, whereby the blood clearance of the yeast-expressed CPG2_3Q was compared against the bacterial (non-glycosylated) CPG2 (produced within the Department) over 5 hr. Enzyme activity was measured using HPLC (136). The HPLC assay was based on the enzyme-catalysed reduction of methotrexate and the peaks formed by the metabolite of methotrexate was measured against a standard curve. This assay was more sensitive than the spectrophotometric assay with a limit of detection of 0.002 U/ml. As shown in Figure 3.12, CPG2_3Q (1.12% injected enzyme activity/g at 5 hr) cleared faster

than the bacterial CPG2 (38.6% injected enzyme activity/g at 5 hrs), although there appeared to be a discrepancy in the injected enzyme units of bacterial CPG2 because of the >100% injected activity/g observed at 1 hr (see Table 3.2). The study revealed the following: 1) CPG2_3Q remained gycosylated; 2) the Con A column was not a reliable measure of the ability of CPG2_3Q to bind mannose receptors *in vivo*; and 3) the limited sensitivity of the Con A column to detect additional glycosylations, other than N-linked glycosylations. The results suggested that other glycosylations were present on CPG2_3Q, which were likely to be O-linked. Further manipulation of CPG2 would be necessary to remove additional glycosylations in order to evade the mannose receptor.
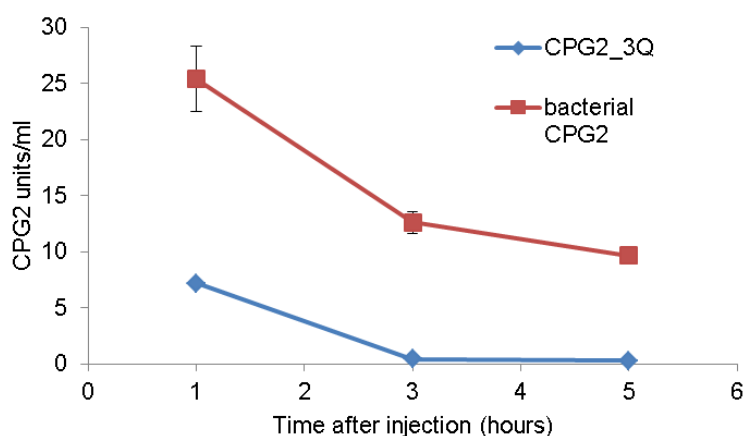


**Figure 3.12 Plasma clearance of CPG2_3Q and bacterial non-glycosylated CPG2 in mice**
Hairy balb/c mice were given yeast-expressed CPG2_3Q (blue) or bacterial CPG2WT (red) (25 U per mouse, i.v.). CPG2 activity was measured in the blood at 1, 3, and 5 hr after injection. Enzyme activity was measured indirectly by HPLC. (Mean of 2 mice per group ± stdev).

**Table 3.2 Plasma biodistribution of CPG2_3Q in mice over time**
Balb/c mice were given yeast-expressed CPG2_3Q or bacterial CPG2WT (25 U per mouse, i.v.) and enzyme activity measure in the plasma at 1, 3, and 5 hr after injection. Results expressed as the mean enzyme activity of 2 mice per group.

| Time (hr) | CPG2_3Q (% injected activity/g) | Bacterial CPG2WT (% injected activity/g) |
|---|---|---|
| 1 | 28.7 | 101.6 |
| 3 | 1.64 | 50.4 |
| 5 | 1.12 | 38.6 |

### 3.2.3   Removal of O-linked glycosylation from CPG2

Little is known about the pattern and specificity of O-linked glycosylation in *P. pastoris*. In an attempt to knock-out the O-linked residues on CPG2, strategies to mutate CPG2 were undertaken, as explained in the following sections. All O-linked residue mutations were constructed into the CPG2_3Q or mCPG2_3Q gene sequence.

### *3.2.3.1   Rationally predicted mutations: CPG2_3Q_12A*

O-linked glycosylation occurs via serine (Ser) and threonine (Thr) residues. There are 17 Ser and 22 Thr residues per CPG2 monomer. The first attempt to rationally mutate CPG2 focused on surface-located O-glycosylations based on *in silico* predictions. To achieve this, the CPG2 protein sequence was analysed for potential O-glycosylation sites using the program NetOGlyc, which is designed to predict all potential O-glycosylation sites (343). No residues were marked by the program with a high prevalence for O-glycosylation but the highest-rated of the 12 potential surface-located O-glycosylated residues were selected. Surface location was predicted by visual examination of the position of the NetOGlyc predicted residues on a rotating model of the crystal structure. The 12 'surface residues' are shown in the computer-assisted protein model (Molecular Operating Environment) of the crystal structure of CPG2 (PDB 1cg2) (344), Figure 3.13. These residues were substituted to alanine (Ala) to form the protein CPG2_3Q_12A. Figure 3.14 shows the protein sequence CPG2_3Q DNA highlighting the Ser/Thr residues mutated to Ala. Alanine is a neutral amino acid that is also hydrophobic and small, thus preventing any kind of molecular steric hindrance or shifts in protein folding.
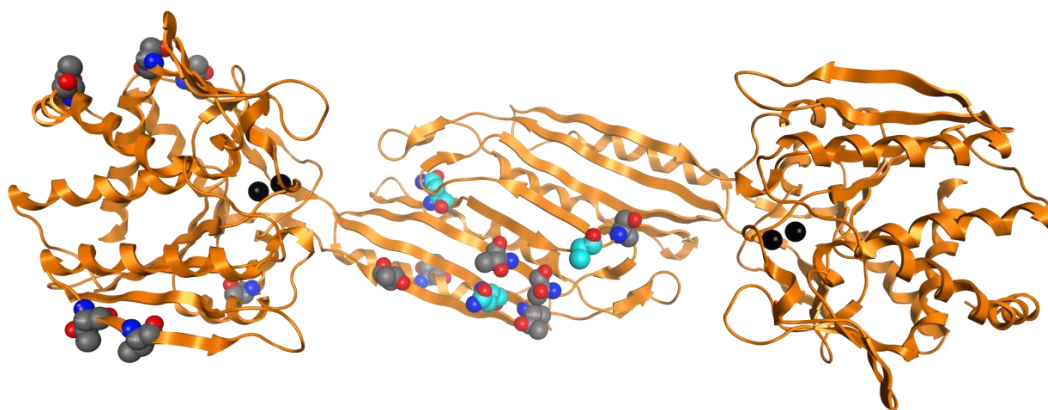
**Figure 3.13 Computer-assisted protein model of (bacterial) CPG2 dimer representing surface modifications for CPG2_3Q_12A**

Location of potential surface located residues involved in O-glycosylation by *P. pastoris* of CPG2 predicted with the program NetOGlyc. The residues are depicted only on the left monomer unit. All 12 residues were mutated to alanine to generate CPG2_3Q_12A (grey/red/blue). The 3 light cyan (aqua blue/red/blue) residues indicate the potential N-glycosylation sites. (The blue and red spheres on each amino acid represent nitrogen and oxygen atoms, respectively). Zinc ions (2x black spheres on both chains) represent the active site. The image was produced using the bacterial CPG2 crystal structure (PDB: 1cg2) with the kind assistance of Dr Paul Gane (Department of Medicinal Chemistry, UCL).

```
A Q K R D N V L F Q A A T D E Q P A V I K
T L E K L V N I E T G T G D A E G I A A A
G N F L E A E L K N L G F T V T R S K S A
G L V V G D N I V G K I K G R G G K N L L
L M S H M D T V Y L K G I L A K A P F R V
E G D K A Y G P G I A D D K G G N A V I L
H T L K L L K E Y G V R D Y G T I T V L F
N T D E E K G S F G S R D L I Q E E A K L
A D Y V L S F E P T S A G D E K L S L G T
S G I A Y V Q V Q I T G K A S H A G A A P
E L G V N A L V E A S D L V L R T M N I D
D K A K N L R F Q W T I A K A G Q V S N I
I P A S A T L N A D V R Y A R N E D F D A
A M K T L E E R A Q Q K K L P E A D V K V
I V T R G R P A F N A G E G G K K L V D K
A V A Y Y K E A G G T L G V E E R T G G G
T D A A Y A A L S G K P V I E S L G L P G
F G Y H S D K A E Y V D I S A I P R R L Y
M A A R L I M D L G A G K H H H H H H - -
```

**Figure 3.14 Primary protein sequence of CPG2_3Q highlighting the rationally predicted Ser/Thr residues**

12 Ser/Thr residues substituted to Ala are highlighted in pink and 3 mutated N-glycosylated residues (Asn→Gln) are highlighted in blue. Full DNA and protein sequence can be found in Section 2.1.1.2. (The sequence originates from the Genbank entry: AAA62842.1 - bacterial CPG Variovorax paradoxus).

CPG2_3Q_12A gene was generated by GenScript Inc. and cloned into the bacterial pUC57 vector. The CPG2_3Q_12A gene was digested with EcoRI and XbaI and cloned into an empty pPICzαB vector and the protein was expressed in methanol-induced yeast culture supernatant at 48 and 72 hr (see Figure 3.15). Two out of the 4 yeast clones expressed protein at these time points, and one of them was taken forward for scaled-up 10 L batch fermentation. The protein was harvested after 72 hr and purified. However, during the final concentration step, after radial bed chromatography, the concentration of CPG2_3Q_12A did not sufficiently increase from start to end. Starting OD at 280nm was 0.084 in 500 ml increased only to 0.118. Insufficient protein was produced during the fermentation to run through a gel-filtration column. Furthermore, the resultant CPG2_3Q_12A had very low activity (<10 U/mg).



**Figure 3.15 Protein expression of CPG2_3Q_12A at 48 and 72 hr in shake flask cultures**
Lane 1: marker, lane 2-5: expression of CPG2_3Q_12A from 4 yeast cell clones at 48 hr post-methanol induction; lane 6-9: expression of CPG2_3Q_12A from the same yeast cell clones at 72 hr post-methanol induction; lane 10: positive control. Protein was detected with anti-His/anti-mouse-HRP. 2 out of 4 yeast clones expressed the protein. (MW markers in kDa).

### 3.2.3.2 *Mass spectrometry-predicted mutations*

In the second approach to address the O-glycosylation status of *P. pastoris*-generated CPG2-3Q, mass spectrometry (MS) was used to identify and define the Ser/Thr residues that were occupied. MS is a separation technique that generates charged molecules or molecule fragments within a heterogeneous sample that can be identified by differences in their mass-to-charge ratio. MS was performed in collaboration with Dr Daniel Spencer at Ludger Ltd (Culham Science Centre,

Oxfordshire). MS confirmed the presence of O-glycosylated glycopeptides, and a total of 10 residues were identified as depicted in the computer-assisted model of the CPG2 crystal structure (Figure 3.16), and in the CPG2_3Q protein sequence (Figure 3.16). The glycans on the first two threonine residues (T55 and T57) were definitively ascribed as intact glycopeptides and the remainder glycans were identified in glycopeptides that had been liberated from the denatured protein. The predicted amino acid substitutions of the potentially O-glycosylated Ser/Thr residues are listed in Table 3.3.
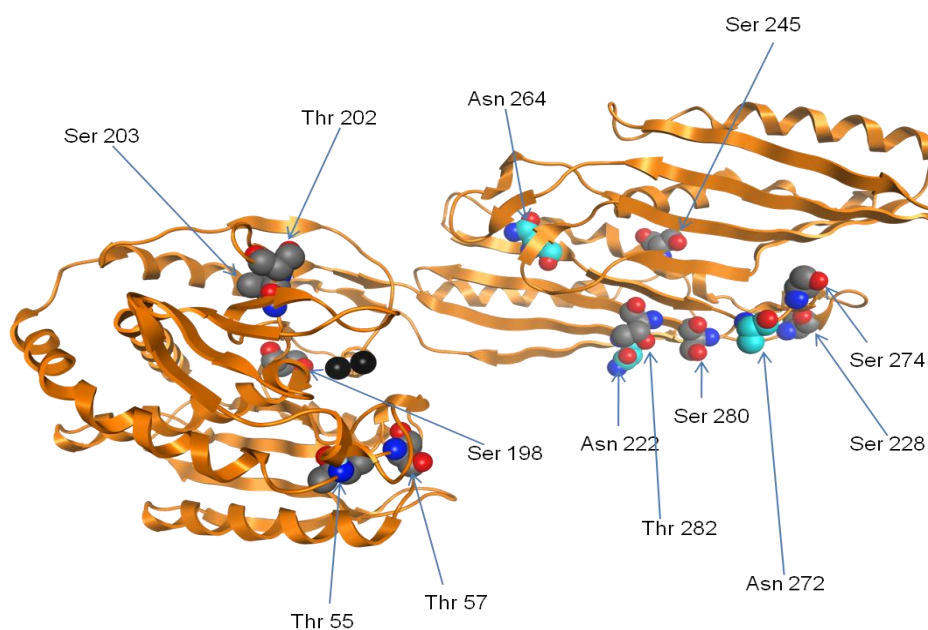


**Figure 3.16 Computer-assisted protein model of (bacterial) CPG2 monomer illustrating the MS-predicted O-glycosylated Ser/Thr residues**

10 Ser/Thr residues (grey/red/blue) and 3 Asn residues (aqua blue/red/blue) are illustrated on a single CPG2 monomer chain. (The blue and red spheres on each amino acid represent nitrogen and oxygen atoms, respectively). Zinc ions (2x black spheres) represent the active site. The image was produced using the bacterial CPG2 crystal structure (PDB 1cg2) with the kind assistance of Dr Paul Gane (Department of Medicinal Chemistry, UCL).

```
A   Q   K   R   D   N   V   L   F   Q   A   A   T   D   E   Q   P   A   V   I   K
T   L   E   K   L   V   N   I   E   T   G   T   G   D   A   E   G   I   A   A   A
G   N   F   L   E   A   E   L   K   N   L   G   F   T   V   T   R   S   K   S   A
G   L   V   V   G   D   N   I   V   G   K   I   K   G   R   G   G   K   N   L   L
L   M   S   H   M   D   T   V   Y   L   K   G   I   L   A   K   A   P   F   R   V
E   G   D   K   A   Y   G   P   G   I   A   D   D   K   G   G   N   A   V   I   L
H   T   L   K   L   L   K   E   Y   G   V   R   D   Y   G   T   I   T   V   L   F
N   T   D   E   K   G   S   F   G   S   R   D   L   I   Q   E   E   A   K   L
A   D   Y   V   L   S   F   E   P   T   S   A   G   D   E   K   L   S   L   G   T
S   G   I   A   Y   V   Q   V   Q   I   T   G   K   A   S   H   A   G   A   A   P
E   L   G   V   N   A   L   V   E   A   S   D   L   V   L   R   T   M   N   I   D
D   K   A   K   N   L   R   F   Q   W   T   I   A   K   A   G   Q   V   S   N   I
I   P   A   S   A   T   L   N   A   D   V   R   Y   A   R   N   E   D   F   D   A
A   M   K   T   L   E   E   R   A   Q   Q   K   K   L   P   E   A   D   V   K   V
I   V   T   R   G   R   P   A   F   N   A   G   E   G   G   K   K   L   V   D   K
A   V   A   Y   Y   K   E   A   G   G   T   L   G   V   E   E   R   T   G   G   G
T   D   A   A   Y   A   A   L   S   G   K   P   V   I   E   S   L   G   L   P   G
F   G   Y   H   S   D   K   A   E   Y   V   D   I   S   A   I   P   R   R   L   Y
M   A   A   R   L   I   M   D   L   G   A   G   K   H   H   H   H   H   H   -   -
```

**Figure 3.17 Primary protein sequence of CPG2_3Q highlighting the MS-predicted O-glycosylated Ser/Thr residues**

The 10 Ser/Thr residues selected for mutation are highlighted in yellow and 3 mutated N-glycosylated residues (Asn→Gln) are highlighted in blue. Full DNA and protein sequence can be found in Section 2.1.1.2. (The sequence originates from the Genbank entry: AAA62842.1 - bacterial CPG2 Variovorax paradoxus).

**Table 3.3 Summary of the MS-predicted O-glycosylated Ser/Thr residues, their location within CPG2 and suggested amino acid substitutions for cloning**

T57N denotes T57 to N57 substitution.

| Residue position | Location of amino acid | Note | Suggested substitution |
|---|---|---|---|
| T55 | Buried | potentially near active site | Gln (Q), Val (V) or Ala (A) OR Asn (N) + T57N |
| T57 | Near surface, frame work oxygen on surface | potentially near active site | Asn (N) |
| S198 | Buried | | Asn (N) or Ala (A) |
| T202 | Semi surface | | Gln (Q) |
| S203 | Semi surface | | Gln (Q) |
| S228 | Surface | at dimerisation interface | Gln (Q) or Ala (A) or Asn (N) |
| S245 | Buried | at dimerisation interface | Asn (N) or Ala (A) |
| S274 | Surface | at dimerisation interface | Gln (Q) or Ala (A) |
| S280 | Surface | at dimerisation interface | Gln (Q) or Ala (A) |
| T282 | Surface | at dimerisation interface | Gln (Q) or Ala (A) |

The position of T55 and T57 molecules within CPG2 were both located very close to the active site (the zinc ions depicted as black spheres), as illustrated in Figure 3.18A and B (respectively). Interestingly, T55 was buried within the molecule and not exposed on the surface (Figure 3.18A). T55 was shown to be linked to lysine 143 by hydrogen (H) bonds, which was also very near the active site. As a result, mutating T55 could potentially quench enzyme activity. However, the H bond with K143 may have already broken if residues have had to fold and orientate differently to accommodate for the glycan chains in *P. pastoris*-expressed protein. T57 is a surface residue in contact with a water molecule (see Figure 3.18B), which helps to make it available for glycosylation. By mutating T57 to N57, the bond with water is not lost, although it is a more bulky amino acid.
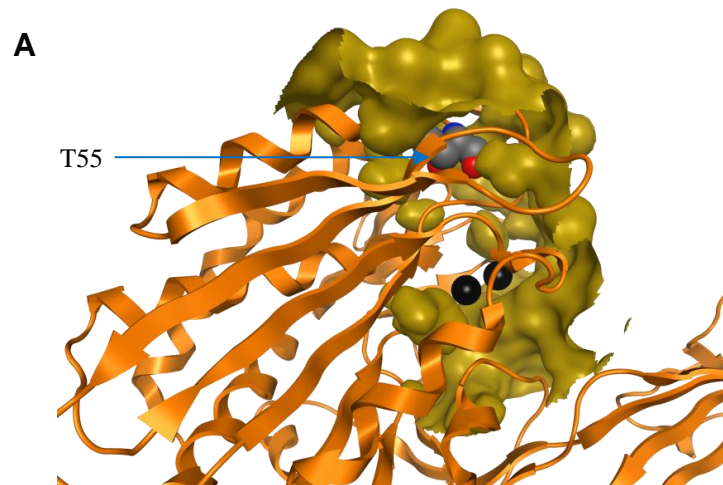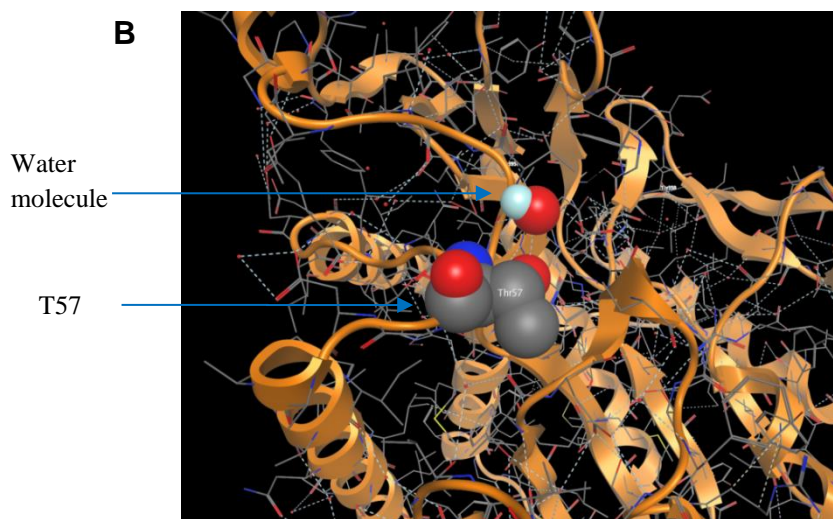
**Figure 3.18 Computer-assisted representation of the location of residues T55 and T57 within CPG2**

A) T55 (grey/red/blue) shown here as buried and in close proximity to the active site (Zinc ions, black spheres). B) T57 (grey/red/blue) close to the surface and hydrogen bonded to a water molecule (red/light blue). Red sphere, oxygen atom; blue sphere, nitrogen atom; light blue sphere, hydrogen atom. The image was produced using the bacterial CPG2 crystal structure (PDB: 1cg2) with the kind assistance of Dr Paul Gane (Department of Medicinal Chemistry, UCL).

Five mutated constructs of CPG2_3Q containing T55 and/or T57 substitutions were proposed for cloning, as shown in Table 3.3. T55 was substituted with glutamine (T55Q; charge is similar), valine (T55V; hydrophobic but isosterically similar), alanine (T55A; small and hydrophobic), asparagine (T55N), or asparagine in the presence of a T57 substitution to asparagine (T55N_T57N). Gene sequences of 145 base pairs (…NIE**TGT**…), each containing the amino acid change, were ordered from GenScript Inc. The 5 genes were substituted individually with PstI and XhoI restriction enzymes into the pPICZαB_mCPG2_3Q vector (as mentioned in Section 3.2.2.2). Protein was expressed in methanol-induced yeast culture supernatant at 24, 48 and 72 hr and enzyme activity of the mutated mCPG2_3Q constructs was tested on the UV-spectrophotometer and/or by HPLC. The results are summarised in Table 3.4. Protein expression, as determined by Western blot using anti-His and anti-CPG2 antibodies, was very weak (almost visible with naked eye) for all 5 mutants. Enzyme activity was not detected on the spectrophotometer but activity down to 0.002 U/ml could be detected with HPLC. The T55V mutant was found to exhibit the most activity at 72 hr expression in shake flasks, which was almost half of that detected for mCPG2_3Q. Nevertheless, a yeast clone was chosen to be taken forward for

scaled-up batch fermentation. The purified protein was loaded and run through a Superdex 75 column. The FPLC profile is shown in Figure 3.19. The T55V purified protein was found to exhibit activity of 274 U/ml (see Table 3.4).

Due to the high enzyme activity obtained with T55V, two additional mutated mCPG2_3Q constructs were generated: T55**V**_T57**N** and T55**V**_T57**V**. These were cloned and expressed in yeast in the same way as described above. The mutations were successful and adequate concentrations of protein were produced by fermentations. FPLC profile of the purified protein is shown in Figure 3.19. However, these constructs showed decreased enzyme activity compared to the parent T55V construct - 181 and 122 U/ml for T55**V**_T57**N** and T55**V**_T57**V**, respectively (see Table 3.4).

**Table 3.4 T55 and/or T57 mutated constructs of CPG2 and their corresponding enzyme activities**

The constructs that were taken forward for fermentation are shown in bold. *Enzyme activity was measured using HPLC, except for T55V_T57N and T55V_T57V, which were measured on the UV-spectrophotometer.

| Clone | Sequence Change | Enzyme activity (U/ml) 72hrs shake flasks* | Specific activity (U/mg) of purified protein | Total yield (mg) purified protein from 9 L feedstock |
|---|---|---|---|---|
| mCPG2_3Q | actggtact | **1.06** | **231** | **166.3** |
| T55Q | **cag**ggtact | 0.01 | | |
| T55V | **gtt**ggtact | **0.47** | **152.4** | **44.5** |
| T55A | **gct**ggtact | 0.32 | | |
| T55N_T57N | **aac**ggt**aac** | 0.06 | | |
| T57N | actggt**aac** | 0.13 | | |
| T55V_T57N | **gtt**ggt**aac** | **<1** | **50** | **75** |
| T55V_T57V | **gtt**ggt**gtt** | **<1** | **29** | **84** |
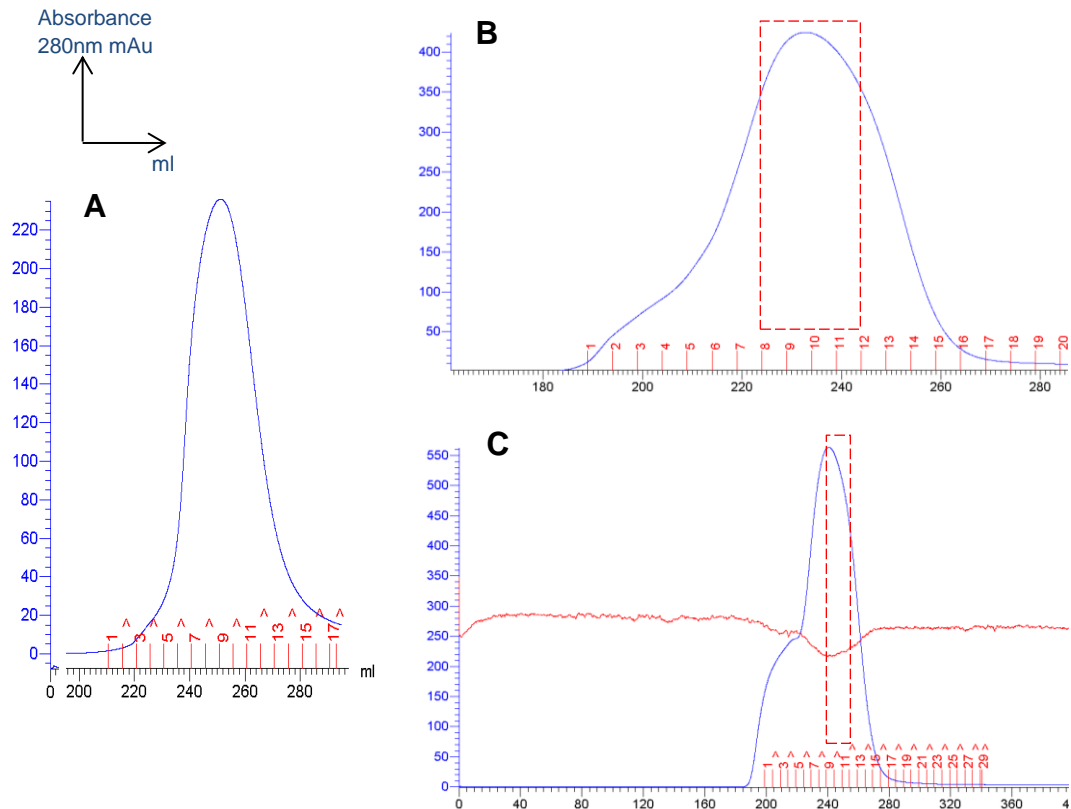
**Figure 3.19 FPLC profile of purified mCPG2_3Q mutated constructs: A) T55V, B) T55V_T57N and C) T55V_T57V**

25 ml of purified protein from the fermentor was applied to a Superdex 75 column. 0.5 ml fractions were collected. B) 8-12 fractions, inclusive, were pooled, C) 9-12 fractions, inclusive, were pooled.

The loss of enzyme activity was probably the direct result of the mutated T55 and T57 residues, which may have caused a disruption in proper folding of the protein leading to a distorted binding/catalytic site. The FPLC profiles appeared to convey this as shown by the broad shape of the peaks for the doubly-mutated constructs (Figure 3.19 B and C), in contrast to the peak for singly-mutated T55V construct (Figure 3.19A). Consistent with this explanation, conservation analysis revealed that the T55 and T57 residues are highly conserved within CPG2 (Figure 3.20) with an amino acid conservation score of 9; the highest conservation score that can be obtained between sequences (345).
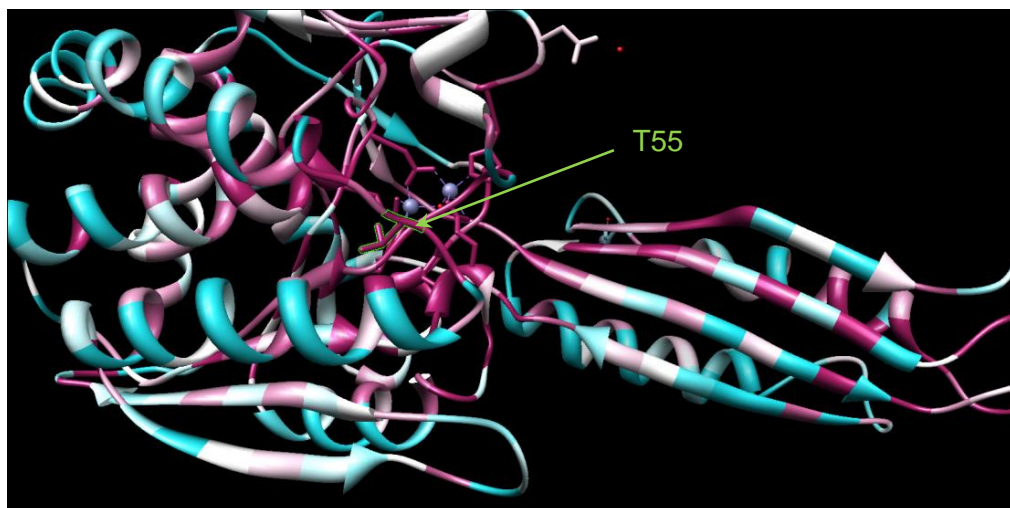
**Figure 3.20 Structural computation of bacterial CPG2 highlighting the conserved (pink), medium conserved (white) and non-conserved (blue) residues**

T55 is shown here in a green outline indicating that it is a highly conserved residue (dark pink). Conservation analysis of CPG2 scores were calculated against homologous sequences using the Consurf server programme http://consurftest.tau.ac.il/ (Image and computational analyses are courtesy of Harpal Sahota, Institute of Structural and Molecular Biology, Birkbeck College, London).

To determine whether the mutations had an effect on the clearance of yeast CPG2 *in vivo*, an experiment was conducted in mice, as previously described in Section 3.2.2.2.1. Twenty-five units of purified protein was injected i.v. into balb/c hairy mice and enzyme activity measured in blood at 1, 3 and 5 hr. The constructs to be measured included bacterial CPG2 (provided by Mologic Ltd), yeast-expressed mCPG2_3Q, yeast-expressed CPG2 (provided by Mologic Ltd), T55V and T55V_T57N mutated constructs. Unfortunately, the mutated constructs, T55V and T55V_T57N, cleared too rapidly to be detected. Bacterial CPG2 and mCPG2_3Q were detected and % injected activity/g noted in Table 3.5.

**Table 3.5 Plasma biodistribution of mCPG2_3Q and bacterial CPGWT in mice**

Balb/c mice were given yeast-expressed mCPG2_3Q or bacterial CPG2 (25 U per mouse, i.v.) and enzyme activity measure in the plasma at 1, 3, and 5 hr after injection. Enzyme activity was measured by methotrexate catalysed-reduction on UV-spectrophotometer. Results expressed as the mean enzyme activity of 2 mice per group. N/D: not detected

| Time (hrs) | mCPG2_3Q (% injected activity/g) | Bacterial CPG2WT (% injected activity/g) |
|---|---|---|
| 1 | 17.2 | 61.2 |
| 3 | N/D | 31.2 |
| 5 | N/D | N/D |

## 3.3 Discussion

The work detailed in this Chapter described strategies to create non-glycosylated MFECP for the proposed 3-phase ADEPT system. The strategies to deglycosylate MFECP have focused on the CPG2 component of the fusion protein, mainly because it is most susceptible to glycosylation by *P. pastoris*, but also most vulnerable to modifications that could affect its functional activity. The strategies investigated included using deglycosylating enzymes and genetically mutating the glycan-linked residues, both of which failed to generate a non-glycosylated yeast-expressed protein.

Stability tests showed that the clinical grade batches of fusion protein appeared to be degraded after long-term storage at -80°C, but had not lost activity. This degradation may have occurred as a result of protease cleavage during the fermentation process, since MFECP contained a Kex2 protease cleavage site (Lys-Arg) located at the point of fusion between the antibody and enzyme. Removal of this site could potentially prevent partial degradation of the protein. The enzyme activity, 120 U/mg, was slightly lower than that recorded at the time of production (124 U/mg) (196), which was expected after long term storage. The fusion protein was also shown to be thermostable over 96 hr at 37°C.

The removal of sugars from glycoproteins is usually achieved by enzymatic or chemical methods. The main drawback of these methods is the lack of specific approaches to remove O-linked sugars. Previous studies identified N-linked glycosylations on the enzyme moiety of MFECP (137) as a result of yeast expression in *P. pastoris*, and O-linked glycosylations were believed to exist on the protein but this was not proven. Enzymes currently available for deglycosylation are only specific for the removal of N-linked glycosylations. These enzymes removed the N-linked glycosylations on MFECP at Asn/GlcNAc sites and detection with biotinylated Con A revealed the presence of a small, single band on the Western blot. A Con A column was used to check the glycosylation status of PNGase F- and EndoHf-treated MFECP and revealed an apparently non-glycosylated fusion protein since it eluted in the binding phase. The same occurred when the Con A column was used to check the glycosylation status of the genetically mutated CPG2 construct, CPG2_3Q. Thus, genetic substitution of the N-glycosylated sites meant that either O-linked glycosylations were absent on CPG2 or the O-linked glycosylations were short-chained branches that could not be distinguished by the Con A in the column. Nevertheless, it was certain that no N-glycosylations existed on CPG2_3Q since Con A primarily recognises α-mannose residues part of the N-glycan core structure, that is, residues arranged in a tri-mannosyl {Manα(1,3)[Manα(1,6)]Man} configuration (346) (347) (348) (16). As a result, the Con A column only verified the N-glycosylation status of enzyme-treated MFECP and CPG2_3Q but not the overall glycosylation status. Furthermore, the rapid blood clearance of CPG2_3Q (compared to non-glycosylated bacterial CPG2) *in vivo* proved that the CPG2_3Q remained glycosylated, and thus the absence of N-glycosylations were insufficient to halt the enhanced clearance of the enzyme by the mannose receptors in the liver. By 5 hr CPG2_3Q and bacterial CPG2 had cleared from the circulation at 1.12 and 38.6 % injected enzyme activity/g, respectively. Previous clearance studies showed that by 6 hr 13 and < 0.004 % injected enzyme activity/g of bacterial CPG2 (136) and *P. pastoris*-expressed MFECP (138), respectively, remained in the circulation.

The FPLC profile of CPG2_3Q presented a skewed Gaussian-shaped peak, which indicated partial dimerization, perhaps resulting from an improperly folded protein. Since CPG2 naturally dimerises non-covalently, the N-linked mutation on residue Asn-264 may have impeded the complete dimerisation of CPG2_3Q. This was

supported by the fact that the Asn-264 residue in MFECP was not glycosylated because it appeared to be an important residue involved in dimerisation and enzyme activity (342). Besides, Springer and colleagues (342) showed that mutation of all 3 N-glycosylation sites in CPG2 led to recovery of the enzyme's activity and affinity for the prodrug.

The presence of O-linked glycosylations, which occupy the Ser/Thr residues upon post-translational modification in *P. pastoris*, was addressed separately. O-linked glycosylations are less easy to categorise and there is no specific enzyme to cleave O-linked glycosylations, like there is for N-linked glycosylations. Thorpe and colleagues (349) (350) were first to mention the removal or modification of glycosylation on the ricin immunotoxin in order to improve the retention of the protein in circulation and preventing hepatic clearance. Chemical methods for O-deglycosylation include alkaline hydrazinolysis, trifluoromethanesulfonic acid and alkaline borohydride for β-elimination, which are used to liberate oligosaccharides from the protein. These are not specific and usually require very high or low pH conditions, which can lead to loss of protein structure and enzyme activity. Chemical treatments are usually ideal for detecting the presence and residue location of glycosylations in mass spectrometry (MS) analysis. To improve the tumour-to-blood ratios in ADEPT, Houba *et al*. (151) reported the complete deglycosylation of the human enzyme, β-glucuronidase, by treatment with sodium periodate and sodium borohydride. Recovery of enzyme activity was 95% and the antibody-enzyme conjugate cleared slower than the glycosylated conjugate.

In an attempt to remove the potential O-linked glycosylations on CPG2_3Q, the DNA sequence was rationally mutated on 12 surface Ser/Thr residues, creating CPG2_3Q_12A. Unfortunately, these mutations proved detrimental to the protein's enzyme activity. This was probably caused by the mutations, such that, too many residues were mutated, the wrong residues were mutated, alanine was used for all substitutions, and/or the lack of residues to glycosylate by *P. pastoris* led to improper protein folding. Alanine is the smallest hydrophobic amino acid and using this residue to replace otherwise larger, polar amino acids may have caused difficulties in proper folding of the protein. Indeed, glycosylation in yeast aids in the proper folding and expression of proteins, such that many proteins do not fold properly when

unglycosylated, and instead aggregate (351) (352) (353). Protein O-glycosylation has roles in modulating the function of secretory proteins by enhancing their stability and solubility and affording protection from degradation by proteases (354). In filamentous fungi, protein O-glycosylation contributes to proper maintenance of fungal morphology, development and differentiation (355).

In a second attempt to remove the O-glycosylations from CPG2_3Q, MS analysis was used to identify the residues that were glycosylated. MS is a valuable tool for analysing protein modifications, and is being increasingly used in glycoproteomics (356) to, 1) distinguish and identify glycosylated protein and peptides, 2) determine the N- and O-glycosylation sites and the degree of occupancy, and 3) analyse the structures of the attached glycan moieties (357) (358) (359) (360) (361). MS analysis revealed 10 O-glycosylated Ser/Thr sites to potentially mutate. Interestingly, only 3 of the 10 experimentally identified O-glycosylation sites were amongst the 12 predicted by NetOGlyc and neither of the definitively ascribed T55 nor T57 were amongst the 3 sites predicted by both approaches. With the O-glycosylated residues identified, the substituting residues were predicted, this time, taking into account the sites of occupancy within the protein molecule.

Interestingly, in computer-modelling of the bacterial CPG2 crystal structure, it became clear that the orientation of some of the residues may have shifted as a result of glycosylation processing, which doesn't exist in bacteria. For example, S245 on CPG2_3Q, which was found to be O-glycosylated in *P. pastoris*, appeared to be buried in bacterial CPG2. This was probably because the protein had to accommodate for the glycan chains and therefore would have folded in a different orientation. Furthermore, this residue is located at the dimerization interface, which may explain the reduced enzyme activity observed for glycosylated *P. pastoris*-expressed MFECP and CPG2 compared to the non-glycosylated bacterial CPG2 (~ 600 U/ml, reported by Mologic Ltd). In fact, studies have clearly demonstrated that glycosylation can impact enzyme catalysis (362) (363). For example, Grinnell and colleagues found that elimination of the glycosylation sites on various glycoforms of the antithrombotic serine protease human protein C (HPC), by site-directed mutagenesis, led to an increase in the catalytic rates (Kcat) without apparent changes

in substrate binding affinities (KM) (364). Similar findings have been found with other proteins (365) (366) (367).

The codon-optimised mCPG2_3Q from Mologic Ltd was more amenable to genetic manipulation and has resulted in a higher enzyme activity when expressed in *P. pastoris* compared to CPG2_3Q constructed from the original bacterial plasmid sequence in-house. The T55/T57 mutated constructs were, therefore, cloned into mCPG2_3Q gene sequence and the T55V mutant, which possessed the highest enzyme activity in shake flask cultures, was taken forward for large-scale production. The success of the genetic manipulation led to the production of two T55_T57 double mutants. Asn was chosen for the T55V_T57**N** mutant because of its size and polar nature which is similar to threonine. Valine was chosen for T55V_T57**V** simply because of the success with T55V, alone. Unfortunately, the enzyme activity of CPG2 was further reduced by the extra mutations, although the protein yield was high when expressed in yeast. Conservation analysis of the CPG2 sequence revealed T55 and T57 to be highly conserved residues, which may be the contributing to the reduced enzyme activities of the double T55_T57 mutants in relation to the singly mutated T55V construct and, subsequently, the reduced enzyme activity of this mutant in relation to mCPG2_3Q. Conservation grades for the N-linked residues, Asn-222, -264 and -272, are 1, 9 and 3, respectively (9 indicates a highly conserved residue). This clearly explained the reason for glycosylation occurring on Asn-222 and -272, but not -264 when CPG2 is expressed in *P. pastoris*.

The major advantage of using a yeast expression system is the ease of protein production, including shorter process times and high production yields, especially of recombinant mAbs and mAb fragments (368). *P. pastoris* glycosylation processing is not complex in the type of glycan structures or patterns it forms, like in mammalian cells, but rather the challenge is determining the site and occupancy of O-linked glycosylation on a single residue. Bacterial protein expression systems are popular because bacteria are easy to culture, grow fast and produce high yields of recombinant protein. However, multi-domain eukaryotic proteins expressed in bacteria are often non-functional because the cells are not equipped to accomplish the required post-translational modifications and molecular folding. Also, many proteins may be expressed as insoluble aggregates in inclusion bodies and are often

difficult to recover without harsh denaturants and subsequent cumbersome refolding procedures. For example, bacterial expression of MFECP was previously shown to generate impractically low yields (136) (195). Mammalian expression systems usually produce functional protein, but the yield is low, cost of production is high and mammalian cell culturing is time-consuming. Nevertheless, their comprehensive post-translational processing machinery results in glycosylation patterns suitable for clinical use and different to those in *P. pastoris*, so potentially, will not bind to the mannose receptors in the liver.

Approaches to deglycosylate proteins produced in *P. pastoris* have principally focused on N-glycosylation, which exhibits an organised post-translational pattern. Strategies have included: glycosylation inhibitors, for example, tunicamycin, which has previously been used to block N-linked glycosylation on CPG2 in mammalian cells (342); and N-linked glycoengineering in *P. pastoris* by inactivation and/or over-expression of certain enzymes (369) (370) (371) (372) (373). Characterisation and removal of O-linked glycosylations in *P. pastoris* in this manner have been more difficult to achieve. Until very recently, only inhibitors of the protein O-mannosyltransferase (pmt) enzyme had been employed as a means to inhibit O-linked glycosylation in *P. pastoris, S. cerevisiae* and the protease-deficient yeast strain, *Ogataea minuta* (374) (375). A means to reduce non-desirable mannose O-glycosyations would be to genetically engineer yeast *P. pastoris*. A recent paper identified and characterised the protein-O-mannosyltransferase (PMT) gene family in *P. pastoris* and demonstrated how O-glycosylation in *P. pastoris* could be manipulated by creating PMT-knockout strains and/or using PMT inhibitors (376). The authors noted the importance of O-mannose chain-length in addition to the overall extent of glycosylation. For example, it was found that PMT1 and PMT2 knockouts led to significantly reduced O-glycosylation on the expressed protein, which correlated with a decrease in O-glycan occupancy from 20 to 3-4 moles of glycan per mole of protein (376).

Other strategies, which do not involve removal of glycosylation, instead focus on slowing clearance of the fusion protein by using blocking reagents (377); and/or increasing circulation time of the protein by polyethylene glycol (PEG) modification, or FcRn-mediated recycling (378) (379). Mannan, which blocks the mannose

receptors in the liver, increased blood enzyme levels in mice by 200-fold 5 hr-post administration of MFECP, compared to MFECP alone (196). PEG-modification of bacterial β-glucuronidase was investigated in order to improve the stability and pharmacokinetics of antibody-β-glucuronidase conjugates in ADEPT (209). PEGylated conjugates exhibited greater tumour uptake and decreased normal tissue binding of antibody-β-glucuronidase conjugates. Although, more than 3 PEG molecules were found to affect enzyme activity, the antibody-enzyme conjugate was stable in serum regardless of PEG modification.

## 3.4   Summary

This Chapter proposed that the current ADEPT system could be modified in order to improve the pharmacokinetics of ADEPT in a 3-phase treatment system. In principle, a non-glycosylated fusion protein would slow clearance of the fusion protein from blood resulting in increased enzyme retention in the tumour. To this end, the use of deglycosylating enzymes was too expensive and was effectively limited to the removal of N-linked glycosylations on MFECP. Genetic manipulation of the N-linked glycosylated residues on CPG2 generated a functionally active protein (CPG2_3Q) upon expression in *P. pastoris*. However, its rapid clearance *in vivo* suggested the presence of O-linked glycosylation. Mass spectrometry revealed 10 O-linked residues in CPG2_3Q, of which, 2 (T55 and T57) were definitively ascribed. Various mutated constructs were generated, with T55V exhibiting the highest activity. The success of this mutant led to the creation of the double mutated constructs, T55V_T57N and T55V_T57V, both of which exhibited lower enzyme activities compared to T55V. T55 and T57 were found to be highly conserved residues, and thus proved that the removal of *P. pastoris* O-linked glycosylation on CPG2 is challenging.

University College London

# CHAPTER 4

Pharmacokinetic and Pharmacodynamic Challenges of Antibody-Directed
Enzyme Prodrug Therapy (ADEPT)

Carima Andrady

# 4 Investigating the DNA Damage Response to ADEPT

## 4.1 Introduction

It is believed that certain DNA damage response mechanisms play a role in the lack of effective therapeutic benefit after one cycle of ADEPT. In mice bearing colorectal carcinoma xenografts, a single therapy dose of MFECP followed by the ZD2767P prodrug led to a short-lived tumour response, whilst repeat dosing led to sustained tumour regression (138). This implies that a single treatment with ADEPT does not result in tumour eradication. However, multiple cycles of treatment are likely to invoke an immune reaction against CPG2 leading toxicity (380) and induce drug resistance. Immunosuppression is also not an ideal solution (381).

Early ADEPT studies indicated that potent DNA interstrand cross-links (ICLs) are induced following successful prodrug-to-active drug conversion *in vitro*, *in vivo* and clinical biopsies (242) (246) (139). Initial repair of these ICLs, by unhooking, was found to take place over time post-ADEPT (246), however the occurrence of other or downstream DNA repair processes was not indicated. It is proposed that DNA damage repair processes, in addition to ICL unhooking, are occurring in response to a single cycle of ADEPT and contributing to the low therapeutic efficacy.

### 4.1.1 Aims and Objectives

The aim: to investigate the formation of and response to DNA damage following a single cycle of ADEPT *in vitro* and *in vivo*. The objectives:

1. To determine the growth inhibitory effect of ADEPT on antigen-positive and antigen-negative cancer cell lines.
2. To measure the formation and initial repair of DNA ICLs.
3. To measure the γ-H2AX response.
4. To determine the RAD51 response.

## 4.2    Results

### 4.2.1    Growth inhibition studies: Determining the effect of ADEPT on cell proliferation

The growth inhibitory effect of a single cycle of ADEPT was tested on CEA$^{+ve}$ (SW1222) and CEA$^{-ve}$ (A375M) cell lines. The SRB assay was performed to determine the concentration of prodrug required to inhibit the growth of cells by 50% following conversion to the active drug by the localised antibody-enzyme fusion protein, MFECP. The cells were incubated with 0.1 U/ml MFECP for an hour followed by the ZD2767P prodrug at various concentrations for another hour and subsequently incubated in drug-free media for 96 hr, as described in Section 2.2.4.1. The MFECP concentration was chosen based on previous studies conducted by Monks (382), who showed that 0.1 U/ml of CPG2 was sufficient for maximal ZD2767P activation within 1 hr incubation. The cells were fixed and stained with SRB - a bright pink aminoxanthene dye with two sulphonic acid groups, which under mildly acidic conditions binds electrostatically to basic amino acid residues of proteins in fixed cells. Figure 4.1 revealed a mean GI$_{50}$ of 0.12 ($\pm$0.03) $\mu$M prodrug for SW1222 cells, although growth inhibition was initiated at prodrug concentrations > 0.03 $\mu$M. For CEA$^{-ve}$ A375M cells (Figure 4.2), growth inhibition was apparent but the effect was observed with a greater concentration of prodrug, that is, mean GI$_{50}$ 0.55 ($\pm$0.06) $\mu$M. This was more than 5 times higher than the GI$_{50}$ value for ADEPT-treated SW1222 cells. These results demonstrated the highly specific nature of the enzyme for the prodrug, and furthermore that prodrug was activated and conversion to the active drug has a growth inhibitory effect on the cells. However, it is likely that due to the nature of the *in vitro* protocol, in which the prodrug was added directly to the fusion protein, residual unbound fusion protein was contributing to growth inhibition, as demonstrated by the non-antigen-specific A375M cells.
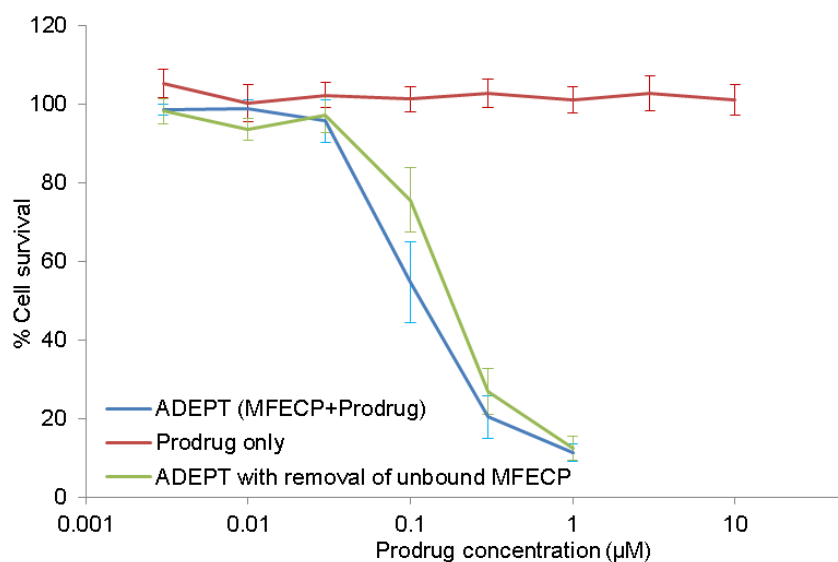
**Figure 4.1 *In vitro* growth inhibition in CEA-expressing SW1222 cells treated with a single cycle of ADEPT**

SW1222 cells were treated with 0.1 U/ml MFECP for 1hr followed by various concentrations of the prodrug for 1 hr. Cells were then incubated in drug-free media for 96 hr and treated with SRB. For the graph indicated in green, fusion protein was removed from the media prior to adding the prodrug. (mean ± SEM).
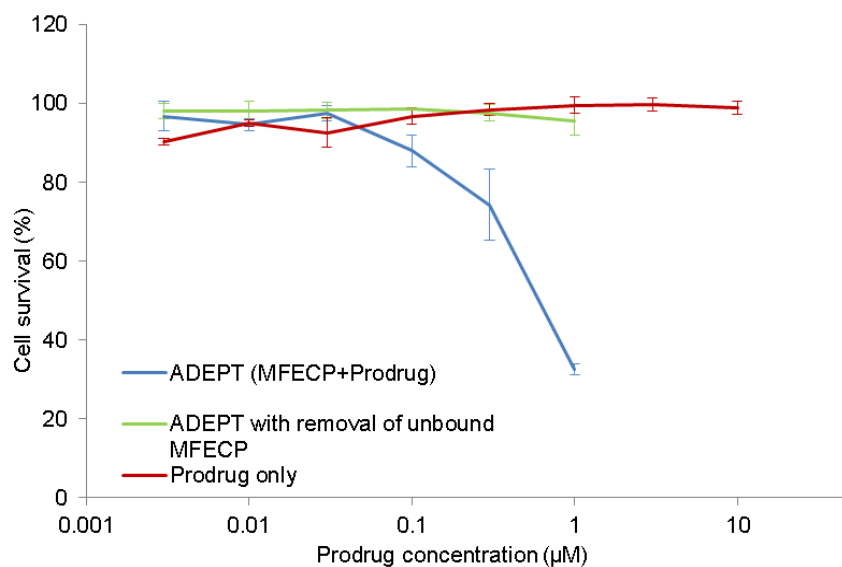


**Figure 4.2 *In vitro* growth inhibition in non-CEA-expressing A375M cells treated with a single cycle of ADEPT**

A375M cells were treated with 0.1 U/ml MFECP for 1hr followed by various concentrations of the prodrug for 1 hr. Cells were then incubated in drug-free media for 96 hr and treated with SRB. For the graph indicated in green, fusion protein was removed from the media prior to adding the prodrug. (mean ± SEM).

In view of this, the protocol was adapted accordingly. Growth inhibition was evaluated on cells that had been washed of excess MFECP prior to prodrug addition. The effect of growth inhibition caused by ADEPT on SW1222 cells was the same whether or not residual fusion protein is removed prior to prodrug (Figure 4.1). The only difference was the mean $GI_{50}$ was greater, at 0.19 ($\pm$0.03) $\mu$M, when the unbound fusion protein was removed. When the same protocol was applied to A375M cells, no growth inhibitory effect was observed. This clearly demonstrated the highly specific targeting effect of ADEPT provided by the anti-CEA antibody. Thus, although the fusion protein did not bind to the cells, its presence in the media still rendered it active towards the prodrug, unless it was removed. This could be a potential problem *in vivo* if the fusion protein is not permitted to clear from the blood and healthy tissues prior to prodrug administration.

The prodrug and fusion protein were also tested individually in order to verify that these components on their own did not have a growth inhibitory effect on the cells. The fusion protein did not have any effect on the cells and was similar to that of non-treated cells. Prodrug alone also showed no growth inhibitory effect on the cells up to 10 $\mu$M. However, there was a growth inhibitory effect on cells at prodrug concentrations >10 $\mu$M, as shown in Figure 4.3. Interestingly, the effect in SW1222 cells was greater than in A375M cells, with a mean $GI_{50}$ of 27 ($\pm$6.75) $\mu$M and 96 ($\pm$12.12) $\mu$M, respectively.
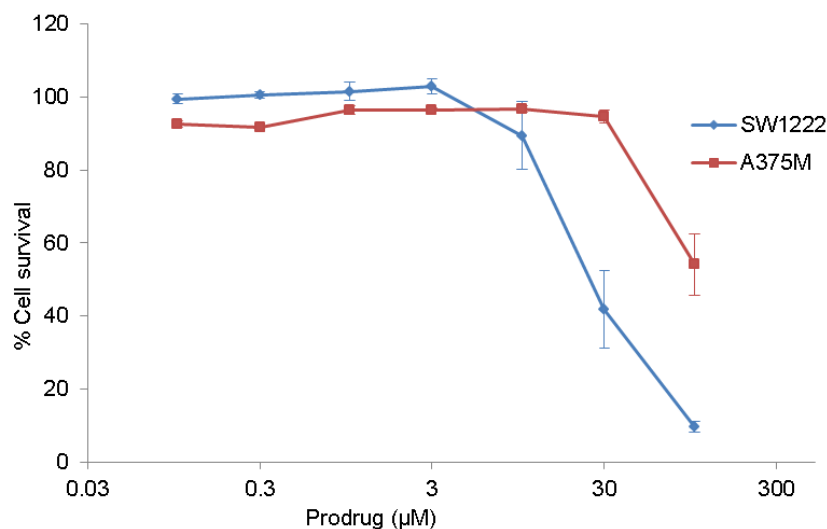
**Figure 4.3** ***In vitro*** **growth inhibition in CEA- and non-CEA-expressing cells treated with prodrug only**

SW1222 and A375M cells were treated various concentrations of prodrug for 1 hr, incubated in drug-free media for 96 hr and then treated with SRB. (mean ± SEM).

## 4.2.2 DNA ICL damage by ADEPT

The modified single-cell gel electrophoresis assay, also known as the comet assay, was originally developed to measure strand breaks, and has been adapted to measure interstrand cross-linking and repair (383) (384). The comet assay uses X-ray irradiation to introduce a fixed level of random DNA strand breaks in the cells. The strand breaks migrate in an electrophoretic field depending on the presence (and extent) of interstrand cross-linking. The extent of DNA damage is quantitated by image analysis to produce a tail moment, defined by Olive *et al.* (385). The method is described in more detail in Section 2.2.4.2. Examples of the typical comet images were taken, where each orange sphere represents a single cell-containing DNA (Figure 4.4).
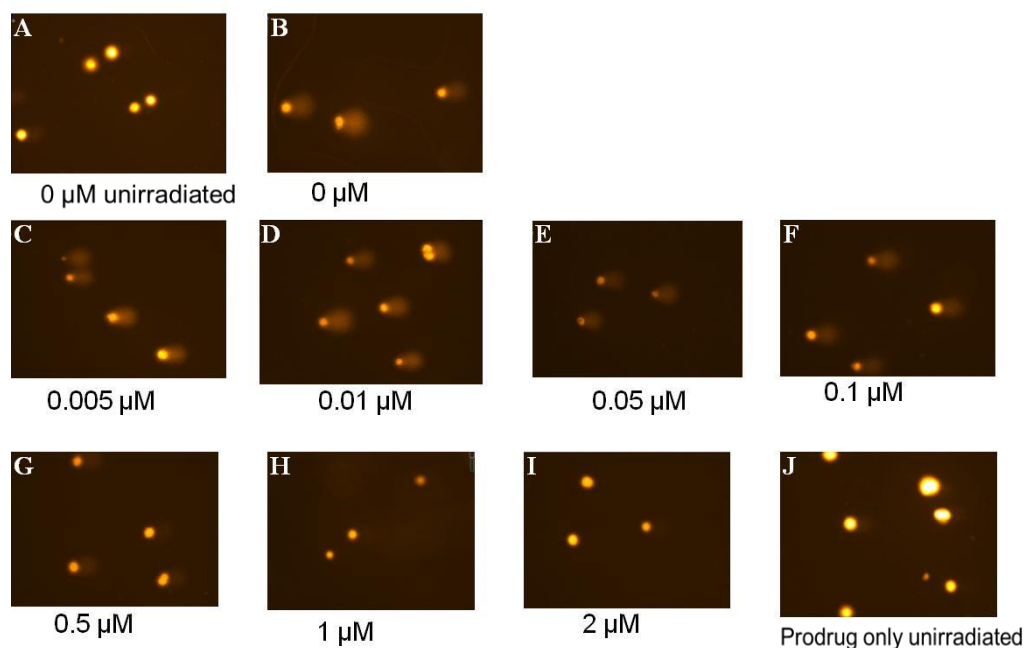
**Figure 4.4 Typical comet images of SW1222 colorectal carcinoma cells treated with increasing concentrations of the ZD2767 prodrug**

(A) Non-ADEPT-treated, unirradiated tumour cells. After irradiation (17.5 Gy) of non-ADEPT-treated tumour cells, distinct comets were observed (B). ADEPT-treated, irradiated tumour cells (C-I) were exposed to 0.1 U/ml MFECP for 1hr followed by 0.005-2 µM prodrug for 1 hr. (J) Prodrug-only (2 µM), unirradiated tumour cells. In all images nuclei were stained with propidium iodide. Original magnification, x20.

## 4.2.2.1 Measuring ICL formation and unhooking (initiation of repair) in vitro

A standard curve for X-ray irradiation dose in non-drug-treated SW1222 cells was performed to establish an optimum radiation dose (Gy) that produced satisfactory DNA strand break levels in the cells. Ideally, the dose should give a head-to-tail DNA ratio of approximately 1:1. An X-ray dose of 17.5 Gy was sufficient for all comet assay experiments. In untreated, unirradiated SW1222 cells no DNA damage was detected and the DNA remained intact, as shown in Figure 4.4 A. Following irradiation of cells with 17.5 Gy, the resulting shorter DNA fragments migrated from the bulk of the DNA during electrophoresis to produce the typical comet images (Figure 4.4 B).

Cells were treated with ADEPT following the *in vitro* protocol previously outlined for the growth inhibition assays and varying the prodrug concentration. When

ADEPT-treated cells were irradiated (Figure 4.4 C-I), comet tails were visible but with decreased length and intensity compared with irradiated untreated cells. The images showed that comet tail length is inversely proportional to prodrug concentration (Figure 4.4 C-I). The comet heads were larger and of greater intensity compared with the untreated irradiated cells (Figure 4.4 B) as a result of the retention of DNA by the prodrug-induced ICLs. The decrease in comet tail moment compared with untreated irradiated cells was used to quantitate the level of DNA ICLs formed upon treatment with ADEPT, as shown in the dose-response curve, Figure 4.5. The concentration of prodrug required to cause 50% cross-linking in SW1222 cells was 0.21 ($\pm$ 0.02) $\mu$M.
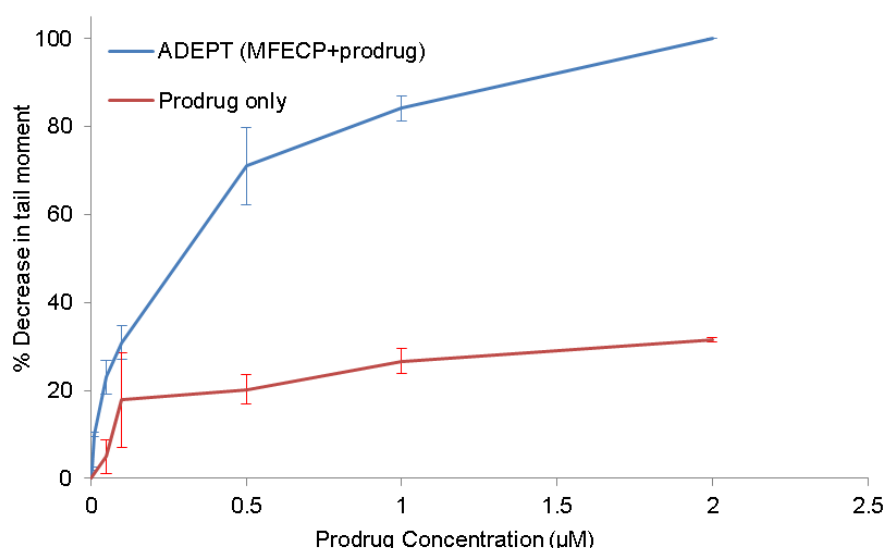


**Figure 4.5 Formation of ADEPT-induced DNA ICLs in SW1222 colorectal carcinoma cells**
Cells were treated with 0.1U/ml of MFECP for 1 hr followed by various concentrations (0-2$\mu$M) of prodrug for 1hr, and DNA ICLs measured using the comet assay. Results are expressed as percentage decrease in tail moment for 50 cells per experiment analysed (n = 3, mean $\pm$ SEM). Percentage decrease in tail moment is directly proportional to the levels of cross linking.

Prodrug alone did not induce single-strand breakage in unirradiated cells (Figure 4.4 J) and these cells showed similar profiles to the untreated cells (Figure 4.4 A). A dose response curve of irradiated prodrug-only-treated SW1222 cells is shown in Figure 4.5. The results indicated low-level cross-linking <30%, which appeared to correlate with the low toxicity seen in the growth inhibition assays up to 3 $\mu$M prodrug. However, at concentrations >3 $\mu$M, the formation of DNA ICLs steadily increased with increasing prodrug concentration but less than 50% cross-links were

formed at prodrug concentrations as high as 100 µM (Figure 4.6). To investigate the cross-linking effect of the prodrug over a longer incubation period, the prodrug was incubated with the cells for 3 hr, as opposed to 1hr. As shown in Figure 4.6, there was no difference in the formation of ICLs with increasing prodrug concentration over time, except by 3hr some ICLs may have repaired, as indicated by the lowered response. ICL formation in cells treated with only the fusion protein were comparable with the untreated cells, indicating that the fusion protein alone had no cytotoxic effect on the tumour cells.
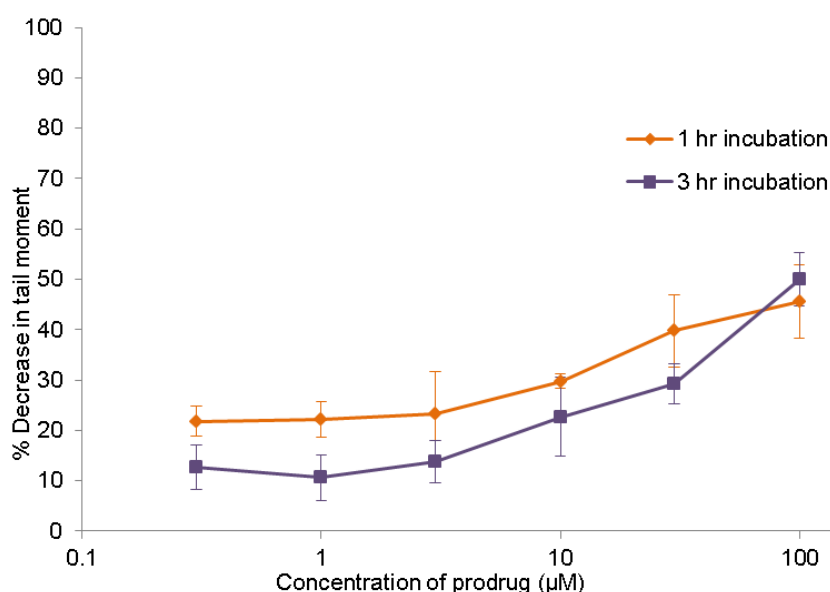


**Figure 4.6 *In vitro* formation of DNA ICLs produced by the prodrug alone in SW1222 colorectal carcinoma cells measured using the comet assay**

Cells were treated with 0.3-100µM prodrug for 1hr. Results are expressed as percentage decrease in tail moment for 50 cells per experiment analysed (mean ± SEM).

Next, the time course of ICL formation and repair was assessed in SW1222 cells treated with ADEPT using 0.25 µM prodrug, which was previously shown to generate > 50% cross-links. ICLs were found to form rapidly following ADEPT treatment, peaking at 1hr (Figure 4.7). This rapid increase was followed by an equally rapid reduction in ICLs by 4 hr. The decrease in level of ICLs at 48 hr (expressed as the % unhooking at 48 hr-post-ADEPT) was 72%. The experiment indicated that ICLs form immediately following ADEPT, and this most likely commenced during prodrug incubation (as indicated by the 40% cross-linking at 0

hr). Moreover, the data indicated that DNA damage repair occurred, albeit the initial stages of ICL repair, in colon carcinoma cells exposed to ADEPT.
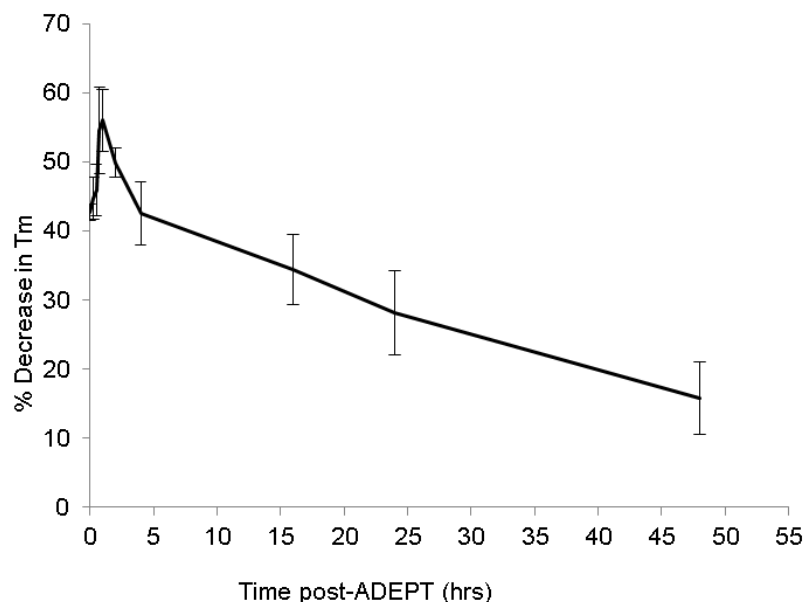


**Figure 4.7 DNA ICL formation in SW1222 cells over time post-ADEPT**

Cells were treated with ADEPT using 0.25 μM prodrug. After prodrug incubation the cells were incubated in drug-free medium and samples were taken at different time points over 48 hr. ICLs were measured using the comet assay. Results are the mean ± SEM of 50 cells from 3 independent experiments.

### 4.2.2.2  *Measuring ICL formation and unhooking (initiation of repair) in vivo*

ICL formation and unhooking was measured in response to a single-cycle treatment of ADEPT in cells isolated from SW1222 colon carcinoma xenografts and peripheral blood lymphocytes (PBLs) isolated from whole blood perfusions from mice. The mice were given 1000 U/kg MFECP followed by 70 mg/kg ZD2767P prodrug 6, 7 and 8 hr later. The tumours and blood were removed at 1, 3 and 24 hr post-treatment. This *in vivo* ADEPT protocol was followed according to that previously used by Sharma *et al.* (138) and is explained in Section 2.2.5.2.

The results from the comet assay are presented as irradiated and unirradiated comet tail moments in Figure 4.8 and Figure 4.9 for tumours and PBLs (respectively),

which were extracted from individual mice at different time points post-ADEPT (4 mice per time point). The presence of ICLs was indicated by a decrease in the irradiated tail moment of the ADEPT-treated samples compared to the untreated samples. (Note: tail moment is the product of the percentage DNA in the comet tail and the distance between the means of the head and tail distributions). As shown in Figure 4.8, at 1 hr-post-ADEPT there was a significant ($p<0.0001$) decrease in irradiated DNA tail moment compared to the non-treated, with a mean percentage reduction in tail moment of 100% ($\pm 4.00$) (using Equation 2.2, Section 2.2.5.2). This suggested, firstly, that ADEPT caused DNA damage in the form of DNA ICLs in the tumour cells *in vivo*, and secondly, that these ICLs formed rapidly. At 3 and 24hr-post-ADEPT, ICL formation persisted with statistically significant ($p<0.0001$) mean percentage reduction in tail moments of 72% ($\pm15.75$) and 55% ($\pm13.02$), respectively. This indicated that ICLs persisted over 24hr-post-ADEPT *in vivo*, and the fewer ICLs being formed at 24 hr implied that cross-links were being unhooked (statistically significant, $p<0.0001$). The unirradiated tail moment values indicated low level ICL formation, which may be background DNA damage in the tissues caused by various endogenous metabolic reactions.
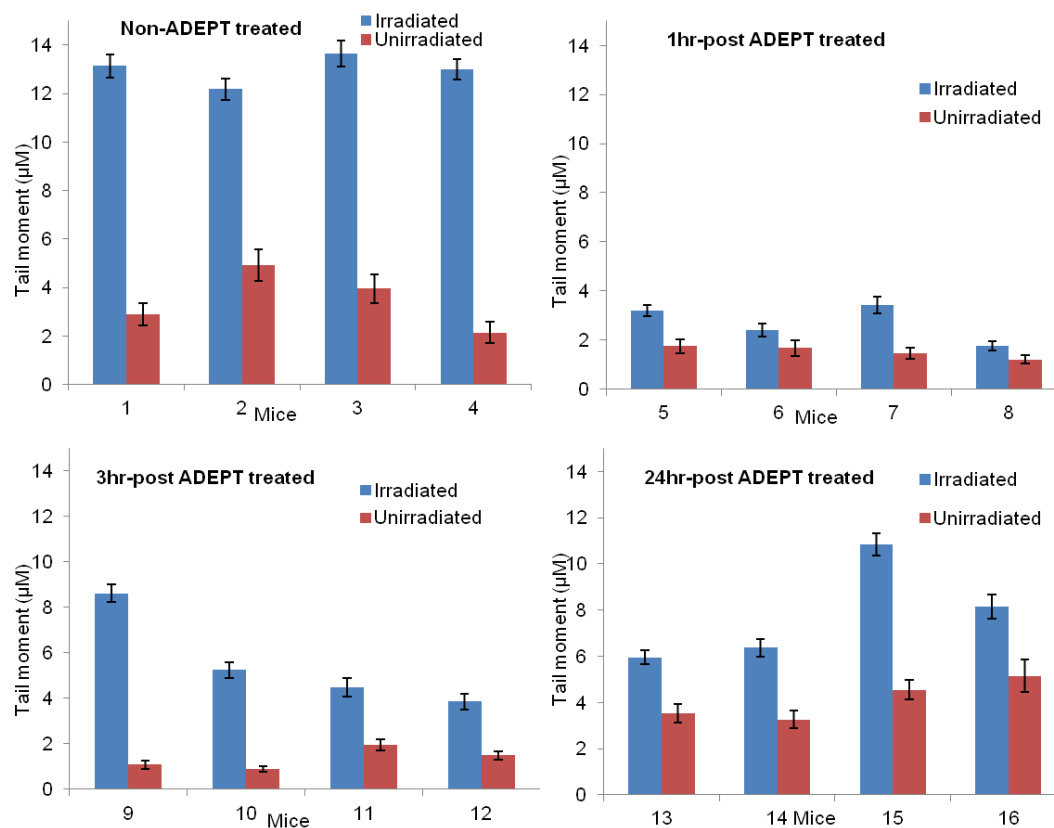
**Figure 4.8 DNA interstrand cross-linking in SW1222 xenograft tumour tissue**

Nude mice (4 per test group) bearing SW1222 tumours were injected (i.v.) with 1000 U/kg MFECP followed by 70 mg/kg ZD2767P (i.p.) at 6, 7 and 8 hr later. Tumours were excised at 1, 3 and 24 hr after the last prodrug dose, and processed immediately into single-cell suspensions. The study also included a non-ADEPT treated group. The cells were irradiated with X-rays at a dose of 17.5 Gy and ICLs were measured using the comet assay. Results are expressed as mean tail moment for 50 cells ± SEM per mouse, where the tail moment is inversely proportional to cross-linking. (Tail moment is the product of the percentage DNA in the comet tail and the distance between the means of the head and tail distributions).

Figure 4.9 illustrates the irradiated and unirradiated tail moment values for PBLs which came from the same mice whose tumour xenografts were examined in Figure 4.8. The tail moments for the PBLs in ADEPT-treated mice appeared to show few deviations from those of the PBLs in non-treated mice, with mean percentage reduction in tail moments of 17% (± 4.63), 6% (± 7.22) and 7% (±10.41) at 1, 3 and 24 hr-post-ADEPT, respectively. The large difference in cross-linking at 1 hr compared to 3 and 24 hr may have resulted from peripheral activation of the prodrug or accumulation of prodrug in certain areas. Data collected from the PBLs validated the principle of ADEPT *in vivo*, that is, site-specific activation of the prodrug.
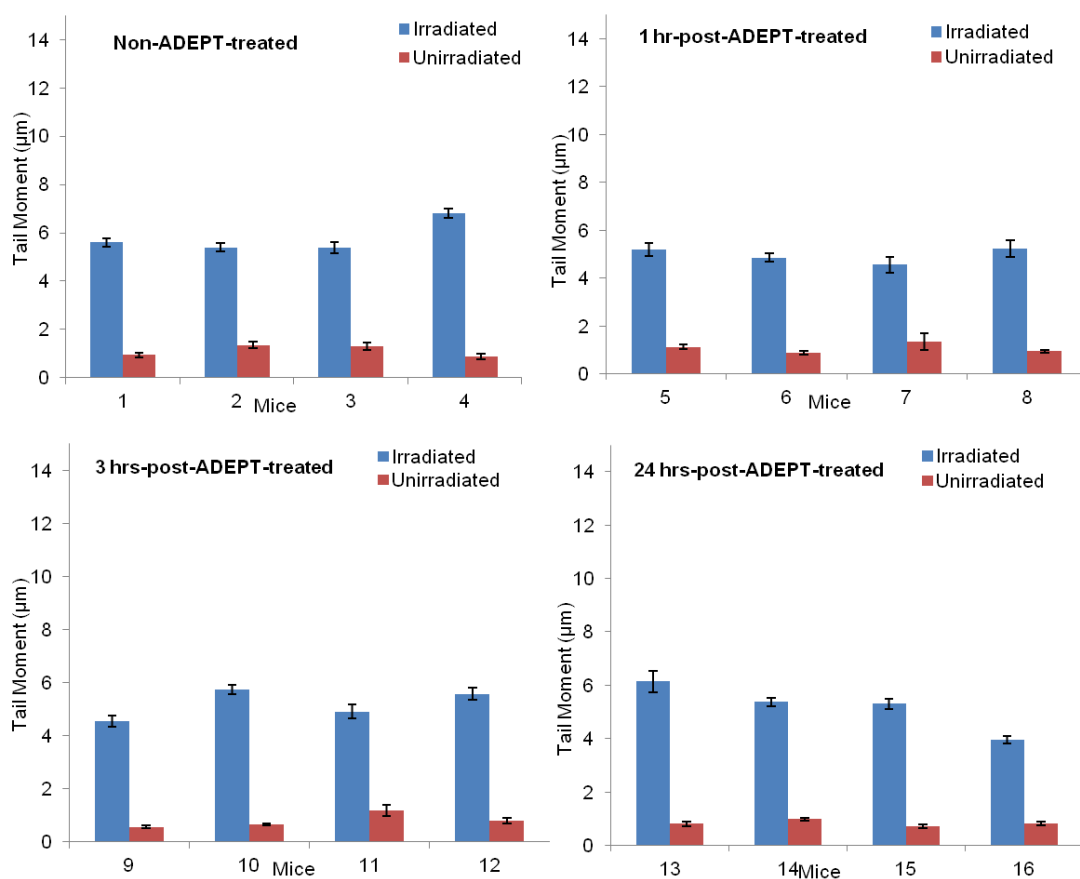
**Figure 4.9 DNA interstrand cross-linking in peripheral blood lymphocytes derived from ADEPT-treated mice bearing SW1222 tumour xenografts**

Nude mice (4 per test group) bearing SW1222 tumours were injected (i.v.) with 1000 U/kg MFECP followed by 70 mg/kg ZD2767P (i.p.) at 6, 7 and 8 hr later. Blood perfusions were collected at 1, 3 and 24 hr after the last prodrug dose, and processed immediately into single-cell suspensions. The study also included a non-ADEPT treated group. The cells were irradiated with X-rays at a dose of 17.5 Gy and ICLs were measured using the comet assay. Results are expressed as mean tail moment for 50 cells ± SEM per mouse, where the tail moment is inversely proportional to cross-linking. (Tail moment is the product of the percentage DNA in the comet tail and the distance between the means of the head and tail distributions).

## 4.2.3  The DNA damage response to ADEPT

To complement the findings of ICL unhooking *in vitro* and *in vivo*, phosphorylation of H2AX histone protein, that is, γ-H2AX, was measured following a single cycle of ADEPT. It has been reported γ-H2AX accumulates at sites of DSBs to form discrete

nuclear foci (308) (310). Since its discovery, γ-H2AX has been widely used as a highly sensitive, prognostic marker of DNA damage and has been clinically validated as a pharmacodynamic marker of DNA damage in response to ICL-inducing agents (320) (386) (338) (387).

### 4.2.3.1 *Measuring γ-H2AX foci formation in vitro*

Figure 4.10 shows a dose response of γ-H2AX foci in SW1222 cells was measured at 3 hr-post-ADEPT (blue) or prodrug alone (red). Briefly, cells were incubated with 0.1 U/ml fusion protein for 1 hr (or drug-free media for prodrug alone) followed by various concentrations of prodrug for 1 hr and incubated in drug-free medium for 3 hr. The cells were then trypsinised, fixed onto slides and incubated with an anti-γ-H2AX monoclonal antibody. Foci were detected when a fluorophore-conjugated antibody was applied and microscope images were acquired for counting. In the ADEPT-treated cells, the γ-H2AX response, which is defined as the average number of foci per cell, steadily increased with increasing prodrug concentration post-treatment. In the prodrug-only treatment a weak γ-H2AX response indicated low levels of DNA damage incurred, with an average number of foci per cell less than 2. Foci formation in cells treated with fusion protein alone were comparable with the untreated cells.
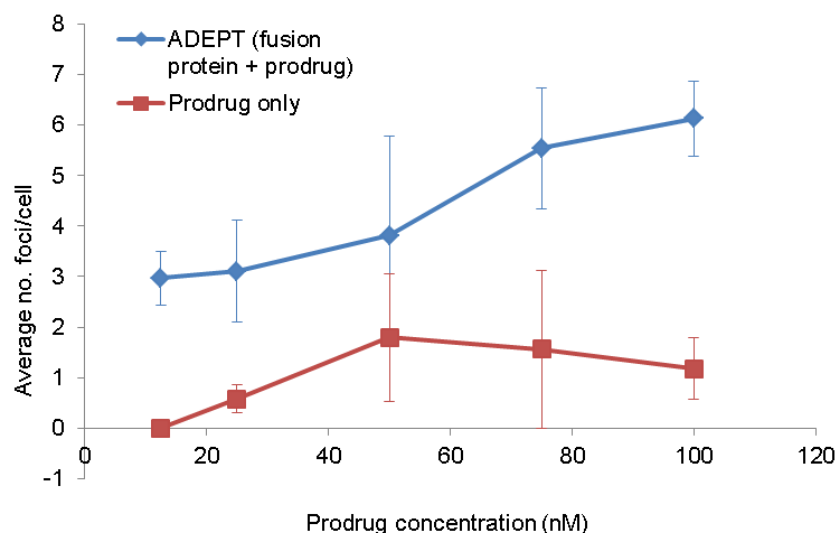
**Figure 4.10 Dose response of γ-H2AX foci in SW1222 cells following exposure to ADEPT (blue) or prodrug alone (red)**

Cells were incubated with fusion protein for 1hr followed by the prodrug for 1 hr at various concentrations (blue), or incubated with prodrug only (red). Following 3 hr in drug-free medium, the cells were trypsinised, fixed and stained with an anti-γ-H2AX antibody. 100 foci were counted per dose per experiment and normalised against foci in the non-treated cells (mean ± SEM).

In order to determine the persistence of γ-H2AX over time, foci formation was measured in cells post-ADEPT over 48 hr, as previously conducted with the comet assay. Representative images of γ-H2AX foci detected in SW1222 cells over time post-ADEPT are shown in Figure 4.11. This pattern is graphically represented as average foci per cell at the same time points in Figure 4.12. γ-H2AX foci induction clearly peaked at 3 hr-post ADEPT, although foci were present as early as 0-1 hr-post ADEPT, as shown in Figure 4.12. A weaker peak of induction followed at 16 and 24 hr-post treatment. The strong γ-H2AX response at 3 hr-post-ADEPT was found to lag behind the peak ICL formation by 2 hr, suggesting the recruitment of repair proteins at the site of DNA damage is stimulated by ICL-associated DSBs (320) (307) (306) (319). Furthermore, the rapid increase in foci formed by 3 hr was followed by a rapid decline to near-baseline levels by 8 hr, which probably indicated resolution of the intermediary DSBs by downstream repair pathways. The second γ-H2AX peak observed at 24 hr-post-ADEPT is thought to be linked to growth arrest of cells in G2 phase of the cell cycle (see Section 5).
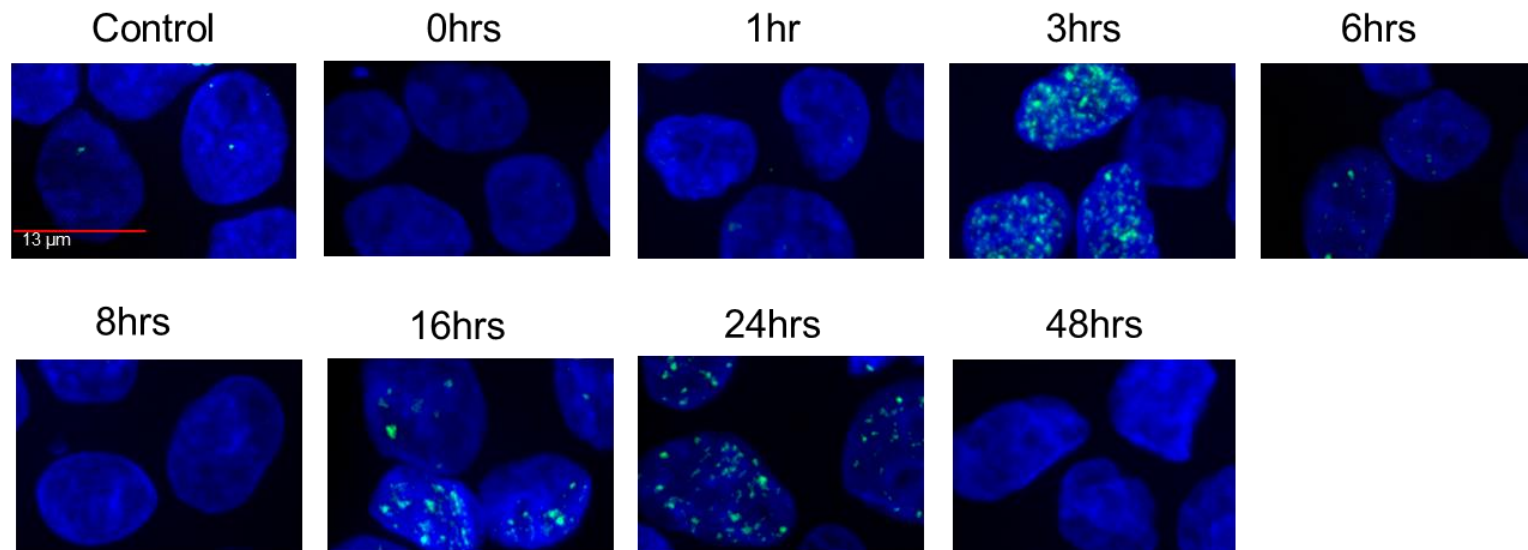
**Figure 4.11 Representative images of SW1222 cells showing γ-H2AX foci over time post-ADEPT**

Cells were treated with ADEPT using a prodrug concentration of 50 nM followed by post-incubation in drug-free medium for the times shown. Nuclei (blue) were stained with 4',6-diamidino-2-phenylindole (DAPI), and foci (green) were detected with an anti-γ-H2AX antibody/Alexa Fluor 488 fluorophore-conjugated antibody. Images were visualised with a Perkin Elmer Ultraview Spinning Disk Confocal, driven by Volocity Acquisition (63x oil immersion objective).
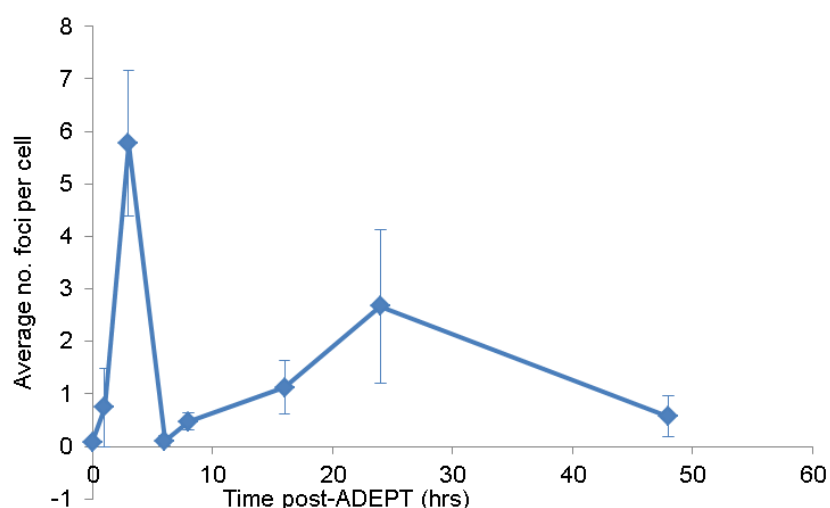
**Figure 4.12 γ-H2AX foci induction in SW1222 cells over time post-ADEPT**

Cells were incubated with the fusion protein for 1 hr followed by 50 nM prodrug for 1 hr and post-incubation in drug-free medium for the times shown. 100 foci were counted per time point per experiment and average foci per cell was normalised against non-treated cells. (mean ± SEM).

### 4.2.3.2. *Measuring γ-H2AX foci formation in vivo*

The versatile nature of the immunofluorescence assay allowed subsequent measurement of γ-H2AX foci in tumour cells and PBLs from immune-compromised mice bearing SW1222 xenografts treated with a single cycle of ADEPT (as previously mentioned in Section 4.2.2.2). Gamma-H2AX foci were detected at each time point post-ADEPT for each individual mouse (Figure 4.13). The background level of γ-H2AX foci in the non-treated tumour samples was less than 1 focus per cell. At 1hr-post-ADEPT the levels of foci were almost comparable to the control with a mean number of foci per cell (compared to the untreated) of 1.90 (±0.48). Gamma-H2AX foci formed increased at 3 hr and 24 hr-post-ADEPT, with mean number of foci per cell 4.03 (±0.50) ($p<0.0001$) and 6.75 (±0.49), respectively. This pattern demonstrated that a DNA damage response formed and persisted over time in response to ADEPT-induced DNA damage. Furthermore, the γ-H2AX response increased relatively rapidly, doubling in foci formation, between 1 and 3 hr-post-ADEPT. This suggested a very active period of time during which repair proteins likely accumulated at the site of DNA damage *in vivo*.
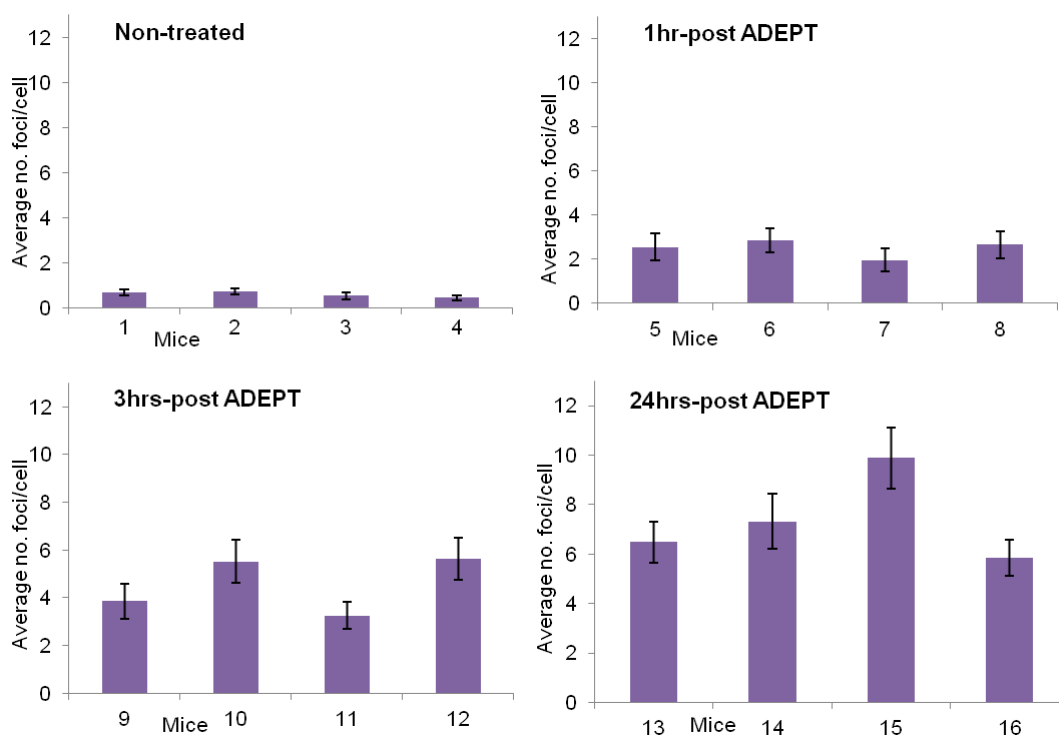
137

**Figure 4.13 γ-H2AX response in ADEPT-treated SW1222 tumour xenografts**

Gamma-H2AX foci were detected and quantified in colorectal carcinoma tumour cells by immunofluorescence using a biotin conjugated anti-γ-H2AX antibody/Alexa Fluor 488 conjugated streptavidin. Tumours derived from the previously described *in vivo* study where mice were treated with ADEPT and tissues excised at 1, 3 and 24 hr after the last prodrug dose. (100 cells were counted per mouse ± SEM).

Figure 4.14 represents the γ-H2AX response in PBLs analysed at various time points post-ADEPT in mice. The levels of foci formed at each time point changed relatively little compared to the untreated tumour cells, with mean foci per cell (compared to the untreated) 0.12 (±0.16), 0.85 (±0.15) and 1.61 (±0.32) at 1, 3 and 24 hr-post-ADEPT, respectively. Although the response is low compared to the tumours, detection of foci probably indicated presence of peripheral damage caused by activation of prodrug or accumulation of inactivated prodrug.
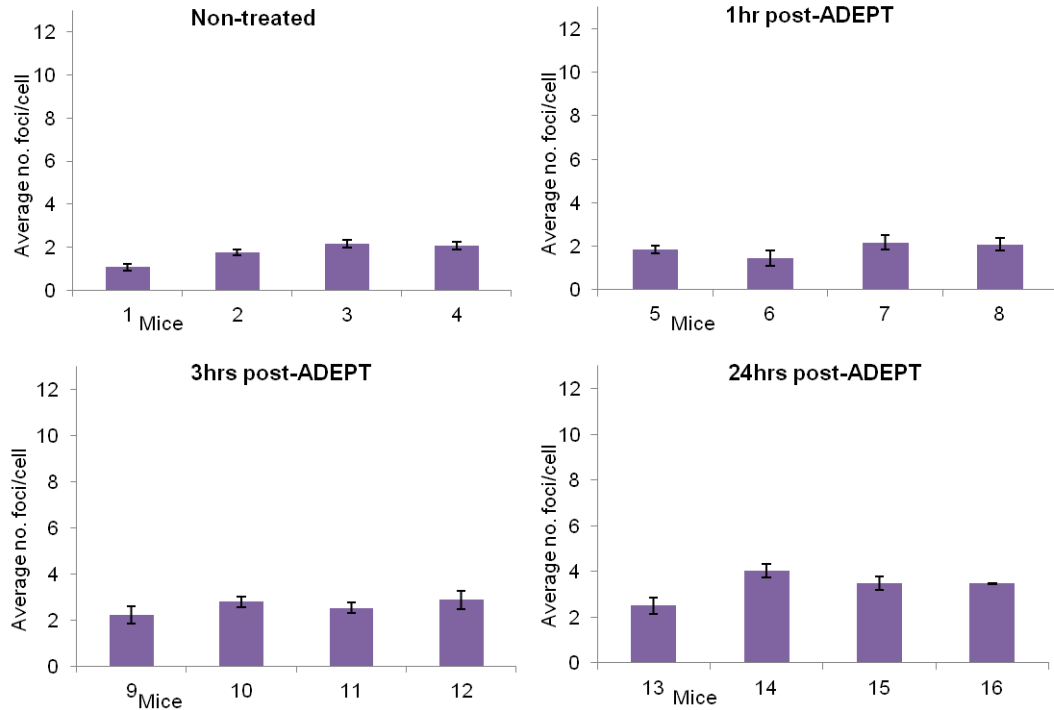
**Figure 4.14 γ-H2AX response in peripheral blood lymphocytes (PBLs) derived from ADEPT-treated mice bearing SW1222 tumour xenografts**

Gamma-H2AX foci were detected and quantified in PBLs by immunofluorescence using a biotin conjugated anti-γ-H2AX antibody/Alexa Fluor 488 conjugated streptavidin. PBLs derived from the previously described *in vivo* study where mice were treated with ADEPT and tissues excised at 1, 3 and 24 hr after the last prodrug dose. (100 cells were counted per mouse ± SEM).

## 4.2.4 DNA damage repair: Is there a role for homologous recombination (HR) following ADEPT?

To determine whether HR was involved in the later stages of ICL repair, RAD51 response was measured by immunofluorescence in the same way as previously described in Section 4.2.3. In humans, RAD51 is a 339-amino acid protein and is the essential initiator of the HR repair pathway, which is responsible for mediating error-free repair of DSBs (388). RAD51 protein forms nuclear complexes in the form of microscopically-detectable foci in response to ionising radiation and DNA damaging agents. It is these foci which are thought to represent sites where repair takes place (328) (389).

In SW1222 cells the RAD51 response was marked at 6 hr-post-ADEPT followed by a smaller peak of induction at 24 hr (Figure 4.15). The 6-hr peak observed here followed the γ-H2AX response peak at 3 hr, and suggested that repair by HR occurred in response to ADEPT-induced ICL damage. In addition, the data is supportive of the formation of DSBs as intermediates during ICL repair. The second wave of foci induction is probably linked to the γ-H2AX peak also observed at 24 hr and may indicate repair occurring during later stages in the cell cycle.
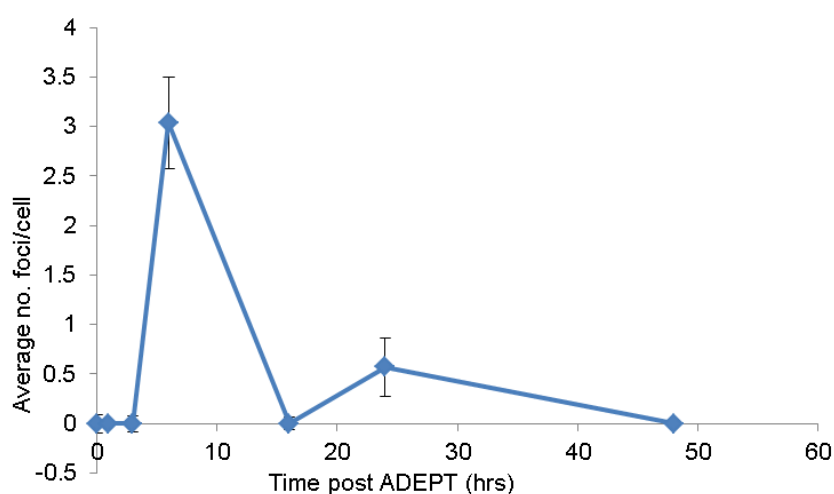


**Figure 4.15 RAD51 foci induction in SW1222 cells over time post-ADEPT**
Cells were incubated with the fusion protein for 1 hr followed by 50 nM prodrug for 1 hr and post-incubation in drug-free medium for the times shown. Cells were fixed and stained with anti-RAD51 antibody followed by an Alexa Fluor conjugated antibody. Results are mean of 100 foci counted per time point (mean ± SEM).

When RAD51 foci were measured in SW1222 colorectal carcinoma xenografts, there was no clear pattern in response to ADEPT-induced damage (Figure 4.16), in contrast to that seen *in vitro*. There was a difference in foci levels between the non-treated and treated tumour samples, however mean foci per cell per time point post-ADEPT was relatively equal, that is 5.5 (±0.33), 5.4 (±0.33) and 5.4 (±0.33) at 1, 3 and 24 hr, respectively. This was probably because peak of induction *in vivo* was missed if it had occurred between 3 and 24 hrs-post ADEPT. Besides, the presence of detectable foci at each time point varied between the mice per time point and this variation was more evident at 24 hr, which could suggest varied rates of DSB repair.
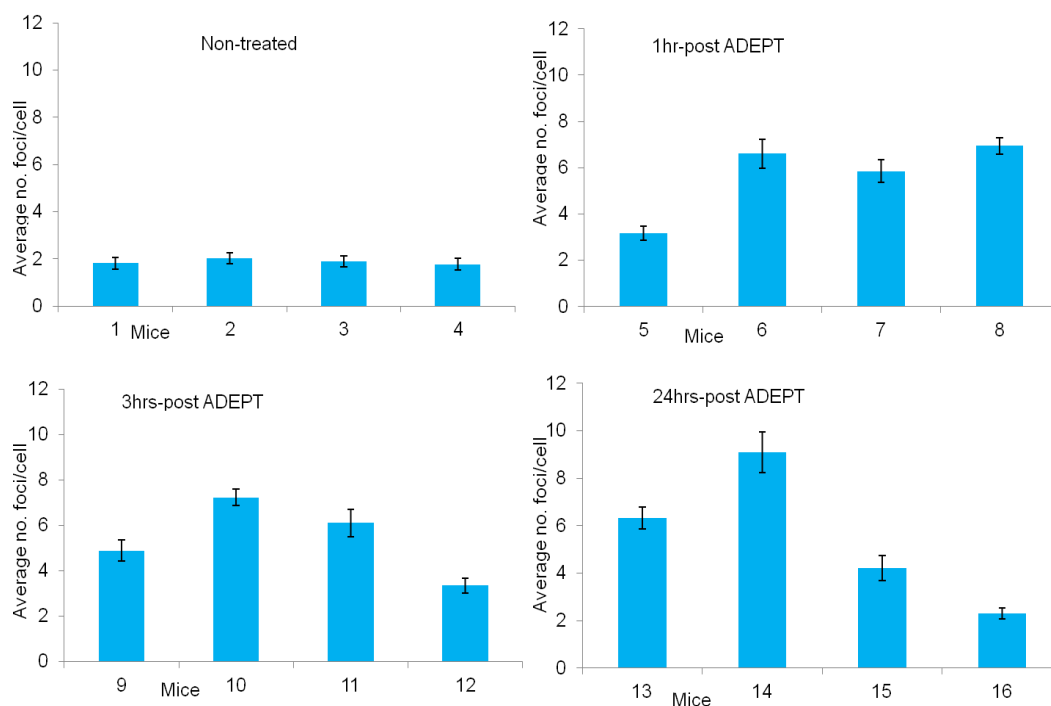
**Figure 4.16 RAD51 foci measured in ADEPT-treated SW1222 tumour xenografts**

RAD51 foci were detected and quantified in colorectal carcinoma tumour cells by immunofluorescence using an anti-RAD51 antibody and Alexa Fluor 488 conjugated secondary antibody. Tumours derived from the previously described *in vivo* study where mice were treated with ADEPT and tissues excised at 1, 3 and 24 hr after the last prodrug dose. (100 cells counted per mouse ± SEM).

## 4.3    Discussion

The work detailed in this Chapter contributes to the understanding of the processes involved in DNA damage formation and repair in response to a single cycle of ADEPT in colon carcinoma SW1222 cells *in vitro* and *in vivo*. Studies showed that the cytotoxicity of ADEPT is the result of potent DNA damage lesions, that is ICLs. Experimental work investigating the γ-H2AX response in ADEPT-treated cells suggested the importance and complexity of DNA repair mechanisms. The cellular and DNA damage response following ADEPT were evaluated.

The effect of ADEPT on tumour cell proliferation was assessed using the SRB assay, which revealed a $GI_{50}$ of 0.12 μM and 0.55 μM in colorectal carcinoma and melanoma cell lines, respectively. This correlated well with previously reported $GI_{50}$

values for ADEPT using the ZD2767P prodrug, which were found to be 0.04-2.2 μM in colorectal tumour and non-small cell lung cancer (NSCLC) cell lines (247) (246). These were relatively cytotoxic $GI_{50}$ concentrations in comparison to other nitrogen mustard drugs, such as chlorambucil (26 μM LS174T cells, 79 μM LoVo cells) (247), melphalan (~50 μM LoVo cells) (270) and a monofunctional analogue of ZD2767 (18-38 μM for all comparable colorectal cell lines) (247). Thus, the greater cytotoxicity of bifunctional alkylating agents is probably a result of their ability to induce toxic DNA ICLs.

Earlier studies that reported $GI_{50}$ values with the ZD2767P prodrug were conducted without the antibody component of the fusion protein (246). All *in vitro* protocols described, incorporated the antibody-enzyme fusion protein, however it was necessary to rule out any binding by the fusion protein to the $CEA^{-ve}$ A375M cells. Thus, to mimic the treatment conditions *in vivo* (where the fusion protein is allowed to clear from the circulation before prodrug can be given), unbound fusion protein was removed from the cells prior to prodrug addition. The $GI_{50}$ in SW1222 cells was 0.19 μM, with the removal/wash step proving to be a less sensitive protocol but a more genuine reflection of ADEPT (difference of 0.07 μM compared to when unbound fusion protein was not removed). As expected, there was no growth inhibitory effect in A375M cells. This demonstrated the highly specific targeting action of ADEPT and also the importance of the individual components of ADEPT.

The growth inhibitory effect of the ZD2767P prodrug alone was also assessed and proved to have no effect on SW1222 cells at prodrug concentrations less than 10 μM, which is in accordance with data obtained with LS174T cells (246). *In vivo*, administration of prodrug alone was found not to slow tumour growth (138); and in patients the prodrug was shown to cause little toxicity (135). However, the prodrug was found to have an effect on tumour cells at concentrations greater than 10 μM, that is, approximately 100-fold differential in potency compared to ADEPT (or rather the active drug) in SW1222 and A375M cells, with $GI_{50}$ of 27 and 96 μM, respectively. Similar findings were also found when LoVo cells were exposed to the active drug alone or the prodrug alone (133). A number of possible physiochemical-related reasons could explain the growth inhibition observed at high concentrations of prodrug alone. For example, the balance between the lipophilicity and

hydrophilicity of the ZD2767P prodrug may be compromised at high concentrations (390), and this is in addition to its short half-life. Its ability to induce DNA damaging ICLs with increasing prodrug dose up to 100 μM was ultimately weaker than the action of the active drug in ADEPT, with low levels of ICLs persisting up to 3 μM before a notable increase was observed. The potency of ADEPT prodrugs has been relatively low, in the micromolar (μM) range. It is theoretically possible to use new and more potent prodrugs that would be too toxic to administer as standard chemotherapeutics. Tietze and colleagues (391) (392) showed that it is possible to design and apply *in vivo* prodrugs >4800 times less toxic than the corresponding active drug. Two novel pyrrolobenzodiazapiene-based prodrugs were investigated for use in ADEPT and found to be more potent (picomolar range) than nitrogen mustards (393).

Clonogenic assays are useful for determining the potency of a drug but provide little detail as to how the drug affects the cell. Since the prodrug used here in ADEPT was a nitrogen mustard derivative, cross-links were believed to be the principle DNA damage lesion responsible for its potency, and therefore, cytotoxicity (394) (242) (395) (396) (264). A good correlation between the extent of cross-linking and cytotoxicity was previously demonstrated in response to ADEPT (246) (247). The modified comet assay was used to measure ICLs and their subsequent unhooking in response to a single cycle of ADEPT, *in vitro* and *in vivo*. The comet assay was originally developed to measure DNA strand breaks (397). The modified comet assay is more sensitive, requires fewer cells and can be appropriately applied for clinical blood and tissue samples (398) (246) (399) (400) (401) (402) (403) (139) (404) (387). The dose response experiment revealed a prodrug concentration of 0.21 μM was required to cause 50% cross-linking in SW1222 cells. LS174T colorectal carcinoma cells were shown to be less sensitive to cross-linking at prodrug concentrations of 0.5-1 μM (246). It has been suggested that cross-linking may be a determinant of cellular sensitivity, more so than genetic p53 status (247) (338), especially since SW1222 cells are p53-defective and LS174T cells are p53 wild-type (405).

Drug concentrations that give rise to 50-70% cross-links are routinely used for investigating ICL induction and repair. The time course experiment for ICL

formation post-ADEPT showed that ICLs formed rapidly *in vitro* and *in* vivo. The data revealed that ADEPT-induced ICLs peaked at 1hr in SW1222 cells, and suggested they probably start forming immediately upon prodrug administration. ICLs formed within 10 min upon exposure of cells to 0.02, 0.2, 2 μM ZD2767P (+CPG2) with no increase in damage seen over 50 min (247). Furthermore, there was no evidence of a decrease in ICL levels over 1 hr (suggesting no repair or stable adducts). Rapid cross-link formation is consistent with studies investigating the highly reactive ZD2767D active drug, which has a short plasma half-life (< 2 min) (133). Mechlorethamine-induced ICLs have been shown to peak at 1 hr-post-treatment (322) (288) (320) (406), and for melphalan this was 16 hr in NSCLC cells (338). Nitrogen mustard-induced ICLs are generally quite unstable with a half-life of 2 hr, which contributes to their decreased toxicity and therapeutic benefit compared to other, more stable ICLs (407) induced by pyrrolobenzodiazapienes (PBD) (393). DNA cross-links formed by PBDs have been shown to be more resistant to repair (408) (409,), reducing the probability of clinical resistance developing.

Unhooking of these ICLs commenced within an hour following the peak of damage in SW1222 cells, with 47% cross-links unhooked by 24 hr and 72% unhooked by 48 hr. Unhooking of ICLs is thought to be carefully orchestrated by specific NER nucleases that cause the covalent bond holding the strands of DNA together to flip out and leave a stable adduct, thus removing the cytotoxic lesion (see Figure 1.6). When mice bearing SW1222 xenografts were treated with ADEPT, cross-links formed rapidly within 1 hr and they persisted in samples taken at 3 and 24 hr-post-treatment, with an estimated 45% of cross-links unhooked by 24 hr (considering there were 100% cross-links at 1 hr). This correlated well with the *in vitro* data, although earlier time points (before 1 hr) would be required in order to elucidate a definite peak in cross-linking *in vivo*. Despite the overall consensus, ICL unhooking varied between the tumours over time, in particular, tail moments for tumour samples from mice no.9 at 3 hr and no.15 at 24 hr. Webley *et al.* (246) also showed that cells from LS174T xenografts exposed to ADEPT (using the F(ab')$_2$ conjugate plus ZD2767P) had extensive ICL formation after 1 hr, which was significantly reduced at 24 hr, supposedly as a result of repair activity. In the Phase I ADEPT clinical trial, a reduction in tail moment by 58% was seen in a tumour sample from one patient, indicating effective localisation of MFECP and prodrug activation in the tumour

(139). Cross-linking was not observed in PBLs taken from the same patient at the same time as the treated tumour biopsy, thus, demonstrating the specificity and selectivity of ADEPT. Similarly, PBLs taken from the ADEPT-treated mice displayed low levels of cross-linking, though, ICLs detected at 1 hr-post-ADEPT were notably higher (17% reduction in tail moment) than at 3 and 24 hr. DNA damage exhibited here may be the result of peripheral prodrug activation, since the tumours exhibited extensive cross-linking. Indeed, cross-linking in PBLs from the 31 patients treated in the ADEPT trial ranged from 0% to 27%, with only two patient samples displaying >20% reduction in tail moment (139).

Mammalian ICL repair is complex, involving the concerted action of multiple repair pathways (303). Studies investigating ICL repair suggest DSBs are formed as an intermediary lesion during unhooking (323) (284) (269) (288). DSBs have been shown to trigger a γ-H2AX response following IR (310) and, to a less proportional extent, following alkylating agents (313) (410) (320) (411) (338). The role of γ-H2AX is to recruit DNA repair and cell cycle checkpoint proteins required for the efficient processing of DNA DSBs. Thus, γ-H2AX induction following ICL DNA damage is a way of determining the DNA damage response. Specifically, the DNA damage response to ADEPT-induced ICLs was less understood and thus, explored. In SW1222 cells, γ-H2AX foci could be detected at very low concentrations of prodrug (in combination with the fusion protein), as low at 12.5 nM. The peak of γ-H2AX formation was detected at 3 hr-post-ADEPT, that is 2 hr following the peak of ICLs. Similar timings were observed in mechlorethamine-treated human fibroblasts (320). The findings suggested that H2AX is phosphorylated within a few hours of DNA damage, possibly in response to ICL-associated DSBs, which are believed to form upon unhooking of ICLs. An additional smaller γ-H2AX foci peak was observed at 24 hr-post-ADEPT, the significance of which cannot be explained from these assays alone. The response was believed to be associated with repair of (non-ICL-related) DSBs, which are thought to occur in the G2/M phase of the cell cycle (411). Additionally, ICL-induced DSBs (and other repair intermediates) may arise at later time points post-treatment as replication forks, previously blocked by ICLs, are restored, bypassed or restarted (411).

When the DNA damage response was measured *in vivo,* a statistically significant increase in γ-H2AX foci formation was observed over time post-ADEPT in SW1222 tumour xenografts. Gamma-H2AX levels ranged from 2 foci per cell at 1 hr to 10 foci per cell at 24 hr-post-treatment. Encouragingly, higher levels of γ-H2AX foci were observed in the tumours than in time-matched PBLs. The γ-H2AX foci per cell in PBLs ranged from 1 at 1 hr to 4 at 24 hr-post-treatment. The γ-H2AX response pattern observed in the tumours tied in well with the increase in comet tail moment, or rather, unhooking of cross-links over time. For example, where ICL formation was found to be greatest at 1 hr, the γ-H2AX response was weakest and vice versa at 24 hr-post-ADEPT. In particular, tumour cells from one mouse (no.15) that exhibited the greatest number of γ-H2AX foci per cell, also displayed the largest comet tail moment post-treatment, further indicating that ICL unhooking correlated with γ-H2AX response as a result of ICL-associated DSB formation. The γ-H2AX response was found to persist over time *in vivo*, although more time points before and after 24 hr would be needed to clarify the biphasic response observed *in vitro*. Disappearance of γ-H2AX foci is believed to reflect dephosphorylation by protein phosphatases (412) (413), and thus, the removal of crosslinks (414) leading to the release of repair proteins to complete the DNA repair process (415).

There is conflicting evidence on the functional relevance of γ-H2AX (416). The formation of γ-H2AX does not simply imply a direct repair response to DSBs induced during ICL repair, since γ-H2AX has been shown to be induced in HR-defective cells and independently of readily detectable ICL-associated DSBs (319) (320) (288) (322). H2AX-deficient cells showed only mild defects in DNA damage checkpoint control and DNA repair, suggesting that H2AX assists in, but is not critical for DNA damage checkpoint activation and DNA repair processes (319) (321) (321). Interestingly, a potent pyrrolobenzodiazepene, SJG136, was found to induce a γ-H2AX response in clinical tumour samples and PBLs at 24 hrs-post-treatment (417) (387), despite the persistence of ICLs, with very little ICL unhooking (408). This may reflect the non-distorting nature of the cross-links produced by this agent and which may evade early detection by the repair machinery (418).

According to the literature, the γ-H2AX response in SW1222 cells exposed to ADEPT likely indicated the accumulation of proteins required for repair, namely the

HR and TLS pathways which are involved in the processing of (ICL-associated) DSBs (268) (269) (270) (411) (271) (272). DNA damage repair proteins recruited by γ-H2AX to the site of DNA damage include the MRE11/RAD50/NBS1 (MRN) complex, BRCA1, RAD51, MDC1 and FANCD2 – all major components of HR repair pathway (307) (419) (296). Paull *et al*. (307) demonstrated that γ-H2AX foci formed within a few minutes of DNA damage and accounted for the patterns of RAD50, RAD51 and BRCA1 foci seen much later during recovery from DNA damage.

RAD51 is the central protein involved in controlling strand invasion and recombination in human cells during repair in response to DNA damage by DSBs (420) (421). RAD51 foci have been previously visualised by immunofluorescence after exposure of cells to exogenous agents (338) (85) (337). RAD51 foci induction over time post-ADEPT displayed a biphasic response, with the earlier 6-hr peak being the strongest and this was followed by another smaller peak at 24 hr. This biphasic response was also observed in cells treated with cisplatin (338). It would appear that the first peak is indicative of HR repair of ICL-associated DSBs, especially since there was a γ-H2AX response 3 hr earlier. However, the recruitment of RAD51 to damage sites has been shown to function independently of H2AX phosphorylation status (422) (423). RAD51 foci were found to interact with ICL-stalled forks before DSB formation (330) and it is believed this may function to prevent fork breakage/degradation in order to initiate strand invasion as soon as the DSB has formed (424). RAD51 has also been shown to mediate restart of transiently stalled forks, but this function is not linked to foci formation or to its role in DSB repair (425). The control of RAD51 protein levels is thought to be partially cell-cycle dependent (426), which may explain the 24 hr peak of induction and it's possible link to repair of non-ICL-related DSBs.

The RAD51 response was detected in tumour xenografts, but in contrast to *in vitro* data, there was no obvious pattern of induction post-ADEPT, as seen with γ-H2AX. With the peak of induction occurring at 6 hr *in vitro*, it is likely the peak *in vivo* was missed, as only a few selected time points were obtained. Nevertheless, the results could also indicate the existence of RAD51-independent mechanisms of repair taking place *in vivo* (427) (428) (429) (430). Mixed responses for RAD51 upon treatment

with ICL-inducing agents have been previously reported (338) (387). For example, Wu and colleagues (387) found that RAD51 foci persisted or were absent in HR-defective cells in response to cisplatin treatment. The role of RAD51 and other HR-related proteins would need to be investigated further in response to ADEPT-induced ICL damage *in vitro* and *in vivo*.

## 4.4    Summary

The results presented here have clearly shown that there is a DNA damage response to a single cycle of ADEPT. Growth inhibition assays with antigen-positive and −negative cell lines showed that ADEPT is specific in its action. The comet assay demonstrated that ADEPT is selectively toxic causing ICL damage, which formed rapidly by 1 hr in colorectal carcinoma cells *in vitro* and *in vivo*. ICLs were found to unhook over 48 hr and this correlated with a DNA damage response, represented by an increase in the γ-H2AX response at 3 hr-post ADEPT and 24 hr *in vivo*. The γ-H2AX response indicated the accumulation of repair factors at the site of DNA damage and the possible presence of ICL-associated DSBs. A marked increase in RAD51 foci at 6 hr *in vitro* confirmed the presence of DSBs and moreover, the repair of these DSBs by HR. Further investigation of HR status *in vivo* is warranted. Taken together, the results indicate DNA damage repair in response to a single-cycle of ADEPT, which could potentially be manipulated to improve clinical therapeutic efficacy.

University College London

# CHAPTER 5

Pharmacokinetic and Pharmacodynamic Challenges of Antibody-Directed Enzyme Prodrug Therapy (ADEPT)

Carima Andrady

# 5 Approaches to Target the DNA Damage Response Pathway

## 5.1 Introduction

The pharmacodynamic response to a single cycle of ADEPT, as assessed in Chapter 4, indicated the occurrence of DNA damage repair contributing to the lack of an effective tumour response. This was evidenced by the unhooking of ICLs, a γ-H2AX response and a RAD51 response; with the latter indicating the involvement of HR repair which is favoured in S or G2 phases of the cell cycle. In order to improve the therapeutic efficacy of ADEPT, it was proposed that selected genes and/or proteins could be inactivated (or activated) which would interfere with the repair process.

The development of inhibitors for targeting the DNA damage repair pathway has been of considerable interest over the last few years as novel cancer therapeutic agents in their own right and/or in combination with existing therapies (431) (259). Of particular interest is targeting the cell cycle. In the event of DNA damage, normal cell cycling activity must halt in order for repair (or apoptosis) to take place; and this is mediated by cell cycle checkpoint kinases, Chk1 and Chk2, depending on the type of damage incurred and/or cell cycle phase (432) (257). Chk1 is important in regulating the intra-S and G2 phases in preparation for cell division, as demonstrated in biochemical and genetic analyses (433) (434). Selectively targeting and inhibiting Chk1 has emerged as an interesting therapeutic strategy for p53-deficient/defective cancers (435) (436) (437). By inhibiting Chk1, cancer cells are forced through the G2-to-M transition in the face of DNA damage induced by genotoxic agents (e.g. ADEPT), as the G1/S phase arrest will be compromised by the lack of p53. An explanation of the proposed mechanism is illustrated in Figure 5.1. This is the principle of *synthetic lethality*, which is a term used to describe two events (e.g. mutations/inactivation/inhibition) that individually do not compromise survival but together are lethal (438) (439). With this strategy in mind, it was hypothesised that the therapeutic potential of a single cycle of ADEPT could be enhanced by inhibiting Chk1 using clinically tested Chk1 inhibitors.
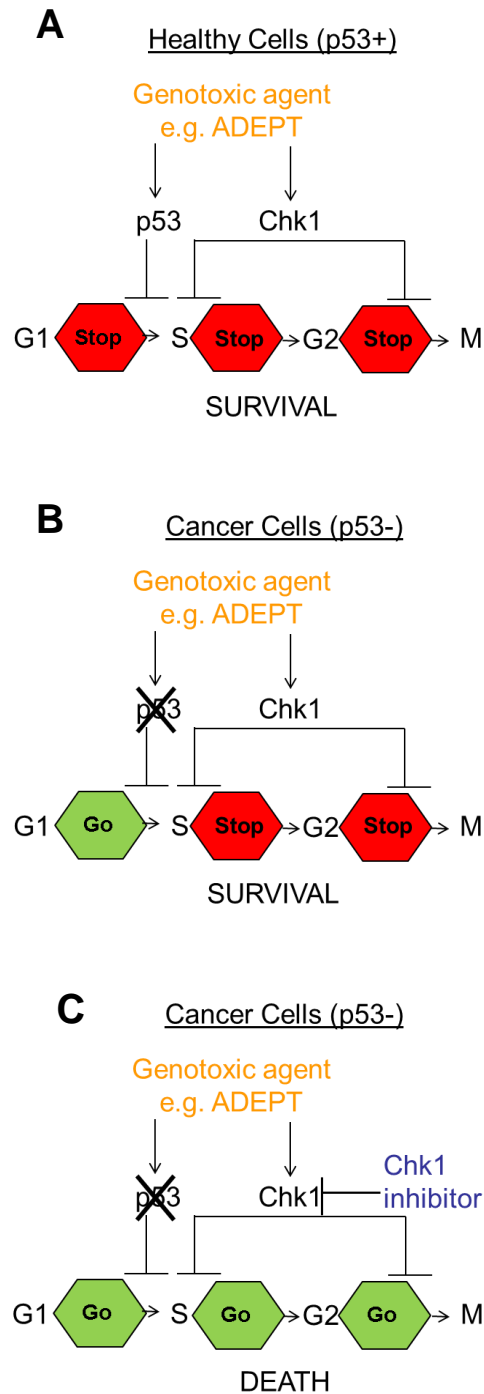
**Figure 5.1 Synthetic lethal interaction as a proposed approach to improving the therapeutic response of ADEPT**

Normal cells are capable of sustaining checkpoints in the presence of functional p53 and active Chk1 for as long as needed when DNA is damaged (A). Most cancer cells lack a functional p53 pathway and therefore are unable to arrest in G1 when their DNA is damaged, but they are able to activate the S- and G2-checkpoints through the Chk1 pathway (B). This gives tumour cells time to repair any damage and promotes their survival. When p53-deficient cancer cells are subjected to genotoxic agents that induce replicative stress in combination with Chk1 inhibition they lose all three checkpoints and progress through the cell cycle without repairing their DNA damage. This results in

preferential killing of p53-deficient tumour cells whilst avoiding normal cell toxicity (C). (Taken and adapted from Ma *et al*., 2011 (440)).

### 5.1.1 Aims and Objectives

The aim: to investigate an intervention strategy to augment tumour cell-kill by a single cycle of ADEPT. The objectives:

1. To determine the transcript regulation profile of a defined set of genes involved in DNA damage response signalling.
2. To identify cell cycle checkpoints that would impede DNA damage repair
3. To evaluate the effect of Chk1 inhibitors in combination with ADEPT.

## 5.2 Results

### 5.2.1 Identifying changes in regulation of DNA damage response genes post-ADEPT

Real-time PCR is generally considered the gold standard for gene expression measurement. The specificity of the $RT^2$ PCR array system, which uses the SYBR® Green assay, guarantees the amplification of a single gene in each reaction meaning that levels of expression confidently reflects the gene of interest.

The expression of 84 genes involved in DNA damage signalling and repair was measured in response to a single-cycle of ADEPT in order to determine, and possibly manipulate, the DNA damage response or repair mechanisms (as observed in Chapter 4) at the mRNA level. Cells were treated with ADEPT using a prodrug concentration of 0.25 μM, which is equivalent to the concentration used to determine ICL peak formation and unhooking post-ADEPT. Total RNA extracted from the cells was converted to cDNA and gene expression was quantified using real-time PCR. Figure 5.2 shows the gene expression pattern of SW1222 cells at 1, 3 and 24 hr-post-ADEPT, compared to untreated cells. The difference in gene expression in the ADEPT-treated samples compared to the non-treated samples was conveyed as a fold regulation value using the $RT^2$ Profiler PCR array data analysis software. The

fold regulation value is the difference between the normalised gene expression (that is, average cycle threshold (Ct) value of gene of interest minus average Ct value of house-keeping genes) in the ADEPT-treated samples compared to the normalised gene expression of the untreated samples. Genes that exhibited greater than 2-fold increase in gene expression in ADEPT-treated cells compared to untreated cells are highlighted in red, and those that exhibited a greater than 2-fold decrease in expression are shown in green. The values for these genes are represented in Table 5.1. Gene nomenclature and average Ct values per gene analysed are documented in the Appendix 1A and 1B.

Due to the cost of the assay, time points investigated post-ADEPT were limited to 1, 3 and 24 hr. These time points were chosen based on the *in vitro* assays used to determine ICL formation, ICL unhooking and γ-H2AX response. Internal quality control genes were included in each plate per sample analysed. These included house-keeping genes for normalising Ct values, a genomic DNA control for detecting non-transcribed DNA contamination, reverse transcriptase control genes for detecting efficiency of the cDNA synthesis and positive PCR control genes for detecting efficiency of the PCR reaction.
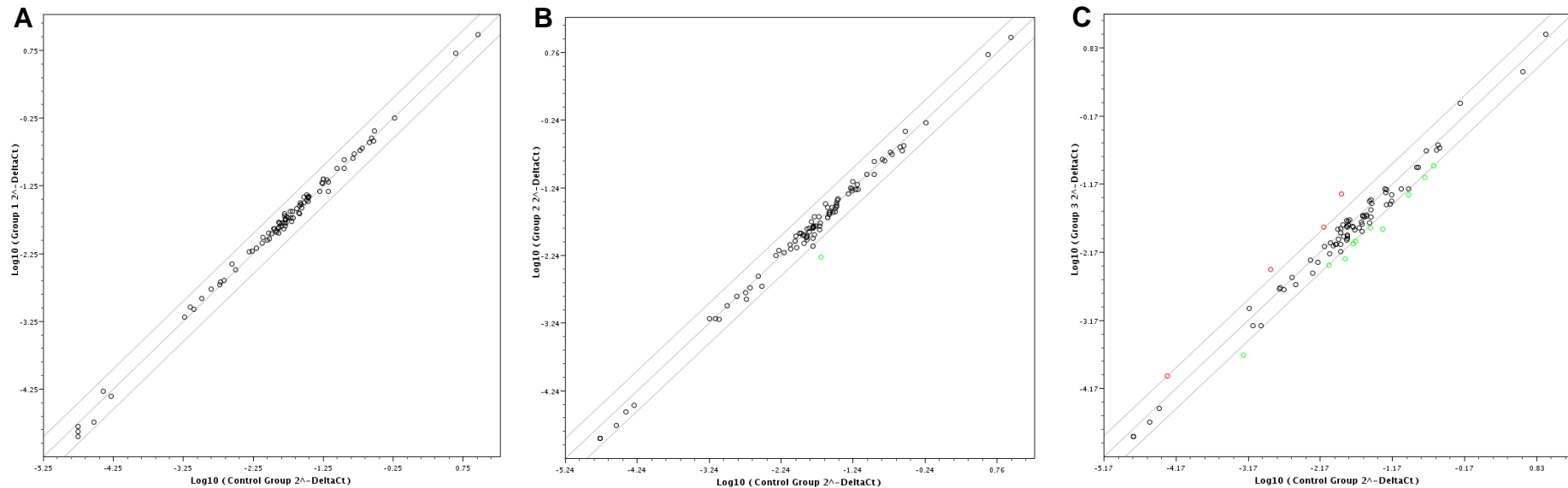
**Figure 5.2 Real time PCR analysis of the change in expression of 84 genes involved in DNA damage signalling at 1 (A), 3 (B) and 24 (C) hr-post-ADEPT in SW1222 cells**

Cells were treated with ADEPT and, following 1hr incubation with 0.25 μM prodrug,, cells were post-incubated with drug-free media for 1, 3 and 24 hr. RNA was extracted at these time points and cDNA synthesised prior to PCR. Mean Ct values were computed from four separate ADEPT experiments. A change in gene expression in the ADEPT-treated cells compared to the untreated cells is conveyed as a fold regulation value. Genes which show increased expression by more than 2-foldcompared to non-ADEPT-treated cells are shown in red and those which show decreased expression less than -2-foldare shown in green. Data was analysed using the RT$^2$ Profiler PCR data analysis software (SABiosciences).

**Table 5.1 DNA damage response gene expression values that changed more than two-fold following ADEPT compared to untreated cells**

Values were computed from four independent ADEPT experiments, as mentioned in Figure 5.2 using the RT$^2$ Profiler PCR data analysis software (SABiosciences). *Values regarded as significant p value ≤ 0.008 (when compared to non-treated).

| Gene name | | Fold regulation values (compared to non-treated) | | |
|---|---|---|---|---|
| Abbreviation | Full name/description | 1hr | 3hr | 24hr |
| BTG2 | B-cell translocation gene 2 | 1.20 | 1.03 | 2.71 |
| *DDIT3 | DNA-damage-inducible transcript 3 | 1.20 | 1.09 | 3.71 |
| DMC1 | DMC1 dosage suppressor of mck1 homolog, meiosis-specific homologous recombination (yeast) | -1.18 | -1.47 | 2.00 |
| FEN1 | Flap structure-specific endonuclease 1 | -1.08 | -1.05 | -3.36 |
| XRCC6 | X-ray repair complementing defective repair in Chinese hamster cells 6 | -1.06 | -1.12 | -2.03 |
| IGHMBP2 | Immunoglobulin mu binding protein 2 | -1.01 | 1.05 | -2.02 |
| LIG1 | Ligase 1 | -1.10 | -3.74 | -2.11 |
| *MLH3 | MutL homolog 3 (E. coli) | 1.06 | 1.09 | 2.09 |
| NBN | Nibrin | -1.15 | 1.21 | -2.77 |
| *PCNA | Proliferating cell nuclear antigen | -1.01 | 1.03 | -2.24 |
| PNKP | Polynucleotide kinase 3'-phosphatase | -1.03 | -1.41 | -2.17 |
| TP73 | Tumour protein p73 | 1.11 | 1.17 | -2.77 |
| *UNG | Uracil-DNA glycosylase | 1.22 | 1.25 | -2.35 |
| *XPA | Xerodermapigmentosum, complementation group A | 1.13 | -1.05 | -2.16 |

It is interesting to note that the change in gene expression increases over time post-ADEPT, being greater at 24 hr-post-ADEPT compared to 1 hr. This is illustrated, in Figure 5.2, by the broad distribution of the data points (fold regulation values) at 24 hr compared to the more centralised distribution at 1 hr. This confirms that even at the gene level ADEPT is having an effect on the cells up to 24 hr after receiving treatment. Nevertheless, of the 84 DNA damage signalling/repair genes analysed,

only four genes showed a greater than 2-fold increase in expression (red) at 24 hr-post-ADEPT (Figure 5.2) (Table 5.1). The number of genes that decreased in expression by more than 2-fold (green) was much greater at 24 hr and, additionally, LIG1 (ligase) gene showed decreased expression at 3 hr-post-ADEPT. The down-regulation of the genes, FEN1, LIG1, PCNA, PNKP and UNG, suggested that base excision repair (BER) may be involved, possibly repairing ADEPT-induced DNA monoadducts. The down-regulated expression of these genes indicated a form of negative feedback regulation at 24 hr. This is supported by the fact that expression of BTG2, which encodes a protein involved in cell cycle regulation, is up-regulated at the same time. In addition, DDIT3 - an inducer of cell cycle arrest (441), was also found to be up-regulated. Thus, ADEPT may be having an effect on the regulation of the cell cycle. The large number of genes down-regulated post-ADEPT was an unexpected finding and the results of the analysis provided little information for targeted intervention studies.

To determine possible biological interactions of the differently regulated genes at 24 hr post-treatment, the PCR array dataset was imported into the Ingenuity Pathway Analysis Tool (IPA) (Ingenuity H Systems, Redwood City, CA, USA www.ingenuity.com). The IPA tool was used here to determine direct and indirect interactions between the products of those genes with altered expression and also of those not involved in the PCR array analysis. A graphical representation of these interactions at 24 hr-post-ADEPT is shown in Figure 5.3. There appeared to be a strong association with PCNA, which suggested an important role for this gene/protein following ADEPT-induced DNA damage. In addition, there was an association with cyclin A, with direct links to FEN1, LIG1 and PCNA. Cyclin A is associated with control of DNA replication (442) and mediating cell cycle progression by interacting with cyclin-dependent kinases (CDKs).
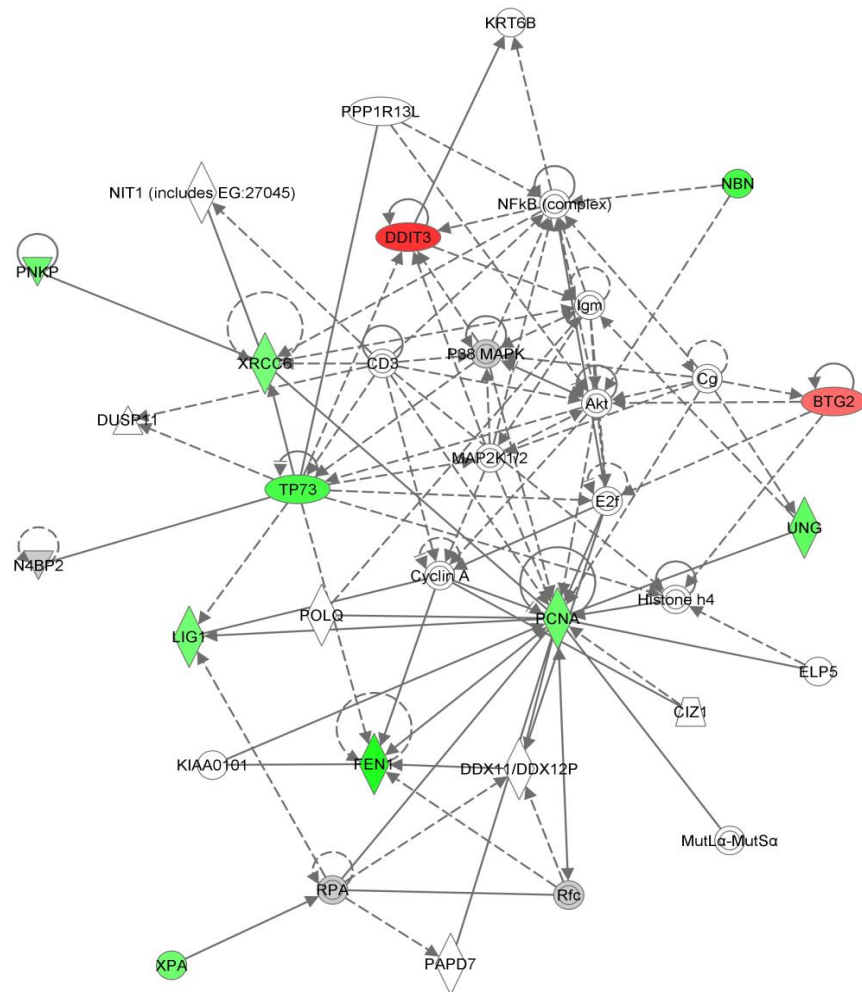
**Figure 5.3 Ingenuity Pathways Analysis (IPA) summary of the 24 hr-post-ADEPT PCR array dataset**

The protein molecules with altered gene expression are highlighted in red (up-regulated) or green (down-regulated). The protein molecules of genes are represented as nodes and the biological relationship between two nodes is represented as a line. A solid line represents a direct interaction and a dotted line represents an indirect interaction. All lines are supported by at least one reference from the Ingenuity Knowledge database (www.ingenuity.com; Ingenuity H Systems, Redwood City, CA, USA).

To establish whether protein expression correlated with the altered gene expression observed at 24 hr-post-ADEPT, SW1222 cells were treated with ADEPT in the same way (as above), lysed at 1, 3, 24 and 48 hr-post-treatment and 15 µg cell lysate loaded onto 4-20% Tris/Gly gels for separation by SDS-PAGE. Protein was transferred onto PVDF membrane and stained with respective antibodies for detection of PCNA and NBS1 (gene name, NBN, Table 5.1). Protein was detected at all time points in ADEPT-treated and untreated cells as shown in Figure 5.4.

Interestingly, protein expression levels of PCNA increased at 24 hr-post-ADEPT by an average density of 1.4-fold (±0.2) compared to untreated; contrary to its relative gene expression (Table 5.1). By 48 hr, expression had reduced to levels comparable to the untreated with an average density of 1.1 (±0.13).



untreated    1      3      24     48 (hrs)

PCNA (36 kDa)

NBS1 (95 kDa)

β-actin (42 kDa)
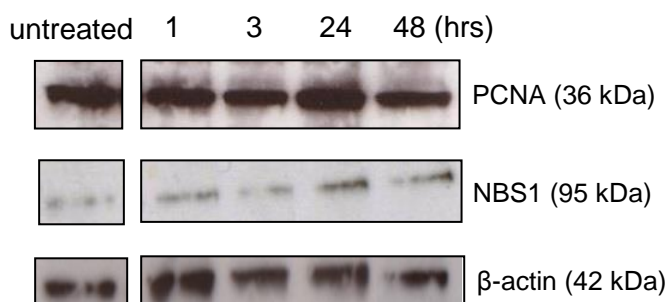
**Figure 5.4 SW1222 cellular expression of PCNA and NBS1 proteins at 1, 3, 24 and 48 hr-post-ADEPT**

Cells were treated with a single cycle of ADEPT and then incubated in drug-free media. Cells were lysed at respective time points post-ADEPT and lysate loaded onto Tris/Gly gels. Protein was separated by SDS-PAGE, and PCNA and NBS1 were detected by Western blot. β-actin protein was used as experimental loading control. Images are representative of at least two independent experiments.

NBS1 protein expression appeared to increase over time post-ADEPT with an average density of 3-fold (±0.6) at 24 hr and 3.8-fold by 48 hr, compared to the non-treated (Figure 5.4). In contrast, the relative gene expression at 24 hr post-ADEPT was down-regulated. Thus, it was deduced that protein expression appeared not to correlate directly with gene expression from the PCR arrays but showed a different pattern of regulation that is probably more suggestive of real-time DNA repair mechanisms taking place in response to ADEPT. The expression of other proteins with altered gene expression was not pursued further as antibodies for these were not available in our lab, and would have been a costly expense solely for this purpose.

## 5.2.2   Analysing cell cycle activity in response to ADEPT

Negative regulation of the cell cycle, as highlighted by the up-regulation of anti-proliferative genes - BTG2 and DDIT3, prompted an investigation into cell cycling activity post-ADEPT in SW1222 cells. To investigate the cell cycling activity in

response to a single cycle of ADEPT, the proportion of cells at different phases of the cell cycle was analysed by fluorescence activated cell sorting (FACS), and Chk1 and Chk2 proteins, which control cell cycle progression, were measured.

Cells were treated with ADEPT using experimental conditions which caused > 50% cross-links. Propidium iodide was used to stain fixed cells and cell cycle analysis was conducted by FACS. Cell cycle phases were gated and analysed as follows: sub-G1 consists of cell debris; G0/G1 represents cells in resting phase or preparing for DNA replication (all cells are 2N); S represents cells in the process of DNA replication; G2/M consists of cells preparing to divide and/or in the process of mitosis (all cells are 4N). There was no difference in the proportion of cells in each cell cycle phase at 3 or 6 hr with or without ADEPT, as shown in Figure 5.5. In untreated SW1222 cells the fraction of cells in G0/G1 remained unchanged over time (Figure 5.5 B); although a decrease in cells in G2/M phase was observed from 23% at 3 hr to 11% at 48 hr. In contrast, ADEPT induced an apparent growth arrest at G2/M phase at 24 hr following treatment and causing a large proportion of cells to reside in G2/M phase at 24 hr (35%) (Figure 5.5 A), compared to untreated normal cycling cells (15%) (Figure 5.5 B). At 48 hr-post-ADEPT, the proportion of cells in G2/M remained greater than in the untreated cells, but had reduced to 23%, which may suggest recovery from the growth arrest. The proportion of cells in S-phase remained relatively constant over time for untreated (19-24%) and ADEPT-treated cells (20-28%). There was also no significant difference in the sub-G1 fraction, which was used to assess the level of cell death, between ADEPT-treated and untreated cells. These data suggested that cells exposed to ADEPT are not killed more than untreated cells, and cells can overcome an initial cell cycle arrest at G2/M caused by ADEPT.
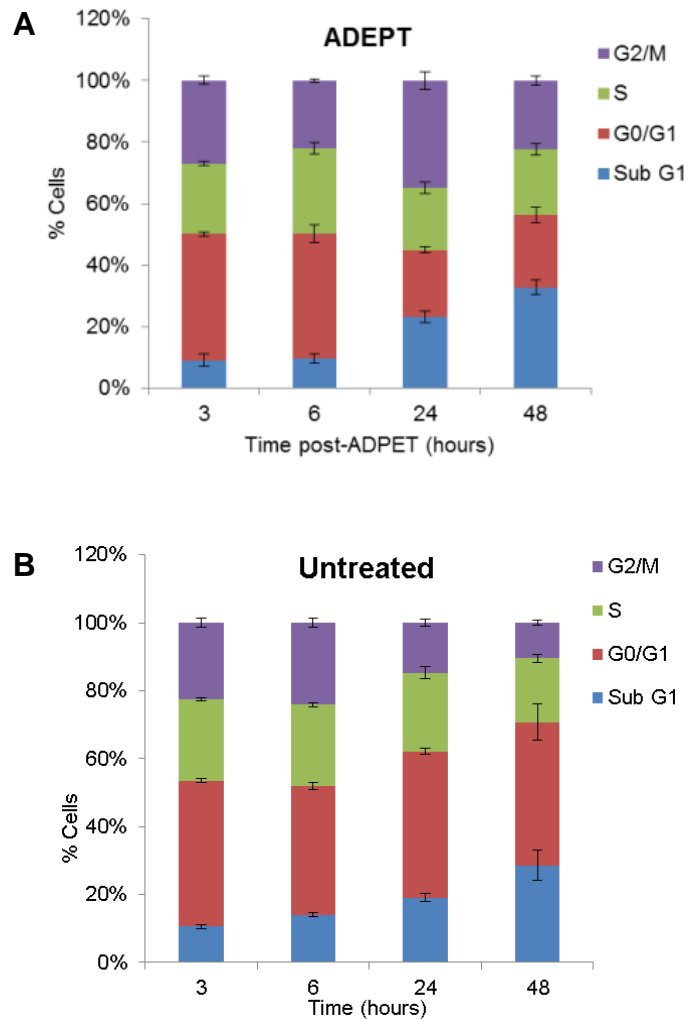
**Figure 5.5 Cell cycling activity in ADEPT-treated (A) and untreated (B) SW1222 cells**

G2/M cell cycle arrest is evident in ADEPT-treated cells compared to untreated cells. SW1222 cells were treated with or without ADEPT followed by incubation in drug-free medium for different lengths of time. Cells were fixed with 70% cold ethanol and stained with 50 μg/ml propidium iodide (PI) solution per million cells. Cell solution was analysed by flow cytometry. Cell cycle phases: Sub G1, G0/G1, S and G2/M. Data are representative of at least 4 independent experiments, mean ± SEM.

The activation of the cell cycle checkpoint kinases, Chk1 and Chk2, in ADEPT-treated cells was assessed by measuring the expression of phosphorylated Chk1 (Chk1-p) and phosphorylated Chk2 (Chk2-p) by Western blotting (Figure 5.6). Briefly, SW1222 cells were treated with ADEPT in the same way (as mentioned in Section 5.2.1), lysed at 1, 3, 24 and 48 hr-post-ADEPT and 15 μg cell lysate was loaded onto 4-20% Tris/Gly gels and separated by SDS-PAGE. Protein was transferred onto a PVDF membrane and stained with anti-Chk1-p and Chk2-p antibodies. The relative difference in protein expression in ADEPT-treated cells

compared to untreated cells was quantified using Image J analysis software. Chk1-p levels increased over 24 hr-post-ADEPT by up to 2.3-fold (±0.07), relative to the untreated cells. By 48 hr, expression had decreased to 0.8-fold (±0.38) compared to untreated cells. Chk1-p expression in untreated SW1222 cells did not change over 48 hr, and its presence, and change in expression levels, has previously been detected in normal cycling cancer cells (443). Chk2-p expression was also detected post-ADEPT and increased over time by more than double from 1.5-fold (±0.09) at 1 hr to 4.4-fold (±2.5) at 48 hr, relative to the untreated.
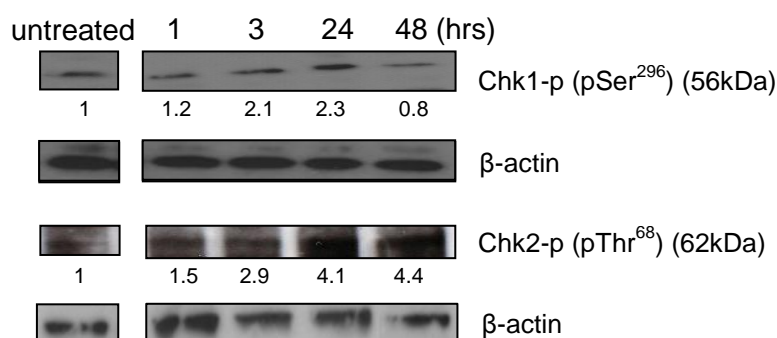


**Figure 5.6 Chk1-p and Chk2-p expression is up-regulated in ADEPT-treated SW1222 cells**
Cells were treated with a single cycle of ADEPT (as described in the Methods) and lysed at different time points. Data is representative of at least 2 independent experiments, and protein expression relative to the untreated was quantified by densitometry using Image J. β-actin protein was used as an experimental control.

Collectively, these data suggested a link between increased presence of activated Chk1 and G2/M growth arrest at 24 hr following ADEPT, as a result of DNA damage repair. Furthermore, the decrease in activation of Chk1 at 48 hr and increase in Chk2 over time may be associated with the recovery of cells back to normal cell cycling activity in response to ADEPT.

### 5.2.3 Evaluating the cellular response to ADEPT in combination with Chk1 inhibitors

The first Chk1 inhibitor to be developed was UCN-01 (7-hydroxystaurosporine). It is classified as a non-specific inhibitor because it has been shown to act on several kinases, including Chk1, Chk2, MAPKAP kinase (MK2) and protein kinase C (PKC)

(444) (445) (446). Due to the non-selective nature of UCN-01, more potent, specific Chk1 inhibitors were subsequently developed, some of which are analogues of the UCN-01 compound, for example, PF-477736. Both UCN-01 and PF-477736 were assessed for their Chk1 inhibitory effect on SW1222 cells in combination with ADEPT.

### 5.2.3.1 Determining the growth inhibition potential of ADEPT in combination with Chk1 inhibitors

SRB assays were used to determine whether combination treatment of ADEPT and Chk1 inhibitors, UCN-01 or PF-477736, could potentiate growth inhibition of SW1222 cells compared to ADEPT alone. Preliminary experiments were conducted to determine the concentrations of each inhibitor which would inhibit 10-20% of cells. Briefly, cells were exposed to increasing concentrations of each Chk1 inhibitor (separately) for 96 hr before SRB reagent was applied (Figure 5.7). Sub-toxic doses of the inhibitors on SW1222 cells that could be used in combination with ADEPT were found to be 25 nM UCN-01 and 0.1 μM PF-477736.
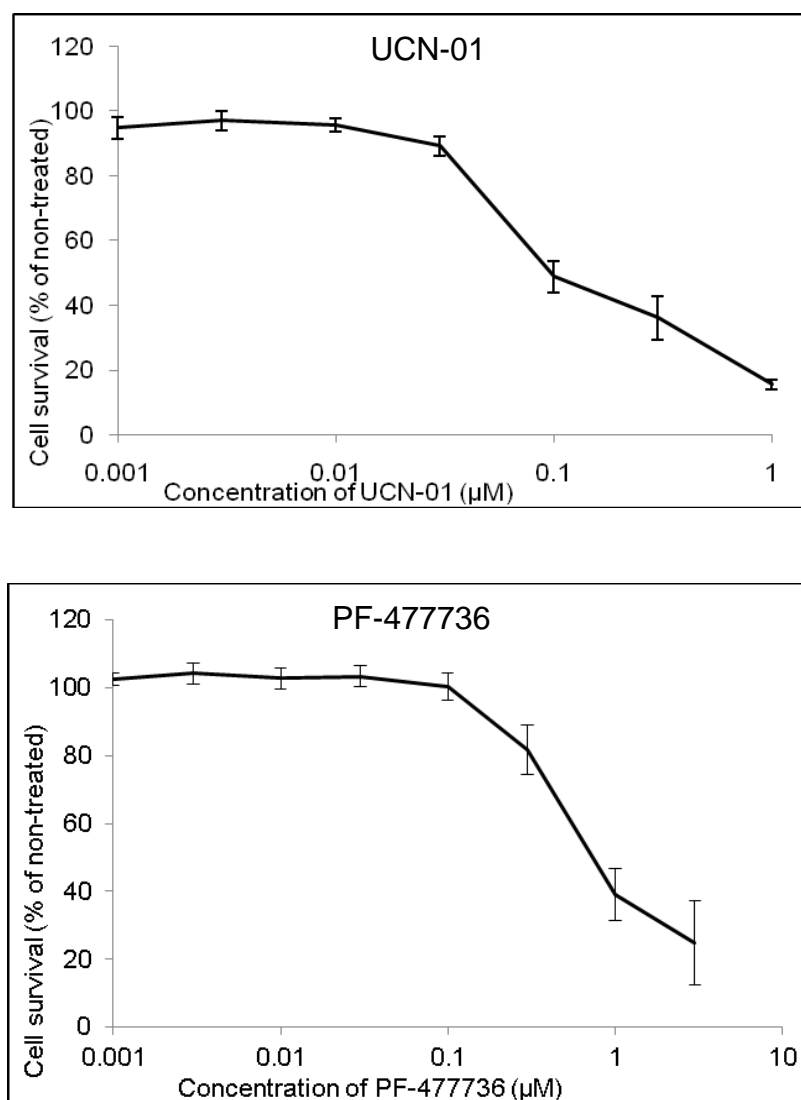
**Figure 5.7 Determining the sub-toxic dose of UCN-01 or PF-477736**

SW1222 cells were treated with increasing concentrations of each inhibitor and incubated for 96 hr and SRB applied. Data are representative of 3 independent experiments, mean ± SEM.

Combination experiments were conducted using increasing concentrations of the ADEPT prodrug (alone or with the fusion protein) in the presence of either 25 nM UCN-01 or 0.1 μM PF-477736. ADEPT combined with PF-477736 caused 50% growth inhibition at a lower prodrug concentration than ADEPT did alone (Figure 5.8). This corresponded to a $GI_{50}$ of 0.13 (± 0.03) μM for ADEPT/PF-477736, as opposed to 0.17 (± 0.02) μM for ADEPT alone. The $GI_{50}$ of ADEPT in combination with UCN-01 was 0.18 (± 0.02) μM, which was similar to ADEPT alone (Figure 5.8). However, at concentrations of > 0.2 μM prodrug, there appeared to be a more rapid increase in growth inhibition compared to ADEPT alone. We also showed that

the prodrug or fusion protein alone in combination with either Chk1 inhibitor had no growth inhibitory effect on the cells (Figure 5.8). Additionally, there was no effect on cells incubated in the presence of 25 nM UCN-01 or 0.1 μM PF-477736 over 96 hr and absorbance readings were similar to that of untreated cells.
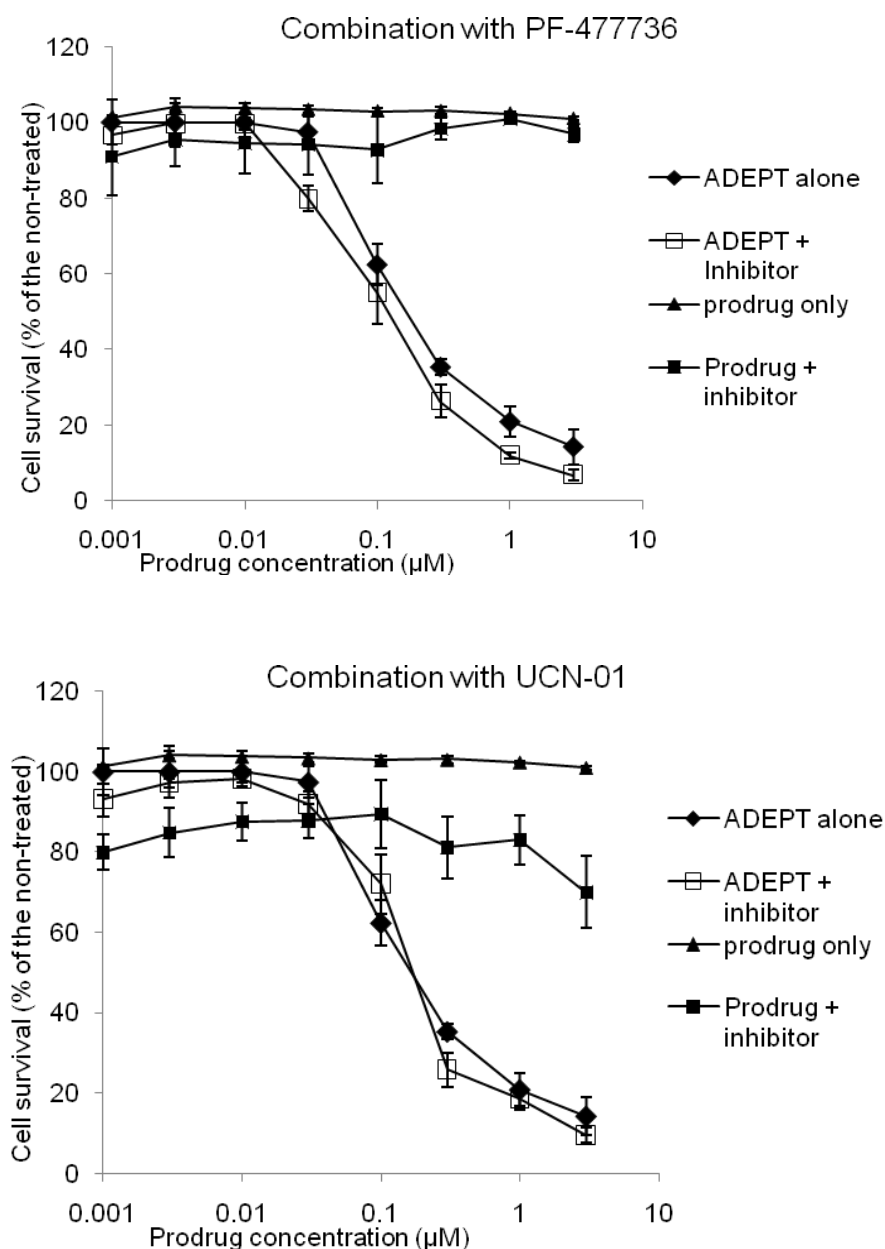


**Figure 5.8 Growth inhibitory effect of Chk1 inhibitors in combination with ADEPT**

Cells were treated with: ADEPT alone; ADEPT plus Chk1 inhibitor (0.1 μM PF-477736 or 25 nM UCN-01); prodrug alone; or prodrug plus Chk1 inhibitor (0.1 μM PF-477736 or 25 nM UCN-01). Following treatment cells were incubated in drug-free medium with or without Chk1 inhibitor (0.1 μM PF-477736 or 25 nM UCN-01) for 96 hr and SRB applied. Plots are representative of 3 independent experiments, mean ± SEM.

Unfortunately, these results do not show that the combination therapy is (statistically) favourable, in terms of growth inhibition, compared to ADEPT alone. In the context of combination therapy, it would be necessary to investigate the methodology of these growth experiments further and to determine the existence of synergy. [Note: the Chou-Talalay combination index (CI) method (447, 448)) was used to test for synergy between the effect of ADEPT and Chk1 inhibition using the growth inhibition values. The CI algorithm, based on the laws of mass action, has been used by researchers to determine synergism with drug combinations, particularly in cancer therapy as listed in the review by Chou and Talalay (449). However, appropriate assumptions regarding synergism using these growth inhibition values could not be deduced at the time]. In light of the data presented, it was postulated whether the effect of the drug combinations could be recognised in a different experiment, namely cell cycling by FACs. A concentration of 0.3 μM prodrug, which was found to induce approximately 75% growth inhibition, was sufficiently potent but not too toxic to test therapeutic efficacy in subsequent *in vitro* experiments.

### 5.2.3.2 *Chk1 inhibitors attenuate G2/M arrest and augment cell death in ADEPT-treated cells*

In light of the growth inhibition experiments it was think that To determine whether the combination therapies had an effect on cell cycling, The established concentrations of ADEPT and Chk1 inhibitor combinations were subsequently used to assess the effect on cell cycling activity. SW1222 cells were treated with ADEPT using 0.3 μM prodrug in the presence of 25 nM UCN-01 or 0.1 μM PF-477736. Cells were then cultured in media containing Chk1 inhibitor and harvested at different time points post-ADEPT. In the presence of Chk1 inhibition, ADEPT-treated cells appeared to undergo normal cell cycling for at least 6 hours after treatment (Figure 5.9, and also Appendix 2 for individual stacked column charts). At 24 hr-post-ADEPT in the presence of inhibitor, cells underwent growth arrest at the G2/M phase, compared to cells treated with the inhibitor alone. This demonstrated that changes in the cell cycle were due to the effect of ADEPT. In cells treated with the sub-toxic dose of Chk1 inhibitor alone, cell cycling was comparable to normal

untreated cells (Figure 5.9). This confirms that any changes in the cell cycle are due to the effect of ADEPT, with Chk1 acting as a sensitiser. At 24 hr-post-ADEPT plus UCN-01, 34% cells were in G2/M phase compared to 19% with UCN-01 alone; and ADEPT plus PF-477736, 38% cells were in G2/M phase compared to 15% with PF-477736 alone (Figure 5.10). Notably, at 48 hr post-treatment, cells treated with ADEPT in presence of UCN-01 or PF-477736 showed a significant ($p < 0.001$) decrease in the proportion of cells in G2/M, 13% and 10% (respectively) (Figure 5.10). This equated to 72% (ADEPT plus PF-477736) or 63% (ADEPT plus UCN-01) decrease from 24 to 48 hr post-treatment, compared to 35% with ADEPT alone. This suggested that in the presence of Chk1 inhibition a greater proportion of cells were able to overcome the G2/M block and re-enter the cell cycle (mitosis) compared to ADEPT alone.
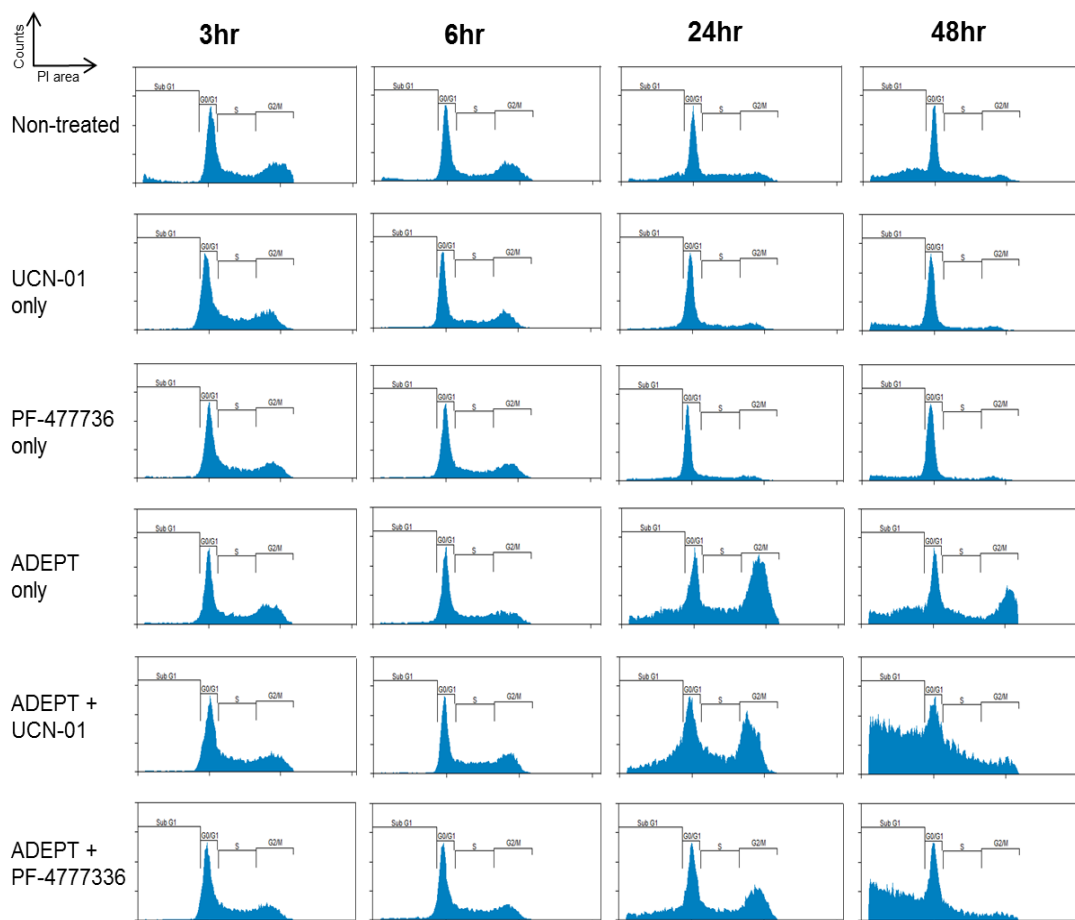
**Figure 5.9 Representative cell cycle analyses of SW1222 cells treated with or without ADEPT and in the presence of Chk1 inhibitors**

Cells were exposed to Chk1 inhibitor alone (25 nM UCN-01 or 0.1 μM PF-477736) alone, or in combination with ADEPT (0.3 μM prodrug). Following treatment, cells were fixed with 70% cold ethanol and stained with 50 μg/ml propidium iodide (PI) solution per million cells. Cell solution was analysed by flow cytometry. Data taken from individual experiments are representative of the calculated means. Graphical portions refer to cell cycle phases (L to R): Sub G1, G0/G1, S, G2/M.
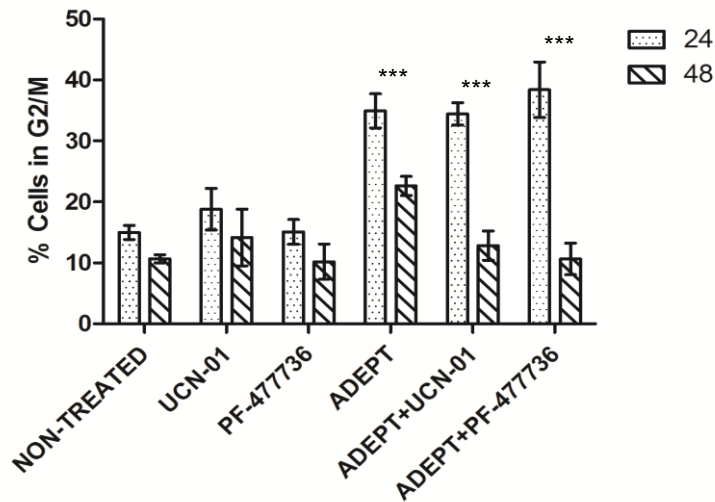
**Figure 5.10 G2/M cell fraction at 24 and 48 hr-post-ADEPT (± Chk1 inhibition)**
SW1222 cells were treated with or without ADEPT in combination with UCN-01 or PF-477736, as described in Figure 5.9. Non-treated and ADEPT data were taken from Figure 5.5. Data are representative of at least 3 independent experiments, mean ± SEM. *** $p < 0.001$ of the difference between 24 and 48 hr.

Interestingly, the large decrease in the G2/M fraction at 48 hr-post ADEPT in the presence of Chk1 inhibitor coincided with an increase in sub-G1 fraction (dead cells) (Figure 5.9 and Figure 5.11). Up to 24 hr, any differences in the sub-G1 fraction between non-treated, ADEPT alone and ADEPT in the presence of Chk1 inhibitors had been relatively small and non-significant. By 48 hr cell death was significantly higher in ADEPT plus Chk1 inhibitor with 49% and 52% fraction of cells in sub-G1, compared to 33% following ADEPT alone ($p< 0.001$) (Figure 5.11). When the data was analysed without the sub-G1 portion (data not shown), there was little difference between cell cycling of the ADEPT-treated cells in the presence and absence of Chk1 inhibitors. These data suggested that UCN-01 and PF-477736 promote cell cycle progression through the G2-to-M checkpoint, and any cells containing damaged DNA, ultimately die.
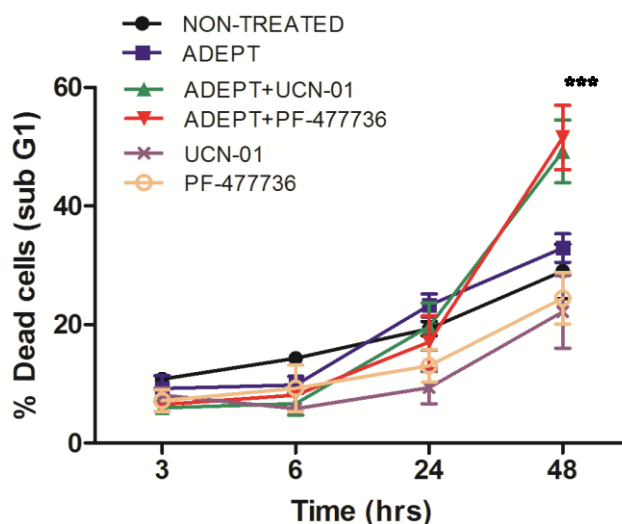
**Figure 5.11 Change in proportion of dead cells post-ADEPT (± Chk1 inhibition)**
SW1222 cells were treated with or without ADEPT in combination with UCN-01 or PF-477736, as described in Figure 5.9. Non-treated and ADEPT data were taken from Figure 5.5. Data are representative of at least 3 independent experiments, mean ± SEM. *** p < 0.001 of the difference between 24 and 48 hrs.

The expression of Chk1-p and Chk2-p following treatment with ADEPT plus UCN-01 or PF-477736, was determined by Western blotting. SW1222 cells were treated with ADEPT in the presence of 25 nM UCN-01 or 0.1 µM PF-477736, as described previously, and non-ADEPT-treated cells were exposed to the same concentrations of inhibitor only. Cells were lysed at 1, 3, 24 and 48 hr-post-ADEPT, 15-20 µg cell lysate loaded onto 4-20% Tris/Gly gels and the protein mixture separated by SDS-PAGE. Protein was transferred onto PVDF membrane and stained with anti-Chk1-p and Chk2-p antibodies. The relative difference in expression of ADEPT-treated cells, compared to non-ADEPT-treated cells, was quantified by Image J. In the presence of UCN-01 or PF-477736, Chk1-p expression increased at 3 hr in ADEPT-treated cells 1.6- and 1-fold (±0.65 and ±0.21), respectively, relative to the non-ADEPT-treated (Figure 5.12A and B). By 24 hr-post-ADEPT expression levels of Chk1-p were down-regulated by 0.5- and 0.4-fold difference (±0.3 and ±0.37) in the presence of UCN-01 or PF-477736 (respectively). By 48 hr-post-ADEPT, Chk1-p levels below baseline levels of the non-ADEPT-treated cells were sustained. These findings suggested diminished Chk1 activity at 24 hr-post ADEPT as a result of Chk1 inhibition, when compared with the increased Chk1-p levels observed in ADEPT-only-treated cells (Figure 5.13 B). Chk2-p expression in cells treated with ADEPT

plus UCN-01 increased up to 24 hr by 2-fold (± 0.7), and by 48 hr levels decreased to 0.8-fold (±0.03), relative to non-ADEPT-treated cells. In the presence of PF-477736, Chk2-p expression increased steadily over 48 hr following ADEPT by 1.4-fold (±0.4), relative to the non-ADEPT-treated cells (Figure 5.12A). The data suggested low levels of Chk2 activity possibly caused by Chk1 inhibition following ADEPT, compared to ADEPT alone (Figure 5.12B), and may indicate a role for Chk2 in response to ADEPT.
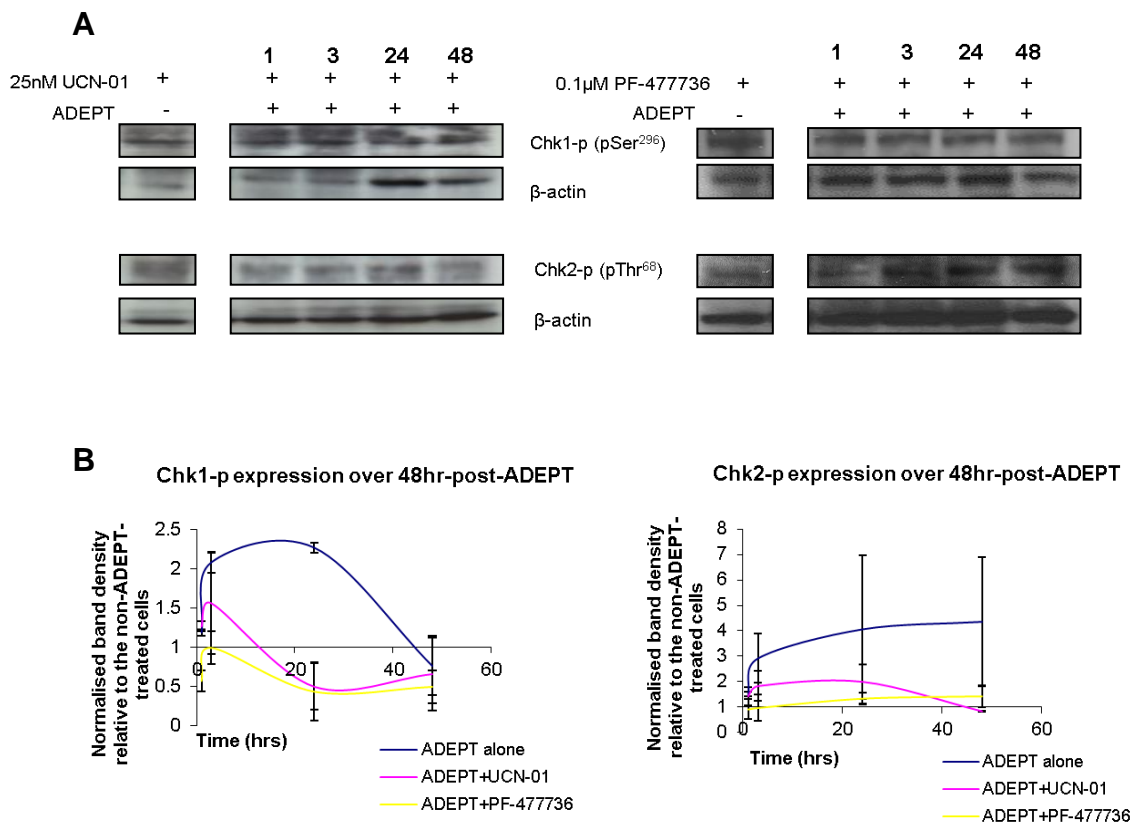


**Figure 5.12 Expression of Chk1-p (Ser296) and Chk2-p (Thr68) in SW1222 cells treated with ADEPT in combination with Chk1 inhibitors**

Cells were treated with ADEPT in combination with UCN-01 or PF-477736, as described previously. A) Specific bands for Chk1-p and Chk2-p generated by Western blotting. B) In the presence of Chk1 inhibitors, low levels of activated Chk1 and Chk2 were observed compared to cells treated with ADEPT alone (data taken from Figure 5.6), where < 1-fold difference was considered below levels of that in the non-ADEPT-treated cells. Data are representative of at least 2 independent experiments, and protein expression relative to the non-ADEPT-treated cells was quantified by densitometry using Image J. β-actin protein was used as an experimental control.

Together, the results revealed that Chk1 inhibitors sensitised ADEPT-treated cells to cell death, although the overall cycling of live ADEPT-treated cells remained unchanged; and Chk1 inhibition by UCN-01 and PF-477736 was specific for Chk1.

## 5.3 Discussion

The data presented in this Chapter described and investigated approaches to enhance the therapeutic potential of a single cycle of ADEPT by attempting to target the DNA damage signalling/repair pathways. In the first instance, DNA damage response to ADEPT at the gene level was investigated but found to provide little information regarding strategies for intervention. Secondly, it was hypothesised that the therapeutic potential of a single cycle of ADEPT would be enhanced by inhibiting cell cycle checkpoint activation. The hypothesis was tested using clinically validated Chk1 inhibitors, UCN-01 and PF-477736, which were found to potentiate the cytotoxicity of ADEPT in SW1222 cells.

### 5.3.1 Identifying changes in regulation of DNA damage response genes post-ADEPT

Regulation of gene expression was assessed in response to a single cycle of ADEPT using the $RT^2$ PCR array system containing 84 primers for genes involved in DNA damage signalling. Of the large pool of genes quantified in SW1222 cells treated with to ADEPT, only 14 were found to undergo changes in their transcript levels at 24 hr post-treatment compared to the non-treated cells. Furthermore, the gene expression changes were small in magnitude and down-regulation was the predominant effect. Similarly, in an assessment of various DNA damaging compounds, alkylating agents caused fewer and less robust changes in the expression of the smallest number of genes, although they were found to be the most mutagenic compounds tested (compared to reactive oxygen species and topoisomerase inhibitors) in lymphoma cells (450). It is believed that the down-regulation of the genes, namely, PCNA, FEN-1, LIG1, UNG, PNKP, may be the result of a negative feedback mechanism linked to BER. BER is a highly coordinated, multistep pathway that corrects small DNA modifications or damaged DNA bases resulting from

cellular metabolism such as methylation, deamination and hydroxylation (451). Bifunctional alkylating agents induce monoadducts, in addition to ICLs, which may be repaired via the BER pathway. In fact, monoadducts constitute the majority of lesions by nitrogen mustards; however they are not potent enough to cause a tumour response.

In long-patch BER, PCNA recruits base-specific glycosylases and apurinic/apyrimidinic (AP) endonuclease (452) (453) to the damaged site (454) (455). The damaged DNA fragment, otherwise known as a 5' overhanging flap, is removed by the FEN-1 protein (456) (457), which is recruited by PCNA (458). PNKP primes the DNA strand-break ends with hydroxyl or phosphate groups prior to ligation by DNA ligase I (LIG1) in DNA synthesis (459). Uracil DNA glycosylases (UNG) recognise uracil in DNA, which may arise either by spontaneous deamination of cytosine or by the mis-incorporation by DNA polymerases during DNA synthesis in BER (460).

In addition to its role in BER, FEN-1 also has important roles in DNA replication and homologous recombination (HR) (461) (462). In fact, research has linked HR repair in response to BER strand-break intermediates (463), and BER in ICL repair has also been noted (273). Furthermore, there is evidence to support the role of BER in mediating cisplatin toxicity (464). Thus, targeting proteins involved in BER has been suggested as a strategy to enhance the sensitivity of tumour cells to alkylating agents (465). One study showed that targeting FEN-1 with an inhibitor increased the cytotoxic effect of the alkylating agent, temozolomide (466).

Quantifying changes in mRNA levels does not provide any information about the post-transcriptional and post-translational modifications of mRNA-to-protein product. These modifications, including acetylation, phosphorylation, methylation and ubiquitinylation (to name a few), are involved in orchestrating the chromatin responses to DNA damage (312) and may have dramatic effects on the overall function of the resulting protein. Thus, two genes were selected to assess their respective cellular protein levels post-ADEPT. Western blot analysis revealed up-regulation of PCNA at 24 hr, which did not correlate with the down-regulated gene expression at this time point. This probably tells us: a) the protein undergoes post-

translational modifications that allow it to have a significant impact (or not) on the cell; and/or b) gene regulation is an early event in response to the constant changing cell environment. Since PCNA, along with other BER/replication-related genes, were down-regulated, it would suggest that the decrease in PCNA transcript levels was a negative response to the elevated protein levels reflecting the real-time changes occurring in the cells. With that, the elevated PCNA protein levels at 24 hr-post-ADEPT was supportive of its role in repair and/or DNA synthesis which corresponded to cell cycle arrest at 24 hr-post-ADEPT. By 48 hr, PCNA protein levels returned to normal suggesting repair was complete and cells returned to normal cycling. NBS1 protein was also analysed since gene expression was down-regulated at 24 hr and it is a protein involved in DNA damage repair, specifically being recruited by γ-H2AX to sites of DSBs. Similar to PCNA, NBS1 protein levels were found to be up-regulated at 24 and 48 hr-post-ADEPT.

The genes that exhibited up-regulated expression at 24 hr following exposure to ADEPT - BTG2 and DDIT3 – have been shown to be involved in the negative regulation of cell cycle progression (467) (468) (441) and cell proliferation (469) in response to DNA damage, and are also associated with apoptosis. The up-regulation of these genes in SW1222 cells may be associated with G2/M growth arrest observed in these cells at 24 hr upon exposure to ADEPT. In lymphoma cells exposed to alkylating agents, G2/M arrest was also observed at 24 hr post-treatment (470) (450) and this was accompanied by an increase in transcript levels of BTG2 (450). DDIT3 (CHOP) protein elevation was also observed in response to alkylating agents, including methyl methanosulphate (471) (472).

### 5.3.2   Analysing cell cycle activity in response to ADEPT

The G2/M growth arrest observed in SW1222 cells at 24 hr-post-ADEPT indicated that cells were undergoing DNA damage repair, as discussed in Chapter 4. It would appear that this arrest was most likely induced by stalled replication forks caused by ICLs (424), since there is no evidence that ICLs alone inactivate G1 or G2 cell cycle checkpoints, suggesting that they are tolerated by the cell until the DNA replication fork is encountered (281). ADEPT-treated cells appeared to overcome this G2 arrest

at 48 hr, indicating perhaps the presence of non-damaged and/or repaired cells that resumed normal cycling as a viable population. Thus, a delay in the cell cycle was sufficient to circumvent the potentially toxic effects of the activated nitrogen mustard drug (473) (470). Moreover, there appeared to be little difference in the dead cell (sub-G1) population between non-treated and ADEPT-treated cells over 48 hr, further highlighting the fact that repair was occurring in response to a single cycle of ADEPT.

Cell cycling activity was also assessed by means of Chk1 and Chk2 kinases, which are involved in checkpoint control and DNA damage repair in the G2-to-M and G1-to-S phases (respectively) (435) (474). Up-regulated expression of Chk1-p at 3 and 24 hr-post-ADEPT indicated activation of Chk1. Interestingly, this increase in Chk1 phosphorylation appeared to correlate with the G2/M growth arrest observed at 24 hr-post-ADEPT. Activated Chk1 phosphorylates the cell cycle phosphatase, Cdc25C, which prevents the dephosphorylation and activation of cyclin-dependent kinase 1 (Cdk1), resulting in blockade of G2/M transition and delay in mitotic entry (475) (476). Another role for Chk1 is in DNA repair, notably HR, which preferentially occurs in G2 phase (477). This is supported by studies showing that Chk1 is involved in the phosphorylation and recruitment of RAD51 (Chapter 4) to DNA repair foci (478) (479) (335). By 48 hr, activated Chk1 levels decreased to less than baseline/control levels, which may correlate with the resume of normal cell cycling and possibly resolution of DNA damage repair.

When the same cells were analysed for Chk2 activity, protein levels of Chk2-p were found to increase over 48 hr-post-ADEPT reaching 4-fold difference compared to the untreated cells by 24 hr. The findings may implicate a role for Chk2 in controlling or mediating DNA damage repair and/or cell cycle arrest (478) (480). In camptothecin-treated colon cancer cells, Chk2-p increased progressively up to 72 hr-post-drug treatment whilst phosphorylated Chk1 was found to disappear by 48 hr (478). Indeed, activation of Chk2 at later time points post-drug treatment may function as a negative regulatory mechanism in the cell cycle and have an anti-apoptotic effect in response to DNA damage (481). There is substantial overlap in the activities of Chk1 and Chk2. For example, in cisplatin-induced DNA cross-linking and replication stress, both Chk1 and Chk2 were activated in an ATR-dependent manner (482).

### 5.3.3 Evaluating the cellular response to ADEPT in combination with Chk1 inhibitors

With data supporting a role for Chk1 activation during ADEPT-induced G2/M arrest, it was hypothesised that inhibition of Chk1 would impede growth arrest and DNA repair and lead to increased tumour cell death (483) (484). Mechanistic studies to inhibit G2/M arrest induced by alkylating agents had already begun in the early 1990s (470) (485). UCN-01 was one of the first Chk1 inhibitor compounds to show promising pre-clinical anti-cancer therapy as a single agent (486) (487) (488), and in combination with various DNA damaging agents (489) (490) (491), due to its anti-proliferative effects and cytostatic properties in several human tumour cells lines (492) (493). UCN-01 is the only inhibitor to have undergone extensive pre-clinical and clinical investigation, however due to its relative high affinities for multiple cell cycle kinases, second-generation inhibitors were developed with greater selectivity for Chk1. Second-generation Chk1 inhibitors include: PF-477736 (494) (495), AZD7762 (496) (497), SAR-020106 (498) and XL-844 (499). Potentiation of gemcitabine efficacy by these compounds has been demonstrated in xenograft models and clinical trials (500) (440). UCN-01 and second-generation Chk1 inhibitors in combination with DNA damaging agents have demonstrated particular success in p53-defective/deficient tumour cells (501) (502) (503) (504) (505). The combined effect of loss of p53 and inhibition of Chk1 are believed to create a synthetic lethal interaction. Synthetic lethality was first shown to be an effective anti-cancer strategy in BRCA1-deficient tumour cells with poly(ADP-ribose) polymerase (PARP) inhibitors. Inhibition of Chk1 in p53$^{-/-}$colon carcinoma cell lines was shown to abrogate G2/M arrest and increase cytotoxicity induced by irradiation and cisplatin (506); and gemcitabine (496). Nevertheless, there is surmounting evidence to show that Chk1 inhibition can be just as effective in cancer cells irrespective of p53 status (507) (508) (509). The SW1222 colon carcinoma cell line studied here possessed a p53-defective gene (405) and its corresponding protein was also shown to be absent in Western blotting (personal communication with Dr Hassan Shahbakhti). The effect of Chk1 inhibition in ADEPT-treated p53-defective SW1222 cells was proposed a synthetic lethal interaction; and first and second generation Chk1 inhibitors, UCN-01 and PF-477736, were used to test this.

The growth inhibition (SRB) assay was used to determine the concentrations of Chk1 inhibitor and prodrug that could be combined together. For combination experiments the concentrations of inhibitor were selected based on a $GI_{10-20}$, that is, a sub-toxic dose that alone did not demonstrate growth inhibition on SW1222 cells. ADEPT in combination with PF-477736 had a greater growth inhibitory effect ($GI_{50}$ of 0.13 µM) than that observed for ADEPT alone ($GI_{50}$ 0.17 µM) and ADEPT in combination with UCN-01 ($GI_{50}$ 0.18 µM). These results, however, were not reflective of the data obtained from the cell cycling studies, which may suggest a review of the methodology used to determine growth inhibition/cell viability would be necessary for future work. Indeed, cell cycling studies showed that viable tumour cells (untouched by the toxic insults) continued normal cycling, and it's these cells which may have been detected in the growth inhibition assay, especially if they had 96 hr to recover post-drug regimen.

Growth arrest of cells in G1, intra-S and G2 in response to DNA damage is a well-documented phenomenon that permits cells to repair damaged DNA before, during or after replication and before mitosis (respectively). As inhibitors of Chk1, UCN-01 and PF-477736 have been shown to abrogate S- and G2- phase arrest in cells undergoing DNA damage (438). It was shown here that UCN-01 and PF-477736 attenuated G2/M arrest at 48 hr-post-ADEPT (fraction of cells: 13 and 10%, respectively), compared to ADEPT alone (23%) and inhibitor only (19 and 15%, respectively). This was paralleled with a significantly large increase in cell death at 48 hr (sub-G1 fraction: 49 and 52%) when ADEPT was combined with UCN-01 and PF-477736 (respectively), compared to ADEPT alone (33%). The findings suggested that a greater proportion of cells in G2/M (at 24 hr-post-ADEPT) exited this arrest, by 48 hr. An increase in cell death was observed in Chk1-deficient/-inhibited cells exposed to antimetabolites, cytarabine or gemcitabine (510) (504). Since the integrity of the replication fork during cell cycling relies on Chk1, in the absence of Chk1, increased cell death was found to result from three cellular events (according to researchers (511) (512)): activation of late origin firing, destabilization of stalled replication forks and cell cycle progression from G1/S directly to mitosis. The increased sub-G1 fraction at 48 hr, observed here, implied that cells were probably forced to enter mitosis regardless of DNA damage incurred or repaired. It is thought

that the damaged cells died by a process known as mitotic catastrophe, prior to apoptosis. Mitotic catastrophe is an event in which a cell is destroyed during mitosis because of aberrant chromosome segregation or DNA damage resulting in multiple micronuclei (513). The occurrence of mitotic catastrophe was not determined here, although it has been shown to be a feature of ICL-induced death in mammalian cells (251, 513).

A change in Chk1 and Chk2 was also observed in cells treated with ADEPT in combination with UCN-01 or PF-477736. A small increase in Chk1-p expression was observed over 3 hr-post-ADEPT, and this was followed by a decrease in levels by 24 hr to below baseline/control levels, and low Chk1-p expression levels persisted up to 48 hr. This was in contrast to the increase in Chk1-p expression in ADEPT-only-treated cells. Indeed, decreased Chk1-p (Ser$^{296}$) expression is a recognised biomarker of Chk1 inhibition (514) (438) (498) (497). Knockdown of ATR mediates the phosphorylation of Ser$^{345}$ and Ser$^{317}$ on Chk1, which in turn mediates autophosphorylation of Ser$^{296}$ (515). In general, levels of Chk1-p were low (compared to non-ADEPT-treated), which suggested Chk1 activation was being inhibited by UCN-01 or PF-477736. Chk1 activity was particularly low in PF-47736-treated cells, emphasising the selective nature of this inhibitor. PF-477736 has been shown to specifically inhibit Chk1 with an IC$_{50}$ value of 0.49 nM (494), and for UCN-01 an IC$_{50}$ value of 11 nM was reported (440). Both inhibitors have been shown to inhibit Chk2 with a 100-fold selectivity ratio (440). Interestingly, the pattern or timing of inhibition observed here occurred earlier (24 hr-post-ADEPT) compared to the attenuation of G2/M growth arrest (48 hr-post-ADEPT). Like most protein kinase inhibitors, Chk1 inhibitors function by competitive inhibition of the ATP binding pocket (516) (515). It would be interesting to assess the lasting inhibitory activity (> 48 hr-post-ADEPT) of these agents at the phosphorylation level and the corresponding cell cycling phases. Measuring total Chk1 levels would have provided further quantitative information regarding the relative levels of phosphorylated Chk1 compared to non-phosphorylated Chk1.

Chk2 activity was observed in ADEPT-treated cells in the presence of Chk1 inhibitors, and there were differences between the two inhibitors. Chk2-p expression levels increased up to 24 hr post-ADEPT/UCN-01 combination, which was similar to

that in ADEPT-only-treated cells. At 48 hr, expression decreased to levels below baseline, which was not observed in ADEPT-only-treated cells. This is may have indicated suppression of Chk2 phosphorylation by Chk1 inhibitors, since Chk1 inhibitors have been shown to target Chk2 (514). In the presence of PF-477736, Chk2-p expression increased over 48 hr in ADEPT-treated cells. The increase in Chk2 observed with the Chk1 inhibitors implied that Chk2 may have had a compensatory effect as a result of the inhibition of Chk1 phosphorylation (517), concomitant with cell cycle arrest at 24 hr-post-ADEPT. It is believed that G2/M arrest (with or without inhibitors) is mediated in part by Chk2 (478) (480) (518) (519). One event demanding Chk2 function is the generation of DSBs in S phase, that is, when Chk2 increases the rate of phosphate exchange on Cdc25A residues targeted by Chk1 (520), and amplifying the "housekeeping" function of Chk1. The findings implicated a role for Chk2 inhibitors in increasing ADEPT-induced cell death. Castedo and colleagues (481) showed that inhibition of Chk2 reduced doxorubicin-induced G2 blockade and concomitantly increased the frequency of apoptotic cells. However, the rationale for Chk2 inhibitors remains unclear and may depend on the cell's genetic background and the genotoxic agent employed (521). The equivocal findings observed here with Chk2 activity in response to the ADEPT/Chk1 inhibitor combination would require further investigation to determine, specifically, the role of Chk2 in ADEPT.

To-date the majority of clinical trials designed to test pre-clinically well-established Chk1 inhibitors in combination with DNA-damaging agents have yet to produce reliable proof-of-concept data. Clinical trial dose-limiting toxicities have varied between compounds and various combinations. Clinical progression with UCN-01 as a single agent or in combination with chemotherapy has been hindered by unfavourable pharmacokinetic and toxicity profiles owing to the compound's high affinity for human α1-acid glycoprotein (522) (523) (524). LY2603618 – one of the first-generation inhibitors - is currently undergoing phase II trials in combination with cisplatin and pemetrexed in metastatic non-small cell lung cancer, and with gemcitabine in pancreatic cancer (525). In the phase I trial of PF-477736 in combination with gemcitabine, 3 patients (out of 36 at the time of publication) exhibited partial responses (526). The trial was terminated early, although one patient

remained on the study until a complete response was observed (study completion 2011) (527).

## 5.4 Summary

It was proposed that control and/or regulation of the DNA damage response to a single cycle of ADEPT could be manipulated to enhance the tumour cell response. To this end it was shown that DNA damage signalling gene profile arrays did not generate a tractable strategy for intervention studies. However, it did provide a genetic fingerprint of the tumour response to ADEPT. A number of genes involved in DNA damage repair and replication were down-regulated at 24 hr-post-treatment, and additionally the small number of genes involved in cell cycle control, prompted an investigation into the cycling activity of SW1222 cells post-ADEPT. A G2/M arrest 24 hr-post-treatment was observed and coincided with an elevation in phosphorylated Chk1 expression at 3 hr and 24 hr compared to unperturbed cells. It was hypothesised that Chk1 inhibition represented a therapeutic strategy for creating a "synthetic lethal" response by overriding the last checkpoint defence against damage induced by genotoxic agents in p53-defective tumour cells. A 75% growth inhibitory concentration of the ADEPT prodrug was established in combination with Chk1 inhibitors, UCN-01 or PF-477736, and found to augment the cell killing capacity of ADEPT in p53-defective SW1222 cells by attenuating G2/M-phase arrest and increasing cell death 48 hr-post treatment. The data indicated that inhibition of Chk1 activity could significantly improve the therapeutic response to single-cycle ADEPT.

University College London

# CHAPTER 6

Pharmacokinetic and Pharmacodynamic Challenges of Antibody-Directed
Enzyme Prodrug Therapy (ADEPT)

Carima Andrady

# 6   Thesis Summary and Future Directions

The aim of the work undergone in this thesis has been to investigate the parameters that would facilitate the development of an enhanced single-cycle ADEPT system. Two parameters were investigated: the first was to develop a favourable pharmacokinetic profile of the current antibody enzyme fusion protein; and the second was to define and manipulate the pharmacodynamic tumour profile of the response to a single cycle of ADEPT.

## 6.1   Addressing the pharmacokinetic challenges

How can ADEPT be delivered most safely and effectively to tumours? In the most recent Phase I ADEPT trial where patients were administered multiple cycles of ADEPT, an increased incidence of myelosuppression was observed (199). The myelosuppression was most likely caused by the generation of activated prodrug in non-tumour tissues, possibly due to the presence of MFECP in these tissues. Furthermore, it had been noted by single and repeated ADEPT trials that the fusion protein cleared too rapidly. A successful ADEPT system requires that a) tumour CPG2 is high and b) non-tumour CPG2 activity is low or absent, at the time of prodrug administration. Failure to achieve a) would lead to reduced therapeutic efficacy, and failure of b) would lead to increased toxicity. It was hypothesised in Chapter 3 that a non-glycosylated fusion protein would accomplish both a) and b), if combined with a glycosylated clearing agent, as outlined in the proposed 3-phase ADEPT (Figure 3.1). Two factors had to be considered - firstly the need to characterise the glycosylations, particularly the O-glycosylations, on the fusion protein/CPG2 and, this was followed by the need to generate a functional and intact non-glycosylated fusion protein/enzyme.

Various approaches to remove the N- and O-linked glycosylations from CPG2 in *P. pastoris* were explored. N-linked glycosylations proved relatively easy to remove without greatly affecting the enzyme activity. O-linked glycosylations were identified by mass spectrometry, but proved more challenging to remove. T55/T57

mutated CPG2 constructs exhibited reduced enzyme activity and exhibited rapid clearance *in vivo*. Full characterisation of glycosylations on proteins from biological systems remains a challenge because of the attachment of structurally different glycans (microheterogeneity) that can occupy different glycosylation sites (macroheterogeneity) on a protein. Mass spectrometry (MS) is widely used for the analysis of glycans because it provides a link between mass and composition. One of the major challenges that hinder the analysis of O-glycosylations is the unwanted side reactions occurring once the oligosaccharides are released from the protein backbone (termed 'peeling') (528). For this purpose, the analysis of the intact glycoprotein and/or glycopeptides, obtained after protease or chemical digestion, is required, especially for identifying site-specific glycosylation. The T55 and T57 residues, in particular, were characterised in this way - in a glycopeptide. Analysis of glycopeptides is by far the most efficient but also challenging process of characterising O-linked glycosylations. As O-glycosylation sites are not indicated by specific consensus motifs, direct analysis of these glycopeptides is especially difficult. Glycosylation analysis at the native intact protein level has the advantage of requiring less sample handling, but chromatography and MS techniques are still in their infancy compared with measurements at the peptide and glycan level. A recent study described a highly sensitive MS technique to profile, characterise and quantify the complex micro-heterogeneity, such as glycosylation, on intact native monoclonal antibodies and antibody-drug conjugates (529).

To produce glyco-free MFECP in yeast *P. pastoris* would be ideal, but whilst it was relatively uncomplicated to identify, characterise and manipulate N-linked glycosylations, the same was not true for O-linked glycosylations. However, obtaining glyco-free MFECP is not impossible, and additionally, progress has been made to try and remove O-linked glycosylations in *P. pastoris*-derived proteins (376) (374). Nevertheless, O-linked glycosylations are mostly linear and complete removal of these glycosylations in MFECP may disrupt the tertiary and quaternary structure of the protein, which in turn, would affect overall protein function, such as antigen binding and enzyme activity. Thus, an alternative solution would be to generate a non-mannosylated glycosylated fusion protein that exhibits mammalian glycosylation patterns. Springer and colleagues (342) were able to successfully generate enzymatically functional CPG2 in mammalian cells, provided the N-linked

glycosylated residues had been mutated. With the current availability and practicality of employing mammalian cell lines for protein production, stable (non-transient) expression of MFECP could effectively be established. For example, the FIp-In™ technology (Invitrogen) is a stable mammalian expression system that allows for site-specific integration of the gene of interest into the mammalian genome. Moreover, it would be of interest to use a glycoengineered *P. pastoris* strain capable of producing mammalian-like glycoforms (530).

## 6.2   Addressing the pharmacodynamic challenges

How can the therapeutic response to ADEPT be augmented? Repair of DNA damage inflicted by the activated prodrug was previously shown to be a limiting factor in the efficacy of ADEPT (246). Alkylating agents were originally chosen for use in the CPG2 ADEPT system because *in vitro* they maintain a log-linear tumour cell kill over a wide range of doses (531). The data presented in Chapter 4 demonstrated the cytotoxicity of the activated prodrug *in vitro* and *in vivo*, and also the repair capacity of cancer cells to effectively remove DNA damaging adducts. Activation of the prodrug was evidenced by the rapid formation of DNA ICL damage, whilst repair was found to occur slowly. In fact, 72% of ICLs, which formed within 1 hr following ADEPT, were unhooked by 48 hr *in vitro*. ICL damage poses a unique DNA repair problem. ICLs are repaired via a multistep process composed mainly of the nucleotide excision repair (NER), translesion synthesis (TLS) and homologous recombination (HR) pathways, as current literature states (270) (338) (411) (532). Future work would investigate the role of other DNA repair pathways activated in response to ADEPT, including (but not limited to): BER (base excision repair), which was evidenced from the gene profiling arrays; and the Fanconi anaemia pathway, which is important in co-ordinating and regulating ICL repair processes (533).

As part of identifying the DNA damage response to ADEPT, $\gamma$-H2AX foci induction was detected in ADEPT-treated cells at 3 and 24 hr-post-ADEPT (Chapter 4). The 3 hr timing of induction appeared to fit well with previous findings observed in tumour

cells exposed solely to nitrogen mustard drugs (320); and this indicated an immediate repair response to ICL damage, namely, ICL repair-associated DSBs. This pattern was also consistent with the biphasic RAD51 response. The first (and more prominent) peak of RAD51 foci induction was detected at 6 hr-post-ADEPT, which was considered to reflect repair of ICL-associated DSBs by homologous recombination (HR). However, if HR repair occurs during S or G2 phase of the cell cycle (477) then this did not fit with the G2 arrest observed at 24 hr-post-ADEPT. Additionally, a clear RAD51 response pattern was not observed *in vivo*, and it was deduced that the role and regulation of RAD51 in HR in response to ADEPT would need to be explored further (421).

*In vivo* data obtained on ICL damage and unhooking over time were found to follow a similar pattern to that obtained *in vitro*. Moreover, the γ-H2AX response correlated well with ICL unhooking at 24 hr following therapy, such that, tumours exhibiting the greatest number of γ-H2AX foci per cell, also displayed the largest comet tail moment post-treatment. The biphasic γ-H2AX pattern observed *in vitro* (but not *in vivo*) was a novel finding, and the peak in γ-H2AX foci at 24 hr would appear to coincide with a number of other genetic, protein and cellular changes discovered in this thesis, in response to ADEPT. Olive at al. (414) suggested that cells must transit S phase in order to stimulate H2AX phosphorylation leading to foci induction at 24 hr. Indeed, G2/M growth arrest (Chapter 5) was found to occur at 24 hr-post-ADEPT, and the γ-H2AX response here was thought to reflect the slow repair of (non-ICL-related) DSBs (411). This was further supported by the second (smaller) peak of RAD51 induction also detected at 24 hr-post-ADEPT (534). It was also interesting to note that the increase in activated Chk1 observed at 3 and 24 hr in ADEPT-treated cells (Chapter 5) correlated with γ-H2AX foci peak induction. It is believed that activation (phosphorylation) of Chk1 following therapy could be an indirect (rather than direct) consequence of ICL-associated DNA damage (535), such as the signals induced by stalled replication forks and/or γ-H2AX.

As an important cell cycle signalling molecule in the DNA damage response pathway, the relative gene expression of Chk1 in SW1222 cells was found to be unchanged over time following ADEPT. This was not the case when levels of the protein were analysed (as mentioned above); and the same pattern ensued for Chk2,

PCNA and NBS proteins, and their respective genes. When an array of DNA damage signalling genes were analysed from cells treated with ADEPT, a noticeable change in gene expression was observed at 24 hr (Chapter 5). However, a change in expression was found in only 17% of the gene array, and most of the genes were down-regulated at 24 hr-post-ADEPT. Interestingly, this down-regulation was thought to reflect the negative regulation of transcription activity, in particular the genes involved in the BER pathway and DNA replication. Thus, ceasing repair activity when it was no longer needed. Negative regulation of repair activity was observed at 48 hr-post-ADEPT, which was denoted by a reduction in γH2AX foci (regulated by the dephosphorylating phosphatases), a significant reduction in the proportion of cells in G2/M phase, and decreased levels of phosphorylated Chk1 (as the G2/M arrest was lifted). Furthermore, the genes (BTG2 and DDIT3), whose levels of expression were up-regulated at 24 hr following ADEPT, are negative regulators of cell cycle progression suggesting their possible involvement in mediating G2/M growth arrest. Negative regulation of the DNA damage response is a crucial event in cells and serves to limit signalling and repair in space and time, disassembly of repair complexes and prevent unwanted DNA repair (536).

ICL unhooking, γ-H2AX and RAD51 responses all pointed towards repair activity in response to a single cycle of ADEPT. Yet, when the cell cycle was analysed, repair activity was most strikingly observed in the negligible differences in cell death populations between ADEPT-treated and non-treated cells (Chapter 5). In general, tumour cells are relatively resistant to cell death induction. DNA ICL repair reflects, in part, acquired drug resistance which is a major clinical impediment to successful cancer therapy (399) (400). This "chemoresistance" is coupled with intrinsic tumour resistance including, epigenetic mechanisms, tumour microenvironmental influences and tumour heterogeneity (537). A prominent feature of tumours is their p53 genetic signature, which may also contribute to tumour drug resistance or sensitivity. Although the p53 gene is not a clinical marker of drug resistance, tumour cells harbouring mutated p53 are likely to be more resistant to drugs compared to p53 wild-type cells when treated with a variety of molecules (538). The p53-defective nature of the SW1222 cell-line was used to our advantage to increase the therapeutic response to ADEPT by inhibiting the mediator of G2/M arrest, Chk1, in the proposed synthetic lethal interaction. Since G2/M arrest and elevated levels of phosphorylated

Chk1 were active in ADEPT-treated SW1222 cells, it was hypothesised that inhibition of Chk1 would impede growth arrest and DNA repair, and lead to increased tumour cell death. To this end, clinically compatible Chk1 inhibitors, UCN-01 or PF-477736, were used as a means to improve the tumour response to ADEPT.

UCN-01 or PF-477736 combined with the ADEPT prodrug were found to: attenuate ADEPT-induced G2/M arrest as demonstrated by the 72% decrease in G2/M fraction from 24 to 48 hr, compared to 35% reduction with ADEPT alone; and increase cell death to ~ 50%, compared to 33% by 48 hr. Although the cells exhibited a greater response to the ADEPT/PF-477736 combination, the differences between the two Chk1 combinations were not significant. UCN-01 and PF-477736 were shown to inhibit active Chk1 as phosphorylated Chk1 expression was down-regulated by 24 hr. The effect on phosphorylated Chk2 was not clear and would require further investigation. There were no significant differences observed between the first and second generation Chk1 inhibitors, though, growth inhibition studies showed that ADEPT/PF-477736 combination appeared to have greater (not statistically significant) cell kill effect compared to ADEPT alone. However, insufficient time and consolidation of the methodology and data prohibited obtaining conclusive assumptions.

Cell cycle experiments conducted here provided the initial basis for exploring the pharmacodynamic endpoints determining the DNA damage response (as defined in Chapter 4) and, ultimately, therapeutic efficacy. Indeed, depletion of Chk1 activity in combination with chemotherapy agents has been shown to result in persistent $\gamma$-H2AX expression and loss of RAD51 localisation to nuclear foci in response to DNA damage, both of which are involved in mediating repair (497) (539). It would be necessary to contrast this work with the effect of Chk1 inhibition in ADEPT-treated p53 wild-type cells, which would essentially establish the validity of synthetic lethality ("hard" or "soft" (540)).

## 6.3  ADEPT in perspective

Efforts to optimise cytotoxic delivery remain an important issue in cancer therapy. The specificity of targeting by the antibody in ADEPT provides a safe and effective means of delivering a toxic chemotherapeutic directly to the tumour. Similar to ADEPT, the concept of antibody-drug conjugates (ADCs) is based on combining the strengths of each molecule whilst eliminating the weaknesses of each individual approach. With an improvement in linker technology and the approval of two ADCs, there has been resurgence in ADC development and use in early phase clinical trials (105). However, the efficacy of ADCs is still limited by toxicity (accumulation in the liver and partial release of the payload), immunogenicity towards the antibody and/or the toxic payload and poor penetration of solid tumours (541). The challenges posed by ADCs presents an ideal opportunity for ADEPT to make a major contribution to cancer therapy.

Achieving optimal clinical efficacy without toxicity is difficult to obtain in cancer therapy and remains a persistent challenge. Clinically, one cycle of therapy is not usually effective in cancer patients. Multiple cycles of therapy, however, brings with it the increased incidence of immunogenicity and clinical drug resistance. In this thesis, I proposed strategies to address the pharmacokinetic and pharmacodynamic challenges of ADEPT that limit its clinical efficacy. Glyco-free MFECP was proposed as the primary approach towards attempting to control the clearance of antibody-enzyme, and this would be proceeded by a clearing agent that would facilitate maximal tumour-to-blood ratios. The idea, although challenging, is not impossible to achieve, and there are opportunities to pursue this area further. Assessing the DNA damage response to ADEPT generated interesting information and indicated repair was occurring in response to a single cycle of therapy. The data also provided a base on which to identify a strategy to overcome DNA damage repair. The work with Chk1 inhibitors demonstrated a unique strategy to improve the therapeutic response to ADEPT, and demands further investigation *in vitro* and *in vivo*.

University College London

# APPENDIX

Pharmacokinetic and Pharmacodynamic Challenges of Antibody-Directed Enzyme Prodrug Therapy (ADEPT)

Carima Andrady

# Appendix 1

**Appendix 1A: PCR profiling arrays**

Average Ct values for DNA damage signalling/repair gene profiling arrays (Section 5.2.1) derived from ADEPT-treated and non-treated SW1222 cells using the RT$^2$ Profiler PCR data analysis software (SABiosciences). Average of 4 independent experiments.

| Symbol | Average Ct | | | | Standard Deviation | | | |
|---|---|---|---|---|---|---|---|---|
| | Control | 1hr | 3hrs | 24hrs | Control | 1hr | 3hrs | 24hrs |
| ABL1 | 24.90 | 23.94 | 24.10 | 24.77 | 0.88 | 0.96 | 0.73 | 0.48 |
| ANKRD17 | 23.37 | 22.57 | 22.86 | 23.10 | 1.03 | 0.96 | 0.53 | 0.27 |
| APEX1 | 20.91 | 19.99 | 19.91 | 20.93 | 1.12 | 1.08 | 1.48 | 0.39 |
| ATM | 29.68 | 28.66 | 29.11 | 28.76 | 1.17 | 1.41 | 0.77 | 0.70 |
| ATR | 25.13 | 24.33 | 24.59 | 25.19 | 0.95 | 1.09 | 0.80 | 0.41 |
| ATRX | 28.23 | 27.43 | 28.16 | 27.73 | 0.95 | 0.89 | 0.63 | 0.28 |
| BRCA1 | 24.07 | 23.26 | 23.62 | 23.45 | 1.34 | 1.18 | 0.78 | 0.28 |
| BTG2 | 28.67 | 27.76 | 28.01 | 26.85 | 2.18 | 1.14 | 0.72 | 1.40 |
| CCNH | 24.81 | 23.96 | 24.43 | 24.94 | 1.12 | 0.98 | 0.75 | 0.41 |
| CDK7 | 24.13 | 23.16 | 23.73 | 23.52 | 1.12 | 1.05 | 0.62 | 0.71 |
| CHEK1 | 23.35 | 22.36 | 22.73 | 23.68 | 1.20 | 1.12 | 0.54 | 0.72 |
| CHEK2 | 25.18 | 24.07 | 24.65 | 24.76 | 1.16 | 1.10 | 0.55 | 0.95 |
| CIB1 | 21.51 | 20.84 | 21.03 | 21.07 | 0.54 | 0.96 | 0.75 | 0.64 |
| CIDEA | 34.26 | 34.29 | 34.36 | 34.29 | 0.86 | 0.78 | 0.55 | 0.28 |
| CRY1 | 24.13 | 23.38 | 23.87 | 24.57 | 0.65 | 1.07 | 0.50 | 0.70 |
| DDB1 | 23.19 | 22.39 | 22.76 | 23.67 | 0.78 | 1.07 | 0.48 | 0.75 |
| DDIT3 | 25.43 | 24.52 | 24.70 | 23.16 | 0.67 | 0.76 | 0.98 | 0.55 |
| DMC1 | 33.42 | 33.01 | 33.36 | 32.04 | 0.87 | 1.14 | 0.47 | 0.87 |
| ERCC1 | 25.46 | 24.77 | 25.10 | 25.08 | 0.79 | 0.95 | 0.65 | 0.80 |
| ERCC2 | 25.18 | 24.51 | 25.54 | 25.41 | 0.86 | 0.98 | 1.71 | 0.78 |
| EXO1 | 24.60 | 23.83 | 23.49 | 24.83 | 0.80 | 1.07 | 0.65 | 1.08 |
| FANCG | 25.56 | 24.98 | 24.99 | 25.39 | 0.88 | 1.01 | 0.47 | 1.22 |
| FEN1 | 23.52 | 22.99 | 22.98 | 24.89 | 1.15 | 1.11 | 0.42 | 1.79 |
| XRCC6 | 21.16 | 20.58 | 20.71 | 21.80 | 1.07 | 1.03 | 0.68 | 0.90 |
| GADD45A | 26.86 | 25.93 | 26.01 | 26.41 | 1.05 | 1.16 | 0.71 | 2.02 |
| GADD45G | 28.27 | 27.56 | 27.85 | 27.80 | 0.84 | 1.04 | 0.43 | 0.62 |
| GML | 35.00 | 35.00 | 35.00 | 35.00 | 0.00 | 0.00 | 0.00 | 0.00 |
| GTF2H1 | 25.11 | 24.53 | 24.13 | 24.50 | 0.53 | 0.92 | 0.71 | 0.39 |
| GTF2H2 | 24.04 | 23.27 | 23.31 | 24.28 | 0.87 | 1.28 | 0.33 | 0.59 |
| GTSE1 | 25.91 | 25.31 | 25.64 | 25.57 | 0.60 | 0.94 | 0.63 | 0.45 |
| HUS1 | 25.15 | 24.38 | 24.56 | 25.36 | 0.96 | 0.98 | 0.52 | 0.61 |
| IGHMBP2 | 26.00 | 25.36 | 25.31 | 26.63 | 0.94 | 1.01 | 0.26 | 1.17 |
| IP6K3 | 35.00 | 34.50 | 35.00 | 35.00 | 0.00 | 0.67 | 0.00 | 0.00 |
| XRCC6BP1 | 26.51 | 25.75 | 25.87 | 26.51 | 0.99 | 1.17 | 0.65 | 0.80 |
| LIG1 | 24.78 | 24.27 | 26.07 | 25.48 | 1.21 | 1.20 | 4.21 | 1.47 |
| MAP2K6 | 25.16 | 24.66 | 25.15 | 25.24 | 1.29 | 0.85 | 0.55 | 0.96 |
| MAPK12 | 29.50 | 28.75 | 29.16 | 29.61 | 0.98 | 1.22 | 0.95 | 0.88 |
| MBD4 | 24.01 | 23.22 | 23.24 | 23.63 | 0.62 | 0.98 | 0.80 | 0.34 |
| MLH1 | 24.42 | 23.61 | 23.91 | 24.22 | 0.47 | 0.83 | 0.81 | 0.12 |

| | | | | | | | | |
|---|---|---|---|---|---|---|---|---|
| MLH3 | 26.23 | 25.50 | 25.50 | 24.79 | 0.58 | 1.00 | 0.88 | 0.40 |
| MNAT1 | 25.03 | 24.27 | 24.57 | 24.43 | 0.53 | 0.97 | 0.78 | 0.76 |
| MPG | 23.43 | 22.56 | 22.71 | 22.94 | 0.52 | 0.92 | 0.85 | 0.37 |
| MRE11A | 27.69 | 26.54 | 27.05 | 27.25 | 0.79 | 1.27 | 0.73 | 0.59 |
| MSH2 | 23.34 | 22.36 | 22.39 | 22.95 | 0.46 | 1.04 | 0.76 | 0.69 |
| MSH3 | 25.17 | 24.18 | 24.67 | 24.48 | 0.71 | 1.13 | 0.79 | 0.75 |
| MUTYH | 25.46 | 24.49 | 25.25 | 24.87 | 0.75 | 1.17 | 0.64 | 1.14 |
| N4BP2 | 26.21 | 25.24 | 25.71 | 25.74 | 0.62 | 0.99 | 0.48 | 1.04 |
| NBN | 25.24 | 24.79 | 24.36 | 26.33 | 0.65 | 2.46 | 0.59 | 1.59 |
| NTHL1 | 24.49 | 24.02 | 24.14 | 24.54 | 0.66 | 1.22 | 0.95 | 0.56 |
| OGG1 | 25.46 | 25.03 | 25.03 | 25.98 | 0.64 | 1.16 | 0.56 | 0.51 |
| PCBP4 | 24.48 | 24.06 | 24.14 | 24.99 | 0.57 | 0.94 | 0.24 | 0.55 |
| PCNA | 21.59 | 20.95 | 20.93 | 22.38 | 0.70 | 1.26 | 0.64 | 0.54 |
| AIFM1 | 22.34 | 21.83 | 22.03 | 22.92 | 0.69 | 1.09 | 0.85 | 0.44 |
| PMS1 | 24.86 | 24.46 | 24.57 | 24.79 | 0.50 | 1.08 | 0.52 | 0.46 |
| PMS2 | 24.37 | 23.79 | 23.90 | 24.31 | 0.61 | 1.09 | 0.35 | 0.62 |
| PMS2P3 | 24.26 | 23.53 | 23.90 | 24.27 | 0.44 | 1.13 | 0.25 | 0.69 |
| PNKP | 24.87 | 24.26 | 24.75 | 25.60 | 0.50 | 1.08 | 0.37 | 1.52 |
| PPP1R15A | 25.10 | 24.19 | 24.98 | 24.69 | 0.70 | 1.26 | 0.30 | 1.34 |
| PRKDC | 21.87 | 21.12 | 21.37 | 21.87 | 0.76 | 1.29 | 0.37 | 0.94 |
| RAD1 | 26.73 | 25.91 | 25.77 | 27.03 | 0.44 | 1.07 | 0.52 | 0.89 |
| RAD17 | 25.35 | 24.71 | 24.84 | 24.69 | 0.60 | 0.92 | 0.86 | 0.21 |
| RAD18 | 24.07 | 23.46 | 23.44 | 23.95 | 0.89 | 1.03 | 0.63 | 0.33 |
| RAD21 | 21.04 | 20.35 | 20.86 | 21.03 | 0.85 | 0.96 | 0.60 | 0.47 |
| RAD50 | 25.46 | 24.72 | 25.13 | 25.65 | 0.94 | 1.14 | 0.45 | 1.07 |
| RAD51 | 28.06 | 27.36 | 27.58 | 27.83 | 0.71 | 1.17 | 0.77 | 0.38 |
| RAD51B | 25.59 | 24.90 | 25.41 | 24.90 | 0.83 | 0.89 | 0.73 | 0.58 |
| RAD9A | 25.95 | 25.00 | 25.06 | 26.08 | 0.80 | 1.11 | 0.63 | 0.55 |
| RBBP8 | 24.48 | 23.69 | 23.67 | 24.64 | 0.71 | 0.85 | 0.80 | 0.40 |
| REV1 | 25.66 | 24.81 | 25.02 | 25.63 | 0.92 | 1.16 | 0.30 | 0.57 |
| RPA1 | 22.68 | 21.85 | 22.02 | 22.94 | 0.94 | 1.28 | 0.71 | 0.88 |
| SEMA4A | 27.52 | 26.80 | 27.54 | 27.58 | 1.06 | 0.89 | 0.97 | 1.86 |
| SESN1 | 25.79 | 25.05 | 24.94 | 25.69 | 1.17 | 1.03 | 0.68 | 0.93 |
| SMC1A | 23.09 | 22.52 | 22.76 | 23.52 | 0.80 | 1.07 | 0.39 | 0.63 |
| SUMO1 | 23.11 | 22.96 | 22.51 | 23.21 | 0.81 | 1.28 | 0.49 | 0.37 |
| TP53 | 33.82 | 32.78 | 33.70 | 33.65 | 0.51 | 1.11 | 0.63 | 0.87 |
| TP73 | 29.95 | 29.15 | 29.11 | 31.04 | 0.76 | 1.24 | 0.47 | 0.63 |
| TREX1 | 25.33 | 24.53 | 24.66 | 25.23 | 0.56 | 1.17 | 0.56 | 0.43 |
| UNG | 22.34 | 21.41 | 21.41 | 23.19 | 0.59 | 1.08 | 0.87 | 0.34 |
| XPA | 24.08 | 23.25 | 23.54 | 24.82 | 0.52 | 0.86 | 0.53 | 0.27 |
| XPC | 25.16 | 24.31 | 24.64 | 24.78 | 0.67 | 0.94 | 0.46 | 0.54 |
| XRCC1 | 24.43 | 23.55 | 24.00 | 24.25 | 0.92 | 1.16 | 0.65 | 0.81 |
| XRCC2 | 25.71 | 24.81 | 24.92 | 25.62 | 0.79 | 1.10 | 0.34 | 0.95 |
| XRCC3 | 29.11 | 28.22 | 28.49 | 29.59 | 1.04 | 1.35 | 0.70 | 1.77 |
| ZAK | 24.28 | 23.27 | 23.65 | 24.18 | 1.08 | 1.18 | 0.52 | 0.85 |
| B2M | 20.96 | 20.50 | 20.62 | 20.78 | 0.55 | 1.07 | 0.80 | 0.28 |
| HPRT1 | 21.94 | 21.36 | 21.31 | 21.89 | 0.43 | 1.13 | 0.80 | 0.34 |
| RPL13A | 19.95 | 19.37 | 19.50 | 18.76 | 0.44 | 0.91 | 0.74 | 0.68 |
| GAPDH | 16.01 | 15.28 | 15.30 | 15.38 | 0.59 | 1.19 | 0.95 | 0.49 |
| ACTB | 17.07 | 16.18 | 16.14 | 17.22 | 0.55 | 1.05 | 0.47 | 0.26 |

Appendix

## Appendix 1B: PCR profiling arrays

The change in the regulation of DNA damage signalling/repair genes derived from ADEPT-treated SW1222 cells (compared to non-treated cells) was computed using the $RT^2$ Profiler PCR data analysis software (SABiosciences). Cut-off is 2 for up-regulation and -2 for down-regulation. (Average of four independent experiments). According to the $RT^2$ Profiler PCR data analysis software: **A -** the gene's expression is relatively low in one sample and reasonably detected in the other sample suggesting that the actual fold-change value is at least as large as the calculated and reported fold-change result; **B -** gene's average threshold cycle is relatively high (> 30), meaning that its relative expression level is low, in both control and test samples; **C -** gene's average threshold cycle is either not determined or greater than the defined cut-off value (35), in both samples meaning that its expression was undetected, making this fold-change result erroneous and un-interpretable.

| | Up/Down Regulation (comparing to control group) | | | | | |
| | 1hr | | 3hrs | | 24hrs | |
| Symbol | Fold Change | Comment | Fold Change | Comment | Fold Change | Comment |
|---|---|---|---|---|---|---|
| ABL1 | 1.24 | OKAY | 1.14 | OKAY | 0.85 | OKAY |
| ANKRD17 | 1.11 | OKAY | 0.93 | OKAY | 0.93 | OKAY |
| APEX1 | 1.21 | OKAY | 1.31 | OKAY | 0.76 | OKAY |
| ATM | 1.29 | OKAY | 0.97 | OKAY | 1.45 | OKAY |
| ATR | 1.11 | OKAY | 0.95 | OKAY | 0.74 | OKAY |
| ATRX | 1.11 | OKAY | 0.68 | OKAY | 1.09 | OKAY |
| BRCA1 | 1.12 | OKAY | 0.89 | OKAY | 1.18 | OKAY |
| BTG2 | 1.20 | OKAY | 1.03 | OKAY | 2.71 | OKAY |
| CCNH | 1.15 | OKAY | 0.85 | OKAY | 0.70 | OKAY |
| CDK7 | 1.25 | OKAY | 0.87 | OKAY | 1.18 | OKAY |
| CHEK1 | 1.26 | OKAY | 1.00 | OKAY | 0.61 | OKAY |
| CHEK2 | 1.38 | OKAY | 0.94 | OKAY | 1.03 | OKAY |
| CIB1 | 1.01 | OKAY | 0.91 | OKAY | 1.04 | OKAY |
| CIDEA | 0.62 | B | 0.61 | B | 0.75 | B |
| CRY1 | 1.07 | OKAY | 0.79 | OKAY | 0.57 | OKAY |
| DDB1 | 1.11 | OKAY | 0.88 | OKAY | 0.55 | OKAY |
| DDIT3 | 1.20 | OKAY | 1.09 | OKAY | 3.71 | OKAY |
| DMC1 | 0.85 | B | 0.68 | B | 2.00 | B |
| ERCC1 | 1.02 | OKAY | 0.84 | OKAY | 1.00 | OKAY |
| ERCC2 | 1.01 | OKAY | 0.51 | OKAY | 0.65 | OKAY |
| EXO1 | 1.08 | OKAY | 1.41 | OKAY | 0.65 | OKAY |
| FANCG | 0.95 | OKAY | 0.97 | OKAY | 0.87 | OKAY |
| FEN1 | 0.93 | OKAY | 0.95 | OKAY | 0.30 | OKAY |
| XRCC6 | 0.95 | OKAY | 0.89 | OKAY | 0.49 | OKAY |
| GADD45A | 1.21 | OKAY | 1.18 | OKAY | 1.05 | OKAY |
| GADD45G | 1.05 | OKAY | 0.88 | OKAY | 1.07 | OKAY |
| GML | 0.64 | C | 0.65 | C | 0.77 | C |
| GTF2H1 | 0.95 | OKAY | 1.29 | OKAY | 1.17 | OKAY |
| GTF2H2 | 1.09 | OKAY | 1.09 | OKAY | 0.65 | OKAY |
| GTSE1 | 0.97 | OKAY | 0.79 | OKAY | 0.98 | OKAY |
| HUS1 | 1.08 | OKAY | 0.98 | OKAY | 0.66 | OKAY |
| IGHMBP2 | 0.99 | OKAY | 1.05 | OKAY | 0.49 | OKAY |
| IP6K3 | 0.90 | B | 0.65 | C | 0.77 | C |

| | | | | | |
|---|---|---|---|---|---|
| XRCC6BP1 | 1.08 | OKAY | 1.02 | OKAY | 0.77 | OKAY |
| LIG1 | 0.91 | OKAY | 0.27 | OKAY | 0.47 | OKAY |
| MAP2K6 | 0.90 | OKAY | 0.66 | OKAY | 0.73 | OKAY |
| MAPK12 | 1.07 | OKAY | 0.83 | OKAY | 0.71 | OKAY |
| MBD4 | 1.11 | OKAY | 1.12 | OKAY | 1.01 | OKAY |
| MLH1 | 1.12 | OKAY | 0.93 | OKAY | 0.88 | OKAY |
| MLH3 | 1.06 | OKAY | 1.09 | OKAY | 2.09 | OKAY |
| MNAT1 | 1.08 | OKAY | 0.90 | OKAY | 1.17 | OKAY |
| MPG | 1.16 | OKAY | 1.08 | OKAY | 1.08 | OKAY |
| MRE11A | 1.42 | OKAY | 1.02 | OKAY | 1.05 | OKAY |
| MSH2 | 1.26 | OKAY | 1.26 | OKAY | 1.01 | OKAY |
| MSH3 | 1.27 | OKAY | 0.93 | OKAY | 1.25 | OKAY |
| MUTYH | 1.24 | OKAY | 0.76 | OKAY | 1.15 | OKAY |
| N4BP2 | 1.25 | OKAY | 0.92 | OKAY | 1.07 | OKAY |
| NBN | 0.87 | OKAY | 1.21 | OKAY | 0.36 | OKAY |
| NTHL1 | 0.88 | OKAY | 0.84 | OKAY | 0.74 | OKAY |
| OGG1 | 0.86 | OKAY | 0.88 | OKAY | 0.54 | OKAY |
| PCBP4 | 0.85 | OKAY | 0.83 | OKAY | 0.54 | OKAY |
| PCNA | 0.99 | OKAY | 1.03 | OKAY | 0.45 | OKAY |
| AIFM1 | 0.91 | OKAY | 0.81 | OKAY | 0.51 | OKAY |
| PMS1 | 0.84 | OKAY | 0.80 | OKAY | 0.81 | OKAY |
| PMS2 | 0.95 | OKAY | 0.91 | OKAY | 0.80 | OKAY |
| PMS2P3 | 1.06 | OKAY | 0.84 | OKAY | 0.76 | OKAY |
| PNKP | 0.97 | OKAY | 0.71 | OKAY | 0.46 | OKAY |
| PPP1R15A | 1.20 | OKAY | 0.71 | OKAY | 1.02 | OKAY |
| PRKDC | 1.07 | OKAY | 0.93 | OKAY | 0.77 | OKAY |
| RAD1 | 1.13 | OKAY | 1.28 | OKAY | 0.63 | OKAY |
| RAD17 | 0.99 | OKAY | 0.93 | OKAY | 1.21 | OKAY |
| RAD18 | 0.97 | OKAY | 1.01 | OKAY | 0.83 | OKAY |
| RAD21 | 1.03 | OKAY | 0.74 | OKAY | 0.77 | OKAY |
| RAD50 | 1.06 | OKAY | 0.82 | OKAY | 0.68 | OKAY |
| RAD51 | 1.04 | OKAY | 0.91 | OKAY | 0.91 | OKAY |
| RAD51B | 1.03 | OKAY | 0.74 | OKAY | 1.24 | OKAY |
| RAD9A | 1.23 | OKAY | 1.21 | OKAY | 0.71 | OKAY |
| RBBP8 | 1.11 | OKAY | 1.15 | OKAY | 0.69 | OKAY |
| REV1 | 1.15 | OKAY | 1.02 | OKAY | 0.79 | OKAY |
| RPA1 | 1.14 | OKAY | 1.03 | OKAY | 0.64 | OKAY |
| SEMA4A | 1.05 | OKAY | 0.65 | OKAY | 0.74 | OKAY |
| SESN1 | 1.07 | OKAY | 1.18 | OKAY | 0.83 | OKAY |
| SMC1A | 0.95 | OKAY | 0.82 | OKAY | 0.57 | OKAY |
| SUMO1 | 0.71 | OKAY | 0.99 | OKAY | 0.71 | OKAY |
| TP53 | 1.31 | B | 0.71 | B | 0.86 | B |
| TP73 | 1.11 | OKAY | 1.17 | OKAY | 0.36 | A |
| TREX1 | 1.11 | OKAY | 1.04 | OKAY | 0.82 | OKAY |
| UNG | 1.22 | OKAY | 1.25 | OKAY | 0.43 | OKAY |
| XPA | 1.13 | OKAY | 0.96 | OKAY | 0.46 | OKAY |
| XPC | 1.14 | OKAY | 0.94 | OKAY | 1.00 | OKAY |
| XRCC1 | 1.18 | OKAY | 0.88 | OKAY | 0.87 | OKAY |
| XRCC2 | 1.19 | OKAY | 1.13 | OKAY | 0.82 | OKAY |
| XRCC3 | 1.19 | OKAY | 1.01 | OKAY | 0.55 | OKAY |
| ZAK | 1.28 | OKAY | 1.01 | OKAY | 0.82 | OKAY |
| B2M | 0.88 | OKAY | 0.83 | OKAY | 0.88 | OKAY |

| HPRT1 | 0.96 | OKAY | 1.02 | OKAY | 0.80 | OKAY |
|-------|------|------|------|------|------|------|
| RPL13A | 0.95 | OKAY | 0.89 | OKAY | 1.75 | OKAY |
| GAPDH | 1.06 | OKAY | 1.07 | OKAY | 1.19 | OKAY |
| ACTB | 1.17 | OKAY | 1.25 | OKAY | 0.69 | OKAY |

# Appendix 2
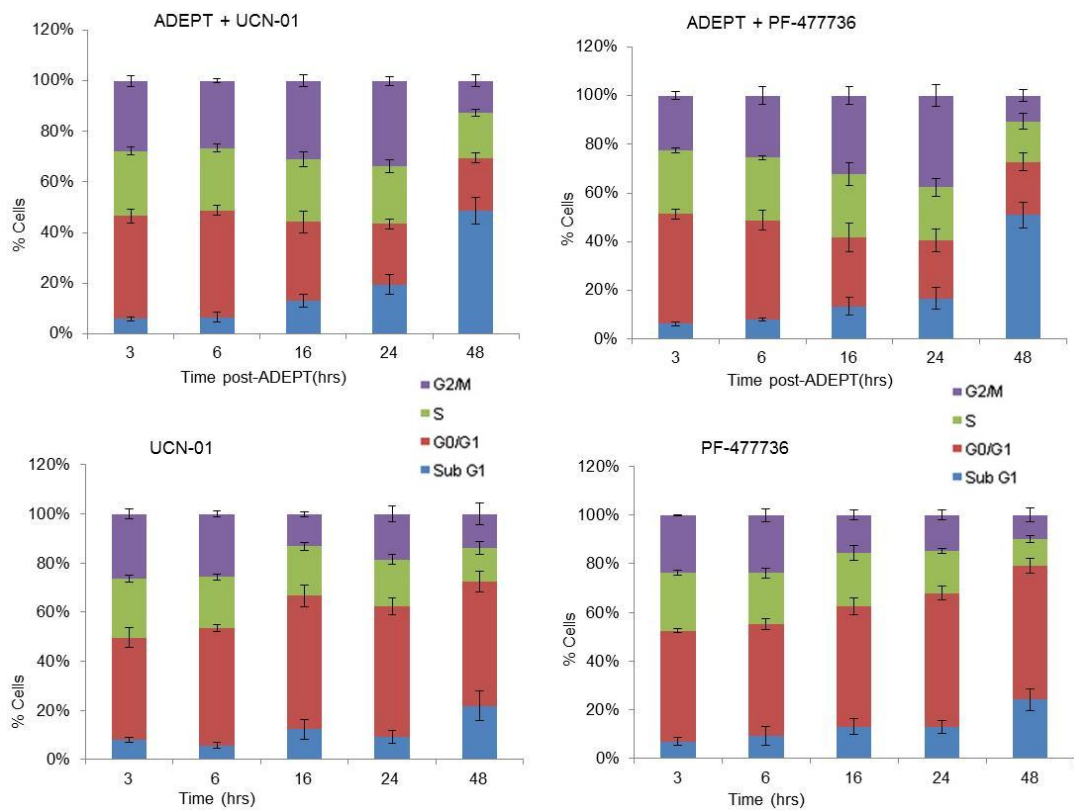


**Appendix 2: Cell cycle analysis of ADEPT in the presence of Chk1 inhibitors**

SW1222 cells were treated with ADEPT using 0.3 μM prodrug (or a drug-free media) and 25 nM UCN-01 or 0.1 μM PF-477736. Cells were subsequently cultured in medium containing respective Chk1 inhibitor alone and harvested at different time points.

# **Extra-Curricular Development**

## **Poster presentations**

- UCL Graduate School Poster Competition – March 2010 and 2011
- Student Day (UCL/NIMR) – May 2010
- UCL Cancer Institute Symposium – July 2011

## **Conferences**

- Global Proteins Summit, London, June 2009
- MicroRNAs and Translation Regulation in Cancer, London, November 2009
- Phage Display symposium, Cambridge, September 2010
- EORTC symposium Berlin, November 2010
- NCRI, UK, November 2011

## **Skills courses**

- Personal and Professional Management Skills
- Confidence Building
- Abstract writing and poster presentations – ThinkWrite™ courses
- Creative thesis writing
- Time-management
- Various career development seminars and career fairs, including Nature Expo 2010 and 2012

## **Supervising and teaching**

- Work experience/summer project students (GCSE-level, A'Level and undergraduate level)
- Practical course for MSc Cancer students (2009 and 2010)

- Public engagement activities, including the Open Day for the UCL Macmillan Cancer Centre

## Work experience

NIHR/Wellcome Cancer Clinical Trials Centre, 2013

## Publications

Andrady C, Sharma S, Chester K. Antibody-Enzyme Fusion Proteins for Cancer Therapy, 2011. *Immunotherapy* 3(2):193-211 (see thesis attachment at the back)

Andrady C *et al*. Synergistic Lethality of Chk1 Inhibitors and Antibody-Directed Enzyme Prodrug Therapy (ADEPT), 2014. Biochemical Pharmacology (submission in progress)

University College London

# BIBLIOGRAPHY

Pharmacokinetic and Pharmacodynamic Challenges of Antibody-Directed
Enzyme Prodrug Therapy (ADEPT)

Carima Andrady

# **References**

1.  Hanahan D, Weinberg RA. The hallmarks of cancer. Cell. 2000;100:57-70.

2.  Hanahan D, Weinberg R. Hallmarks of Cancer: The Next Generation. Cell. 2011;144(5):646-74.

3.  Smith SC, Theodorescu D. Learning therapeutic lessons from metastasis suppressor proteins. Nature reviews Cancer. 2009;9(4):253-64.

4.  Stratton MR, Campbell PJ, Futreal PA. The cancer genome. Nature. 2009;458(7239):719-24.

5.  Klein CA. Parallel progression of primary tumours and metastases. Nature reviews Cancer. 2009;9(4):302-12.

6.  (IARC) G. Section of Cancer Information 2010. Available from: globocan.iarc.fr.

7.  UK CR. Cancer Mortality Statistics Iin the UK in 2010 2013. Available from: cruk.org/cancerstats.

8.  Aggarwal S. Targeted cancer therapies. Nat Rev Drug Discov. 2010;9(6):427-8.

9.  Strebhardt K, Ullrich A. Paul Ehrlich's magic bullet concept: 100 years of progress. Nature reviews Cancer. 2008;8(6):473-80.

10. Currie GA, Basham C. Serum mediated inhibition of the immunological reactions of the patient to his own tumour: a possible role for circulating antigen. BrJCancer. 1972;26(6):427-38.

11. Rosenberg SA, Terry WD. Passive immunotherapy of cancer in animals and man. AdvCancer Res. 1977;25:323-88.

12. Kohler G, Milstein C. Continuous cultures of fused cells secreting antibody of predefined specificity. Nature. 1975;256(5517):495-7.

13. de StGroth SF, Scheidegger D. Production of monoclonal antibodies: strategy and tactics. JImmunolMethods. 1980;35(1-2):1-21.

14. Kabat EA. THE MOLECULAR WEIGHT OF ANTIBODIES. The Journal of Experimental Medicine. 1939;69(1):103-18.

15. Porter RJ. Prolonged suppression by x-ray of adaptation for the secondary antibody response. ProcSocExpBiolMed. 1962;111:583-4.

16. Reeke GN, Jr., Becker JW, Edelman GM. The covalent and three-dimensional structure of concanavalin A. IV. Atomic coordinates, hydrogen bonding, and quaternary structure. Journal of Biological Chemistry. 1975;250(4):1525-47.

17. Edelman GM. Antibody structure and molecular immunology. Science (New York, NY). 1973;180(88):830-40.

18. Padlan EA. Anatomy of the antibody molecule. MolImmunol. 1994;31(3):169-217.

19. Wu TT, Kabat EA. An analysis of the sequences of the variable regions of Bence Jones proteins and myeloma light chains and their implications for antibody complementarity. The Journal of Experimental Medicine. 1970;132(2):211-50.

20. Skerra A, Pluckthun A. Assembly of a functional immunoglobulin Fv fragment in Escherichia coli. Science (New York, NY). 1988;240(4855):1038-41.

21. Porter RR. Separation and isolation of fractions of rabbit gamma-globulin containing the antibody and antigenic combining sites. Nature. 1958;182(4636):670-1.

22. Scott AM, Wolchok JD, Old LJ. Antibody therapy of cancer. Nature reviews Cancer. 2012;12(4):278-87.

23. Adams GP, Weiner LM. Monoclonal antibody therapy of cancer. Nat Biotechnol. 2005;23(9):1147-57.

24. Weiner LM, Surana R, Wang S. Monoclonal antibodies: versatile platforms for cancer immunotherapy. Nat Rev Immunol. 2010;10(5):317-27.

25. Shawler DL, Bartholomew RM, Smith LM, Dillman RO. Human immune response to multiple injections of murine monoclonal IgG. The Journal of Immunology. 1985;135(2):1530-5.

26. Schroff RW, Foon KA, Beatty SM, Oldham RK, Morgan AC, Jr. Human anti-murine immunoglobulin responses in patients receiving monoclonal antibody therapy. Cancer research. 1985;45(2):879-85.

27. Goodman GE, Beaumier P, Hellstrom I, Fernyhough B, Hellstrom KE. Pilot trial of murine monoclonal antibodies in patients with advanced melanoma. JClinOncol. 1985;3(3):340-52.

28. Boulianne GL, Hozumi N, Shulman MJ. Production of functional chimaeric mouse/human antibody. Nature. 1984;312(5995):643-6.

29. Morrison SL, Johnson MJ, Herzenberg LA, Oi VT. Chimeric human antibody molecules: mouse antigen-binding domains with human constant region domains. ProcNatlAcadSci USA. 1984;81(21):6851-5.

30. Colcher D, Pavlinkova G, Beresford G, Booth BJ, Choudhury A, Batra SK. Pharmacokinetics and biodistribution of genetically-engineered antibodies. QJNuclMed. 1998;42(4):225-41.

31. Jones PT, Dear PH, Foote J, Neuberger MS, Winter G. Replacing the complementarity-determining regions in a human antibody with those from a mouse. Nature. 1986;321(6069):522-5.

32. Riechmann L, Clark M, Waldmann H, Winter G. Reshaping human antibodies for therapy. Nature. 1988;332(6162):323-7.

33. Winter G, Harris WJ. Humanized antibodies. Trends in pharmacological sciences. 1993;14(5):139-43.

34. Beckman RA, Weiner LM, Davis HM. Antibody constructs in cancer therapy: protein engineering strategies to improve exposure in solid tumors. Cancer. 2007;109(2):170-9.

35. Holliger P, Hudson PJ. Engineered antibody fragments and the rise of single domains. Nat Biotech. 2005;23(9):1126-36.

36. Byrd JC, Waselenko JK, Maneatis TJ, Murphy T, Ward FT, Monahan BP, et al. Rituximab therapy in hematologic malignancy patients with circulating blood tumor cells: association with increased infusion-related side effects and rapid blood tumor clearance. JClinOncol. 1999;17(3):791-5.

37. Seidman A, Hudis C, Pierri MK, Shak S, Paton V, Ashby M, et al. Cardiac dysfunction in the trastuzumab clinical trials experience. JClinOncol. 2002;20(5):1215-21.

38. Piccart-Gebhart MJ, Procter M, Leyland-Jones B, Goldhirsch A, Untch M, Smith I, et al. Trastuzumab after adjuvant chemotherapy in HER2-positive breast cancer. NEnglJMed. 2005;353(16):1659-72.

39. Moore GL, Chen H, Karki S, Lazar GA. Engineered Fc variant antibodies with enhanced ability to recruit complement and mediate effector functions. MAbs. 2010;2(2):181-9.

40. McCafferty J, Griffiths AD, Winter G, Chiswell DJ. Phage antibodies: filamentous phage displaying antibody variable domains. Nature. 1990;348(6301):552-4.

41. Winter G, Griffiths AD, Hawkins RE, Hoogenboom HR. Making antibodies by phage display technology. AnnuRev Immunol. 1994;12:433-55.

42. Mao S, Gao C, Lo CH, Wirsching P, Wong CH, Janda KD. Phage-display library selection of high-affinity human single-chain antibodies to tumor-associated carbohydrate antigens sialyl Lewisx and Lewisx. ProcNatlAcadSci USA. 1999;96(12):6953-8.

43. Lonberg N, Taylor LD, Harding FA, Trounstine M, Higgins KM, Schramm SR, et al. Antigen-specific human antibodies from mice comprising four distinct genetic modifications. Nature. 1994;368(6474):856-9.

44. Green LL, Hardy MC, Maynard-Currie CE, Tsuda H, Louie DM, Mendez MJ, et al. Antigen-specific human monoclonal antibodies from mice engineered with human Ig heavy and light chain YACs. Nat Genet. 1994;7(1):13-21.

45. Lonberg N. Human monoclonal antibodies from transgenic mice. HandbExpPharmacol. 2008 (181):69-97.

46. Smith GP. Filamentous fusion phage: novel expression vectors that display cloned antigens on the virion surface. Science (New York, NY). 1985;228(4705):1315-7.

47.     Better M, Chang CP, Robinson RR, Horwitz AH. Escherichia coli secretion of an active chimeric antibody fragment. Science (New York, NY). 1988;240(4855):1041-3.

48.     Marks JD, Hoogenboom HR, Bonnert TP, McCafferty J, Griffiths AD, Winter G. By-passing immunization. Human antibodies from V-gene libraries displayed on phage. JMolBiol. 1991;222(3):581-97.

49.     Marks JD, Hoogenboom HR, Griffiths AD, Winter G. Molecular evolution of proteins on filamentous phage. Mimicking the strategy of the immune system. Journal of Biological Chemistry. 1992;267(23):16007-10.

50.     Kempeni J. Preliminary results of early clinical trials with the fully human anti-TNFalpha monoclonal antibody D2E7. AnnRheumDis. 1999;58 Suppl 1:I70-I2.

51.     Weinblatt ME, Keystone EC, Furst DE, Moreland LW, Weisman MH, Birbara CA, et al. Adalimumab, a fully human anti-tumor necrosis factor alpha monoclonal antibody, for the treatment of rheumatoid arthritis in patients taking concomitant methotrexate: the ARMADA trial. Arthritis Rheum. 2003;48(1):35-45.

52.     Yip YL, Ward RL. Application of phage display technology to cancer research. CurrPharmBiotechnol. 2002;3(1):29-43.

53.     Hoogenboom HR. Selecting and screening recombinant antibody libraries. Nat Biotech. 2005;23(9):1105-16.

54.     Persson MA, Caothien RH, Burton DR. Generation of diverse high-affinity human monoclonal antibodies by repertoire cloning. ProcNatlAcadSci USA. 1991;88(6):2432-6.

55.     Knappik A, Ge L, Honegger A, Pack P, Fischer M, Wellnhofer G, et al. Fully synthetic human combinatorial antibody libraries (HuCAL) based on modular consensus frameworks and CDRs randomized with trinucleotides. JMolBiol. 2000;296(1):57-86.

56.     Rothe C, Urlinger S, Lohning C, Prassler J, Stark Y, Jager U, et al. The human combinatorial antibody library HuCAL GOLD combines diversification of all six CDRs according to the natural immune system with a novel display method for efficient selection of high-affinity antibodies. JMolBiol. 2008;376(4):1182-200.

57.     Hanes J, Jermutus L, Weber-Bornhauser S, Bosshard HR, Pluckthun A. Ribosome display efficiently selects and evolves high-affinity antibodies in vitro from immune libraries. ProcNatlAcadSci USA. 1998;95(24):14130-5.

58.     Boder ET, Wittrup KD. Yeast surface display for directed evolution of protein expression, affinity, and stability. Methods Enzymol. 2000;328:430-44.

59.     Boder ET, Wittrup KD. Yeast surface display for screening combinatorial polypeptide libraries. Nat Biotechnol. 1997;15(6):553-7.

60.     Feldhaus MJ, Siegel RW, Opresko LK, Coleman JR, Feldhaus JM, Yeung YA, et al. Flow-cytometric isolation of human antibodies from a nonimmune Saccharomyces cerevisiae surface display library. Nat Biotechnol. 2003;21(2):163-70.

61.     Alonso-Camino V, Sanchez-Martin D, Compte M, Sanz L, Alvarez-Vallina L. Lymphocyte display: a novel antibody selection platform based on T cell activation. PLoSOne. 2009;4(9):e7174.

62.     Yang XD, Jia XC, Corvalan JR, Wang P, Davis CG, Jakobovits A. Eradication of established tumors by a fully human monoclonal antibody to the epidermal growth factor receptor without concomitant chemotherapy. Cancer research. 1999;59(6):1236-43.

63.     Hecht JR, Patnaik A, Berlin J, Venook A, Malik I, Tchekmedyian S, et al. Panitumumab monotherapy in patients with previously treated metastatic colorectal cancer. Cancer. 2007;110(5):980-8.

64.     Van CE. Integration of the anti-EGFR agent panitumumab into clinical practice in metastatic colorectal cancer. ClinAdvHematolOncol. 2007;5(8):611-3.

65.     Tan AR, Moore DF, Hidalgo M, Doroshow JH, Poplin EA, Goodin S, et al. Pharmacokinetics of cetuximab after administration of escalating single dosing and weekly fixed dosing in patients with solid tumors. ClinCancer Res. 2006;12(21):6517-22.

66.     Jain RK. Physiological barriers to delivery of monoclonal antibodies and other macromolecules in tumors. Cancer Res. 1990;50(3 Suppl):814s-9s.

67.     Inbar D, Hochman J, Givol D. Localization of antibody-combining sites within the variable portions of heavy and light chains. ProcNatlAcadSci USA. 1972;69(9):2659-62.

68.     Huston JS, Levinson D, Mudgett-Hunter M, Tai MS, Novotny J, Margolies MN, et al. Protein engineering of antibody binding sites: recovery of specific activity in an anti-digoxin single-chain Fv analogue produced in Escherichia coli. ProcNatlAcadSci USA. 1988;85(16):5879-83.

69.     Bird RE, Hardman KD, Jacobson JW, Johnson S, Kaufman BM, Lee SM, et al. Single-chain antigen-binding proteins. Science (New York, NY). 1988;242(4877):423-6.

70.     Yokota T, Milenic DE, Whitlow M, Schlom J. Rapid tumor penetration of a single-chain Fv and comparison with other immunoglobulin forms. Cancer Res. 1992;52(12):3402-8.

71.     Tolner B, Smith L, Hillyer T, Bhatia J, Beckett P, Robson L, et al. From laboratory to Phase I/II cancer trials with recombinant biotherapeutics. EurJCancer. 2007;43(17):2515-22.

72.     Nelson AL, Reichert JM. Development trends for therapeutic antibody fragments. Nat Biotechnol. 2009;27(4):331-7.

73.     Begent RH, Verhaar MJ, Chester KA, Casey JL, Green AJ, Napier MP, et al. Clinical evidence of efficient tumor targeting based on single-chain Fv antibody selected from a combinatorial library. Nat Med. 1996;2(9):979-84.

74.     Adams GP, Schier R. Generating improved single-chain Fv molecules for tumor targeting. JImmunolMethods. 1999;231(1-2):249-60.

75.     Adams GP, Schier R, McCall AM, Simmons HH, Horak EM, Alpaugh RK, et al. High affinity restricts the localization and tumor penetration of single-chain fv antibody molecules. Cancer Res. 2001;61(12):4750-5.

76.     Wochner RD, Strober W, Waldmann TA. The role of the kidney in the catabolism of Bence Jones proteins and immunoglobulin fragments. The Journal of Experimental Medicine. 1967;126(2):207-21.

77.     Wu AM, Senter PD. Arming antibodies: prospects and challenges for immunoconjugates. Nat Biotechnol. 2005;23(9):1137-46.

78.     Todorovska A, Roovers RC, Dolezal O, Kortt AA, Hoogenboom HR, Hudson PJ. Design and application of diabodies, triabodies and tetrabodies for cancer targeting. JImmunolMethods. 2001;248(1-2):47-66.

79.     Pluckthun A, Pack P. New protein engineering approaches to multivalent and bispecific antibody fragments. Immunotechnology. 1997;3(2):83-105.

80.     Holliger P, Prospero T, Winter G. "Diabodies": small bivalent and bispecific antibody fragments. ProcNatlAcadSci USA. 1993;90(14):6444-8.

81.     Olafsen T, Cheung CW, Yazaki PJ, Li L, Sundaresan G, Gambhir SS, et al. Covalent disulfide-linked anti-CEA diabody allows site-specific conjugation and radiolabeling for tumor targeting applications. Protein engineering, design & selection : PEDS. 2004;17(1):21-7.

82.     FitzGerald K, Holliger P, Winter G. Improved tumour targeting by disulphide stabilized diabodies expressed in Pichia pastoris. Protein Eng. 1997;10(10):1221-5.

83.     Huang BC, Davern S, Kennel SJ. Mono and bivalent binding of a scFv and covalent diabody to murine laminin-1 using radioiodinated proteins and SPR measurements: effects on tissue retention in vivo. JImmunolMethods. 2006;313(1-2):149-60.

84.     Slavin-Chiorini DC, Kashmiri SV, Schlom J, Calvo B, Shu LM, Schott ME, et al. Biological properties of chimeric domain-deleted anticarcinoma immunoglobulins. Cancer research. 1995;55(23 Suppl):5957s-67s.

85.     Kenanova V, Olafsen T, Crow DM, Sundaresan G, Subbarayan M, Carter NH, et al. Tailoring the pharmacokinetics and positron emission tomography imaging properties of anti-

carcinoembryonic antigen single-chain Fv-Fc antibody fragments. Cancer research. 2005;65(2):622-31.

86.     Kenanova V, Olafsen T, Williams LE, Ruel NH, Longmate J, Yazaki PJ, et al. Radioiodinated versus radiometal-labeled anti-carcinoembryonic antigen single-chain Fv-Fc antibody fragments: optimal pharmacokinetics for therapy. Cancer research. 2007;67(2):718-26.

87.     Natarajan A, Xiong CY, Albrecht H, DeNardo GL, DeNardo SJ. Characterization of site-specific ScFv PEGylation for tumor-targeting pharmaceuticals. BioconjugChem. 2005;16(1):113-21.

88.     Pasut G, Veronese FM. PEGylation for improving the effectiveness of therapeutic biomolecules. Drugs Today (Barc). 2009;45(9):687-95.

89.     Kubetzko S, Balic E, Waibel R, Zangemeister-Wittke U, Pluckthun A. PEGylation and multimerization of the anti-p185HER-2 single chain Fv fragment 4D5: effects on tumor targeting. Journal of Biological Chemistry. 2006;281(46):35186-201.

90.     Ilinskaya ON, Koschinski A, Repp H, Mitkevich VA, Dreyer F, Scholtz JM, et al. RNase-induced apoptosis:Fate of calcium-activated potassium channels. Biochimie. 2008;90(5):717-25.

91.     Yazaki PJ, Kassa T, Cheung CW, Crow DM, Sherman MA, Bading JR, et al. Biodistribution and tumor imaging of an anti-CEA single-chain antibody-albumin fusion protein. NuclMedBiol. 2008;35(2):151-8.

92.     Graff CP, Chester K, Begent R, Wittrup KD. Directed evolution of an anti-carcinoembryonic antigen scFv with a 4-day monovalent dissociation half-time at 37 degrees Celsius. Protein EngDesSel. 2004;17(4):293-304.

93.     Goldenberg DM, Sharkey RM. Novel radiolabeled antibody conjugates. Oncogene. 2007;26(25):3734-44.

94.     Pastan I, Hassan R, FitzGerald DJ, Kreitman RJ. Immunotoxin treatment of cancer. AnnuRevMed. 2007;58(1):221-37.

95.     Khawli LA, Hu P, Epstein AL. Cytokine, chemokine, and co-stimulatory fusion proteins for the immunotherapy of solid tumors. HandbExpPharmacol. 2008 (181):291-328.

96.     Andrady C, Sharma SK, Chester KA. Antibody-enzyme fusion proteins for cancer therapy. Immunotherapy. 2011;3(2):193-211.

97.     Sharkey RM, Goldenberg DM. Perspectives on cancer therapy with radiolabeled monoclonal antibodies. JNuclMed. 2005;46 Suppl 1:115S-27S.

98.     Goldenberg DM, Sharkey RM, Paganelli G, Barbet J, Chatal JF. Antibody pretargeting advances cancer radioimmunodetection and radioimmunotherapy. JClinOncol. 2006;24(5):823-34.

99. Green DJ, Pagel JM, Pantelias A, Hedin N, Lin Y, Wilbur DS, et al. Pretargeted radioimmunotherapy for B-cell lymphomas. ClinCancer Res. 2007;13(18 Pt 2):5598s-603s.

100. De Lorenzo C, Nigro A, Piccoli R, D'Alessio G. A new RNase-based immunoconjugate selectively cytotoxic for ErbB2-overexpressing cells. FEBS Letts. 2002;516(1-3):208-12.

101. De Lorenzo C, Arciello A, Cozzolino R, Palmer DB, Laccetti P, Piccoli R, et al. A fully human antitumor immunoRNase selective for ErbB-2-positive carcinomas. Cancer Res. 2004;64(14):4870-4.

102. De Lorenzo C, D'Alessio G. Human anti-ErbB2 immunoagents--immunoRNases and compact antibodies. FEBS J. 2009;276(6):1527-35.

103. Bernstein ID. Monoclonal antibodies to the myeloid stem cells: therapeutic implications of CMA-676, a humanized anti-CD33 antibody calicheamicin conjugate. Leukemia. 2000;14(3):474-5.

104. Ravandi F. Gemtuzumab ozogamicin: one size does not fit all--the case for personalized therapy. Journal of clinical oncology : official journal of the American Society of Clinical Oncology. 2011 Feb 1;29(4):349-51.

105. Lambert JM. Drug-conjugated antibodies for the treatment of cancer. British journal of clinical pharmacology. 2013 Aug;76(2):248-62.

106. Alley SC, Okeley NM, Senter PD. Antibody-drug conjugates: targeted drug delivery for cancer. CurrOpinChemBiol. 2010;14(4):529-37.

107. Lewis Phillips GD, Li G, Dugger DL, Crocker LM, Parsons KL, Mai E, et al. Targeting HER2-Positive Breast Cancer with Trastuzumab-DM1, an Antibody–Cytotoxic Drug Conjugate. Cancer research. 2008;68(22):9280-90.

108. Junttila T, Li G, Parsons K, Phillips G, Sliwkowski M. Trastuzumab-DM1 (T-DM1) retains all the mechanisms of action of trastuzumab and efficiently inhibits growth of lapatinib insensitive breast cancer. 2011;128(2):347-56.

109. Verma S, Miles D, Gianni L, Krop IE, Welslau M, Baselga J, et al. Trastuzumab Emtansine for HER2-Positive Advanced Breast Cancer. New England Journal of Medicine. 2012;367(19):1783-91.

110. Bagshawe KD. Antibody directed enzymes revive anti-cancer prodrugs concept. BrJCancer. 1987;56(5):531-2.

111. Bagshawe KD, Springer CJ, Searle F, Antoniw P, Sharma SK, Melton RG, et al. A cytotoxic agent can be generated selectively at cancer sites. BrJCancer. 1988;58(6):700-3.

112. Senter PD, Saulnier MG, Schreiber GJ, Hirschberg DL, Brown JP, Hellstrom I, et al. Anti-tumor effects of antibody-alkaline phosphatase conjugates in combination with etoposide phosphate. ProcNatlAcadSciUSA. 1988;85(13):4842-6.

113. Senter PD, Springer CJ. Selective activation of anticancer prodrugs by monoclonal antibody-enzyme conjugates. AdvDrug DelivRev. 2001;53(3):247-64.

114. Rooseboom M, Commandeur JN, Vermeulen NP. Enzyme-catalyzed activation of anticancer prodrugs. Pharmacol Rev. 2004;56(1):53-102.

115. Rautio J, Kumpulainen H, Heimbach T, Oliyai R, Oh D, Jarvinen T, et al. Prodrugs: Design and clinical applications. NatRevDrug Discov. 2008;7(3):255-70.

116. Taylorson CJ EH, Tarragona-Fiol A, Rabin BR, Boyle FT, Hennam JF, Blakey DC, Marsham PR, Heaton DW, Davies DH, Slater AM, Hennequin LFA., inventor patent 5985, 281. 1999.

117. Lowe H. Design, Construction and Evaluation of a Humanised ADEPT System: University College London, University of London; 2011.

118. Lowe HL, Sharma S, Bagshawe KD, Chester K. Antibody Directed Enzyme Prodrug Therapy (ADEPT). In: Little M, editor. Recombinant Antibodies for Immunotherapy: Cambridge University Press; 2009.

119. Senter PD, Schreiber GJ, Hirschberg DL, Ashe SA, Hellstrom KE, Hellstrom I. Enhancement of the in vitro and in vivo antitumor activities of phosphorylated mitomycin C and etoposide derivatives by monoclonal antibody-alkaline phosphatase conjugates. Cancer Res. 1989;49(21):5789-92.

120. Senter PD. Activation of prodrugs by antibody-enzyme conjugates: a new approach to cancer therapy. The FASEB Journal. 1990;4(2):188-93.

121. Wallace PM, Senter PD. In vitro and in vivo activities of monoclonal antibody-alkaline phosphatase conjugates in combination with phenol mustard phosphate. Bioconjugate chemistry. 1991;2(5):349-52.

122. Haenseler E, Esswein A, Vitols KS, Montejano Y, Mueller BM, Reisfeld RA, et al. Activation of methotrexate-.alpha.-alanine by carboxypeptidase A monoclonal antibody conjugate. Biochemistry. 1992;31(3):891-7.

123. Vitols KS, Haag-Zeino B, Baer T, Montejano YD, Huennekens FM. Methotrexate-{alpha}-Phenylalanine: Optimization of Methotrexate Prodrug for Activation by Carboxypeptidase A-Monoclonal Antibody Conjugate. Cancer research. 1995;55(3):478-81.

124. Perron MJ, Page M. Activation of methotrexate-phenylalanine by monoclonal antibody--carboxypeptidase A conjugate for the specific treatment of ovarian cancer in vitro. British journal of cancer. 1996;73(3):281-7.

125. Smith GK, Banks S, Blumenkopf TA, Cory M, Humphreys J, Laethem RM, et al. Toward Antibody-directed Enzyme Prodrug Therapy with the T268G Mutant of Human Carboxypeptidase A1 and Novel in Vivo Stable Prodrugs of Methotrexate. Journal of Biological Chemistry. 1997;272(25):15804-16.

126. Wolfe LA, Mullin RJ, Laethem R, Blumenkopf TA, Cory M, Miller JF, et al. Antibody-Directed Enzyme Prodrug Therapy with the T268G Mutant of Human Carboxypeptidase A1: In Vitro and in Vivo Studies with Prodrugs of Methotrexate and the Thymidylate Synthase Inhibitors GW1031 and GW1843. Bioconjugate chemistry. 1999;10(1):38-48.

127. Hao XK, Liu JY, Yue QH, Wu GJ, Bai YJ, Yin Y. In vitro and in vivo prodrug therapy of prostate cancer using anti-gamma-Sm-scFv/hCPA fusion protein. Prostate. 2006;66(8):858-66.

128. Springer CJ, Antoniw P, Bagshawe KD, Searle F, Bisset GM, Jarman M. Novel prodrugs which are activated to cytotoxic alkylating agents by carboxypeptidase G2. JMedChem. 1990;33(2):677-81.

129. Springer CJ, Bagshawe KD, Sharma SK, Searle F, Boden JA, Antoniw P, et al. Ablation of human choriocarcinoma xenografts in nude mice by antibody-directed enzyme prodrug therapy (ADEPT) with three novel compounds. EurJCancer. 1991;27(11):1361-6.

130. Bagshawe KD, Sharma SK, Springer CJ, Antoniw P, Boden JA, Rogers GT, et al. Antibody directed enzyme prodrug therapy (ADEPT): clinical report. DisMarkers. 1991;9(3-4):233-8.

131. Bagshawe KD, Sharma SK, Springer CJ, Antoniw P. Antibody directed enzyme prodrug therapy: a pilot-scale clinical trial. Tumor Targeting. 1995;1(1):17-29.

132. Bagshawe KD, Begent RHJ. First clinical experience with ADEPT. AdvDrug DelivRev. 1996;22(3):365-7.

133. Blakey DC, Burke PJ, Davies DH, Dowell RI, East SJ, Eckersley KP, et al. ZD2767, an improved system for antibody-directed enzyme prodrug therapy that results in tumor regressions in colorectal tumor xenografts. Cancer Res. 1996;56(14):3287-92.

134. Napier MP, Sharma SK, Springer CJ, Bagshawe KD, Green AJ, Martin J, et al. Antibody-directed enzyme prodrug therapy: Efficacy and mechanism of action in colorectal carcinoma. ClinCancer Res. 2000;6(3):765-72.

135. Francis RJ, Sharma SK, Springer C, Green AJ, Hope-Stone LD, Sena L, et al. A phase I trial of antibody directed enzyme prodrug therapy (ADEPT) in patients with advanced colorectal carcinoma or other CEA producing tumours. British journal of cancer. 2002;87(6):600-7.

136. Bhatia J, Sharma SK, Chester KA, Pedley RB, Boden RW, Read DA, et al. Catalytic activity of an in vivo tumor targeted anti-CEA scFv::carboxypeptidase G2 fusion protein. IntJCancer. 2000;85(4):571-7.

137. Medzihradszky KF, Spencer DI, Sharma SK, Bhatia J, Pedley RB, Read DA, et al. Glycoforms obtained by expression in Pichia pastoris improve cancer targeting potential of a recombinant antibody-enzyme fusion protein. Glycobiology. 2004;14(1):27-37.

138. Sharma SK, Pedley RB, Bhatia J, Boxer GM, El-Emir E, Qureshi U, et al. Sustained tumor regression of human colorectal cancer xenografts using a multifunctional mannosylated fusion protein in antibody-directed enzyme prodrug therapy. ClinCancer Res. 2005;11(2):814-25.

139. Mayer A, Francis RJ, Sharma SK, Tolner B, Springer CJ, Martin J, et al. A phase I study of single administration of antibody-directed enzyme prodrug therapy with the recombinant anti-carcinoembryonic antigen antibody-enzyme fusion protein MFECP1 and a bis-iodo phenol mustard prodrug. ClinCancer Res. 2006;12(21):6509-16.

140. Senter PD, Su PC, Katsuragi T, Sakai T, Cosand WL, Hellstrom I, et al. Generation of 5-fluorouracil from 5-fluorocytosine by monoclonal antibody-cytosine deaminase conjugates. BioconjugChem. 1991;2(6):447-51.

141. Kerr DE, Garrigues US, Wallace PM, Hellstrom KE, Hellstrom I, Senter PD. Application of monoclonal antibodies against cytosine deaminase for the in vivo clearance of a cytosine deaminase immunoconjugate. BioconjugChem. 1993;4(5):353-7.

142. Wallace PM, MacMaster JF, Smith VF, Kerr DE, Senter PD, Cosand WL. Intratumoral generation of 5-fluorouracil mediated by an antibody-cytosine deaminase conjugate in combination with 5-fluorocytosine. Cancer Res. 1994;54(10):2719-23.

143. Aboagye EO, Artemov D, Senter PD, Bhujwalla ZM. Intratumoral conversion of 5-fluorocytosine to 5-fluorouracil by monoclonal antibody-cytosine deaminase conjugates: noninvasive detection of prodrug activation by magnetic resonance spectroscopy and spectroscopic imaging. Cancer research. 1998;58(18):4075-8.

144. Deckert PM, Renner C, Cohen LS, Jungbluth A, Ritter G, Bertino JR, et al. A33scFv-cytosine deaminase: A recombinant protein construct for antibody-directed enzyme-prodrug therapy. BrJCancer. 2003;88(6):937-9.

145. Coelho V, Dernedde J, Petrausch U, Panjideh H, Fuchs H, Menzel C, et al. Design, construction, and in vitro analysis of A33scFv::CDy, a recombinant fusion protein for antibody-directed enzyme prodrug therapy in colon cancer. IntJOncol. 2007;31(4):951-7.

146. Schellmann N, Panjideh H, Fasold P, Bachran D, Bachran C, Deckert PM, et al. Targeted tumor therapy with a fusion protein of an antiangiogenic human recombinant scFv and yeast cytosine deaminase. Journal of immunotherapy (Hagerstown, Md : 1997). 2012 Sep;35(7):570-8.

147. Abraham R, Aman N, von BR, Darsley M, Kamireddy B, Kenten J, et al. Conjugates of COL-1 monoclonal antibody and beta-D-galactosidase can specifically kill tumor cells by generation of 5-fluorouridine from the prodrug beta-D-galactosyl-5-fluorouridine. Cell Biophys. 1994;24-25:127-33.

148. Fang L, Battisti RF, Cheng H, Reigan P, Xin Y, Shen J, et al. Enzyme specific activation of benzoquinone ansamycin prodrugs using HuCC49DeltaCH2-beta-galactosidase conjugates. JMedChem. 2006;49(21):6290-7.

149. Yu Y, Fang L, Sun D. Biodistribution of HuCC49DeltaCH2-beta-galactosidase in colorectal cancer xenograft model. IntJ Pharm. 2010;386(1-2):208-15.

150. Haisma HJ, Boven E, van MM, de JJ, van dV, Pinedo HM. A monoclonal antibody-beta-glucuronidase conjugate as activator of the prodrug epirubicin-glucuronide for specific treatment of cancer. British journal of cancer. 1992;66(3):474-8.

151. Houba PH, Boven E, Haisma HJ. Improved characteristics of a human beta-glucuronidase-antibody conjugate after deglycosylation for use in antibody-directed enzyme prodrug therapy. BioconjugChem. 1996;7(5):606-11.

152. Houba PH, Boven E, van der Meulen-Muileman IH, Leenders RG, Scheeren JW, Pinedo HM, et al. Pronounced antitumor efficacy of doxorubicin when given as the prodrug DOX-GA3 in combination with a monoclonal antibody beta-glucuronidase conjugate. IntJ Cancer. 2001;91(4):550-4.

153. Wang SM, Chern JW, Yeh MY, Ng JC, Tung E, Roffler SR. Specific Activation of Glucuronide Prodrugs by Antibody-targeted Enzyme Conjugates for Cancer Therapy. Cancer Res. 1992;52(16):4484-91.

154. Bosslet K, Czech J, Hoffmann D. Tumor-selective prodrug activation by fusion protein-mediated catalysis. Cancer Res. 1994;54(8):2151-9.

155. Florent JC, Dong X, Gaudel G, Mitaku S, Monneret C, Gesson JP, et al. Prodrugs of anthracyclines for use in antibody-directed enzyme prodrug therapy. JMedChem. 1998;41(19):3572-81.

156. De Graaf M, Boven E, Oosterhoff D, van der Meulen-Muileman IH, Huls GA, Gerritsen WR, et al. A fully human anti-Ep-CAM scFv-beta-glucuronidase fusion protein for selective chemotherapy with a glucuronide prodrug. BrJCancer. 2002;86(5):811-8.

157. Biela BH, Khawli LA, Hu P, Epstein AL. Chimeric TNT-3/human beta-glucuronidase fusion proteins for antibody-directed enzyme prodrug therapy (ADEPT). Cancer BiotherRadiopharm. 2003;18(3):339-53.

158. Chen KC, Wu SY, Leu YL, Prijovich ZM, Chen BM, Wang HE, et al. A humanized immunoenzyme with enhanced activity for glucuronide prodrug activation in the tumor microenvironment. BioconjugChem. 2011;22(5):938-48.

159. Svensson HP, Kadow JF, Vrudhula VM, Wallace PM, Senter PD. Monoclonal antibody-beta-lactamase conjugates for the activation of a cephalosporin mustard prodrug. BioconjugChem. 1992;3(2):176-81.

160. Vrudhula VM, Senter PD, Fischer KJ, Wallace PM. Prodrugs of doxorubicin and melphalan and their activation by a monoclonal antibody-penicillin-G amidase conjugate. J MedChem. 1993;36(7):919-23.

161. Rodrigues ML, Presta LG, Kotts CE, Wirth C, Mordenti J, Osaka G, et al. Development of a humanized disulfide-stabilized anti-p185HER2 Fv-beta-lactamase fusion protein for activation of a cephalosporin doxorubicin prodrug. Cancer Res. 1995;55(1):63-70.

162. Kerr DE, Vrudhula VM, Svensson HP, Siemers NO, Senter PD. Comparison of recombinant and synthetically formed monoclonal antibody-beta-lactamase conjugates for anticancer prodrug activation. BioconjugChem. 1999;10(6):1084-9.

163. Siemers NO, Kerr DE, Yarnold S, Stebbins MR, Vrudhula VM, Hellstrom I, et al. Construction, expression, and activities of L49-sFv-beta-lactamase, a single-chain antibody fusion protein for anticancer prodrug activation. BioconjugChem. 1997;8(4):510-9.

164. Vrudhula VM, Kerr DE, Siemers NO, Dubowchik GM, Senter PD. Cephalosporin prodrugs of paclitaxel for immunologically specific activation by L-49-sFv-beta-lactamase fusion protein. BioorgMedChemLetts. 2003;13(3):539-42.

165. Alderson RF, Toki BE, Roberge M, Geng W, Basler J, Chin R, et al. Characterization of a CC49-based single-chain fragment-beta-lactamase fusion protein for antibody-directed enzyme prodrug therapy (ADEPT). BioconjugChem. 2006;17(2):410-8.

166. Cortez-Retamozo V, Backmann N, Senter PD, Wernery U, De Baetselier P, Muyldermans S, et al. Efficient cancer therapy with a nanobody-based conjugate. Cancer Res. 2004;64(8):2853-7.

167. Bignami GS, Senter PD, Grothaus PG, Fischer KJ, Humphreys T, Wallace PM. N-(4'-hydroxyphenylacetyl)palytoxin: a palytoxin prodrug that can be activated by a monoclonal antibody-penicillin G amidase conjugate. Cancer research. 1992;52(20):5759-64.

168. Kerr DE, Senter PD, Burnett WV, Hirschberg DL, Hellstrom I, Hellstrom KE. Antibody-penicillin-V-amidase conjugates kill antigen-positive tumor cells when combined with doxorubicin phenoxyacetamide. Cancer ImmunolImmunother. 1990;31(4):202-6.

169. Heinis C, Alessi P, Neri D. Engineering a thermostable human prolyl endopeptidase for antibody-directed enzyme prodrug therapy. Biochemistry. 2004;43(20):6293-303.

170. Afshar S, Asai T, Morrison SL. Humanized ADEPT comprised of an engineered human purine nucleoside phosphorylase and a tumor targeting peptide for treatment of cancer. MolCancer Ther. 2009;8(1):185-93.

171. Sherwood RF, Melton RG, Alwan SM, Hughes P. Purification and properties of carboxypeptidase G2 from Pseudomonas sp. strain RS-16. Use of a novel triazine dye affinity method. EurJBiochem. 1985;148(3):447-53.

172. Lindner HA, Lunin VV, Alary A, Hecker R, Cygler M, Menard R. Essential roles of zinc ligation and enzyme dimerization for catalysis in the aminoacylase-1/M20 family. Journal of Biological Chemistry. 2003;278(45):44496-504.

173. Buchen S, Ngampolo D, Melton RG, Hasan C, Zoubek A, Henze G, et al. Carboxypeptidase G2 rescue in patients with methotrexate intoxication and renal failure. BrJCancer. 2005;92(3):480-7.

174. Tuffaha HW, Omar SA. Glucarpidase rescue in a patient with high-dose methotrexate-induced nephrotoxicity. JOncolPharmPract. 2009.

175. Springer CJ, Poon GK, Sharma SK, Bagshawe KD. Analysis of antibody-enzyme conjugate clearance by investigation of prodrug and active drug in an ADEPT clinical study. Cell Biophys. 1994;24-25:193-207.

176. Springer CJ, Dowell R, Burke PJ, Hadley E, Davis DH, Blakey DC, et al. Optimization of alkylating agent prodrugs derived from phenol and aniline mustards: a new clinical candidate prodrug (ZD2767) for antibody-directed enzyme prodrug therapy (ADEPT). JMedChem. 1995;38(26):5051-65.

177. Begent RH, Keep PA, Searle F, Green AJ, Mitchell HD, Jones BE, et al. Radioimmunolocalization and selection for surgery in recurrent colorectal cancer. BrJSurg. 1986;73(1):64-7.

178. Melton RG, Boyle JM, Rogers GT, Burke P, Bagshawe KD, Sherwood RF. Optimisation of small-scale coupling of A5B7 monoclonal antibody to carboxypeptidase G2. JImmunolMethods. 1993;158(1):49-56.

179. Hammarstrom S. The carcinoembryonic antigen (CEA) family: structures, suggested functions and expression in normal and malignant tissues. SeminCancer Biol. 1999;9(2):67-81.

180. Sharma SK, Bagshawe KD, Springer CJ, Burke PJ, Rogers GT, Boden JA, et al. Antibody directed enzyme prodrug therapy (ADEPT): a three phase system. DisMarkers. 1991;9(3-4):225-31.

181. Philben VJ, Jakowatz JG, Beatty BG, Vlahos WG, Paxton RJ, Williams LE, et al. The effect of tumor CEA content and tumor size on tissue uptake of indium 111-labeled anti-CEA monoclonal antibody. Cancer. 1986;57(3):571-6.

182. Stribbling SM, Martin J, Pedley RB, Boden JA, Sharma SK, Springer CJ. Biodistribution of an antibody-enzyme conjugate for antibody-directed enzyme prodrug therapy in nude mice bearing a human colon adenocarcinoma xenograft. Cancer ChemotherPharmacol. 1997;40(4):277-84.

183. Sharma SK, Bagshawe KD, Burke PJ, Boden RW, Rogers GT. Inactivation and clearance of an anti-CEA carboxypeptidase G2 conjugate in blood after localisation in a xenograft model. BrJCancer. 1990;61(5):659-62.

184. Sharma SK, Bagshawe KD, Burke PJ, Boden JA, Rogers GT, Springer CJ, et al. Galactosylated antibodies and antibody-enzyme conjugates in antibody-directed enzyme prodrug therapy. Cancer. 1994;73(3 Suppl):1114-20.

185. Rogers GT, Burke PJ, Sharma SK, Koodie R, Boden JA. Plasma clearance of an antibody--enzyme conjugate in ADEPT by monoclonal anti-enzyme: its effect on prodrug activation in vivo. British journal of cancer. 1995;72(6):1357-63.

186. Sharma SK, Boden JA, Springer CJ, Burke PJ, Bagshawe KD. Antibody-directed enzyme prodrug therapy (ADEPT). A three-phase study in ovarian tumor xenografts. Cell Biophys. 1994;24-25:219-28.

187. Bagshawe KD. Antibody-directed enzyme prodrug therapy for cancer: Its theoretical basis and application. MolMedToday. 1995;1(9):424-31.

188. Bagshawe KD, Sharma SK. Cyclosporine delays host immune response to antibody enzyme conjugate in ADEPT. TransplantProc. 1996;28(6):3156-8.

189. Blakey DC, Davies DH, Dowell RI, East SJ, Burke PJ, Sharma SK, et al. Anti-tumour effects of an antibody-carboxypeptidase G2 conjugate in combination with phenol mustard prodrugs. BrJCancer. 1995;72(5):1083-8.

190. Chester KA, Begent RH, Robson L, Keep P, Pedley RB, Boden JA, et al. Phage libraries for generation of clinically useful antibodies. Lancet. 1994;343(8895):455-6.

191. Boehm MK, Corper AL, Wan T, Sohi MK, Sutton BJ, Thornton JD, et al. Crystal structure of the anti-(carcinoembryonic antigen) single-chain Fv antibody MFE-23 and a model for antigen binding based on intermolecular contacts. BiochemJ. 2000;346 Pt 2:519-28.

192.    Sainz-Pastor N, Tolner B, Huhalov A, Kogelberg H, Lee YC, Zhu D, et al. Deglycosylation to obtain stable and homogeneous Pichia pastoris-expressed N-A1 domains of carcinoembryonic antigen. IntJBiolMacromol. 2006;39(1-3):141-50.

193.    Chester KA, Mayer A, Bhatia J, Robson L, Spencer DI, Cooke SP, et al. Recombinant anti-carcinoembryonic antigen antibodies for targeting cancer. Cancer ChemotherPharmacol. 2000;46 Suppl:S8-12.

194.    Mayer A, Tsiompanou E, O'Malley D, Boxer GM, Bhatia J, Flynn AA, et al. Radioimmunoguided surgery in colorectal cancer using a genetically engineered anti-CEA single-chain Fv antibody. ClinCancer Res. 2000;6(5):1711-9.

195.    Michael NP, Chester KA, Melton RG, Robson L, Nicholas W, Boden JA, et al. In vitro and in vivo characterisation of a recombinant carboxypeptidase G2::anti-CEA scFv fusion protein. Immunotechnology. 1996;2(1):47-57.

196.    Kogelberg H, Tolner B, Sharma SK, Lowdell MW, Qureshi U, Robson M, et al. Clearance mechanism of a mannosylated antibody-enzyme fusion protein used in experimental cancer therapy. Glycobiology. 2007;17(1):36-45.

197.    Tolner B, Smith L, Begent RH, Chester KA. Expanded-bed adsorption immobilized-metal affinity chromatography. NatProtoc. 2006;1(3):1213-22.

198.    Tolner B, Smith L, Begent RH, Chester KA. Production of recombinant protein in Pichia pastoris by fermentation. NatProtoc. 2006;1(2):1006-21.

199.    Wilkins DK. Conditions for safe and effective ADEPT treatment [Doctoral thesis]: University College London; 2010.

200.    Teicher BA, Chari RV. Antibody conjugate therapeutics: challenges and potential. ClinCancer Res. 2011;17(20):6389-97.

201.    Carter P. Improving the efficacy of antibody-based cancer therapies. Nature reviews Cancer. 2001;1(2):118-29.

202.    Tabrizi MA, Tseng CM, Roskos LK. Elimination mechanisms of therapeutic monoclonal antibodies. Drug discovery today. 2006;11(1-2):81-8.

203.    Cartron G, Dacheux L, Salles G, Solal-Celigny P, Bardos P, Colombat P, et al. Therapeutic activity of humanized anti-CD20 monoclonal antibody and polymorphism in IgG Fc receptor FcgammaRIIIa gene. Blood. 2002;99(3):754-8.

204.    Dall'Ozzo S, Tartas S, Paintaud G, Cartron G, Colombat P, Bardos P, et al. Rituximab-dependent cytotoxicity by natural killer cells: influence of FCGR3A polymorphism on the concentration-effect relationship. Cancer research. 2004;64(13):4664-9.

205. Jefferis R. Glycosylation of recombinant antibody therapeutics. BiotechnolProg. 2005;21(1):11-6.

206. Casalini P, Luison E, Menard S, Colnaghi MI, Paganelli G, Canevari S. Tumor pretargeting: role of avidin/streptavidin on monoclonal antibody internalization. JNuclMed. 1997;38(9):1378-81.

207. Marshall D, Pedley RB, Melton RG, Boden JA, Boden R, Begent RH. Galactosylated streptavidin for improved clearance of biotinylated intact and F(ab')2 fragments of an anti-tumour antibody. British journal of cancer. 1995;71(1):18-24.

208. Rowlinson-Busza G, Snook D, Epenetos AA. 90Y-labeled antibody uptake by human tumor xenografts and the effect of systemic administration of EDTA. IntJRadiatOncolBiolPhys. 1994;28(5):1257-65.

209. Cheng TL, Chen BM, Chan LY, Wu PY, Chern JW, Roffler SR. Poly(ethylene glycol) modification of beta-glucuronidase-antibody conjugates for solid-tumor therapy by targeted activation of glucuronide prodrugs. Cancer ImmunolImmunother. 1997;44(6):305-15.

210. Ong GL, Ettenson D, Sharkey RM, Marks A, Baumal R, Goldenberg DM, et al. Galactose-conjugated antibodies in cancer therapy: properties and principles of action. Cancer research. 1991;51(6):1619-26.

211. Henry CA, Clavo AC, Wahl RL. Improved monoclonal antibody tumor/background ratios with exchange transfusions. IntJRadApplInstrumB. 1991;18(5):565-7.

212. Sharkey RM, Primus FJ, Goldenberg DM. Second antibody clearance of radiolabeled antibody in cancer radioimmunodetection. ProcNatlAcadSci USA. 1984;81(9):2843-6.

213. Pedley RB, Dale R, Boden JA, Begent RH, Keep PA, Green AJ. The effect of second antibody clearance on the distribution and dosimetry of radiolabelled anti-CEA antibody in a human colonic tumor xenograft model. IntJ Cancer. 1989;43(4):713-8.

214. Haisma HJ, van MM, Scheffer G, Scheper RJ, Pinedo HM, Boven E. A monoclonal antibody against human beta-glucuronidase for application in antibody-directed enzyme prodrug therapy. Hybridoma. 1995;14(4):377-82.

215. Begent RH, Green AJ, Keep PA, Bagshawe KD, Searle F, Jones BE, et al. Liposomally entrapped second antibody. Lancet. 1983;1(8332):1047-8.

216. Goldenberg DM, Sharkey RM, Ford E. Anti-antibody enhancement of iodine-131 anti-CEA radioimmunodetection in experimental and clinical studies. JNuclMed. 1987;28(10):1604-10.

217. Begent HJ, Chester KA, Bagshawe KD, Keep PA, Searle F, Boden J, et al. Second antibody for improvement of antibody imaging: liposome-entrapped and free preparations in animal and human studies. ClinExpImmunol. 1989;78(2):307-13.

218. Sharkey RM, Boerman OC, Natale A, Pawlyk D, Monestier M, Losman MJ, et al. Enhanced clearance of radiolabeled murine monoclonal antibody by a syngeneic anti-idiotype antibody in tumor-bearing nude mice. IntJCancer. 1992;51(2):266-73.

219. Eno-Amooquaye EA, Searle F, Boden JA, Sharma SK, Burke PJ. Altered biodistribution of an antibody--enzyme conjugate modified with polyethylene glycol. British journal of cancer. 1996;73(11):1323-7.

220. Pimm MV, Demignot S, Gribben SJ. Influence of syngeneic monoclonal anti-idiotypic antibodies to murine monoclonal antibodies against tumour-associated antigens on the biodistribution of their target antibodies and their fragments. JCancer Res ClinOncol. 1993;119(7):408-14.

221. Ong GL, Marria V, Mattes MJ. The fate of antibodies and their radiolabels bound to tumor cells in vitro: the effect of cross-linking at the cell surface and of anti-idiotype antibodies. Cancer ImmunolImmunother. 1994;39(5):325-31.

222. Ashwell G, Morell AG. The role of surface carbohydrates in the hepatic recognition and transport of circulating glycoproteins. AdvEnzymolRelat Areas MolBiol. 1974;41(0):99-128.

223. Ashwell G, Kawasaki T. A protein from mammalian liver that specifically binds galactose-terminated glycoproteins. Methods Enzymol. 1978;50:287-8.

224. Jansen RW, Molema G, Ching TL, Oosting R, Harms G, Moolenaar F, et al. Hepatic endocytosis of various types of mannose-terminated albumins. What is important, sugar recognition, net charge, or the combination of these features. Journal of Biological Chemistry. 1991;266(5):3343-8.

225. Taylor ME, Leaning MS, Summerfield JA. Uptake and processing of glycoproteins by rat hepatic mannose receptor. AmJPhysiol. 1987;252(5 Pt 1):E690-E8.

226. Opanasopit P, Shirashi K, Nishikawa M, Yamashita F, Takakura Y, Hashida M. In vivo recognition of mannosylated proteins by hepatic mannose receptors and mannan-binding protein. AmJPhysiol GastrointestLiver Physiol. 2001;280(5):G879-G89.

227. Jefferis R. Recombinant antibody therapeutics: the impact of glycosylation on mechanisms of action. Trends in pharmacological sciences. 2009;30(7):356-62.

228. Beck A, Wagner-Rousset E, Bussat MC, Lokteff M, Klinguer-Hamour C, Haeuw JF, et al. Trends in glycosylation, glycoanalysis and glycoengineering of therapeutic antibodies and Fc-fusion proteins. CurrPharmBiotechnol. 2008;9(6):482-501.

229. Sears P, Wong CH. Enzyme action in glycoprotein synthesis. Cell MolLife Sci. 1998;54(3):223-52.

230. Strahl-Bolsinger S, Gentzsch M, Tanner W. Protein O-mannosylation. BiochimBiophysActa. 1999;1426(2):297-307.

231. Montesino R, Garcia R, Quintero O, Cremata JA. Variation in N-linked oligosaccharide structures on heterologous proteins secreted by the methylotrophic yeast Pichia pastoris. Protein ExprPurif. 1998;14(2):197-207.

232. Bretthauer RK, Castellino FJ. Glycosylation of Pichia pastoris-derived proteins. Biotechnol Appl Biochem. 1999;30 ( Pt 3):193-200.

233. Gemmill TR, Trimble RB. Overview of N- and O-linked oligosaccharide structures found in various yeast species. BiochimBiophysActa. 1999;1426(2):227-37.

234. Cereghino JL, Cregg JM. Heterologous protein expression in the methylotrophic yeast Pichia pastoris. FEMS MicrobiolRev. 2000;24(1):45-66.

235. Daly R, Hearn MT. Expression of heterologous proteins in Pichia pastoris: a useful experimental tool in protein engineering and production. JMolRecognit. 2005;18(2):119-38.

236. Peter-Katalinic J. Methods in enzymology: O-glycosylation of proteins. Methods Enzymol. 2005;405:139-71.

237. Duman JG, Miele RG, Liang H, Grella DK, Sim KL, Castellino FJ, et al. O-Mannosylation of Pichia pastoris cellular and recombinant proteins. Biotechnol Appl Biochem. 1998;28 ( Pt 1):39-45.

238. Jentoft N. Why are proteins O-glycosylated? Trends BiochemSci. 1990;15(8):291-4.

239. Official U. Glycoprotein and Glycan Analysis - General Considerations. 2011.

240. Ecker M, Mrsa V, Hagen I, Deutzmann R, Strahl S, Tanner W. O-mannosylation precedes and potentially controls the N-glycosylation of a yeast cell wall glycoprotein. EMBO Rep. 2003;4(6):628-32.

241. Mattes WB, Hartley JA, Kohn KW, Matheson DW. GC-rich regions in genomes as targets for DNA alkylation. Carcinogenesis. 1988;9(11):2065-72.

242. Sunters A, Springer CJ, Bagshawe KD, Souhami RL, Hartley JA. The cytotoxicity, DNA crosslinking ability and DNA sequence selectivity of the aniline mustards melphalan, chlorambucil and 4-[bis(2-chloroethyl)amino] benzoic acid. BiochemPharmacol. 1992;44(1):59-64.

243. Kohn KW, Spears CL, Doty P. Inter-strand crosslinking of DNA by nitrogen mustard. JMolBiol. 1966;19(2):266-88.

244.    Pieper RO, Futscher BW, Erickson LC. Transcription-terminating lesions induced by bifunctional alkylating agents in vitro. Carcinogenesis. 1989;10(7):1307-14.

245.    Gargiulo D, Kumar GS, Musser SS, Tomasz M. Structural and function modification of DNA by mitomycin C. Mechanism of the DNA sequence specificity of mitomycins. Nucleic Acids SympSer. 1995 (34):169-70.

246.    Webley SD, Francis RJ, Pedley RB, Sharma SK, Begent RHJ, Hartley JA, et al. Measurement of the critical DNA lesions produced by antibody-directed enzyme prodrug therapy (ADEPT) in vitro, in vivo and in clinical material. British journal of cancer. 2001;84(12):1671-6.

247.    Monks NR, Blakey DC, East SJ, Dowell RI, Calvete JA, Curtin NJ, et al. DNA interstrand cross-linking and TP53 status as determinants of tumour cell sensitivity in vitro to the antibody-directed enzyme prodrug therapy ZD2767. European Journal of Cancer. 2002;38(11):1543-52.

248.    Hayes JD, Wolf CR. Molecular mechanisms of drug resistance. Biochemical Journal. 1990;272(2):281-95.

249.    Hall AG, Tilby MJ. Mechanisms of action of, and modes of resistance to, alkylating agents used in the treatment of haematological malignancies. Blood Rev. 1992;6(3):163-73.

250.    Lord CJ, Ashworth A. The DNA damage response and cancer therapy. Nature. 2012;481(7381):287-94.

251.    Niida H, Nakanishi M. DNA damage checkpoints in mammals. Mutagenesis. 2006;21(1):3-9.

252.    Warmerdam DO, Kanaar R. Dealing with DNA damage: relationships between checkpoint and repair pathways. MutatRes. 2010;704(1-3):2-11.

253.    Branzei D, Foiani M. Regulation of DNA repair throughout the cell cycle. Nat Rev MolCell Biol. 2008;9(4):297-308.

254.    Poehlmann A, Roessner A. Importance of DNA damage checkpoints in the pathogenesis of human cancers. PatholResPract. 2010;206(9):591-601.

255.    Smith J, Tho LM, Xu N, Gillespie DA. The ATM-Chk2 and ATR-Chk1 pathways in DNA damage signaling and cancer. AdvCancer Res. 2010;108:73-112.

256.    Jazayeri A, Falck J, Lukas C, Bartek J, Smith GC, Lukas J, et al. ATM- and cell cycle-dependent regulation of ATR in response to DNA double-strand breaks. Nat Cell Biol. 2006;8(1):37-45.

257.    Nigg EA. Cyclin-dependent protein kinases: key regulators of the eukaryotic cell cycle. BioEssays : news and reviews in molecular, cellular and developmental biology. 1995;17(6):471-80.

258.    Curtin NJ. DNA repair dysregulation from cancer driver to therapeutic target. Nature reviews Cancer. 2012;12(12):801-17.

259.    Curtin NJ. Inhibiting the DNA damage response as a therapeutic manoeuvre in cancer. British journal of pharmacology. 2013 May 17.

260.    Sancar A, Lindsey-Boltz LA, Çonsal-KaÇõmaz K, Linn S. MOLECULAR MECHANISMS OF MAMMALIAN DNA REPAIR AND THE DNA DAMAGE CHECKPOINTS. Annual Review of Biochemistry. 2004;73(1):39-85.

261.    Pallis AG, Karamouzis MV. DNA repair pathways and their implication in cancer treatment. Cancer Metastasis Rev. 2010;29(4):677-85.

262.    Helleday T, Petermann E, Lundin C, Hodgson B, Sharma RA. DNA repair pathways as targets for cancer therapy. Nature reviews Cancer. 2008;8(3):193-204.

263.    Zwelling LA, Michaels S, Schwartz H, Dobson PP, Kohn KW. DNA cross-linking as an indicator of sensitivity and resistance of mouse L1210 leukemia to cis-diamminedichloroplatinum(II) and L-phenylalanine mustard. Cancer Res. 1981;41(2):640-9.

264.    Hansson J, Lewensohn R, Ringborg U, Nilsson B. Formation and removal of DNA cross-links induced by melphalan and nitrogen mustard in relation to drug-induced cytotoxicity in human melanoma cells. Cancer Res. 1987;47(10):2631-7.

265.    Cole RS. Repair of DNA containing interstrand crosslinks in Escherichia coli: sequential excision and recombination. ProcNatlAcadSciUSA. 1973;70(4):1064-8.

266.    McHugh PJ, Sones WR, Hartley JA. Repair of intermediate structures produced at DNA interstrand cross-links in Saccharomyces cerevisiae. MolCell Biol. 2000;20(10):3425-33.

267.    McHugh PJ, Gill RD, Waters R, Hartley JA. Excision repair of nitrogen mustard-DNA adducts in Saccharomyces cerevisiae. Nucleic Acids Res. 1999;27(16):3259-66.

268.    Arnaudeau C, Lundin C, Helleday T. DNA double-strand breaks associated with replication forks are predominantly repaired by homologous recombination involving an exchange mechanism in mammalian cells. JMolBiol. 2001;307:1235-45.

269.    Dronkert MLG, Kanaar R. Repair of DNA interstrand cross-links. Mutation Research/DNA Repair. 2001;486(4):217-47.

270.    McHugh PJ, Spanswick VJ, Hartley JA. Repair of DNA interstrand crosslinks: molecular mechanisms and clinical relevance. Lancet Oncol. 2001;2(8):483-90.

271.    McCabe KM, Olson SB, Moses RE. DNA interstrand crosslink repair in mammalian cells. JCell Physiol. 2009;220(3):569-73.

272.    Sengerova B, Wang AT, McHugh PJ. Orchestrating the nucleases involved in DNA interstrand cross-link (ICL) repair. Cell cycle (Georgetown, Tex). 2011;10(23):3999-4008.

273.    Wilson DM, III, Seidman MM. A novel link to base excision repair? Trends BiochemSci. 2010;35(5):247-52.

274. Vasquez KM. Targeting and processing of site-specific DNA interstrand crosslinks. EnvironMolMutagen. 2010;51(6):527-39.

275. Grompe M, D'Andrea A. Fanconi anemia and DNA repair. HumMolGenet. 2001;10(20):2253-9.

276. Rothfuss A, Grompe M. Repair kinetics of genomic interstrand DNA cross-links: evidence for DNA double-strand break-dependent activation of the Fanconi anemia/BRCA pathway. MolCell Biol. 2004;24(1):123-34.

277. Knipscheer P, Raschle M, Smogorzewska A, Enoiu M, Ho TV, Scharer OD, et al. The Fanconi anemia pathway promotes replication-dependent DNA interstrand cross-link repair. Science (New York, NY). 2009;326(5960):1698-701.

278. Bhagwat N, Olsen AL, Wang AT, Hanada K, Stuckert P, Kanaar R, et al. XPF-ERCC1 participates in the Fanconi anemia pathway of cross-link repair. MolCell Biol. 2009;29(24):6427-37.

279. Zhang N, Liu X, Li L, Legerski R. Double-strand breaks induce homologous recombinational repair of interstrand cross-links via cooperation of MSH2, ERCC1-XPF, REV3, and the Fanconi anemia pathway. DNA repair. 2007;6(11):1670-8.

280. Patel KJ, Joenje H. Fanconi anemia and DNA replication repair. DNA repair. 2007;6(7):885-90.

281. Akkari YM, Bateman RL, Reifsteck CA, Olson SB, Grompe M. DNA replication is required To elicit cellular responses to psoralen-induced DNA interstrand cross-links. MolCell Biol. 2000;20(21):8283-9.

282. Hanada K, Budzowska M, Modesti M, Maas A, Wyman C, Essers J, et al. The structure-specific endonuclease Mus81-Eme1 promotes conversion of interstrand DNA crosslinks into double-strands breaks. EMBO J. 2006;25(20):4921-32.

283. Hanada K. The structure-specific endonuclease Mus81 contributes to replication restart by generating double-strand DNA breaks. Nature StructMolBiol. 2007;14:1096-104.

284. Niedernhofer LJ, Odijk H, Budzowska M, van DE, Maas A, Theil AF, et al. The structure-specific endonuclease Ercc1-Xpf is required to resolve DNA interstrand cross-link-induced double-strand breaks. MolCell Biol. 2004;24(13):5776-87.

285. Legerski RJ. Repair of DNA interstrand cross-links during S phase of the mammalian cell cycle. EnvironMolMutagen. 2010;51(6):540-51.

286. Mu D, Bessho T, Nechev LV, Chen DJ, Harris TM, Hearst JE, et al. DNA interstrand cross-links induce futile repair synthesis in mammalian cell extracts. MolCell Biol. 2000;20(7):2446-54.

287. Kuraoka I, Kobertz WR, Ariza RR, Biggerstaff M, Essigmann JM, Wood RD. Repair of an interstrand DNA cross-link initiated by ERCC1-XPF repair/recombination nuclease. Journal of Biological Chemistry. 2000;275(34):26632-6.

288. De Silva IU, McHugh PJ, Clingen PH, Hartley JA. Defining the roles of nucleotide excision repair and recombination in the repair of DNA interstrand cross-links in mammalian cells. MolCell Biol. 2000;20(21):7980-90.

289. Damia G, Imperatori L, Stefanini M, D'Incalci M. Sensitivity of CHO mutant cell lines with specific defects in nucleotide excision repair to different anti-cancer agents. IntJCancer. 1996;66(6):779-83.

290. Wood RD. Mammalian nucleotide excision repair proteins and interstrand crosslink repair. EnvironMolMutagen. 2010;51(6):520-6.

291. Kunkel TA, Pavlov YI, Bebenek K. Functions of human DNA polymerases eta, kappa and iota suggested by their properties, including fidelity with undamaged DNA templates. DNA repair. 2003;2(2):135-49.

292. Hicks JK, Chute CL, Paulsen MT, Ragland RL, Howlett NG, Gueranger Q, et al. Differential roles for DNA polymerases eta, zeta, and REV1 in lesion bypass of intrastrand versus interstrand DNA cross-links. MolCell Biol. 2010;30(5):1217-30.

293. Ho TV, Scharer OD. Translesion DNA synthesis polymerases in DNA interstrand crosslink repair. EnvironMolMutagen. 2010;51(6):552-66.

294. Downs JA, Lowndes NF, Jackson SP. A role for Saccharomyces cerevisiae histone H2A in DNA repair. Nature. 2000;408(6815):1001-4.

295. Heyer WD, Ehmsen KT, Liu J. Regulation of homologous recombination in eukaryotes. AnnuRev Genet. 2010;44:113-39.

296. Hinz JM. Role of homologous recombination in DNA interstrand crosslink repair. EnvironMolMutagen. 2010;51(6):582-603.

297. Khanna KK, Jackson SP. DNA double-strand breaks: signaling, repair and the cancer connection. Nat Genet. 2001;27(3):247-54.

298. Banath JP, Klokov D, MacPhail SH, Banuelos CA, Olive PL. Residual gammaH2AX foci as an indication of lethal DNA lesions. BMCCancer. 2010;10:4.

299. Soulas-Sprauel P, Rivera-Munoz P, Malivert L, Le GG, Abramowski V, Revy P, et al. V(D)J and immunoglobulin class switch recombinations: a paradigm to study the regulation of DNA end-joining. Oncogene. 2007;26(56):7780-91.

300. Sankaranarayanan K, Wassom JS. Ionizing radiation and genetic risks XIV. Potential research directions in the post-genome era based on knowledge of repair of radiation-induced DNA

double-strand breaks in mammalian somatic cells and the origin of deletions associated with human genomic disorders. MutatRes. 2005;578(1-2):333-70.

301. Sonoda E, Sasaki MS, Morrison C, Yamaguchi-Iwai Y, Takata M, Takeda S. Sister chromatid exchanges are mediated by homologous recombination in vertebrate cells. MolCell Biol. 1999;19(7):5166-9.

302. Li X, Heyer WD. Homologous recombination in DNA repair and DNA damage tolerance. Cell Res. 2008;18(1):99-113.

303. Deans AJ, West SC. DNA interstrand crosslink repair and cancer. Nature reviews Cancer. 2011;11(7):467-80.

304. Frankenberg-Schwager M, Kirchermeier D, Greif G, Baer K, Becker M, Frankenberg D. Cisplatin-mediated DNA double-strand breaks in replicating but not in quiescent cells of the yeast Saccharomyces cerevisiae. Toxicology. 2005;212(2-3):175-84.

305. Collins AR. Mutant rodent cell lines sensitive to ultraviolet light, ionizing radiation and cross-linking agents: a comprehensive survey of genetic and biochemical characteristics. MutatRes. 1993;293(2):99-118.

306. Allen C, Ashley AK, Hromas R, Nickoloff JA. More forks on the road to replication stress recovery. JMolCell Biol. 2011;3(1):4-12.

307. Paull TT, Rogakou EP, Yamazaki V, Kirchgessner CU, Gellert M, Bonner WM. A critical role for histone H2AX in recruitment of repair factors to nuclear foci after DNA damage. Current Biology. 2000;10(15):886-95.

308. Rogakou EP, Pilch DR, Orr AH, Ivanova VS, Bonner WM. DNA Double-stranded Breaks Induce Histone H2AX Phosphorylation on Serine 139. Journal of Biological Chemistry. 1998;273(10):5858-68.

309. Sedelnikova OA, Rogakou EP, Panyutin IG, Bonner WM. Quantitative detection of (125)IdU-induced DNA double-strand breaks with gamma-H2AX antibody. RadiatRes. 2002;158(4):486-92.

310. Rogakou EP, Boon C, Redon C, Bonner WM. Megabase Chromatin Domains Involved in DNA Double-Strand Breaks in Vivo. The Journal of Cell Biology. 1999;146(5):905-16.

311. Lisby M, Rothstein R. Choreography of recombination proteins during the DNA damage response. DNA repair. 2009;8(9):1068-76.

312. Lukas J, Lukas C, Bartek J. More than just a focus: The chromatin response to DNA damage and its role in genome integrity maintenance. Nat Cell Biol. 2011;13(10):1161-9.

313. Bekker-Jensen S, Mailand N. Assembly and function of DNA double-strand break repair foci in mammalian cells. DNA repair. 2010;9(12):1219-28.

314. Sedelnikova OA, Bonner WM. GammaH2AX in cancer cells: a potential biomarker for cancer diagnostics, prediction and recurrence. Cell cycle (Georgetown, Tex). 2006;5(24):2909-13.

315. Olive PL, Banath JP. Phosphorylation of histone H2AX as a measure of radiosensitivity. IntJRadiatOncolBiolPhys. 2004;58(2):331-5.

316. Banath JP, MacPhail SH, Olive PL. Radiation sensitivity, H2AX phosphorylation, and kinetics of repair of DNA strand breaks in irradiated cervical cancer cell lines. Cancer research. 2004;64(19):7144-9.

317. Klokov D, MacPhail SM, Banath JP, Byrne JP, Olive PL. Phosphorylated histone H2AX in relation to cell survival in tumor cells and xenografts exposed to single and fractionated doses of X-rays. RadiotherOncol. 2006;80(2):223-9.

318. Taneja N, Davis M, Choy JS, Beckett MA, Singh R, Kron SJ, et al. Histone H2AX phosphorylation as a predictor of radiosensitivity and target for radiotherapy. Journal of Biological Chemistry. 2004;279(3):2273-80.

319. Celeste A, Fernandez-Capetillo O, Kruhlak MJ, Pilch DR, Staudt DW, Lee A, et al. Histone H2AX phosphorylation is dispensable for the initial recognition of DNA breaks. Nature cell biology. 2003;5(7):675-9.

320. Clingen PH, Wu JY, Miller J, Mistry N, Chin F, Wynne P, et al. Histone H2AX phosphorylation as a molecular pharmacological marker for DNA interstrand crosslink cancer chemotherapy. BiochemPharmacol. 2008;76(1):19-27.

321. Yuan J, Adamski R, Chen J. Focus on histone variant H2AX: to be or not to be. FEBS Lett. 2010;584(17):3717-24.

322. De Silva IU, McHugh PJ, Clingen PH, Hartley JA. Defects in interstrand cross-link uncoupling do not account for the extreme sensitivity of ERCC1 and XPF cells to cisplatin. Nucleic Acids Res. 2002;30(17):3848-56.

323. Huang X, Halicka HD, Darzynkiewicz Z. Detection of histone H2AX phosphorylation on Ser-139 as an indicator of DNA damage (DNA double-strand breaks). CurrProtocCytom. 2004;Chapter 7:Unit.

324. Mimitou EP, Symington LS. DNA end resection: many nucleases make light work. DNA repair. 2009;8(9):983-95.

325. Kowalczykowski SC. Structural biology: snapshots of DNA repair. Nature. 2008;453(7194):463-6.

326. Liu J, Doty T, Gibson B, Heyer WD. Human BRCA2 protein promotes RAD51 filament formation on RPA-covered single-stranded DNA. Nat StructMolBiol. 2010;17(10):1260-2.

327. Rossi MJ, Mazina OM, Bugreev DV, Mazin AV. The RecA/RAD51 protein drives migration of Holliday junctions via polymerization on DNA. ProcNatlAcadSciUSA. 2011;108(16):6432-7.

328. Tarsounas M, Davies D, West SC. BRCA2-dependent and independent formation of RAD51 nuclear foci. Oncogene. 2003;22(8):1115-23.

329. Raschle M, Knipscheer P, Enoiu M, Angelov T, Sun J, Griffith JD, et al. Mechanism of replication-coupled DNA interstrand crosslink repair. Cell. 2008;134(6):969-80.

330. Long DT, Raschle M, Joukov V, Walter JC. Mechanism of RAD51-dependent DNA interstrand cross-link repair. Science (New York, NY). 2011;333(6038):84-7.

331. Budzowska M, Kanaar R. Mechanisms of dealing with DNA damage-induced replication problems. Cell BiochemBiophys. 2009;53(1):17-31.

332. Holloman WK. Unraveling the mechanism of BRCA2 in homologous recombination. Nat StructMolBiol. 2011;18(7):748-54.

333. Tashiro S, Kotomura N, Shinohara A, Tanaka K, Ueda K, Kamada N. S phase specific formation of the human Rad51 protein nuclear foci in lymphocytes. Oncogene. 1996;12(10):2165-70.

334. Forget AL, Kowalczykowski SC. Single-molecule imaging brings Rad51 nucleoprotein filaments into focus. Trends Cell Biol. 2010;20(5):269-76.

335. Bahassi EM, Ovesen JL, Riesenberg AL, Bernstein WZ, Hasty PE, Stambrook PJ. The checkpoint kinases Chk1 and Chk2 regulate the functional associations between hBRCA2 and Rad51 in response to DNA damage. Oncogene. 2008;27(28):3977-85.

336. Graeser M, McCarthy A, Lord CJ, Savage K, Hills M, Salter J, et al. A marker of homologous recombination predicts pathologic complete response to neoadjuvant chemotherapy in primary breast cancer. ClinCancer Res. 2010;16(24):6159-68.

337. Short SC, Giampieri S, Worku M, Alcaide-German M, Sioftanos G, Bourne S, et al. Rad51 inhibition is an effective means of targeting DNA repair in glioma models and CD133+ tumor-derived cells. NeuroOncol. 2011;13(5):487-99.

338. Spanswick VJ, Lowe HL, Newton C, Bingham JP, Bagnobianci A, Kiakos K, et al. Evidence for different mechanisms of 'unhooking' for melphalan and cisplatin-induced DNA interstrand cross-links in vitro and in clinical acquired resistant tumour samples. BMCCancer. 2012;12(1):436.

339. Lee A, Nakano M, Hincapie M, Kolarich D, Baker MS, Hancock WS, et al. The lectin riddle: glycoproteins fractionated from complex mixtures have similar glycomic profiles. OMICS. 2010;14(4):487-99.

340. Skehan P, Storeng R, Scudiero D, Monks A, McMahon J, Vistica D, et al. New colorimetric cytotoxicity assay for anticancer-drug screening. J Natl Cancer Inst. 1990;82(13):1107-12.

341. Olive PL. DNA damage and repair in individual cells: applications of the comet assay in radiobiology. IntJRadiatBiol. 1999;75(4):395-405.

342. Marais R, Spooner RA, Stribbling SM, Light Y, Martin J, Springer CJ. A cell surface tethered enzyme improves efficiency in gene-directed enzyme prodrug therapy. Nat Biotechnol. 1997;15(13):1373-7.

343. Julenius K, Molgaard A, Gupta R, Brunak S. Prediction, conservation analysis, and structural characterization of mammalian mucin-type O-glycosylation sites. Glycobiology. 2005;15(2):153-64.

344. Rowsell S, Pauptit RA, Tucker AD, Melton RG, Blow DM, Brick P. Crystal structure of carboxypeptidase G2, a bacterial enzyme with applications in cancer therapy. Structure. 1997;5(3):337-47.

345. Ashkenazy H, Erez E, Martz E, Pupko T, Ben-Tal N. ConSurf 2010: calculating evolutionary conservation in sequence and structure of proteins and nucleic acids. Nucleic Acids Res. 2010;38(Web Server issue):W529-W33.

346. Goldstein IJ. Studies on the combining sites of concanavalin A. AdvExpMedBiol. 1975;55:35-53.

347. Goldstein IJ, Hollerman CE, Merrick JM. PROTEIN-CARBOHYDRATE INTERACTION. I. THE INTERACTION OF POLYSACCHARIDES WITH CONCANAVALIN A. BiochimBiophysActa. 1965;97:68-76.

348. Goldstein IJ, Hollerman CE, Smith EE. PROTEIN-CARBOHYDRATE INTERACTION. II. INHIBITION STUDIES ON THE INTERACTION OF CONCANAVALIN A WITH POLYSACCHARIDES. Biochemistry. 1965;4:876-83.

349. Thorpe PE, Detre SI, Foxwell BM, Brown AN, Skilleter DN, Wilson G, et al. Modification of the carbohydrate in ricin with metaperiodate-cyanoborohydride mixtures. Effects on toxicity and in vivo distribution. EurJBiochem. 1985;147(1):197-206.

350. Foxwell BM, Donovan TA, Thorpe PE, Wilson G. The removal of carbohydrates from ricin with endoglycosidases H, F and D and alpha-mannosidase. BiochimBiophysActa. 1985;840(2):193-203.

351. Nakatsukasa K, Okada S, Umebayashi K, Fukuda R, Nishikawa S, Endo T. Roles of O-mannosylation of aberrant proteins in reduction of the load for endoplasmic reticulum chaperones in yeast. Journal of Biological Chemistry. 2004;279(48):49762-72.

352. Vegarud G, Christnsen TB. Glycosylation of Proteins: a new method of enzyme stabilization. BiotechnolBioeng. 1975;17(9):1391-7.

353. Sola RJ, Griebenow K. Glycosylation of therapeutic proteins: an effective strategy to optimize efficacy. BioDrugs. 2010;24(1):9-21.

354. Lommel M, Bagnat M, Strahl S. Aberrant processing of the WSC family and Mid2p cell surface sensors results in cell death of Saccharomyces cerevisiae O-mannosylation mutants. MolCell Biol. 2004;24(1):46-57.

355. Goto M. Protein O-glycosylation in fungi: diverse structures and multiple functions. BiosciBiotechnolBiochem. 2007;71(6):1415-27.

356. Tissot B, North SJ, Ceroni A, Pang PC, Panico M, Rosati F, et al. Glycoproteomics: past, present and future. FEBS Lett. 2009;583(11):1728-35.

357. Witze ES, Old WM, Resing KA, Ahn NG. Mapping protein post-translational modifications with mass spectrometry. Nat Methods. 2007;4(10):798-806.

358. Morelle W, Michalski JC. Analysis of protein glycosylation by mass spectrometry. Nat Protoc. 2007;2(7):1585-602.

359. Chen G, Warrack BM, Goodenough AK, Wei H, Wang-Iverson DB, Tymiak AA. Characterization of protein therapeutics by mass spectrometry: recent developments and future directions. Drug discovery today. 2011;16(1-2):58-64.

360. An HJ, Froehlich JW, Lebrilla CB. Determination of glycosylation sites and site-specific heterogeneity in glycoproteins. CurrOpinChemBiol. 2009;13(4):421-6.

361. Medzihradszky KF. Characterization of site-specific N-glycosylation. Methods MolBiol. 2008;446:293-316.

362. Sola RJ, Griebenow K. Chemical glycosylation: new insights on the interrelation between protein structural mobility, thermodynamic stability, and catalysis. FEBS Lett. 2006;580(6):1685-90.

363. Sola RJ, Rodriguez-Martinez JA, Griebenow K. Modulation of protein biophysical properties by chemical glycosylation: biochemical insights and biomedical implications. Cell MolLife Sci. 2007;64(16):2133-52.

364. Grinnell BW, Walls JD, Gerlitz B. Glycosylation of human protein C affects its secretion, processing, functional activities, and activation by thrombin. Journal of Biological Chemistry. 1991;266(15):9778-85.

365. Rudd PM, Joao HC, Coghill E, Fiten P, Saunders MR, Opdenakker G, et al. Glycoforms modify the dynamic stability and functional activity of an enzyme. Biochemistry. 1994;33(1):17-22.

366. Rudd PM, Woods RJ, Wormald MR, Opdenakker G, Downing AK, Campbell ID, et al. The effects of variable glycosylation on the functional activities of ribonuclease, plasminogen and tissue plasminogen activator. BiochimBiophysActa. 1995;1248(1):1-10.

367. Kohen A, Jonsson T, Klinman JP. Effects of protein glycosylation on catalysis: changes in hydrogen tunneling and enthalpy of activation in the glucose oxidase reaction. Biochemistry. 1997;36(9):2603-11.

368. Freyre FM, Vazquez JE, Ayala M, Canaan-Haden L, Bell H, Rodriguez I, et al. Very high expression of an anti-carcinoembryonic antigen single chain Fv antibody fragment in the yeast Pichia pastoris. JBiotechnol. 2000;76(2-3):157-63.

369. Martinet W, Maras M, Saelens X, Jou WM, Contreras R. Modification of the protein glycosylation pathway in the methylotrophic yeast Pichia pastoris. Biotechnology Letters. 1998;20(12):1171-7.

370. Hamilton SR, Davidson RC, Sethuraman N, Nett JH, Jiang Y, Rios S, et al. Humanization of yeast to produce complex terminally sialylated glycoproteins. Science (New York, NY). 2006;313(5792):1441-3.

371. Hamilton SR, Gerngross TU. Glycosylation engineering in yeast: the advent of fully humanized yeast. CurrOpinBiotechnol. 2007;18(5):387-92.

372. Vervecken W, Callewaert N, Kaigorodov V, Geysens S, Contreras R. Modification of the N-glycosylation pathway to produce homogeneous, human-like glycans using GlycoSwitch plasmids. Methods MolBiol. 2007;389:119-38.

373. Jacobs PP, Callewaert N. N-glycosylation engineering of biopharmaceutical expression systems. CurrMolMed. 2009;9(7):774-800.

374. Bobrowicz P, Cook P, Knett W, inventorsProduction of glycoproteins with reduced O-glycosylation. US patent US 2012/0237973AI. 2012.

375. Kuroda K, Kobayashi K, Kitagawa Y, Nakagawa T, Tsumura H, Komeda T, et al. Efficient antibody production upon suppression of O mannosylation in the yeast Ogataea minuta. ApplEnvironMicrobiol. 2008;74(2):446-53.

376. Nett JH, Cook WJ, Chen MT, Davidson RC, Bobrowicz P, Kett W, et al. Characterization of the Pichia pastoris protein-O-mannosyltransferase gene family. PloS one. 2013;8(7):e68325.

377. Byers VS, Pimm MV, Pawluczyk IZ, Lee HM, Scannon PJ, Baldwin RW. Biodistribution of ricin toxin A chain-monoclonal antibody 791T/36 immunotoxin and influence of hepatic blocking agents. Cancer research. 1987 Oct 15;47(20):5277-83.

378. Kontermann RE. Strategies for extended serum half-life of protein therapeutics. CurrOpinBiotechnol. 2011;22(6):868-76.

379. Carter PJ. Introduction to current and future protein therapeutics: a protein engineering perspective. ExpCell Res. 2011;317(9):1261-9.

380. Sharma SK, Bagshawe KD, Melton RG, Begent RH. Effect of cyclosporine on immunogenicity of a bacterial enzyme carboxypeptidase G2 in ADEPT. Transplantation proceedings. 1996 Dec;28(6):3154-5.

381. Chen BM, Cheng TL, Tzou SC, Roffler SR. Potentiation of antitumor immunity by antibody-directed enzyme prodrug therapy. International Journal of Cancer. 2001;94(6):850-8.

382. Monks NR. Determinants of cellular sensitivity to the ZD27267 ADEPT system. UK: University of Newcastle; 1999.

383. Spanswick VJ, Hartley JM, Ward TH, Hartley JA. Measurement of drug-induced DNA interstrand crosslinking using the single-cell gel electrophoresis (comet) assay. Methods MolMed. 1999;28:143-54.

384. Spanswick VJ, Hartley JM, Hartley JA. Measurement of DNA interstrand crosslinking in individual cells using the Single Cell Gel Electrophoresis (Comet) assay. Methods MolBiol. 2010;613:267-82.

385. Olive PL, Banath JP, Durand RE. Heterogeneity in radiation-induced DNA damage and repair in tumor and normal cells measured using the "comet" assay. RadiatRes. 1990;122(1):86-94.

386. Redon CE, Nakamura AJ, Zhang YW, Ji JJ, Bonner WM, Kinders RJ, et al. Histone gammaH2AX and poly(ADP-ribose) as clinical pharmacodynamic biomarkers. ClinCancer Res. 2010;16(18):4532-42.

387. Wu J, Clingen PH, Spanswick VJ, Mellinas-Gomez M, Meyer T, Puzanov I, et al. gamma-H2AX foci formation as a pharmacodynamic marker of DNA damage produced by DNA cross-linking agents: results from two Phase I clinical trials of SJG-136 (SG2000). ClinCancer Res. 2012.

388. Galkin VE, Wu Y, Zhang XP, Qian X, He Y, Yu X, et al. The Rad51/RadA N-terminal domain activates nucleoprotein filament ATPase activity. Structure. 2006;14(6):983-92.

389. Scully R, Chen J, Plug A, Xiao Y, Weaver D, Feunteun J, et al. Association of BRCA1 with Rad51 in mitotic and meiotic cells. Cell. 1997;88(2):265-75.

390. Burke PJ. The design and synthesis of prodrugs for antibody-directed enzyme prodrug therapy (ADEPT). In: Melton RG, Knox R, editors. Enzyme-Prodrug Strategies for Cancer Therapy. New York: Kluwer Academic/Plenum Publishers; 1999. p. 133-54.

391.	Tietze LF, Krewer B. Antibody-Directed Enzyme Prodrug Therapy: A Promising Approach for a Selective Treatment of Cancer Based on Prodrugs and Monoclonal Antibodies. ChemBioDrug Des. 2009;74(3):205-11.

392.	Chen KC, Schmuck K, Tietze LF, Roffler SR. Selective cancer therapy by extracellular activation of a highly potent glycosidic duocarmycin analogue. Molecular pharmaceutics. 2013 May 6;10(5):1773-82.

393.	Masterson LA, Spanswick VJ, Hartley JA, Begent RH, Howard PW, Thurston DE. Synthesis and biological evaluation of novel pyrrolo[2,1-c][1,4]benzodiazepine prodrugs for use in antibody-directed enzyme prodrug therapy. BioorgMed ChemLett. 2006;16(2):252-6.

394.	O'Connor PM, Kohn KW. Comparative pharmacokinetics of DNA lesion formation and removal following treatment of L1210 cells with nitrogen mustards. Cancer Commun. 1990;2(12):387-94.

395.	Panasci L, Henderson D, Torres-Garcia SJ, Skalski V, Caplan S, Hutchinson M. Transport, metabolism, and DNA interaction of melphalan in lymphocytes from patients with chronic lymphocytic leukemia. Cancer research. 1988;48(7):1972-6.

396.	Brox LW, Gowans B, Belch A. L-phenylalanine mustard (melphalan) uptake and cross-linking in the RPMI 6410 human lymphoblastoid cell line. Cancer research. 1980;40(4):1169-72.

397.	Ostling O, Johanson KJ. Microelectrophoretic study of radiation-induced DNA damages in individual mammalian cells. BiochemBiophysRes Commun. 1984;123(1):291-8.

398.	Hartley JM, Spanswick VJ, Gander M, Giacomini G, Whelan J, Souhami RL, et al. Measurement of DNA cross-linking in patients on ifosfamide therapy using the single cell gel electrophoresis (comet) assay. ClinCancer Res. 1999;5(3):507-12.

399.	Spanswick VJ, Craddock C, Sekhar M, Mahendra P, Shankaranarayana P, Hughes RG, et al. Repair of DNA interstrand crosslinks as a mechanism of clinical resistance to melphalan in multiple myeloma. Blood. 2002;100(1):224-9.

400.	Wynne P, Newton C, Ledermann JA, Olaitan A, Mould TA, Hartley JA. Enhanced repair of DNA interstrand crosslinking in ovarian cancer cells from patients following treatment with platinum-based chemotherapy. BrJCancer. 2007;97(7):927-33.

401.	Ledermann JA, Gabra H, Jayson GC, Spanswick VJ, Rustin GJ, Jitlal M, et al. Inhibition of carboplatin-induced DNA interstrand cross-link repair by gemcitabine in patients receiving these drugs for platinum-resistant ovarian cancer. ClinCancer Res. 2010;16(19):4899-905.

402.	Middleton MR, Knox R, Cattell E, Oppermann U, Midgley R, Ali R, et al. Quinone oxidoreductase-2-mediated prodrug cancer therapy. Sci TranslMed. 2010;2(40):40ra50.

403.  Corrie PG, Shaw J, Spanswick VJ, Sehmbi R, Jonson A, Mayer A, et al. Phase I trial combining gemcitabine and treosulfan in advanced cutaneous and uveal melanoma patients. BrJCancer. 2005;92(11):1997-2003.

404.  Puzanov I, Lee W, Chen AP, Calcutt MW, Hachey DL, Vermeulen WL, et al. Phase I pharmacokinetic and pharmacodynamic study of SJG-136, a novel DNA sequence selective minor groove cross-linking agent, in advanced solid tumors. ClinCancer Res. 2011;17(11):3794-802.

405.  Liu Y, Bodmer WF. Analysis of P53 mutations and their expression in 56 colorectal cancer cell lines. ProcNatlAcadSci USA. 2006;103(4):976-81.

406.  Clingen PH, Arlett CF, Hartley JA, Parris CN. Chemosensivity of primary human fibroblasts with defective unhooking of DNA interstrand cross-links. ExpCell Res. 2007;313(4):753-60.

407.  Henriques JA, Brozmanova J, Brendel M. Role of PSO genes in the repair of photoinduced interstrand cross-links and photooxidative damage in the DNA of the yeast Saccharomyces cerevisiae. JPhotochemPhotobiolB. 1997;39(3):185-96.

408.  Hartley JA, Spanswick VJ, Brooks N, Clingen PH, McHugh PJ, Hochhauser D, et al. SJG-136 (NSC 694501), a novel rationally designed DNA minor groove interstrand cross-linking agent with potent and broad spectrum antitumor activity: part 1: cellular pharmacology, in vitro and initial in vivo antitumor activity. Cancer research. 2004;64(18):6693-9.

409.  Clingen PH, De Silva IU, McHugh PJ, Ghadessy FJ, Tilby MJ, Thurston DE, et al. The XPF-ERCC1 endonuclease and homologous recombination contribute to the repair of minor groove DNA interstrand crosslinks in mammalian cells produced by the pyrrolo[2,1-c][1,4]benzodiazepine dimer SJG-136. Nucleic Acids Res. 2005;33(10):3283-91.

410.  Wu JY. Phosphorylation of histone H2AX in response to DNA damage produced by DNA interstrand crosslinking agents: University College London; 2010.

411.  Vare D, Groth P, Carlsson R, Johansson F, Erixon K, Jenssen D. DNA interstrand crosslinks induce a potent replication block followed by formation and repair of double strand breaks in intact mammalian cells. DNA repair. 2012;11(12):976-85.

412.  Chowdhury D, Keogh MC, Ishii H, Peterson CL, Buratowski S, Lieberman J. gamma-H2AX dephosphorylation by protein phosphatase 2A facilitates DNA double-strand break repair. MolCell. 2005;20(5):801-9.

413.  Chowdhury D, Xu X, Zhong X, Ahmed F, Zhong J, Liao J, et al. A PP4-phosphatase complex dephosphorylates gamma-H2AX generated during DNA replication. MolCell. 2008;31(1):33-46.

414.     Olive PL, Banath JP. Kinetics of H2AX phosphorylation after exposure to cisplatin. Cytometry Part B, Clinical cytometry. 2009 Mar;76(2):79-90.

415.     An J, Huang YC, Xu QZ, Zhou LJ, Shang ZF, Huang B, et al. DNA-PKcs plays a dominant role in the regulation of H2AX phosphorylation in response to DNA damage and cell cycle progression. BMCMolBiol. 2010;11:18.

416.     Revet I, Feeney L, Bruguera S, Wilson W, Dong TK, Oh DH, et al. Functional relevance of the histone gammaH2Ax in the response to DNA damaging agents. ProcNatlAcadSci USA. 2011;108(21):8663-7.

417.     Hochhauser D, Meyer T, Spanswick VJ, Wu J, Clingen PH, Loadman P, et al. Phase I study of sequence-selective minor groove DNA binding agent SJG-136 in patients with advanced solid tumors. ClinCancer Res. 2009;15(6):2140-7.

418.     Gregson SJ, Howard PW, Hartley JA, Brooks NA, Adams LJ, Jenkins TC, et al. Design, synthesis, and evaluation of a novel pyrrolobenzodiazepine DNA-interactive agent with highly efficient cross-linking ability and potent cytotoxicity. JMedChem. 2001;44(5):737-48.

419.     Fernandez-Capetillo O, Lee A, Nussenzweig M, Nussenzweig A. H2AX: the histone guardian of the genome. DNA repair. 2004;3(8-9):959-67.

420.     Holthausen JT, Wyman C, Kanaar R. Regulation of DNA strand exchange in homologous recombination. DNA repair. 2010;9(12):1264-72.

421.     Krejci L, Altmannova V, Spirek M, Zhao X. Homologous recombination and its regulation. Nucleic Acids Res. 2012;40(13):5795-818.

422.     Fernandez-Capetillo O, Chen HT, Celeste A, Ward I, Romanienko PJ, Morales JC, et al. DNA damage-induced G2-M checkpoint activation by histone H2AX and 53BP1. Nat Cell Biol. 2002;4(12):993-7.

423.     Sonoda E, Zhao GY, Kohzaki M, Dhar PK, Kikuchi K, Redon C, et al. Collaborative roles of gammaH2AX and the Rad51 paralog Xrcc3 in homologous recombinational repair. DNA repair. 2007;6(3):280-92.

424.     Lambert S, Froget B, Carr AM. Arrested replication fork processing: interplay between checkpoints and recombination. DNA repair. 2007;6(7):1042-61.

425.     Krogh BO, Symington LS. Recombination proteins in yeast. AnnuRev Genet. 2004;38:233-71.

426.     Delacote F, Lopez BS. Importance of the cell cycle phase for the choice of the appropriate DSB repair pathway, for genome stability maintenance: the trans-S double-strand break repair model. Cell cycle (Georgetown, Tex). 2008;7(1):33-8.

427. Wang X, Peterson CA, Zheng H, Nairn RS, Legerski RJ, Li L. Involvement of nucleotide excision repair in a recombination-independent and error-prone pathway of DNA interstrand cross-link repair. MolCell Biol. 2001;21(3):713-20.

428. Sonoda E, Hochegger H, Saberi A, Taniguchi Y, Takeda S. Differential usage of non-homologous end-joining and homologous recombination in double strand break repair. DNA repair. 2006;5(9-10):1021-9.

429. Lundin C. Different roles for nonhomologous end joining and homologous recombination following replication arrest in mammalian cells. MolCell Biol. 2002;22:5869-78.

430. Kass EM, Jasin M. Collaboration and competition between DNA double-strand break repair pathways. FEBS Lett. 2010;584(17):3703-8.

431. Basu B, Yap TA, Molife LR, de Bono JS. Targeting the DNA damage response in oncology: past, present and future perspectives. CurrOpinOncol. 2012;24(3):316-24.

432. Walworth NC. Cell-cycle checkpoint kinases: checking in on the cell cycle. Current opinion in cell biology. 2000 Dec;12(6):697-704.

433. Patil M, Pabla N, Dong Z. Checkpoint kinase 1 in DNA damage response and cell cycle regulation. Cellular and molecular life sciences : CMLS. 2013 Mar 19.

434. Liu Q, Guntuku S, Cui XS, Matsuoka S, Cortez D, Tamai K, et al. Chk1 is an essential kinase that is regulated by Atr and required for the G(2)/M DNA damage checkpoint. Genes & development. 2000 Jun 15;14(12):1448-59.

435. Zhou BB, Anderson HJ, Roberge M. Targeting DNA checkpoint kinases in cancer therapy. Cancer biology & therapy. 2003 Jul-Aug;2(4 Suppl 1):S16-22.

436. Powell SN, DeFrank JS, Connell P, Eogan M, Preffer F, Dombkowski D, et al. Differential sensitivity of p53(-) and p53(+) cells to caffeine-induced radiosensitization and override of G2 delay. Cancer research. 1995 Apr 15;55(8):1643-8.

437. Tenzer A, Pruschy M. Potentiation of DNA-damage-induced cytotoxicity by G2 checkpoint abrogators. Current medicinal chemistry Anti-cancer agents. 2003 Jan;3(1):35-46.

438. Chen T, Stephens PA, Middleton FK, Curtin NJ. Targeting the S and G2 checkpoint to treat cancer. Drug discovery today. 2012 Mar;17(5-6):194-202.

439. Kaelin WG, Jr. Synthetic lethality: a framework for the development of wiser cancer therapeutics. Genome medicine. 2009;1(10):99.

440. Ma CX, Janetka JW, Piwnica-Worms H. Death by releasing the breaks: CHK1 inhibitors as cancer therapeutics. Trends MolMed. 2011;17(2):88-96.

441.    Barone MV, Crozat A, Tabaee A, Philipson L, Ron D. CHOP (GADD153) and its oncogenic variant, TLS-CHOP, have opposing effects on the induction of G1/S arrest. Genes & development. 1994 Feb 15;8(4):453-64.

442.    Jeffrey PD, Russo AA, Polyak K, Gibbs E, Hurwitz J, Massague J, et al. Mechanism of CDK activation revealed by the structure of a cyclinA-CDK2 complex. Nature. 1995 Jul 27;376(6538):313-20.

443.    Brooks K, Oakes V, Edwards B, Ranall M, Leo P, Pavey S, et al. A potent Chk1 inhibitor is selectively cytotoxic in melanomas with high levels of replicative stress. Oncogene. 2013;32(6):788-96.

444.    Kawabe T. G2 checkpoint abrogators as anticancer drugs. Mol Cancer Ther. 2004 Apr;3(4):513-9.

445.    Reinhardt HC, Aslanian AS, Lees JA, Yaffe MB. p53-deficient cells rely on ATM- and ATR-mediated checkpoint signaling through the p38MAPK/MK2 pathway for survival after DNA damage. Cancer cell. 2007 Feb;11(2):175-89.

446.    Courage C, Budworth J, Gescher A. Comparison of ability of protein kinase C inhibitors to arrest cell growth and to alter cellular protein kinase C localisation. British journal of cancer. 1995 Apr;71(4):697-704.

447.    Chou TC, Talalay P. Quantitative analysis of dose-effect relationships: the combined effects of multiple drugs or enzyme inhibitors. AdvEnzyme Regul. 1984;22:27-55.

448.    Chou TC. Drug combination studies and their synergy quantification using the Chou-Talalay method. Cancer research. 2010;70(2):440-6.

449.    Chou TC. Theoretical basis, experimental design, and computerized simulation of synergism and antagonism in drug combination studies. Pharmacol Rev. 2006;58(3):621-81.

450.    Islaih M, Halstead BW, Kadura IA, Li B, Reid-Hubbard JL, Flick L, et al. Relationships between genomic, cell cycle, and mutagenic responses of TK6 cells exposed to DNA damaging chemicals. MutatRes. 2005;578(1-2):100-16.

451.    Barnes DE, Lindahl T. Repair and genetic consequences of endogenous DNA base damage in mammalian cells. Annual review of genetics. 2004;38:445-76.

452.    Helt CE, Wang W, Keng PC, Bambara RA. Evidence that DNA damage detection machinery participates in DNA repair. Cell cycle (Georgetown, Tex). 2005 Apr;4(4):529-32.

453.    Dianova, II, Bohr VA, Dianov GL. Interaction of human AP endonuclease 1 with flap endonuclease 1 and proliferating cell nuclear antigen involved in long-patch base excision repair. Biochemistry. 2001 Oct 23;40(42):12639-44.

454. Matsumoto Y, Kim K, Hurwitz J, Gary R, Levin DS, Tomkinson AE, et al. Reconstitution of proliferating cell nuclear antigen-dependent repair of apurinic/apyrimidinic sites with purified human proteins. Journal of Biological Chemistry. 1999;274(47):33703-8.

455. Matsumoto Y. Molecular mechanism of PCNA-dependent base excision repair. ProgNucleic Acid ResMolBiol. 2001;68:129-38.

456. Prasad R, Dianov GL, Bohr VA, Wilson SH. FEN1 stimulation of DNA polymerase beta mediates an excision step in mammalian long patch base excision repair. The Journal of biological chemistry. 2000 Feb 11;275(6):4460-6.

457. Prasad R, Shock DD, Beard WA, Wilson SH. Substrate channeling in mammalian base excision repair pathways: passing the baton. The Journal of biological chemistry. 2010 Dec 24;285(52):40479-88.

458. Shibata Y, Nakamura T. Defective flap endonuclease 1 activity in mammalian cells is associated with impaired DNA repair and prolonged S phase delay. Journal of Biological Chemistry. 2002;277(1):746-54.

459. Pascucci B, Stucki M, Jonsson ZO, Dogliotti E, Hubscher U. Long patch base excision repair with purified human proteins. DNA ligase I as patch size mediator for DNA polymerases delta and epsilon. The Journal of biological chemistry. 1999 Nov 19;274(47):33696-702.

460. Otterlei M, Warbrick E, Nagelhus TA, Haug T, Slupphaug G, Akbari M, et al. Post-replicative base excision repair in replication foci. EMBO J. 1999;18(13):3834-44.

461. Shen B, Singh P, Liu R, Qiu J, Zheng L, Finger LD, et al. Multiple but dissectible functions of FEN-1 nucleases in nucleic acid processing, genome stability and diseases. BioEssays : news and reviews in molecular, cellular and developmental biology. 2005 Jul;27(7):717-29.

462. Kikuchi K, Taniguchi Y, Hatanaka A, Sonoda E, Hochegger H, Adachi N, et al. Fen-1 facilitates homologous recombination by removing divergent sequences at DNA break ends. MolCell Biol. 2005;25(16):6948-55.

463. Berger SH, Pittman DL, Wyatt MD. Uracil in DNA: consequences for carcinogenesis and chemotherapy. Biochemical pharmacology. 2008 Sep 15;76(6):697-706.

464. Kothandapani A, Dangeti VS, Brown AR, Banze LA, Wang XH, Sobol RW, et al. Novel role of base excision repair in mediating cisplatin cytotoxicity. The Journal of biological chemistry. 2011 Apr 22;286(16):14564-74.

465. Parsons JL, Dianov GL. Co-ordination of base excision repair and genome stability. DNA repair. 2013 May 1;12(5):326-33.

466. Panda H, Jaiswal AS, Corsino PE, Armas ML, Law BK, Narayan S. Amino acid Asp181 of 5'-flap endonuclease 1 is a useful target for chemotherapeutic development. Biochemistry. 2009;48(42):9952-8.

467. Rouault JP, Falette N, Guehenneux F, Guillot C, Rimokh R, Wang Q, et al. Identification of BTG2, an antiproliferative p53-dependent component of the DNA damage cellular response pathway. Nature genetics. 1996 Dec;14(4):482-6.

468. Tirone F. The gene PC3(TIS21/BTG2), prototype member of the PC3/BTG/TOB family: regulator in control of cell growth, differentiation, and DNA repair? Journal of cellular physiology. 2001 May;187(2):155-65.

469. Jauhiainen A, Thomsen C, Strombom L, Grundevik P, Andersson C, Danielsson A, et al. Distinct cytoplasmic and nuclear functions of the stress induced protein DDIT3/CHOP/GADD153. PloS one. 2012;7(4):e33208.

470. O'Connor PM, Ferris DK, White GA, Pines J, Hunter T, Longo DL, et al. Relationships between cdc2 kinase, DNA cross-linking, and cell cycle perturbations induced by nitrogen mustard. Cell growth & differentiation : the molecular biology journal of the American Association for Cancer Research. 1992 Jan;3(1):43-52.

471. Fornace AJ, Jr., Nebert DW, Hollander MC, Luethy JD, Papathanasiou M, Fargnoli J, et al. Mammalian genes coordinately regulated by growth arrest signals and DNA-damaging agents. Molecular and cellular biology. 1989 Oct;9(10):4196-203.

472. Ron D, Habener JF. CHOP, a novel developmentally regulated nuclear protein that dimerizes with transcription factors C/EBP and LAP and functions as a dominant-negative inhibitor of gene transcription. Genes & development. 1992 Mar;6(3):439-53.

473. O'Connor PM, Wassermann K, Sarang M, Magrath I, Bohr VA, Kohn KW. Relationship between DNA cross-links, cell cycle, and apoptosis in Burkitt's lymphoma cell lines differing in sensitivity to nitrogen mustard. Cancer research. 1991 Dec 15;51(24):6550-7.

474. Bartek J, Lukas J. Pathways governing G1/S transition and their response to DNA damage. FEBS letters. 2001 Feb 16;490(3):117-22.

475. O'Connell MJ, Raleigh JM, Verkade HM, Nurse P. Chk1 is a wee1 kinase in the G2 DNA damage checkpoint inhibiting cdc2 by Y15 phosphorylation. The EMBO journal. 1997 Feb 3;16(3):545-54.

476. Boutros R, Dozier C, Ducommun B. The when and wheres of CDC25 phosphatases. Current opinion in cell biology. 2006 Apr;18(2):185-91.

477. Helleday T. Homologous recombination in cancer development, treatment and development of drug resistance. Carcinogenesis. 2010;31(6):955-60.

478. Huang M, Miao Z-H, Zhu H, Cai Y-J, Lu W, Ding J. Chk1 and Chk2 are differentially involved in homologous recombination repair and cell cycle arrest in response to DNA double-strand breaks induced by camptothecins. Molecular Cancer Therapeutics. 2008 June 1, 2008;7(6):1440-9.

479. Sorensen CS. The cell-cycle checkpoint kinase Chk1 is required for mammalian homologous recombination repair. Nature Cell Biol. 2005;7:195-201.

480. Luo Y, Rockow-Magnone SK, Kroeger PE, Frost L, Chen Z, Han EK, et al. Blocking Chk1 expression induces apoptosis and abrogates the G2 checkpoint mechanism. Neoplasia (New York, NY). 2001 Sep-Oct;3(5):411-9.

481. Castedo M, Perfettini JL, Roumier T, Yakushijin K, Horne D, Medema R, et al. The cell cycle checkpoint kinase Chk2 is a negative regulator of mitotic catastrophe. Oncogene. 2004 May 27;23(25):4353-61.

482. Pabla N, Huang S, Mi QS, Daniel R, Dong Z. ATR-Chk2 signaling in p53 activation and DNA damage response during cisplatin-induced apoptosis. The Journal of biological chemistry. 2008 Mar 7;283(10):6572-83.

483. Thompson R, Meuth M, Woll P, Zhu Y, Danson S. Treatment with the Chk1 inhibitor Go6976 enhances cisplatin cytotoxicity in SCLC cells. International journal of oncology. 2012 Jan;40(1):194-202.

484. Montano R, Chung I, Garner KM, Parry D, Eastman A. Preclinical development of the novel Chk1 inhibitor SCH900776 in combination with DNA-damaging agents and antimetabolites. Mol Cancer Ther. 2012 Feb;11(2):427-38.

485. O'Connor PM, Ferris DK, Pagano M, Draetta G, Pines J, Hunter T, et al. G2 delay induced by nitrogen mustard in human cells affects cyclin A/cdk2 and cyclin B1/cdc2-kinase complexes differently. The Journal of biological chemistry. 1993 Apr 15;268(11):8298-308.

486. Ye W, Blain SW. Chk1 has an essential role in the survival of differentiated cortical neurons in the absence of DNA damage. Apoptosis : an international journal on programmed cell death. 2011 May;16(5):449-59.

487. Husain A, Yan XJ, Rosales N, Aghajanian C, Schwartz GK, Spriggs DR. UCN-01 in ovary cancer cells: effective as a single agent and in combination with cis-diamminedichloroplatinum(II)independent of p53 status. Clinical cancer research : an official journal of the American Association for Cancer Research. 1997 Nov;3(11):2089-97.

488. Wu G, Xu L, Lin N, Liu B. UCN-01 induces S and G2/M cell cycle arrest through the p53/p21(waf1) or CHK2/CDC25C pathways and can suppress invasion in human hepatoma cell lines. BMC cancer. 2013;13:167.

489. Bunch RT, Eastman A. Enhancement of cisplatin-induced cytotoxicity by 7-hydroxystaurosporine (UCN-01), a new G2-checkpoint inhibitor. Clinical cancer research : an official journal of the American Association for Cancer Research. 1996 May;2(5):791-7.

490. Mack PC, Gandara DR, Lau AH, Lara PN, Jr., Edelman MJ, Gumerlock PH. Cell cycle-dependent potentiation of cisplatin by UCN-01 in non-small-cell lung carcinoma. Cancer chemotherapy and pharmacology. 2003 Apr;51(4):337-48.

491. Furuta T, Hayward RL, Meng LH, Takemura H, Aune GJ, Bonner WM, et al. p21CDKN1A allows the repair of replication-mediated DNA double-strand breaks induced by topoisomerase I and is inactivated by the checkpoint kinase inhibitor 7-hydroxystaurosporine. Oncogene. 2006 May 11;25(20):2839-49.

492. Gescher A. Analogs of staurosporine: potential anticancer drugs? General pharmacology. 1998 Nov;31(5):721-8.

493. Senderowicz AM, Sausville EA. Preclinical and clinical development of cyclin-dependent kinase modulators. Journal of the National Cancer Institute. 2000 Mar 1;92(5):376-87.

494. Blasina A, Hallin J, Chen E, Arango ME, Kraynov E, Register J, et al. Breaching the DNA damage checkpoint via PF-00477736, a novel small-molecule inhibitor of checkpoint kinase 1. MolCancer Ther. 2008;7(8):2394-404.

495. Zhang C, Yan Z, Painter CL, Zhang Q, Chen E, Arango ME, et al. PF-00477736 mediates checkpoint kinase 1 signaling pathway and potentiates docetaxel-induced efficacy in xenografts. Clinical cancer research : an official journal of the American Association for Cancer Research. 2009 Jul 15;15(14):4630-40.

496. Zabludoff SD, Deng C, Grondine MR, Sheehy AM, Ashwell S, Caleb BL, et al. AZD7762, a novel checkpoint kinase inhibitor, drives checkpoint abrogation and potentiates DNA-targeted therapies. Mol Cancer Ther. 2008 Sep;7(9):2955-66.

497. Morgan MA, Parsels LA, Zhao L, Parsels JD, Davis MA, Hassan MC, et al. Mechanism of radiosensitization by the Chk1/2 inhibitor AZD7762 involves abrogation of the G2 checkpoint and inhibition of homologous recombinational DNA repair. Cancer research. 2010 Jun 15;70(12):4972-81.

498. Walton MI, Eve PD, Hayes A, Valenti M, De Haven Brandon A, Box G, et al. The preclinical pharmacology and therapeutic activity of the novel CHK1 inhibitor SAR-020106. Mol Cancer Ther. 2010 Jan;9(1):89-100.

499. Matthews DJ. Pharmacological abrogation of S-phase checkpoint enhances the anti-tumor activity of gemcitabine in vivo. Cell cycle (Georgetown, Tex). 2007;6:104-10.

500. Dai Y, Grant S. New insights into checkpoint kinase 1 in the DNA damage response signaling network. Clinical cancer research : an official journal of the American Association for Cancer Research. 2010 Jan 15;16(2):376-83.

501. Wang Q, Fan S, Eastman A, Worland PJ, Sausville EA, O'Connor PM. UCN-01: a potent abrogator of G2 checkpoint function in cancer cells with disrupted p53. Journal of the National Cancer Institute. 1996 Jul 17;88(14):956-65.

502. Kohn EA, Ruth ND, Brown MK, Livingstone M, Eastman A. Abrogation of the S phase DNA damage checkpoint results in S phase progression or premature mitosis depending on the concentration of 7-hydroxystaurosporine and the kinetics of Cdc25C activation. The Journal of biological chemistry. 2002 Jul 19;277(29):26553-64.

503. Levesque AA, Fanous AA, Poh A, Eastman A. Defective p53 signaling in p53 wild-type tumors attenuates p21waf1 induction and cyclin B repression rendering them sensitive to Chk1 inhibitors that abrogate DNA damage-induced S and G2 arrest. Mol Cancer Ther. 2008 Feb;7(2):252-62.

504. Syljuasen RG. Inhibition of human Chk1 causes increased initiation of DNA replication, phosphorylation of ATR targets, and DNA breakage. MolCell Biol. 2005;25:3553-62.

505. Koniaras K, Cuddihy AR, Christopoulos H, Hogg A, O'Connell MJ. Inhibition of Chk1-dependent G2 DNA damage checkpoint radiosensitizes p53 mutant human cells. Oncogene. 2001 Nov 8;20(51):7453-63.

506. Carrassa L, Broggini M, Erba E, Damia G. Chk1, but not Chk2, is involved in the cellular response to DNA damaging agents: differential activity in cells expressing or not p53. Cell cycle (Georgetown, Tex). 2004 Sep;3(9):1177-81.

507. Zenvirt S, Kravchenko-Balasha N, Levitzki A. Status of p53 in human cancer cells does not predict efficacy of CHK1 kinase inhibitors combined with chemotherapeutic agents. Oncogene. 2010 Nov 18;29(46):6149-59.

508. Carrassa L, Chil+ R, Lupi M, Ricci F, Celenza C, Mazzoletti M, et al. Combined inhibition of Chk1 and Wee1: In vitro synergistic effect translates to tumor growth inhibition in vivo. Cell cycle (Georgetown, Tex). 2012;11(13):2507-17.

509. Bennett CN, Tomlinson CC, Michalowski AM, Chu IM, Luger D, Mittereder LR, et al. Cross-species genomic and functional analyses identify a combination therapy using a CHK1 inhibitor and a ribonucleotide reductase inhibitor to treat triple-negative breast cancer. Breast Cancer Res. 2012;14(4):R109.

510. Cho SH, Toouli CD, Fujii GH, Crain C, Parry D. Chk1 is essential for tumor cell viability following activation of the replication checkpoint. Cell cycle (Georgetown, Tex). 2005 Jan;4(1):131-9.

511. McNeely S, Conti C, Sheikh T, Patel H, Zabludoff S, Pommier Y, et al. Chk1 inhibition after replicative stress activates a double strand break response mediated by ATM and DNA-dependent protein kinase. Cell cycle (Georgetown, Tex). 2010 Mar 1;9(5):995-1004.

512. Maya-Mendoza A, Petermann E, Gillespie DA, Caldecott KW, Jackson DA. Chk1 regulates the density of active replication origins during the vertebrate S phase. The EMBO journal. 2007 Jun 6;26(11):2719-31.

513. Osawa T, Davies D, Hartley JA. Mechanism of cell death resulting from DNA interstrand cross-linking in mammalian cells. Cell DeathDis. 2011;2:e187.

514. Bucher N, Britten CD. G2 checkpoint abrogation and checkpoint kinase-1 targeting in the treatment of cancer. British journal of cancer. 2008 Feb 12;98(3):523-8.

515. Okita N, Minato S, Ohmi E, Tanuma S, Higami Y. DNA damage-induced CHK1 autophosphorylation at Ser296 is regulated by an intramolecular mechanism. FEBS letters. 2012 Nov 16;586(22):3974-9.

516. Zhao B, Bower MJ, McDevitt PJ, Zhao H, Davis ST, Johanson KO, et al. Structural basis for Chk1 inhibition by UCN-01. The Journal of biological chemistry. 2002 Nov 29;277(48):46609-15.

517. Zaugg K, Su YW, Reilly PT, Moolani Y, Cheung CC, Hakem R, et al. Cross-talk between Chk1 and Chk2 in double-mutant thymocytes. Proceedings of the National Academy of Sciences of the United States of America. 2007 Mar 6;104(10):3805-10.

518. Matsuoka S, Huang M, Elledge SJ. Linkage of ATM to cell cycle regulation by the Chk2 protein kinase. Science (New York, NY). 1998 Dec 4;282(5395):1893-7.

519. Blasina A, de Weyer IV, Laus MC, Luyten WH, Parker AE, McGowan CH. A human homologue of the checkpoint kinase Cds1 directly inhibits Cdc25 phosphatase. Current biology : CB. 1999 Jan 14;9(1):1-10.

520. Sorensen CS, Syljuasen RG, Falck J, Schroeder T, Ronnstrand L, Khanna KK, et al. Chk1 regulates the S phase checkpoint by coupling the physiological turnover and ionizing radiation-induced accelerated proteolysis of Cdc25A. Cancer cell. 2003 Mar;3(3):247-58.

521. Matthews TP, Jones AM, Collins I. Structure-based design, discovery and development of checkpoint kinase inhibitors as potential anticancer therapies. Expert Opin Drug Discov. 2013 Jun;8(6):621-40.

522. Sausville EA, Arbuck SG, Messmann R, Headlee D, Bauer KS, Lush RM, et al. Phase I trial of 72-hour continuous infusion UCN-01 in patients with refractory neoplasms. Journal of clinical oncology : official journal of the American Society of Clinical Oncology. 2001 Apr 15;19(8):2319-33.

523. Perez RP, Lewis LD, Beelen AP, Olszanski AJ, Johnston N, Rhodes CH, et al. Modulation of cell cycle progression in human tumors: a pharmacokinetic and tumor molecular pharmacodynamic study of cisplatin plus the Chk1 inhibitor UCN-01 (NSC 638850). Clinical cancer research : an official journal of the American Association for Cancer Research. 2006 Dec 1;12(23):7079-85.

524. Fuse E, Tanii H, Kurata N, Kobayashi H, Shimada Y, Tamura T, et al. Unpredicted clinical pharmacology of UCN-01 caused by specific binding to human alpha1-acid glycoprotein. Cancer research. 1998 Aug 1;58(15):3248-53.

525. Maugeri-Sacca M, Bartucci M, De Maria R. Checkpoint kinase 1 inhibitors for potentiating systemic anticancer therapy. Cancer treatment reviews. 2013 Aug;39(5):525-33.

526. Brega N, McArthur, G. A., Britten, S. G., et al. Phase I clinical trial of gemcitabine (GEM) in combination with PF-00477736 (PF-736), a selective inhibitor of CHK1 kinase. Journal of Clinical Oncology. 2010;28(Supplement 15 (Abstract 3062)).

527. www.clinicaltrials.gov. US National Institutes of Health US2013 [cited 2013].

528. Merry AH, Neville DC, Royle L, Matthews B, Harvey DJ, Dwek RA, et al. Recovery of intact 2-aminobenzamide-labeled O-glycans released from glycoproteins by hydrazinolysis. Analytical biochemistry. 2002 May 1;304(1):91-9.

529. Rosati S, van den Bremer ET, Schuurman J, Parren PW, Kamerling JP, Heck AJ. In-depth qualitative and quantitative analysis of composite glycosylation profiles and other micro-heterogeneity on intact monoclonal antibodies by high-resolution native mass spectrometry using a modified Orbitrap. mAbs. 2013 Aug 28;5(6).

530. Liu L, Gomathinayagam S, Hamuro L, Prueksaritanont T, Wang W, Stadheim TA, et al. The impact of glycosylation on the pharmacokinetics of a TNFR2:Fc fusion protein expressed in Glycoengineered Pichia Pastoris. Pharmaceutical research. 2013 Mar;30(3):803-12.

531. Frei E, III, Teicher BA, Holden SA, Cathcart KN, Wang YY. Preclinical studies and clinical correlation of the effect of alkylating dose. Cancer research. 1988;48(22):6417-23.

532. Huang Y, Li L. DNA crosslinking damage and cancer - a tale of friend and foe. Translational cancer research. 2013 Jun;2(3):144-54.

533. Kottemann MC, Smogorzewska A. Fanconi anaemia and the repair of Watson and Crick DNA crosslinks. Nature. 2013 Jan 17;493(7432):356-63.

534.   Beucher A, Birraux J, Tchouandong L, Barton O, Shibata A, Conrad S, et al. ATM and Artemis promote homologous recombination of radiation-induced DNA double-strand breaks in G2. The EMBO journal. 2009 Nov 4;28(21):3413-27.

535.   Xiao Z, Xue J, Sowin TJ, Rosenberg SH, Zhang H. A novel mechanism of checkpoint abrogation conferred by Chk1 downregulation. Oncogene. 2005 Feb 17;24(8):1403-11.

536.   Panier S, Durocher D. Push back to respond better: regulatory inhibition of the DNA double-strand break response. Nature reviews Molecular cell biology. 2013 Oct;14(10):661-72.

537.   Fisher R, Pusztai L, Swanton C. Cancer heterogeneity: implications for targeted therapeutics. British journal of cancer. 2013 Feb 19;108(3):479-85.

538.   Lai D, Visser-Grieve S, Yang X. Tumour suppressor genes in chemotherapeutic drug response. Bioscience reports. 2012 Aug;32(4):361-74.

539.   Parsels LA, Morgan MA, Tanska DM, Parsels JD, Palmer BD, Booth RJ, et al. Gemcitabine sensitization by checkpoint kinase 1 inhibition correlates with inhibition of a Rad51 DNA damage response in pancreatic cancer cells. Mol Cancer Ther. 2009 Jan;8(1):45-54.

540.   Lord CJ, Ashworth A. Mechanisms of resistance to therapies targeting BRCA-mutant cancers. Nature medicine. 2013 Nov;19(11):1381-8.

541.   Ricart AD. Immunoconjugates against solid tumors: mind the gap. ClinPharmacol Ther. 2011;89(4):513-23.